

PROGRAMA DE PÓS-GRADUAÇÃO EM CIÊNCIA DOS MATERIAIS

“Study on sugar cane straw ash (SCSA) in alkali-activated binders”

JOÃO CLÁUDIO BASSAN DE MORAES

Ilha Solteira
2017

PROGRAMA DE PÓS-GRADUAÇÃO EM CIÊNCIA DOS MATERIAIS

"Study on sugar cane straw ash (SCSA) in alkali-activated binders"

JOÃO CLÁUDIO BASSAN DE MORAES

Supervisor: Prof. Dr. Jorge Luís Akasaki

Co-Supervisor: Prof. Dr. Jordi Payá Bernabeu

A thesis submitted to the Faculdade de Engenharia – Campus de Ilha Solteira/UNESP, for the degree of Doctor in Materials Science and Engineering.

Area of knowledge: Materials Science and Engineering.

Ilha Solteira
2017

FICHA CATALOGRÁFICA

Desenvolvido pelo Serviço Técnico de Biblioteca e Documentação

M827s Moraes, João Claudio Bassan de.
Study on sugar cane straw ash (SCSA) in alkali-activated binders / João Claudio Bassan de Moraes. -- Ilha Solteira: [s.n.], 2017
187 f. : il.

Tese (doutorado) - Universidade Estadual Paulista. Faculdade de Engenharia de Ilha Solteira. Área de conhecimento: Ciência e Engenharia de Materiais, 2017

Orientador: Jorge Luís Akasaki
Co-orientador: Jorge Juan Payá Bernabeu
Inclui bibliografia

1. Alternative material. 2. Sustainable material. 3. Compressive strength. 4. Microstructural studies.

CERTIFICADO DE APROVAÇÃO

TÍTULO DA TESE: Study on sugar cane straw ash (SCSA) in alkali-activated binders

AUTOR: JOÃO CLAUDIO BASSAN DE MORAES

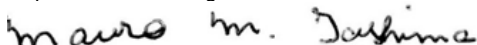
ORIENTADOR: JORGE LUIS AKASAKI

COORIENTADOR: JORGE JUÁN PAYÁ BERNABEU

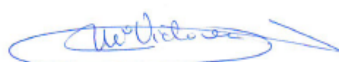
Aprovado como parte das exigências para obtenção do Título de Doutor em CIÊNCIA DOS MATERIAIS, área: CIÊNCIA E ENGENHARIA DOS MATERIAIS pela Comissão Examinadora:



Prof. Dr. JORGE LUIS AKASAKI
Departamento de Engenharia Civil / Faculdade de Engenharia de Ilha Solteira



Prof. Dr. MAURO MITSUUCHI TASHIMA
Departamento de Engenharia Civil / Faculdade de Engenharia de Ilha Solteira



Profa. Dra. MARIA VICTORIA BORRACHERO ROSADO
ICITECH – Instituto de Ciencia y Tecnología del Hormigón / Universitat Politècnica de Valencia



Prof. Dr. HOLMER SAYASTANO JUNIOR
Departamento de Engenharia de Biossistemas / Faculdade de Zootecnia e Engenharia de Alimentos de Pirassununga



Prof. Dr. EMÍLIO CÉSAR CAVALCANTE MELO DA SILVA
CENPES – Centro de Pesquisa da Petrobras / Petróleo Brasileiro

Ilha Solteira, 13 de novembro de 2017

I dedicate this thesis to my
parents, Cássia Regina and
João Batista, and my sister,
Maria Júlia.

ACKNOWLEDGMENTS

I would like to thank my mother Cássia Regina, my father João Batista, my sister Maria Júlia, my aunt Claudia and Meggy to the support and love.

I would like to thank the supervisors and friends, Jorge Akasaki and Jordi Payá, for the knowledge and the opportunity.

I would like to thank the professor and friend Mauro Tashima for helping me in my scientific career and for sharing funny moments.

I would like to thank the professors and friends, José Luiz Melges, María Victoria Borrachero and José Monzó, for the support and knowledge to write the thesis. Thanks also to professor João Carlos Moraes for supporting the qualifying exam. Thanks to professors José Lollo, Rogério Rodrigues, Renato Bertolino, Tsunao and Haroldo Bernardes from Civil Engineering Department for the knowledge provided in my professional career.

I would like to thank my friends from the Civil Engineering Graduate, Priscila, Heitor, Franciéli and Jônatas for the support and funny moments.

I would like to thank all my friends from GIQUIMA, specially to Lourdes and Alba for the strong friendship and for making my year in Valencia very especial. Thanks also to Lucía, Ariel, Patrícia, Jesús, Amin, Yasna, Noelia, Clara, Edwin, Ricardo, Álvaro, Fausto and Manolo "Mister" Paredes. In addition, I would like to thank the researchers and workers from ICITECH for my great year in Valencia.

I would like to thank all my friends from MAC group, João Victor, Adriana, Alex, Danilo, Alan and Thiago Trentin, for the funny and professional moments.

I would like to thank the best neighborhood I ever had in Ilha Solteira: Bruna, Fernanda, Gabriel and Paula.

I would like to thank my friends from Marília, Everton, Bia, Bruno and Renata, for the funny moments.

I would like to thank my friends from Ilha Solteira for the supporting and taking care of me: Estéfani, folks from Equilibrium gym, Mariana Lopes and family, Fernando Tangerino and Angelo Doimo.

I would like to thank my friends from Valencia for one of the best trips I have ever gone: Luigi, Jana, Francesco, Theresa, Lech and Iona.

I would like to thank my virtual friends, but they were closer than ever: Kelly, Gisele and the FC Barcelona group (Caio, Fabielle, Edvande, Drielle, Filipe, Poly and Laiza).

I would like to thank the folks who work in the Civil Engineering Department: Sandra, José Carlos, Juliana, Gilson, Flavio, Ozias, Ademir and Marcelo.

I would like to thank Jaira and Maria Gercy for taking care of me during these years.

I would like to thank CNPq and CAPES for the scholarship.

Finally, thanks to everyone who contributed directly or indirectly to this thesis.

RESUMO

Aglomerantes ativados alcalinamente (AAA) são obtidos da combinação de um precursor sólido (geralmente um aluminossilicato) e uma solução alcalina de alta concentração. As vantagens de utilizar este novo tipo de aglomerante comparado ao cimento Portland, um aglomerante convencional, são as menores emissões de CO₂, menor consumo de energia e a possibilidade de utilizar matérias-primas renováveis e/ou resíduos. Neste sentido, este trabalho apresenta um novo resíduo da indústria da cana-de-açúcar: a folha de cana-de-açúcar. A folha apresenta um poder calorífico interessante; portanto, ela pode ser utilizada como biomassa para produzir energia através de um processo de queima. Depois deste procedimento, é gerado um novo resíduo: a cinza de folha de cana-de-açúcar (CF). Esta cinza não apresenta uma destinação correta, então este trabalho tem como intenção utilizar esta cinza como material-primário em AAA. A CF foi avaliada de duas formas: como precursor sólido e como matéria-primária para produzir a solução alcalina. No primeiro modo, a CF foi utilizada em sistemas combinados com a escória de alto-forno (EAF) ativado com ambas as soluções de NaOH e NaOH/silicato de sódio. No segundo modo, a CF foi utilizada como fonte de sílica para produzir a solução alcalina com o NaOH em AAA baseados em EAF. Os sistemas foram estudados através da resistência à compressão de argamassas e pelo estudo da microestrutura de pastas. Ensaios realizados para avaliar a microestrutura foram a difração de raios-X (DRX), espectroscopia de infravermelho por transformada de Fourier (EITF), análise termogravimétrica (ATG), microscopia eletrônica de varredura (MEV) e porosimetria por intrusão de mercúrio (PIM). Resultados dos ensaios mostraram que a CF melhorou as propriedades mecânicas dos AAA baseados em EAF nos dois modos, como precursor sólido e como fonte de silício para a solução ativadora. Estes resultados permitem concluir que a CF pode ser utilizada em AAA, dando uma destinação ao resíduo.

Palavras-chave: Material alternativo. Material sustentável. Resistência à compressão. Estudos microestruturais.

ABSTRACT

Alkali-activated binders (AAB) are obtained from a combination of a solid precursor (generally an aluminosilicate) and a high concentrated alkaline solution. The advantages of using this new type of binder compared to the Portland cement, a conventional binder, are the less CO₂ emissions, lower energy consumption and the possibility of using renewable and/or residues as raw materials. In this way, this work presents a new residue from the sugar cane industry: the sugar cane straw. The straw presents an interesting calorific value; therefore, it can be utilised as biomass to produce energy by a burning process. After this procedure, it is generated another waste: the sugar cane straw ash (SCSA). This ash does not have an appropriate destination, then this work intends to utilise this ash as raw material in AAB. SCSA was evaluated in both ways: as solid precursor and as raw material to produce the alkaline solution. In the first way, SCSA was utilised in combined systems with blast furnace slag BFS activated with both NaOH and NaOH/sodium silicate solutions. In the second one, the SCSA was utilised as silica source to produce the alkaline solution with NaOH in BFS-based systems. These systems were assessed by the compressive strength of mortars and by microstructural studies on pastes. Tests carried out to assesses their microstructure were X-ray diffraction (XRD), Fourier transform infrared spectroscopy (FTIR), thermogravimetric analysis (TGA), field emission scanning electron microscopy (FESEM), and mercury intrusion porosimetry (MIP). Results of the tests showed that the SCSA improved the mechanical properties of BFS-based AAB in both methods, as solid precursor and as silica source to produce the activating solution. These results allow to conclude that the SCSA can be utilised in AAB, giving it a suitable destination.

Keywords: Alternative material. Sustainable material. Compressive strength. Microstructural studies.

FIGURES LIST

Figure 1.1	Experimental program of the present doctoral thesis	18
Figure 2.1	Scheme of types of binders related to the Ca, Al and M ⁺ content, emphasizing the classification of alkali-activated binders and geopolymers (PROVIS, 2014)	20
Figure 2.2	Development in the accumulated publications number in Scopus/Elsevier database of the words “alkali-activated binders” (dotted line) and “geopolymer” (solid line) presented in title, abstract or keywords (PACHECO-TORGAL et al., 2015)	21
Figure 2.3	Proposed model to formation of BFS-based alkali-activated binders: a) role from the alkalis in the reaction (being R ⁺ the alkaline cation), and b) gel formation (GARCIA-LODEIRO et al., 2015)	23
Figure 2.4	A general view from the N-A-S-H gels produced in the alkaline activation of binders with low Ca-content (GARCIA-LODEIRO et al., 2015)	24
Figure 2.5	Reaction mechanism from the first step named destruction-coagulation: a) dissolution of Si-O-Si bonds, and b) dissolution of Si-O-Al bonds (GARCIA-LODEIRO et al., 2015)	25
Figure 2.6	Reaction mechanism from the second step named coagulation-condensation (GARCIA-LODEIRO et al., 2015)	26
Figure 2.7	Illustration of the gel formation in alkali-activated binders with low Ca-content (GARCIA-LODEIRO et al., 2015)	27
Figure 2.8	Studies on influence of sodium silicate in the compressive strength of BFS-based AAB: a) phosphorous BFS; and b) Acid, neutral and basic BFS (SHI et al., 2006)	29
Figure 2.9	Compressive strength results of combined systems composed by blast furnace slag and red clay brick waste (RCBW/BFS) after 28 days of curing at room temperature (RAKHIMOVA and RAKHIMOV, 2015)	30
Figure 2.10	Compressive strength results of binary systems composed by metakaolin and fly ash (MK/FA) after 7 and 28 days of curing at room temperature (ZHANG et al., 2014)	33
Figure 2.11	Compressive strength evolution of FA/POFA specimens studied in high temperatures (adapted from RANJBAR et al., 2014)	35
Figure 2.12	Comparison between CO ₂ footprints of concretes based on alkali-activated binders and OPC, highlighting the emissions from the alkaline activator (adapted from Turner; Collins, 2013)	37
Figure 2.13	Compressive strength versus reflux time of FCC-based alkali activated binders prepared with different siliceous sources combined with NaOH solutions: G-RHA (ground rice husk ash), O-RHA (original rice husk ash), quartz, control (commercial waterglass solution). Key: full line for compressive strength and dotted line for flexural strength (Bouzón et al., 2014)	38
Figure 2.14	Compressive strength of concrete manufactured with fly ash and palm oil fuel ash (BA geopolymer concrete) compared to one of Portland cement after sulfuric acid attack (ARIFFIN et al., 2013)	39

Figure 2.15	Compressive strength after temperature treatment of OPC mixtures and alkali-activated binders of solid precursors with a) high Ca content and b) low Ca content (TURKER et al., 2016; DUAN et al., 2015)	41
Figure 2.16	Mechanized harvesting of the sugar cane (UNICA, 2016)	42
Figure 2.17	Electrical conductivity of hydrated lime/RHA and hydrated lime/SCSA suspensions (VILLAR-COCINA, 2002)	43
Figure 2.18	Compressive strength of mortars cured after 60 days (GUZMÁN et al., 2011)	44
Figure 3.1	Loss of electrical conductivity (Lc) of suspensions studied at (a) 60 °C; (b) 50 °C; (c) 40 °C; and (d) 30 °C	62
Figure 3.2	pH variation (Δ pH) of the CH/SCSA suspensions at each temperature studied	63
Figure 3.3	DTG curves of the solid part of the suspensions after electrical conductivity measurements at 40 °C.	64
Figure 3.4	FTIR spectra of 3:7 and 5:5 CH/SCSA pastes after 1, 3, 7, and 28 days of curing at 40 °C	66
Figure 3.5	DTG curves of 5:5 and 3:7 CH/SCSA pastes from 1 to 28 days of curing at 40 °C	68
Figure 3.6	SEM images of 3:7 CH/SCSA paste after 28 days of curing cured at 40 °C	70
Figure 4.1	X-Ray Diffraction of SCSA	76
Figure 4.2	SEM images of SCSA	77
Figure 4.3	Compressive strength of Portland cement mortars	80
Figure 4.4	Compressive strength of alkaline activated mortars	81
Figure 5.1	Calculated γ factor for specimens with BFS/SCSA ratios of 85/15, 75/25, 67/33 and 50/50, in the ε value range of 0-0.75, after: a) 3 days of curing, b) 7 days of curing, c) 28 days of curing and d) 90 days of curing (at 25°C)	91
Figure 5.2	DTG curves for the N-100/0 (a), SS50-100/0 (b), N-75/25 (c), SS50-75/25 (d), N-50/50 (e) and SS50-50/50 (f) pastes cured for 7, 28 and 90 days at 25°C	92
Figure 5.3	FTIR spectra for the N-100/0 (a), SS50-100/0 (b), N-75/25 (c), SS50-75/25 (d), N-50/50 (e) and SS50-S50 (f) pastes cured for 7, 28 and 90 days at 25°C	94
Figure 5.4	XRD patterns for the raw materials, BFS and SCSA, and for the N-100/0 and N-50/50 pastes, cured for 28 days at 25°C. (Keys: Q: Quartz; C: Calcite; W: Wollastonite; N: Termonatrite; T: Hydrotalcite; K: Katoite; S: Stratlingite; H: Hydrosodalite; P: Hydrated Nepheline)	95
Figure 5.5	FESEM images of N-100/0 (a and b) and N-50/50 (c and d) after 28 days of curing at 25°C.	96
Figure 6.1	Values of the ϕ ratio for mortars containing SCSA at 7, 28 and 90 days of curing	112

Figure 6.2	XRD patterns of the raw materials (BFS and SCSA) and the pastes 28-0-100/0, 28-0-75/25, 28-0.75-100/0 and 28-0.75-75/25 after 90 days of curing (Key: Q: quartz; C: calcite, H: hydrotalcite; K, katoite; C-S-H: calcium silicate hydrate)	113
Figure 6.3	FTIR spectra of the raw materials (BFS and SCSA) and the pastes 28-0-100/0, 28-0-75/25, 28-0.75-100/0 and 28-0.75-75/25 after 7, 28 and 90 days of curing	114
Figure 6.4	DTG curves of the pastes 28-0-100/0, 28-0-75/25, 28-0.75-100/0 and 28-0.75-75/25 after 7, 28 and 90 days of curing	117
Figure 6.5	Relationships between thermogravimetric mass losses for pastes (P_g , 35-250°C; and P_t , 35-1000°C) and the compressive strength of mortars	118
Figure 6.6	MIP curves of the pastes 28-0-100/0, 28-0-75/25, 28-0.75-100/0 and 28-0.75-75/25 after 90 days of curing: a) differential, and b) accumulated distribution	119
Figure 6.7	FESEM micrographs of BFS activated paste with NaOH (28-0-100/0): a) general view of the paste with an unreacted BFS particle (spot A) and gel (spot B); b) detailed view of the gel; c) in-lens micrograph showing BFS unreacted particle (spot A) and main gel (spot B); d) enlarged zone from c), in which a denser gel is shown (spot C)	120
Figure 6.8	FESEM micrographs of BFS/SCSA activated paste with NaOH (28-0-75/25): a) general view of the paste; b) general view of formed gels (spot D shows a porous gel, and spot E, a compacted gel); c) detailed view of both gels; d) in-lens view (lighter area for porous gel, and darker are for compacted gel)	122
Figure 6.9	FESEM micrographs of BFS activated paste with NaOH and sodium silicate (28-0.75-100/0): a) general view of the paste with some gel formation (spot F shows a porous gel, and spot G, a compacted gel); b) detailed view of formed gels; c) detailed view of sheet-like crystals (spot H, stratlingite); d) pirssonite crystals surrounded by gels	123
Figure 6.10	FESEM micrographs of BFS/SCSA activated paste with NaOH and sodium silicate (28-0.75-75/25): a) general view of the paste with some gel formation (spot J) and a quartz particle (spot K); b) detailed view of compacted gel; c) detailed view of gel; d) pirssonite crystals surrounded by gels.	124
Figure 7.1	Influence of the H_2O/Na_2O ratio by line adjustment on BFS/SCSA proportions of 100/0 (a), 90/10 (b), 80/20 (c) and 70/30 (d) after 3, 7, 28 and 90 days of curing at 25 °C	137
Figure 7.2	σ_{SCSA} factor for SCSA percentage replacements of 10, 20 and 30% after: a) 3; b) 7; c) 28; and d) 90 days of curing at 25 °C	140
Figure 7.3	Best BFS/SCSA proportion for the H_2O/Na_2O ratios of: a) 11.1; b) 13.9; and c) 18.5 after 3, 7, 28 and 90 days of curing at 25 °C	141

Figure 7.4	Non-linear fitting surface of compressive strength values considering all the results after 90 days of curing. Points linked by a solid curve represent the optimum percentage of SCSA in the mixture.	142
Figure 7.5	X-ray diffraction patterns of the raw material and pastes after 90 days of curing: a) BFS and SCSA (raw materials), 19-100/00 and 19-80/20 (pastes); b) BFS and SCSA (raw materials), 19-80/20, 14-80/20 and 11-80/20 (pastes). Key: Q: quartz; C-S-H: semi-crystalline C-S-H; H: hydrotalcite; K: katoite; F: faujasite; C: calcite; S: hydrosodalite	144
Figure 7.6	FTIR spectra of the raw materials (BFS and SCSA) and pastes cured for: a and d) 7 days; b and e) 28 days; and c and f) 90 days at 25 °C. Study on the effect of SCSA content (see a, b and c graphs). Study on the effect of the sodium hydroxide concentration (see d, e and f graphs)	146
Figure 7.7	DTG curves of the pastes: 19-100/0, 19-90/10, 19-80/20 and 19-70/30 cured after a) 7 days, b) 28 days and c) 90 days; and 19-80/20, 14-80/20 and 11-80/20 cured after d) 7 days, e) 28 days and f) 90 days.	149
Figure 7.8	FESEM micrographs of the pastes: a) 19-100/0; and b) 19-80/20 cured after 90 days	151
Figure 7.9	FESEM micrographs of the pastes: a) 19-80/20; b) 14-80/20; and c) 11-80/20 cured after 90 days	152
Figure 8.1	Temperature evolution with time in the dissolution of sodium hydroxide (32.4 g) in water (202.5 g) inside the thermal bottle	165
Figure 8.2	Compressive strength values of mortars (cured at 65 °C for 3 days) with activator prepared by thermal bottle treatment in different reaction time (τ) of 0, 6, 24 and 48 hours	169
Figure 8.3	XRD patterns of raw materials (SCSA and BFS) and pastes (SCSA-1.46-24, SCSA-1.46-0, NH-0 and SS-1.46) cured after 3 days at 65 °C. Keys: Q: quartz; C: calcite; H: hydrotalcite; F: faujasite; C-S-H: calcium silicate hydrate; K: katoite.	171
Figure 8.4	FTIR spectra of raw materials (SCSA and BFS) and pastes (SCSA-1.46-24, SCSA-1.46-0, NH-0 and SS-1.46) cured after 3 days at 65 °C	172
Figure 8.5	DTG curves of pastes (SCSA-1.46-24, SCSA-1.46-0, NH-0 and SS-1.46) cured after 3 days at 65 °C (numbers close to main peaks are in °C)	173
Figure 8.6	FESEM micrographs of the paste SCSA-1.46-24	174
Figure 8.7	FESEM micrographs of the paste SCSA-1.46-0	175
Figure 8.8	Compressive strength values of mortars (cured at 65 °C for 3 days) with activator prepared by thermal bottle treatment in different SiO ₂ /Na ₂ O molar ratio (ϵ) of 0 (only NaOH), 0.73, 1.09, 1.46 and 1.82	176

Figure 8.9	FESEM micrographs of the paste NH-0	178
Figure 8.10	Comparison of compressive strength values of mortars (cured at 65 °C for 3 days and 20 °C for 28 days) obtained from SCSA, SS and RHA	179
Figure 8.11	FESEM micrographs of the paste SS-1.46	181

TABLES LIST

Table 3.1	Chemical composition of SCSA by percentage	60
Table 3.2	Mass loss related to the dehydration of pozzolanic reaction products (P_P) and calcium hydroxide (P_{CH}), and lime fixation of CH:SCSA pastes	68
Table 4.1	Chemical composition of blast furnace slag (BFS) and sugar cane straw ash (SCSA)	78
Table 5.1	Chemical composition of SCSA and BFS by weight percentage	87
Table 5.2	Specimens' names, compressive strength of mortars (MPa) and their standard deviations	91
Table 5.3	Mass losses for the N-100/0, N-75/25, N-50/50, SS50-100/0, SS50-75/25 and SS50-50/50) pastes cured for 7, 28 and 90 days at 25°C in defined temperatures ranges of TGA (35-180°C, 180-250°C and 250-600°C)	93
Table 6.1	Chemical characterisation of the solid precursors utilised in this paper (BFS and SCSA)	105
Table 6.2	Mixture dosage and specimen's names and tests carried out: compressive strength (R_c), X-ray diffraction (XRD), Fourier transform infrared spectroscopy (FTIR), Thermogravimetric analyses (TGA), Mercury intrusion porosimetry (MIP) and Field emission scanning electron microscopy (FESEM)	106
Table 6.3	Compressive strength of mortars (MPa) and their standard deviations	110
Table 6.4	Mass losses (%) for the pastes 28-0-100/0, 28-0-75/25, 28-0.75-100/0 and 28-0.75-75/25 after 7, 28 and 90 days of curing at different temperature ranges (35-250°C, 450-650°C, and total mass loss 35-1000°C)	117
Table 6.5	MIP results of the pastes 28-0-100/0, 28-0-75/25, 28-0.75-100/0 and 28-0.75-75/25 after 90 days of curing	119
Table 7.1	Chemical composition of the raw materials sugar cane straw ash (SCSA) and blast furnace slag (BFS) in weight percentages	134
Table 7.2	Specimen names, mixture designs (H_2O/Na_2O and BFS/SCSA ratios) and tests performed: compressive strength (R_c), X-ray diffraction (XRD), Fourier transform infrared spectroscopy (FTIR), thermogravimetric analysis (TGA) and field emission scanning electron microscopy (FESEM)	136
Table 7.3	Slope values from the graphic compressive strength versus H_2O/Na_2O ratio for the four BFS/SCSA proportions	138
Table 7.4	Mass losses from TGA curves in the 35–250 °C range ($P_{35-200^\circ C}$) and the total mass loss in 35–1000 °C range (P_T) in pastes cured for 7, 28 and 90 days at 25 °C	149
Table 8.1	Chemical composition of BFS, SCSA and RHA in wt%	164
Table 8.2	Mixtures and tests carried out	168
Table 8.3	Mass losses (%) of the pastes SCSA-1.46-24, SCSA-1.46-0, NaOH and SS-1.46 cured after 3 days at 65 °C in the test temperature intervals of 35-300 °C (P_{35-300}) and 300-1000 °C ($P_{300-1000}$)	173

TABLE OF CONTENTS

1	INTRODUCTION	16
1.1	OBJECTIVES	17
2.1	THESIS STRUCTURE	17
2	STATE OF THE ART	19
2.1	ALKALI-ACTIVATED BINDERS	19
2.1.1	Definition	19
2.1.2	History	20
2.1.3	Comparisons to the Portland cement	21
2.1.4	Alkali-activated binders reaction products	22
2.1.5	Solid precursor	27
2.1.6	Alkaline Activators	35
2.1.7	Durability	38
2.2	SUGAR CANE STRAW ASH	42
	REFERENCES	44
3	POZZOLANIC REACTIVITY STUDIES ON SUGAR CANE STRAW ASH	55
3.1	INTRODUCTION	56
3.2	MATERIALS AND METHODS	57
3.2.1	Materials	57
3.2.2	Equipment	58
3.3	RESULTS AND DISCUSSION	59
3.3.1	Sugar Cane Straw Ash Characterization	59
3.3.2	Electrical Conductivity Measurements	60
3.3.3	Fourier Transformed Infrared Spectroscopy	65
3.3.4	Thermogravimetric Analysis	66
3.3.5	Comparison of Results from Different Techniques	69
3.3.6	Scanning Electron Microscopy	69
3.4	CONCLUSIONS	70
	REFERENCES	71
4	PRELIMINARIES STUDIES ON SUGAR CANE STRAW ASH (SCSA) IN MORTARS OF PORTLAND CEMENT/SCSA AND BLAST-FURNACE SLAG/SCSA	74
4.1	INTRODUCTION	75
4.2	EXPERIMENTAL	76
4.2.1	Materials and Equipment	76
4.2.2	Experimental Procedures	78
4.2.2.1	Portland cement mortars	78
4.2.2.2	Alkali-activated mortars	78
4.3	RESULTS AND DISCUSSIONS	79
4.3.1	Compressive Strength of Portland Cement Mortars	79
4.3.2	Compressive Strength of Alkaline Activated mortars	80
4.3	CONCLUSIONS	81
	REFERENCES	81

5	SUGAR CANE STRAW ASH AS SOLID PRECURSOR IN ALKALI-ACTIVATED BINDERS BASED ON BLAST FURNACE SLAG: SOLUTIONS WITH [N+] OF 8 MOL.KG⁻¹ AND SiO₂/Na₂O RATIOS OF 0-0.75	84
5.1	INTRODUCTION	85
5.2	MATERIALS AND METHODS	86
5.2.1	Materials and Equipment	86
5.2.2	Alkali activated binder dosage	88
5.3	RESULTS AND DISCUSSION	88
5.4	CONCLUSIONS	96
	REFERENCES	97
6	SUGAR CANE STRAW ASH AS SOLID PRECURSOR IN ALKALI-ACTIVATED BINDERS BASED ON BLAST FURNACE SLAG: SOLUTIONS WITH [N+] OF 4 MOL.KG⁻¹ AND SiO₂/Na₂O RATIOS OF 0-0.75	100
6.1	INTRODUCTION	101
6.2	MATERIALS AND METHODS	104
6.2.1	Materials	104
6.2.2	Alkali activated binders' dosage and preparation	105
6.2.3	Test procedures for pastes and mortars	105
6.3	RESULTS AND DISCUSSION	107
6.3.1	Compressive strength of mortars	107
6.3.2	Microstructural studies	112
6.3	CONCLUSIONS	124
	REFERENCES	126
7	SUGAR CANE STRAW ASH AS SOLID PRECURSOR IN ALKALI-ACTIVATED BINDERS BASED ON BLAST FURNACE SLAG: SOLUTIONS WITH [N+] OF 6-10 MOL.KG⁻¹	129
7.1	INTRODUCTION	130
7.2	MATERIALS AND METHODS	133
7.2.1	Materials	133
7.2.2	Design of alkali-activated binders	134
7.2.3	Tests carried out for pastes and mortars	134
7.3	RESULTS AND DISCUSSION	137
7.3.1	Compressive strength of mortars	137
7.3.2	Microstructural studies	143
7.3.2.1	<i>X-ray diffraction (XRD)</i>	143
7.3.2.2	<i>Fourier transform infrared spectroscopy (FTIR)</i>	144
7.3.2.3	<i>Thermogravimetric analysis (TGA)</i>	147
7.3.2.4	<i>Field emission scanning electron microscopy (FESEM) and Energy-dispersive X-ray spectroscopy (EDS)</i>	150
7.4	CONCLUSIONS	152
8	SUGAR CANE STRAW ASH AS SILICA SOURCE TO PRODUCE THE ACTIVATING SOLUTION IN ALKALI- ACTIVATED BINDERS BASED ON BLAST FURNACE SLAG	160
8.1	INTRODUCTION	160
8.2	EXPERIMENTAL	162
8.2.1	Materials and Equipment	162

8.2.2	Alkali-activated materials preparation	164
8.2.3	Tests procedures	166
8.2.3	Alkali-activated materials studies	166
8.3	RESULTS AND DISCUSSION	168
8.3.1	Effect of the thermal bottle time (τ) for SCSA/NaOH suspensions (Section 1)	168
8.3.2	Effect of the SiO ₂ /Na ₂ O molar ratio (ϵ) for SCSA/NaOH suspensions (Section 2)	176
8.3.3	Comparison of SCSA to others silica sources (Section 3)	178
8.4	CONCLUSIONS	181
	REFERENCES	182
9	GENERAL CONCLUSIONS	185
10	PROPOSALS FOR FUTURE STUDIES	187

1 INTRODUCTION

Alkali-activated binders (AAB) are the new trend in the research of building construction materials. This type of material is obtained when a silico-aluminous material (also known as solid precursor) is combined with a high concentrated alkaline solution (activating solution) in appropriate proportions. The studies on this type of binder started in the last century with the purpose to reduce the Portland cement consumption. Authors highlighted some advantages of alkali-activated binders' mixtures when compared to the Portland cement: similar or higher compressive strength, improved durability and, mainly, less CO₂ emissions and energy consumption. However, these new kinds of binders present the disadvantages of handling difficult due the high alkalinity, and the several proportions and factors to analyse that influence the mechanical properties of the material (for example, the solid precursor and alkaline solution compositions).

Recent studies focused on the obtainment of new materials source (solid precursors and alkaline solution) for alkali-activated binders' production. The usual materials used as solids precursors are the blast-furnace slag, fly ash and metakaolin. About the alkaline sources in the preparation of the activating solution, hydroxides and silicates are the most common activators. New materials that are being researched in the preparation of alkali-activated binders are, in majority, residues from industry, agro-industry and building construction. This thesis presents a new agro-industry residue from sugar cane production in order to obtain an alkali-activated binder: the sugar cane straw ash (SCSA).

The issue of sugar cane starts in the increase of its production in the last years in Brazil due the production of alcohol and sugar: in only ten years (from 2004/2005 to 2014/2015), the increase was 64%. The state of Sao Paulo, where this research takes place, is the major sugar cane production in Brazil, which represents over than 50% of total production. Another important issue of the sugar cane is the harvesting process. Some years ago, the sugar cane harvesting used to be performed by a burning process in the cultivation area. However, an Agro-environmental protocol was signed to put an end on this burning procedure, making that the mechanized harvesting gains in importance on this scenario. In this type of harvesting, is generated a by-product that is composed by the dried and green leaves, which are mostly left on the cultivation field: the sugar cane straw. Due its interesting

calorific value, which is compared to the sugar cane bagasse, authors are studying new methods to collect and generate energy from this by-product. After this process to obtain energy from the straw, an ash is obtained: the sugar cane straw ash (SCSA). This residue does not present a suitable valorisation, and similar to other ashes from agro-industry (rice husk ash and sugar cane bagasse ash), it can be utilised in the building construction in alkali-activated binders.

2.1 OBJECTIVES

The main objective of this study was to assess the sugar cane straw ash (SCSA) behaviour in alkali-activated binders.

The specific objectives were:

- I) Assess the SCSA reactivity in mixtures of the ash with calcium hydroxide;
- II Evaluate the SCSA as solid precursor in alkali-activated binders based on blast-furnace slag and;
- III) Analyse the SCSA potential as silica source to produce the activating solution.

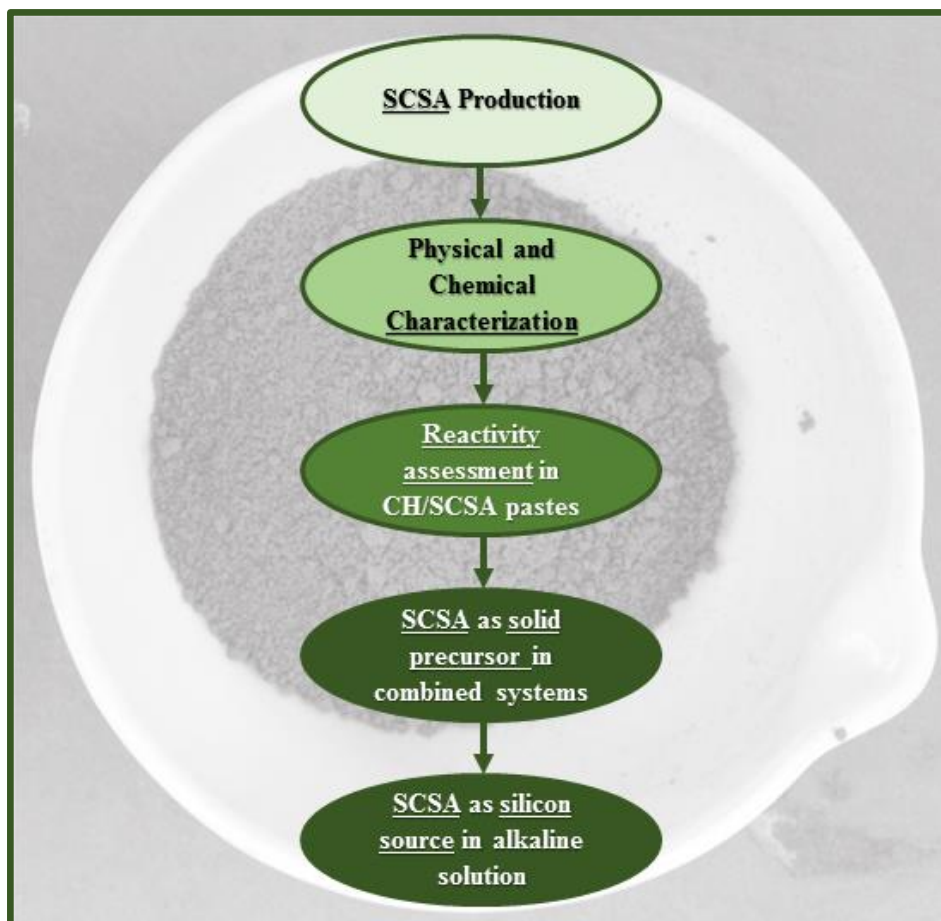
2.2 THESIS STRUCTURE

The SCSA was obtained from an auto-combustion process of the straw, and it was characterized chemically and physically. After, SCSA reactivity was evaluated in calcium hydroxide (CH) pastes by several experimental techniques. Confirmed SCSA good reactivity in these studies, the ash was assessed as solid precursor in binary systems of alkali-activated binders with blast furnace slag (BFS). In the last part of the study, the alkaline solution was prepared by NaOH combined with the SCSA as silicon source in order to replace the use of silicates. The solid precursor utilised in this last work was also the blast furnace slag. Figure 1.1 shows the steps of thesis.

The thesis was divided in 10 chapters, including the Introduction. The Chapter 2 is a State of the Art about alkali-activated binders and sugar cane straw ash. Chapter 3 shows reactivity studies on SCSA in mixtures with calcium hydroxide. Chapter 4 presents the first applications of SCSA in alkali-activated binders. In the Chapters 5, 6 and 7 it is presented studies of SCSA as solid precursor in alkali-activated binders based on BFS. Chapter 8

shows the SCSA as silica source to produce the alkaline solution in BFS-based AAB. Finally, Chapter 9 and 10 presents the general conclusions and proposal for future works.

Figure 1.1 – Experimental program of the present doctoral thesis



2 STATE OF THE ART

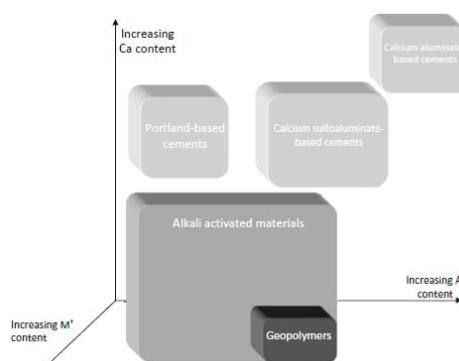
This chapter introduces concepts of alkali-activated binders, empathising definitions, history, comparisons to Portland cement, reaction products, solids precursors, alkaline activator solution and durability. Afterwards, a general view of the background and importance on the SCSA as a construction material is presented, completing this chapter of literature review.

2.1 ALKALI-ACTIVATED BINDERS

2.1.1 Definition

Alkali-activated binders are obtained when an alkaline solution is combined with an amorphous silico-aluminous source (solid precursor), resulting in a material with cementing properties (PACHECO-TORGAL et al., 2015). These types of binders have several denominations as, for example, inorganic polymers, alkali-activated cements, and it is also widely called by “geopolymers”. However, Provis (2014) differs the meaning of alkali-activated binders from geopolymers in the following points. Alkali-activated binders, according to the author, is a combination of a silicate fine solid and an activating alkali metal (in the solid or dissolved forms). That fine solid can be a calcium silicate (as blast furnace slag), or an aluminosilicate (as fly ash and metakaolin). The alkali metal can be obtained from alkali hydroxides, carbonates, silicates, sulphates, aluminates and others sources that can increase the pH and dissolve quicker the fine solid. The author excludes, in his definition, the lime-pozzolan systems and cases that water without the alkaline activator is utilised to make the reaction possible. In the other hand, geopolymer is obtained from the combination of exclusively aluminosilicates (low Ca content) with hydroxides/silicates as alkaline activating solution. From this point of view, any geopolymer can be an alkali-activated binder, but not vice versa. Figure 2.1 illustrate that distinction clearly and compared to others type of binders. In this thesis, the term alkali-activated binders will be adopted to describe that type of construction material.

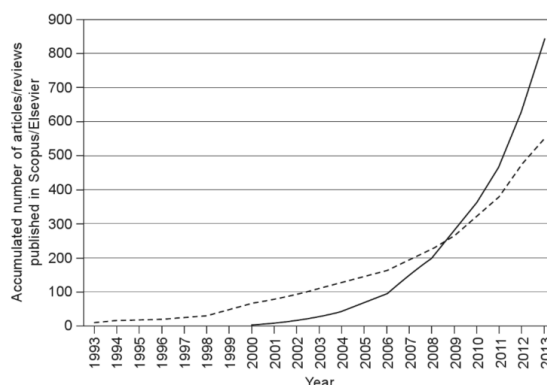
Figure 2.1 – Scheme of types of binders related to the Ca, Al and M⁺ content, emphasizing the classification of alkali-activated binders and geopolymers (PROVIS, 2014)



2.1.2 History

Before to present studies related to alkali-activated binders, this topic shows some important steps of history from alkali-activated binders. The first record of these materials was in 1908 by a patent of Kuhl called “Slag cement and process of making the same”. The researcher combined slag with alkalis sulphate/carbonate, and described its performance as “fully equal to the best Portland cements”. Purdon, in 1940, published a study of slag activated by sodium hydroxide. These studies compared the new binder to the Portland cement mixtures, obtaining similar compressive strength, lower solubility and heat evolution. In the 1950s, Glukhovsky, in Eastern Europe, studied the binders used in the ancient Egypt and Rome. These binders were produced by aluminosilicates with low calcium content, which were denominated as “soil cements” by the author. The next important point was in the 1970s, where the French Joseph Davidovits created the name “geopolymer”, and has patented several formulations of aluminosilicates. In the 80s and 90s, several works about alkali-activated binders took place in the most important scientific journals in the world. However, only after the 2000s, the number of these publications increased drastically (Figure 2.2). The most discussed topics in these recent studies are related to the microstructural properties and characterization, new raw materials and alkaline activators, durability, environmental and others issues (BERNAL et al., 2013; PROVIS, 2014; PACHECO-TORGAL et al., 2015).

Figure 2.2 – Development in the accumulated publications number in Scopus/Elsevier database of the words “alkali-activated binders” (dotted line) and “geopolymer” (solid line) presented in title, abstract or keywords (PACHECO-TORGAL et al., 2015)



2.1.3 Comparisons to the Portland cement

It is known that Portland cement is the most traditional binder utilized nowadays in building construction, and the main purpose to study the alkali-activated binders is to replace it for several reasons. The main advantages of these new binders compared to that conventional binder are: similar or higher strength; resistance to fire and low thermal conductivity; resistance to acid and chemical attack; lower degradation by alkali-silica reaction; good volumetric stability after hardening; adhesion to cement, ceramic, glass and metallic substrates; lower permeability and cost; among others advantages (PROVIS; van DEVENTER, 2014). However, the most important note in the literature is the environmental advantages of alkali-activated binders compared to the Portland cement (DUXSON et al., 2007).

In the Portland cement production, it is emitted 0.66-0.82 ton of CO₂ in atmosphere per 1 ton of binder manufactured. This number put this binder production responsible of 5-8% of CO₂ emissions in the world. Another problem is the use of 2.8-ton non-renewable raw materials (limestone and clay) per 1 ton of Portland cement obtained (GUO et al., 2010). They are heated over than 1400 °C within a rotating kiln, which requires a high-energy consumption to obtain the final product (van DEVENTER et al., 2012; TURNER; COLLINS, 2013). All this information motivated the research of new possibilities do reduce the Portland cement consumption, being one of them the alkali-activated binders. Some of these new materials can release only 0.184 ton of CO₂ per ton of binder produced,

representing a reduction in 50-70% when compared to Portland cement (DAVIDOVITS, 2002; McLELLAN et al., 2011). About the energy consumption, that type of binder can reduce it in 70% (DAVIDOVITS, 2001). In general, the materials used in alkali-activated binders were residues as, for example, fly ash (FA) and fluid catalyst cracking (FCC), which means that the use of these type of binders are environmental friendly for two reasons: the no use of non-renewable raw materials and valorisation of wastes.

2.1.4 Alkali-activated binders reaction products

The results of the combination between the solid precursor and the alkaline solution are, primary, a gel (amorphous phase) and, secondary, the *zeolites* (crystalline phase). Authors divides the studies on reaction products formed in the alkali-activated reaction by the calcium content of the solid precursor in three groups: low (metakolin and fly ash class F), medium (fly ash class C and some combination of binders) and high (blast-furnace slag). The solid precursors with high and low Ca content are that present more information about the reaction products (PROVIS, 2014; PACHECO-TORGAL et al., 2015), whereas the medium presents fewer studies in understating their reaction products.

1) High Ca-content

This group of reaction products, also known as $(\text{Na,K})_2\text{O}-\text{CaO}-\text{Al}_2\text{O}_3-\text{SiO}_2-\text{H}_2\text{O}$ system, is usually obtained from a binder richer of calcium and silicon ($\text{SiO}_2 + \text{CaO} > 70\%$). The information of this sub-topic is based on the alkali-activated binders obtained by the activation of the blast-furnace slag, which is the main solid precursor researched in this group. The main reaction product of activating BFS is the C-A-S-H (calcium silicate hydrate) gel, which is similar to the gel obtained from the Portland cement reaction (GARCIA-LODEIRO et al., 2015). Secondary products are also obtained in the reaction: AFm (as stranglingite), hydrocalcite (due the presence of MgO on the BFS) and zeolites (BERNAL et al., 2014; GARCIA-LODEIRO et al., 2015).

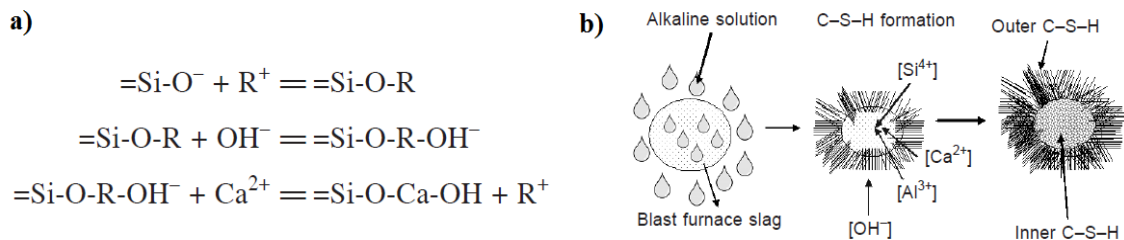
The development of the BFS-based AAB structure is divided in four steps (BERNAL et al., 2014):

- Dissolution of glassy part from the solid precursor;

- Nucleation and growth from the first solid phases;
- Interactions and mechanical binding at the boundaries of the products formed;
- The reactions continue by the chemical equilibrium and diffusion of reactive species through the reaction products formed in older curing time.

The model proposed by these steps is presented in Figure 2.3a. In this model, the alkaline cation, represented as R^+ , works as a catalyser in the beginning of the reaction, and are replaced by Ca^{2+} in a cationic exchange in the sequence of the reaction. However, the alkaline cation returns to participate of the gel structure with the advance of the reaction. Of course, the anions (SiO_4^{4-} and AlO_4^{5-}) also presents an important function, especially in the early ages, as showed in the Figure 2.3b (GARCIA-LODEIRO et al., 2015). The presence of highly condensed anions favours the increase of compressive strength (FERNÁNDEZ-JIMÉNEZ; PUERTAS, 2003).

Figure 2.3 – Proposed model to formation of BFS-based alkali-activated binders: a) role from the alkalis in the reaction (being R^+ the alkaline cation), and b) gel formation (GARCIA-LODEIRO et al., 2015)



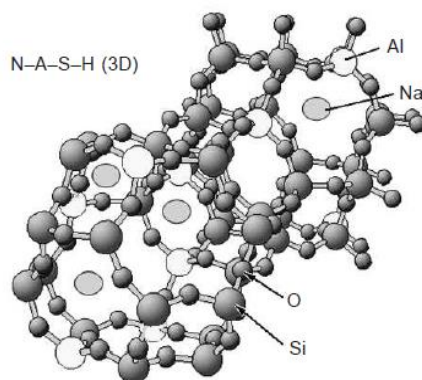
Aluminium has an important role in the alkali-activated binders. The aluminium tetrahedra replaces silicon tetrahedra and permits longer linear chains and inter-chain of Si-O-Al, making that C-S-H gels become two-dimensional C-A-S-H gels. These formed gels are directly influenced by the alkaline activator used in the mixture. The role of alkalis (as Na, K...) is to neutralise the charge balance of the Si replacement by Al (GARCIA-LODEIRO et al., 2015). The activators that are being largely utilised to study the gel formation are the sodium hydroxide and silicate. In general, the presence of silicates, when compared to only hydroxide, make the Ca/Si relation lower (BERNAL et al., 2014) and a higher presence of aluminium in the gel (GARCIA-LODEIRO et al., 2015). The presence of sodium turns the C-A-S-H gel into a (N,C)-A-S-H gel (PROVIS et al., 2015; GARCIA-

LODEIRO et al., 2015). Some authors are trying to describe how the sodium is incorporated to the gel structure by crosslinking, non-crosslinking or replacing of cations (Ca^{2+} by Na^+), and it is not a fully resolved issue (BERNAL et al., 2014; GARCIA-LODEIRO et al., 2015; PROVIS et al., 2015). The understating on AAB-based on solid precursors of high Ca-content increase in the last years by publication of several studies, however, some gel formation issues and the lack of study on other sources of solid precursor should be more studied to real understand the behaviour of this group of reaction products.

II) Low Ca-content

The reaction products studied in this group, also named as $(\text{Na,K})_2\text{O-Al}_2\text{O}_3\text{-SiO}_2\text{-H}_2\text{O}$ system, are obtained from binders composed basically from silicon and aluminium. In this group, the most used solid precursors are fly ash and metakaolin, and the studies on their reaction products will be focused in this topic. The main reaction product from alkaline activation of these binders is the Me-A-S-H (alkaline aluminosilicate hydrate, where Me can be Na, K...) gel. This gel is a three-dimensional inorganic alkaline polymer aluminosilicate, with highly disordered and crosslinked structure (Figure 2.4). The silicon and aluminium are found in the tetrahedral coordination (SiO_4^{4-} and AlO_4^{5-} , respectively), where the alkaline cation balances the extra negative charge from the aluminium tetrahedra replacing the silicon tetrahedra. The secondary products are the zeolites, as faujasite, hydroxysodalite, zeolite P, zeolite Y, and others. These formed products depend on the alkaline activator and curing conditions (PROVIS et al., 2014; GARCIA-LODEIRO et al., 2015).

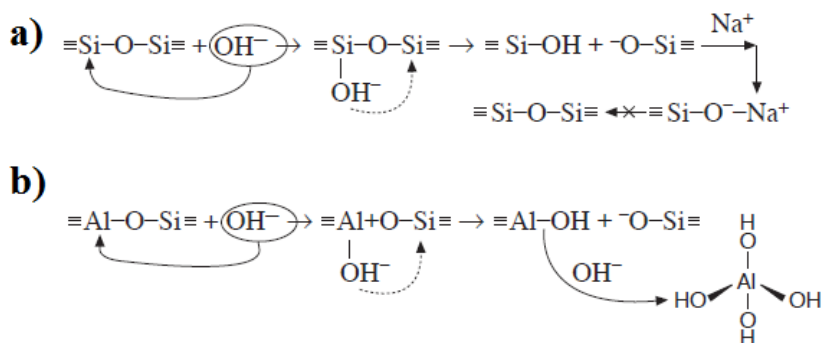
Figure 2.4 – A general view from the N-A-S-H gels produced in the alkaline activation of binders with low Ca-content (GARCIA-LODEIRO et al., 2015)



The reaction mechanism of these AAB products from fly ash and metakaolin activation is presented by three steps: destruction-coagulation, coagulation-condensation and condensation-crystallisation (GARCIA-LODEIRO et al., 2015).

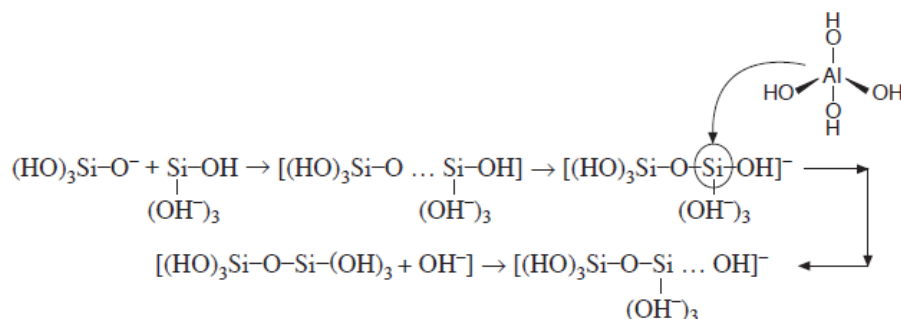
- *Destruction-coagulation*: In the beginning, OH^- ions from the alkaline activator break the bonds siloxane (Si-O-Si). These breaks are possible due the weakening of siloxane by the redistribution of the electronic density from the ions. Then, it is produced silanol ($-\text{Si-OH}$) and sialate ($-\text{Si-O}^-$) groups. The cation from the alkaline activator (Na^+ , K^+ ...) neutralises the negative charge from de sialates, yielding $-\text{Si-O}^-\text{Na}^+$. In this form, the reversion to siloxane is hindered. This information is summarized in Figure 2.5a. The Si-O-Al bonds are also affected by the OH^- ions. The aluminium species is dissolved and form complex species, mainly aluminium tetrahedra (Al(OH)_4^-) (Figure 2.5b).

Figure 2.5 – Reaction mechanism from the first step named destruction-coagulation: a) dissolution of Si-O-Si bonds, and b) dissolution of Si-O-Al bonds (GARCIA-LODEIRO et al., 2015)



- *Coagulation-condensation*: In this step, with the accumulation of ionic species produced in the last step, is favoured the contact between them and polycondensation starts, generating coagulated structures. Silica monomers inter-react and form dimers, trimers, etc. and forming polymers. The aluminium behaves in the same way, where the aluminium tetrahedra replaces the silicon tetrahedra in the structure. The alkaline metal works as a structural component in this step, differently from the first one when worked as catalyst. This information is represented in the Figure 2.6.

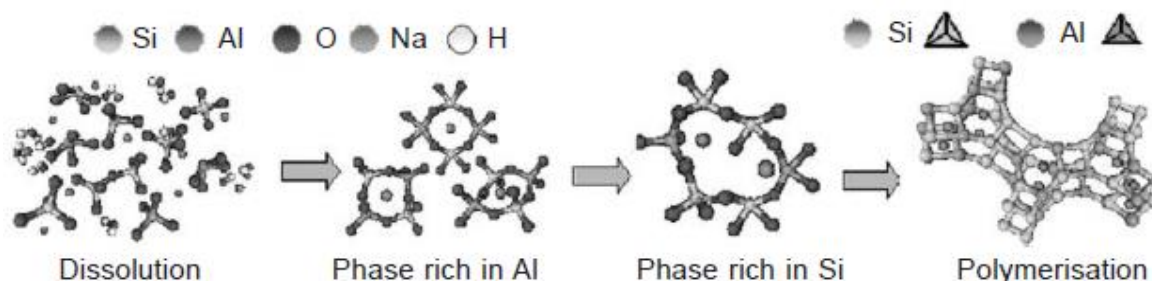
Figure 2.6 – Reaction mechanism from the second step named coagulation-condensation
(GARCIA-LODEIRO et al., 2015)



- *Condensation-crystallisation*: At this final stage, the increase of coagulation favours the precipitation of the reaction products. Their composition depends on the solid precursor, alkaline activator and the curing conditions.

Another model proposed to alkaline activation of only fly ash is showed in the Figure 2.7. In this model, firstly occurs the dissolution of the solid precursor. In the next step, it is highlighted that the first precipitated reaction products are richer in aluminium than silicon. This behaviour is explained due the weaker Al-O bond compared to Si-O bond, which makes that the former dissolves quicker than the latter. After, more Si-O dissolves and raises the concertation of silicon in the gels, producing a richer Si gel. The structural reorganisation and polymerisation of gels determine composition of the polymer, and defines the structure and, consequently, the mechanical behaviour of the alkali-activated binder (GARCIA-LODEIRO et al., 2015). Recent studies focused on the gel formed in these reactions. The improve in the experimental techniques, as nuclear magnetic resonance (NMR), attenuated total reflectance (ATR) and Fourier transform infrared spectroscopy (FTIR), permit to understand better the reactions products. In the next years, due the several raw materials (solid precursors and alkaline activator) that are utilised in alkali-activated binders, the researches in nanostructure and microstructural characterisation increased in numbers and probably will continuous in this way (PALOMO et al., 2014; PROVIS et al., 2015).

Figure 2.7 – Illustration of the gel formation in alkali-activated binders with low Ca-content (GARCIA-LODEIRO et al., 2015)



III) Medium Ca-content

This third and last group is a combination of the two last ones discussed. They are also known as hybrid alkaline cement and are obtained by the alkaline activation of materials (or combination of materials) with SiO_2 , Al_2O_3 and $\text{CaO} > 20\%$. Examples of binders that produce a hybrid cement are the fly ash Class C, and combination of OPC with slag and/or fly ash. The reaction product from their alkaline activation is really complex due the non-uniformity of the raw materials, where can be generated the C-A-S-H, (N,C)-A-S-H and N-A-S-H gels. Stability of these gels are directly related to the pH from the phases obtained: several studies on the pH showed that it favours some type of gel formation. Aluminium and alkali also have an important role in the gel formation, since they can increase the crosslink of the gels. As can be seen, the reaction products of this group present less information when compared to a high and low Ca-content due its complexity, and the based information is mostly empirical (PROVIS; BERNAL, 2014; GARCIA-LODEIRO et al., 2015).

2.1.5 Solid Precursor

Solid precursor is one of the raw materials to produce an alkali-activated binder, where that is basically a fine power composed by silicon and aluminium (and calcium in some cases). The main researched solid precursors and ones that will be discussed are blast-furnace slag, fly ash and metakaolin (PACHECO-TORGAL et al., 2008). After, a general view of others materials (mainly residues) that are being researched to produce alkali-activated binders. In addition, in these topics, will be showed some studies about combined

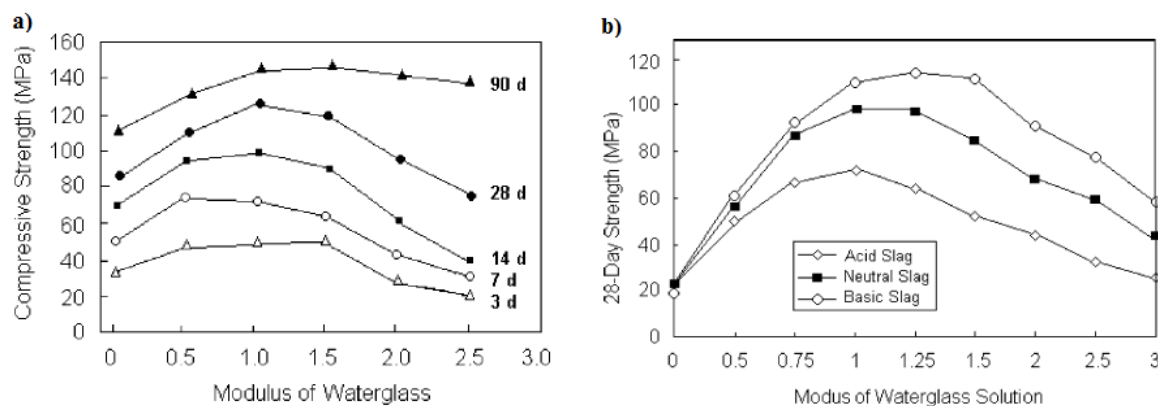
systems (the use of two or more solid precursors), which improve the mechanical properties of alkali-activated binders when compared to which presents only one solid precursor (YUSUF et al., 2014).

1) Blast-furnace slag (BFS)

As showed previously, the first solid precursor that was studied in alkali-activated binders is the blast-furnace slag (BFS) in 1908. This material is a by-product of iron production, and has the presence of calcium, magnesium, silicon and aluminium in its composition. There are several studies focused on properties of alkali-activated binders based on BFS, mainly issues about microstructure, fresh properties, mechanical properties and durability (SHI et al., 2006).

The main reaction product obtained from the alkaline activation of BFS is the C-A-S-H and (Me,C)-A-S-H gels (being Me a N, K...), which its formation was already discussed for solid precursors with high Ca content (PROVIS et al., 2014). The characteristic of this gel is related to several factors (activating solution, curing conditions, etc.), and are directly linked to the mechanical properties. Improving in these properties on BFS based-AAB was previously studied with the use of waterglass combined with a metal hydroxide in the alkaline solution preparation (Figure 2.8) (BROUGH; ATKINSON, 2002; SHI et al., 2006). However, recent studies are highlighting the advantages of using combined systems in order to improve the mechanical properties (RAKHIMOVA and RAKHIMOV, 2015). Some of materials used in combined systems studied in the last years are red clay brick waste (RAKHIMOVA and RAKHIMOV, 2015), palm oil fuel ash (YUSUF et al., 2014), silica fume (HEIKAL et al., 2014) and sugar cane bagasse ash (PEREIRA et al., 2015).

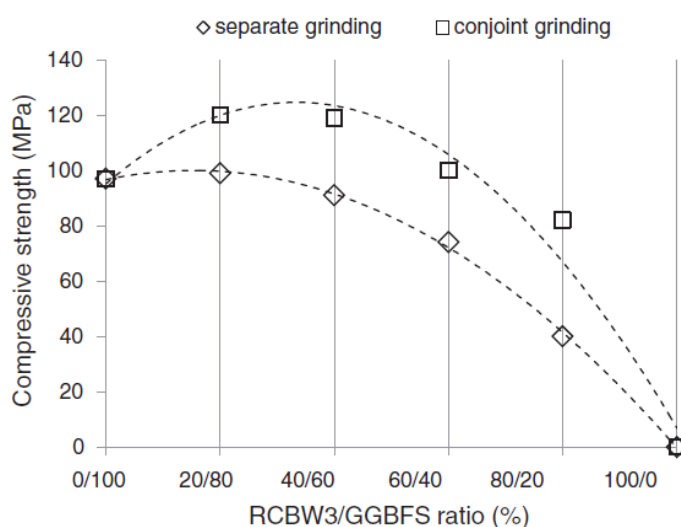
Figure 2.8 – Studies on influence of sodium silicate in the compressive strength of BFS-based AAB: a) phosphorous BFS; and b) Acid, neutral and basic BFS (SHI et al., 2006)



The red clay brick waste (RCBW) is a residue from construction and demolition industries that presents, in its chemical composition, SiO_2 and Al_2O_3 of 70 and 10%, respectively (by mass). The authors concluded that RCBW can replace the BFS until 60% from compressive strength studies, where the optimum stands on the range 20-40% (Figure 2.9). The justifying of the good results using this waste is due to the interaction of aluminosilicates and feldspars from RCBW, and also the presence of amorphous silica that forms hydrates (RAKHIMOVA and RAKHIMOV, 2015). About the palm oil fuel ash (POFA), this is a residue from burning process of the palm empty fruit brunches, palm fibres and palm kernel shell, and the resultant ash is composed by mainly silica (45%) with a high loss on ignition (21%). Studies on this material concluded that the UPOFA (POFA after a treatment) presents an optimum BFS replacement of 20%, which reaches 50% more compressive strength than the control. The authors justify this best replacement percentage by the optimum Ca concentration in the mixture, more Al reactive sourced by the BFS, and the increasing in the amorphousness of the reaction products (YUSUF et al., 2014). Silica fume (SF) is a well-known pozzolanic material. It is a by-product from the silicon or silicon alloys, and presents higher than 95% of high-reactivity amorphous silica. In this study in alkali-activated materials with BFS, the authors replaced this binder by 8% of SF. The authors explained that the higher surface area of SF acts as nucleating agents for formation of C-S-H gel, which increases the compressive strength (HEIKAL et al., 2014). Finally, a residue from sugar cane production, the sugar cane bagasse ash (SCBA), was assessed in alkali-activated binders with interesting results. SCBA replaced BFS in the range of 0-50% by mass, where the authors discovered that the optimum replacement percentage was the

25%. In this percentage of SCBA, the compressive strength presented similar values to the control. The authors concluded that the presence of the sugar cane waste did not cause change in the formed gels from alkali-activated reaction (PEREIRA et al., 2015). The materials studied in binary systems with BFS are mainly composed by silica. All promising results from those studies shows the use of SCSA (which are also composed by silica) an interesting way in combined systems with BFS.

Figure 2.9 – Compressive strength results of combined systems composed by blast furnace slag and red clay brick waste (RCBW/BFS) after 28 days of curing at room temperature (RAKHIMOVA and RAKHIMOV, 2015)



II) Metakaolin (MK)

Metakaolin is a pozzolanic material obtained from the burning process of the kaolin (clay) in the temperature range of 600-850 °C. This material is basically composed by silica and alumina with high degree of amorphous phase and surface area. The first use of metakaolin in alkali-activated binders was by Davidovits in 1979, when the denomination *geopolymer* was proposed. In MK-based AAB, the main reaction product is the Me-A-S-H gel (being Me a Na, K...), where its structure was already discussed for solid precursors with low Ca content. Some studies about influences on this gel formation, and consequently in the mechanical properties, is showed in this topic (PACHECO-TORGAL et al., 2008; RASHAD, 2013a; RASHAD, 2013b).

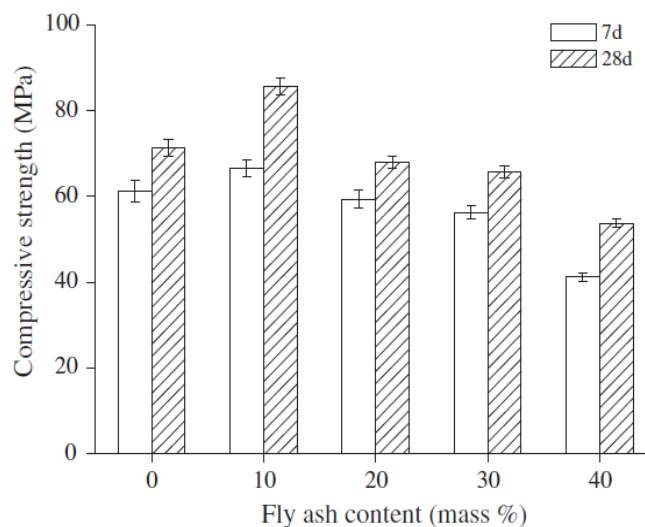
The first influence presented is the alkaline solution. In general, the mechanical properties of MK-based AAB with the combination of alkaline metal silicate/hydroxide is higher than one with only the alkaline metal hydroxide (OZER; SOYER-UZUM, 2015; TYPPAYASAM et al., 2016). About the alkaline metal concentration, there are studies with sodium and potassium, being the former with more works about it. In sodium hydroxide, the Na^+ concentration studied is in the range of 6-15 M (ZHANG et al., 2012; YUSUF et al., 2014; OZER; SOYER-UZUM, 2015; CHENG et al., 2015), whereas, for potassium hydroxide, the K^+ concentration is found in the range of 5-40 M (TAWFIK, A., 2016; TYPPAYASAM et al., 2016). From these studies, the optimum concentration stands in the range of 8-12M (which can vary according to origin of studied metakaolin). For concentrations of the alkaline metal that is outside from this range, it is not able to balance completely the negative charge of the AlO_4^- groups, justifying the worst results in mechanical properties (DUXSON et al., 2005; DUXSON et al., 2007). In addition, for lower concentrations than this range, there is no sufficient alkaline metal to dissolve the metakaolin particles to form polymerized and strength network (WANG et al., 2005). Another factor that influences in the properties of MK-based AAB is the curing temperature. Some authors studied the compressive strength in the range of 20-105°C (PELLISER et al., 2013; ARELLANO-AGUILAR et al., 2014; BING-HUI et al., 2014; CATAURO et al., 2014; TAWFIK et al., 2016; TIPPAYASAM et al., 2016). These studies showed that the higher temperatures (until 80 °C) accelerates the compressive strength development in the first hours when compared to room temperature, however, they became similar after 7-14 days. Now about temperatures above of 80 °C, this caused a decrease in the compressive strength, which was justified by the authors for too rapid setting speed of the matrix that restrained the transformation into a strength structure (BING-HUI et al., 2014). Finally, an important factor that affect the mechanical properties of MK-based AAB is the Si/Al proportion of the mixture (DUXSON et al., 2005; RASHAD, 2013a; OZER; SOYER-UZUM, 2015). The silica and alumina sources are the metakaolin and the waterglass. The chemical composition of the metakaolin cannot be varied in a study; therefore, the Si/Al is varied from the amount of waterglass in the activating solution. Authors concluded that the ideal Si/Al amount is in the range 1.40 to 2.20. In this interval, the microstructure appears glassy, more homogenous, with regular pores. With less Si/Al relation, is showed there is high formation of *zeolite*

structures. For Si/Al higher than this interval, there are presence of unreacted particles and isolated porous.

To end this topic, some studies of combined systems with metakaolin is presented. The aim of use another binder with the metakaolin is to improve its mechanical properties of the final product (ZHANG et al., 2014). The others binders that were used in combined systems are: fly ash (RAJAMMA et al., 2012; ZHANG et al., 2014; PAPA et al., 2014), red mud (HAJJAJI et al., 2013; KAYA; SOYER-UZUN, 2016), boiler slag and rice husk ash (VILLAQUIRÁN-CAICEDO; GUITIÉRREZ, 2015) waste catalyst (CHENG et al., 2015) and palm oil fuel ash (YUSUF et al., 2014).

The studies on fly ash replacing partially metakaolin showed interesting results (Figure 2.10). Authors achieved 15% more compressive strength than the control with a 10% replacement percentage. They give the credits for this improvement due the increase in the reaction extent measured by isothermal calorimetry studies (ZHANG et al., 2014). In studies of metakaolin/red mud, the researchers did not find significantly change in the mechanical properties after 28 days of curing until 40% of replacement percentage (HAJJAJI et al., 2013). When the metakaolin is utilised in a ternary system with boiler slag and rice husk ash, authors achieved improvement of 122% in the compressive strength after 180 days of curing. Now about the waste catalyst replacing partially the metakaolin, researchers found that the optimum replacement percentage was 10% after a compressive strength test. They justify this result by TGA studies, where this replacement percentage presented higher mass loss in the range of 50-300 °C than the control, indicating more reaction products formed (CHENG et al., 2015). Palm oil fuel ash was utilised replacing partially the metakaolin until 70%. The results showed that there is a reduction in the compressive strength of 30% (YUSUF et al., 2014). These results show that is possible to utilise the metakaolin in combined systems with other type of binders.

Figure 2.10 – Compressive strength results of binary systems composed by metakaolin and fly ash (MK/FA) after 7 and 28 days of curing at room temperature (ZHANG et al., 2014)



III) Fly Ash (FA)

Fly ash is a by-product from the energy production by coal burning in thermal plants. The worldwide production is around of 1 billion ton per year, which gives it as one of the most abundant anthropogenic materials (RASHAD, 2014; YAO et al., 2015). The fly ash can be classified in two groups: the Class F and the Class C. The Class F is the fly ash that presents the chemical composition composed by silica and alumina as major oxides. In the other hand, for Class C, there is a considerable quantity of calcium oxide, which gives it a hydraulic characteristic (ASTM, 2015). In this topic, only will be discussed the Fly Ash Class F, which presents better results in alkali-activated studies. This ash presents a glassy aluminosilicate structure with spherical particles, which results in less water demand in mixtures than metakaolin (van DEVENTER et al., 2012). The first study on fly ash in alkali-activated binders was published in 1999 (PALOMO et al., 1999). As the metakaolin and others aluminosilicates materials, the activation of the fly ash generates a Me-A-S-H (being Me a Na, K...) gel. The factors that influences the gel formation, and consequently the mechanical properties, are similar to was discussed previously: metal concentration, curing temperature and $\text{SiO}_2/\text{Na}_2\text{O}$ relation.

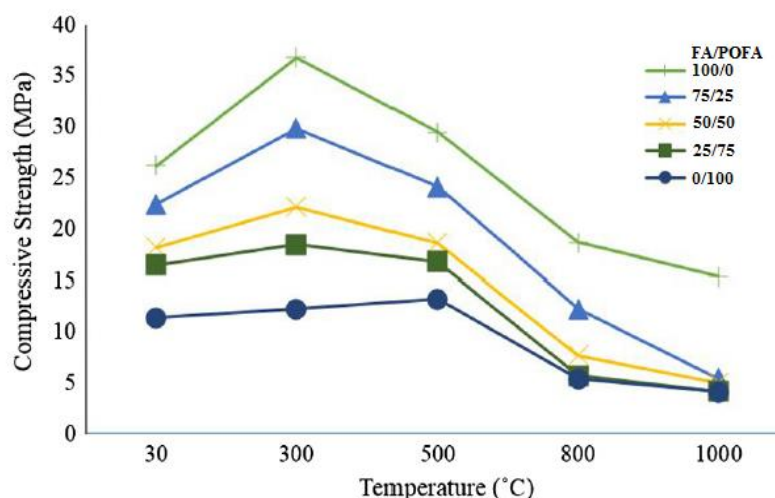
The alkaline metal most utilised in the recent years to activating the fly ash is the sodium by combination of sodium hydroxide and sodium silicate. As the others two solid precursors discussed, fly ash shows better results when activated with waterglass. Authors reported concentrations of this alkaline metal in the range of 3-15M, where these studies showed that the optimum Na^+ concentration are in the range of 9-12 M by compressive strength tests. About the curing temperature, fly ash of Class F is activated only at high temperatures (in the range of 45-115 °C) due its slow reactivity. The optimum curing temperature of fly ash-based AAB from these studies is in the range of 85-115 °C, where a study reaches 120 MPa after 24 hours of curing at 115 °C. The $\text{SiO}_2/\text{Na}_2\text{O}$ relation has an important role in the compressive strength development following these works. This relation was studied in the range of 0-10, where better results are obtained in the range 0.8-1.3 (RYU et al., 2013; GORHAN; KURKLU, 2014; ZHANG et al., 2014; ATIS et al., 2015; CHI, 2015; GUNASEKARA et al., 2015; KAZEMIAN et al., 2015; NIKOLIC et al., 2015).

As the other two solid precursors studied, fly ash was also utilised in AAB combined systems with another binders: sugar cane bagasse ash (CASTALDELLI et al., 2016), palm oil fuel ash (RANJBAR et al., 2014; NADZIRI et al., 2017), blast-furnace slag (MARJANOVIC et al., 2015; DEB et al., 2014), metakaolin and silica fume (RASHAD, 2014).

In studies on binary system of fly ash and sugar cane bagasse ash (SCBA), authors determined that the best FA/SCBA relation is 75/25. The authors highlighted the importance of the SCBA in the compressive strength results in the early curing time at 20 °C. When fly ash was studied with blast-furnace slag, authors detected a compressive strength gain with the increase of this binder. They correlate the compressive strength with the gel composition, Ca/Si and Al/Si relations, where obtained optimum values of these rates of 0.5 and 0.2, respectively (FA/BFS = 25/75). Palm oil fuel ash showed good results when combined with fly ash on high temperature studies. Authors heated samples until 1000 °C and assessed their compressive strengths. The specimens with more palm oil fuel ash in the composition presented less compressive strength loss (Figure 2.11). In studies on fly ash with metakaolin, authors concluded that the most beneficial effect was the increase in the compressive strength. Silica fume also presented good results when combined with fly ash, showing gains in the compressive strength until 7% replacement. From these studies with different binders

combined with fly ash, highlight for the sugar cane bagasse ash, which is an agro-industrial residue as sugar cane straw ash and presented interesting results.

Figure 2.11 – Compressive strength evolution of FA/POFA specimens studied in high temperatures (adapted from RANJBAR et al., 2014)



IV) Other materials

This topic is destined to other materials that are being studied in alkali-activated binders. The list is large, but some of new binders are the being researched recently are: fluid catalytic cracking catalyst residue (TASHIMA et al., 2012a; TASHIMA et al., 2013a), red clay brick waste (REIG et al., 2013a), ceramics wastes (REIG et al., 2013b; REIG et al., 2017), red mud (HE et al., 2013) and vitreous calcium aluminosilicate (TASHIMA et al. 2012b; TASHIMA et al., 2013b). Those studies focused on best alkaline metal molar concentration and $\text{SiO}_2/\text{Me}_2\text{O}$ relation in order to achieve highest mechanical properties.

2.1.6 Alkaline Activators

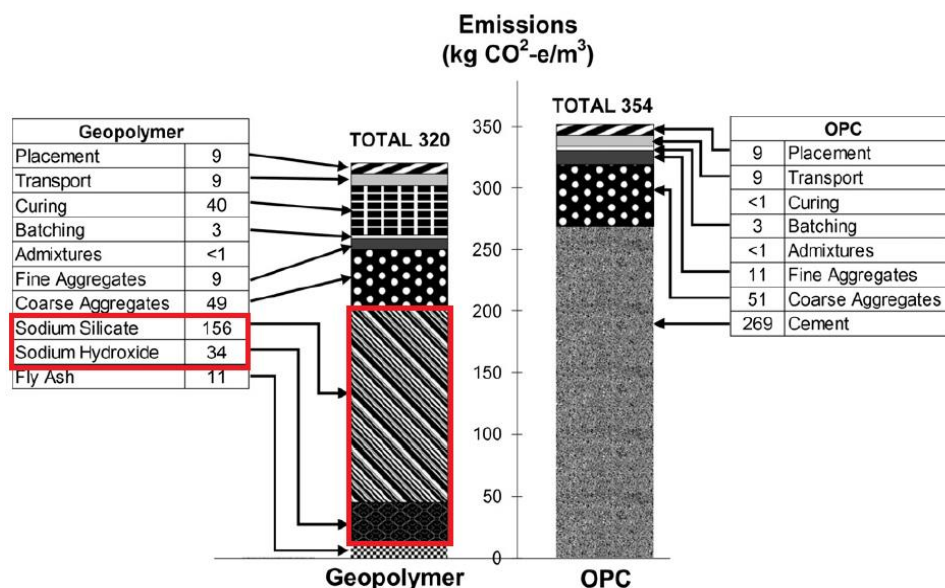
Alkaline solution has an important role in the alkali-activated binders' reaction. They are responsible for the high pH conditions that is necessary to activate the solid precursor (PROVIS; van DEVENTER, 2009). There are six groups that are usually used as alkaline source (SHI et al., 2006):

- a) Caustic alkalis (MeOH , being Me a Na, K, Li...);
- b) Silicates ($\text{Me}_2\text{O} \cdot n\text{SiO}_2$);
- c) Aluminates ($\text{Me}_2\text{O} \cdot n\text{Al}_2\text{O}_3$);
- d) Aluminosilicates ($\text{M}_2\text{O} \cdot \text{Al}_2\text{O}_3 \cdot (2-6)\text{SiO}_2$)
- e) Non-silicate weak acid salts (Me_2CO_3);
- f) Non-silicate strong acid salts: Me_2SO_4 .

From these activators listed, the most commons are the use of sodium hydroxide (NaOH), potassium hydroxide (KOH) and sodium silicate ($\text{Na}_2\text{O} \cdot n\text{SiO}_2$). The sodium-based alkaline activator is cheaper and more available than the potassium-based, consequently, is the most used in alkali-activated binders (SHI et al., 2006). In the other hand, the advantages of potassium-based are the improved phase behaviour (including the less rapid formation of zeolites) and rheology (PROVIS, 2009). The use of silicates combined with hydroxides improve the mechanical properties than those based only by hydroxides (SHI et al., 2006; PROVIS, 2009).

The main advantage from alkali-activated binders over than OPC blends is the less greenhouse gas emission, where the alkaline solution has an important role in releasing this gas. Authors who studied CO_2 footprints of those binders (TURNER; COLLINS, 2013; MELLADO et al., 2014) showed that the most pollutant raw material is the alkaline activator, mainly the waterglass (silicate) (Figure 2.12). The challenge is to increase even more the environmentally characteristic of alkali-activate binders, hence, new ways to replace the use of conventional alkaline source are being researched in the last years.

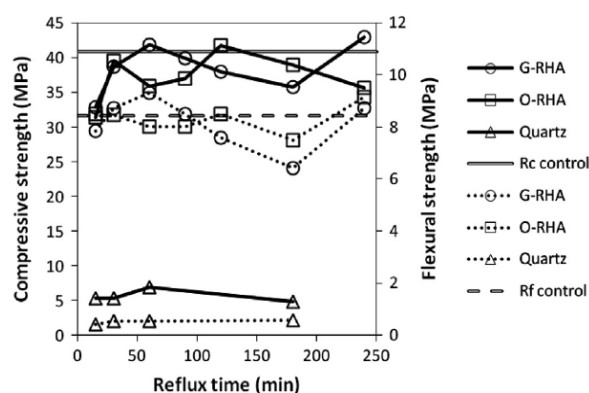
Figure 2.12 – Comparison between CO₂ footprints of concretes based on alkali-activated binders and OPC, highlighting the emissions from the alkaline activator (adapted from Turner; Collins, 2013)



In a study on using potassium-rich biomass ashes to activate metakaolin, authors achieved until 40 MPa after 3 days of curing (PEYS et al., 2016). The evolution of reaction was assessed by calorimetry, attenuated total reflectance Fourier-transformed infrared spectroscopy (ATR-FTIR) and electron probe micro-analysis (EPMA). These tests showed that the biomass ashes reacted with the metakaolin and formed gels. The success of those biomass ashes is due to the high pH (> 13) and over 30% of K₂O in their composition. A study tried to replace the use of silicates by adding rice husk ash (RHA) in activating solution with NaOH by a refluxing dissolution method (BOUZÓN et al., 2014). Results on compressive strength of mortars using FCC as solid precursor showed similar values to a control using sodium silicate after one day of curing, where both reached over than 40 MPa (Figure 2.13). The results were justified due to the high dissolution of the amorphous silica in the sodium hydroxide solution. In the same line in order to replace the use of silicates, a glass waste was also assessed in alkaline solution preparation. Results showed compressive strength fewer than the control with waterglass, however, higher than only activated with NaOH/Na₂CO₃ (PUERTAS; TORRES-CARRASCO, 2014). More recently, sugar cane bagasse ash was evaluated as silica source in the production of activating solution (TCHAKOUTÉ et al., 2017). This new solution presented similar results in compressive

strength tests than the waste glass and rice husk ash in metakaolin-based AAM. These results showed that the alkaline activator influences the mechanical properties of the alkali-activated binders.

Figure 2.13 – Compressive strength versus reflux time of FCC-based alkali activated binders prepared with different siliceous sources combined with NaOH solutions: G-RHA (ground rice husk ash), O-RHA (original rice husk ash), quartz, control (commercial waterglass solution). Key: full line for compressive strength and dotted line for flexural strength (Bouzón et al., 2014)



2.1.7 Durability

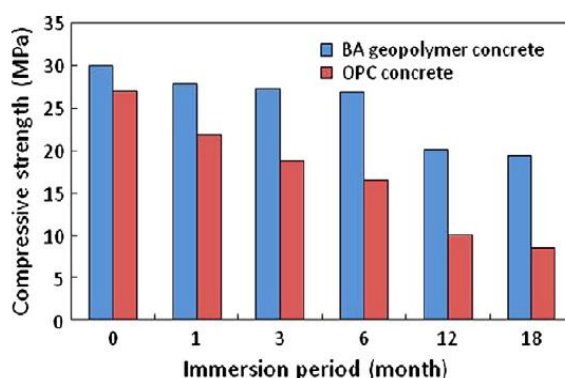
As showed previously, alkali-activated binders can present high compressive strength. However, only this mechanical property is not sufficient, because a construction material should be not only strength, but also durable. Therefore, durability tests on alkali-activated binders are an important issue. These binders were not adopted yet due the lack of full characterization and performance under physicommechanical and chemical conditions (BERNAL; PROVIS, 2014). Therefore, several studies on durability of this type of binder were carried out recently, and it was compared to Portland cement mixtures (MELLADO et al., 2017).

Durability (and compressive strength) of alkali-activated binders is directly linked to their microstructure. Hence, studying the products formed and the porosity of these binders help to understand the durability results of alkali-activated binders. The microstructural of an AAB can vary according to the solid precursor, alkaline solution, solid/liquid ratio, paste content, curing conditions and among others parameters (BERNAL;

PROVIS, 2014). Then, an overview about durability tests and their consequence on alkali-activated binders' microstructure will be presented. These studies are based on acid attack, sulphate attack, chloride penetration, temperature resistance, carbonation, alternate extreme cycles, and alkali-silica reaction.

Alkali-activated binders present good resistance to acid attack when compared to Portland cement mixtures. This is explained by the higher alkalinity of the structure and lower CaO amount in those binders (ABORA et al., 2014; BASCAREVIC, 2015). In general, studies on blast furnace slag, fly ash and metakaolin show less compressive strength and mass losses when compared to Portland cement mixtures (PACHECO-TORGAL et al., 2012; HOSSAIN et al., 2015; DUAN et al., 2015). About studies on binary systems, AAB based on blast-furnace slag and sugar cane bagasse ash (BFS/SCBA) were assessed in acid attack tests were compared to a control mixture composed by only Portland cement. The alkali-activated binder presented a loss in the compressive strength similar for hydrochloride acid and lower for acetic acid when compared to the control one (PEREIRA et al., 2015). In another study of binary systems composed by fly ash and palm oil fuel ash in acid attack, the alkali-activated binders also showed lower compressive strength loss than the Portland cement after an immersion of 18 months in sulfuric acid (Figure 2.14) (ARIFFIN et al., 2013).

Figure 2.14 – Compressive strength of concrete manufactured with fly ash and palm oil fuel ash (BA geopolymer concrete) compared to one of Portland cement after sulfuric acid attack (ARIFFIN et al., 2013)



Sulphate attack impact depends on the salt that alkali-activated binders are exposed. The most used sulphates are the NaSO_4 and MgSO_4 . Whereas MgSO_4 causes a cation-

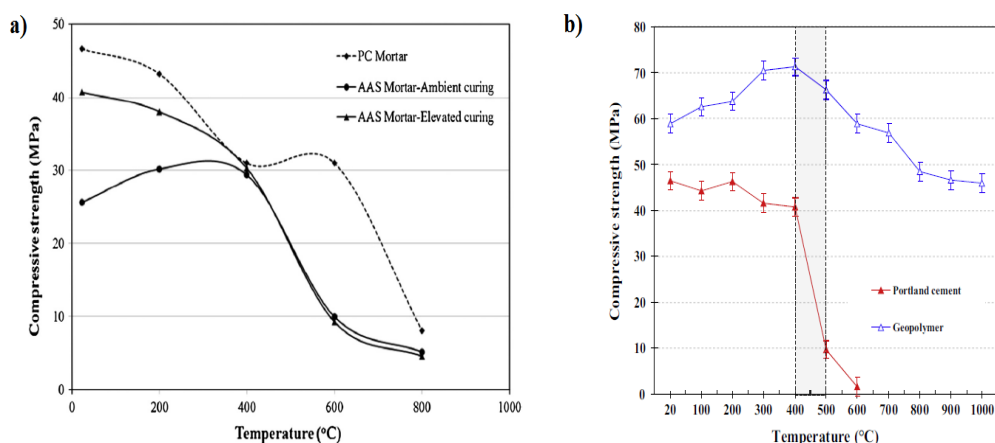
exchange mechanism degrading the gel structure (mainly in Ca-rich structures), leading to formation of M-S-H gels and precipitation of gypsum (in Ca-rich binders), NaSO_4 do not lead any degradation and can promotes the structural evolution of the alkali-activated binders (ISMAIL et al., 2013; BERNAL; PROVIS, 2014). Blast-furnace slag, fly ash and metakaolin specimens were tested in sulphate attack and their showed better results than the Portland cement samples for presenting less expansion and compressive strength loss (CHINDAPRASIRT; CHALEE, 2014; HOSSAIN et al., 2015). In studies on binary systems of BFS/SCBA, MgSO_4 resulted in more compressive strength and mass losses than the NaSO_4 . When compared to the Portland cement mixtures, the alkali-activated binders presented lower compressive strength loss in both sulphates attack (PEREIRA et al., 2015).

Chloride ion penetration is also an important durability study. If is aiming the use of alkali-activated binders as a structure material, they will be used as a reinforced concrete. As know that the chloride ion can induce to corrosion of the steel bars by an electrolytic action; therefore, a low permeability of this ion is required for a durable structure (PACHECO-TORGAL et al., 2012; HOSSAIN et al., 2015). The chloride ion penetration is directly related to the porosity of the material, where authors reported that alkali-activated binders presents lower permeability than the Portland cement ones (BERNAL; PROVIS, 2014). In AAB combined systems containing fly ash and blast furnace slag, authors obtained lower Cl^- concentration in chloride penetration test when compared to a one-system binder (ZHU et al., 2014).

Studies on alkali-activated binders treated at high temperatures are also found in bibliography. Authors found optimistic results in alkali-activated binders until 1200 °C due their high stability (PACHECO-TORGAL et al., 2012). When compared to OPC, the alkali-activated binders produced by solid precursors with low Ca content (as fly ash and metakaolin) show better results than the high Ca content (blast furnace slag). The first class of these binders presents higher stability in the compressive strength with the increase of the temperature treatment (MARTIN et al., 2015; DUAN et al., 2015), whereas the second class showed similar results to OPC (TURKER et al., 2016) (Figure 2.15). Authors justified the first comparison (first class and OPC) due the pore structure of the AAB be able to absorb the stress of water pressure that tends to evaporate at higher temperatures, whereas the OPC pore structure is not able to do it under similar conditions. In addition, XRD analysis presented a halo from the gel structure of AAB after the treatment at 800 °C. In the other

hand, the similar results by the second class is verified in TGA studies, where both, AAB and OPC specimens, presented a significant reduction in the mass loss related to the hydrate products that are responsible for the compressive strength. Binary systems of AAB were also studied in temperature treatment by the combination of metakaolin and fly ash, where authors achieved an optimum proportion of 50/50 by mass after expose specimens until 800 °C (ZHANG et al., 2014). The influence of the activator was also evaluated in thermal tests. Whereas AAB produced by sodium as alkali activator presented deterioration and loss in the compressive strength after 800 °C, potassium-based AAB presented problems only after 1000 °C (PANIAS et al., 2015).

Figure 2.15 – Compressive strength after temperature treatment of OPC mixtures and alkali-activated binders of solid precursors with a) high Ca content and b) low Ca content (TURKER et al., 2016; DUAN et al., 2015)



Carbonation is also an important issue studied for alkali-activated binders. In general, it depends on the type of the solid precursor, the nature/concentration of the alkaline solution and, consequently, the porous size from the final binder. In normal conditions, AAB presents similar or lower carbonation rates than the OPC mixtures (BERNAL; PROVIS, 2014; HOSSAIN et al., 2015). There are studies on the behaviour of alkali-activated binders at alternate extreme cycles, as the freeze-thaw. Authors showed that alkali-activated binders presented better performance than OPC mixtures, where the former can endure more and presents less compressive strength loss in those type of durability tests. Alkali-silica reactions still a complex issue for alkali-activated binders due few studies, whereas for OPC presents several studies. In some of those studies, alkali-activated binders showed to be less

susceptive when compared to OPC mixtures. The presence of calcium has an important role in the expansion of the binders (PACHECO-TORGAL et al., 2012).

As showed in the last paragraphs, there are several durability studies reported on alkali-activated binders in the last years. However, more studies must be done to know the real limits of these new type of binders, since there are many types of solid precursors and alkaline solutions being researched.

2.2 SUGAR CANE STRAW ASH (SCSA)

Sugar cane straw ash is obtained after a burning process of the straw. The interesting in the sugar cane straw arises a few years ago in Brazil for two reasons: the increase in sugar cane production and the mechanized harvesting.

The cultivation of sugar cane increased in the last years in Brazil mainly to obtain ethanol, and put the country as the major producer in the world (FAOSTAT, 2016). The production in 2004/2005 was 385.2 million tons, and increased to 632 million tons in 2014/2015, showing an increase of 64% in only ten years (UNICA, 2016). Some years ago, the sugar cane used to be burned in open-air, which facilitated the process of harvesting. Due to environmental and health risks, a Brazilian law nº 11.241/2002 prohibited gradually this harvesting mode until 2031. However, an Agro-environmental Protocol was assigned by stakeholders of sugar cane production chain reduces this deadline to 2018 (RIBEIRO; FICARELLI, 2010; LEAL et al., 2013a). With these law and protocol, the mechanized harvesting gained importance as a method to collect the sugar cane (Figure 2.16).

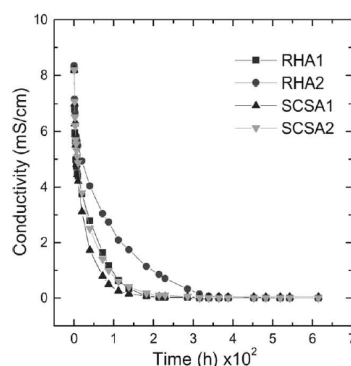
Figure 2.16 – Mechanized harvesting of the sugar cane (UNICA, 2016)



After harvesting the sugar cane with these machines, is obtained a by-product that are composed by green and dry leaves, which is called by sugar cane straw. The amount of straw obtained is 140 kg per 1000 kg of sugar cane harvested (BNDES; CGEE, 2008; LEAL et al., 2013a). Authors stated that some part of this straw should be in the field to protect the soil, however, a part can be used as biomass to generate energy, as the bagasse are being used nowadays (LEAL et al., 2013b). Many studies are being carried out in order to collect the straw from the field (LEMOS et al., 2014) and to obtain energy from the straw due its interesting calorific value and economic point of view (LOMBARDI et al., 2012; MORAES et al., 2012; MESA-PÉREZ et al., 2013; ALVES et al., 2015). This process of energy generation by a burning process yields an inorganic ash composed mainly by silicon dioxide: the sugar cane straw ash (SCSA) (ALVES et al., 2015). The SCSA do not present a suitable valorisation and, considering others agro-industrial ashes destinations, it can be utilised in building construction (MADURWAR et al., 2013).

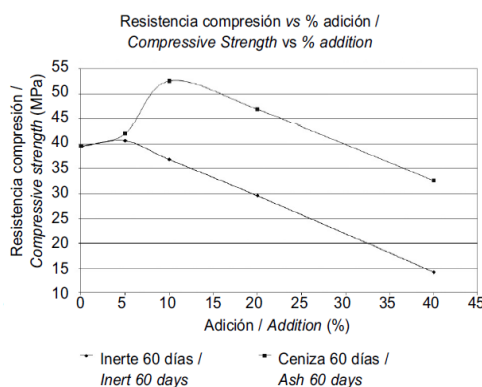
The SCSA was already assessed previously by its potential reactivity and as a construction material, but not in alkali-activated binders. The reactivity of SCSA was evaluated by Villar-Cociña (2002) and Frías et al. (2005 and 2007) in systems of hydrated lime/SCSA. The researchers concluded that the SCSA presents high reactivity, and it can be compared to a well-known pozzolanic material: rice husk ash (RHA) (Figure 2.17). In other study, Calligaris et al. (2015) assessed the SCSA reactivity replacing partially the Portland cement in 20% by X-ray diffraction (XRD) analysis. Authors found pozzolanic behaviour due to crystals analysis on XRD after 90 days of curing: less $\text{Ca}(\text{OH})_2$ and higher ettringite (Aft) in pastes with presence of SCSA when compared to a control without the ash.

Figure 2.17 – Electrical conductivity of hydrated lime/RHA and hydrated lime/SCSA suspensions (VILLAR-COCIÑA, 2002)



About studies with the application of SCSA as construction material, Rodrigues et al. (2013) assessed the ash in cement composites on mechanical and durability (accelerated ageing) tests. According to the authors, the SCSA presented pozzolanic characteristics and high porosity of these particles. The researchers obtained that the mechanical properties of specimens with SCSA presented similar values to the control. Regarding to the durability test, specimens with SCSA showed improved results than compared to the control one. By the results obtained, they concluded that the SCSA could replace partially the Portland cement by 20% in mass in these composites studied. In studies of Portland cement mortars, Oliveira et al. (2015) assessed a combined effect of sugar cane straw and bagasse ashes. The researches obtained that 20% replacement of Portland cement by SCSA presented similar values of compressive strength to the control. In another study of Portland cement mortars, Guzmán et al. (2011) studied replacements by SCSA until 40%. The authors concluded that the optimum replacement percentage is in the range 10-20% after studies on compressive strength of 60 curing days (Figure 2.18).

Figure 2.18 – Compressive strength of mortars cured after 60 days (GUZMÁN et al., 2011)



All these SCSA studies showed that the ash presents high reactivity and a potential to be utilised in alkali-activated binders.

REFERENCES

ABORA, K.; BELEÑA, I.; BERNAL, S. A.; DUNSTER, A.; NIXON, P. A.; PROVIS, J. L.; TOGNIT-HAMOU, A.; WINNEFELD, F. Durability and Testing – Chemical Matrix

Degradation Processes. In: PROVIS, J.; van DEVENTER, J. S. J. *Alkali Activated Materials: State-of-the-Art Report*. New York, London: Springer, 2014.

ALVES, M.; PONCE, G. H. S. F.; SILVA, M. A.; ENSINAS, A. V. *Surplus electricity production in sugarcane mills using residual bagasse and straw as fuel*. **Energy**, v. 91, p. 751-757, 2015.

ARIFFIN, M. A. M.; BHUTTA, M. A. R.; HUSSIN, M. W.; TAHIR, M. M.; AZIAH, N. *Sulfuric acid resistance of blended ash geopolymer concrete*. **Construction and Building Materials**, v. 43, p. 80-86, 2013.

ARRELLANO-AGUILAR, R.; BURCIAGA-DÍAS, O.; GOROKHOVSKY, A.; ESCALANTE-GARCÍA, J. I. *Geopolymer mortars based on a low grade metakaolin: Effects of the chemical composition, temperature and aggregate:binder ratio*. **Construction and Building Materials**, v. 50, p. 642-648, 2014.

ASTM C618-15. Standard Specification for Coal Fly Ash and Raw or Calcined Natural Pozzolan for Use in Concrete, ASTM International, West Conshohocken, PA, 2015.

ATIS, C. D.; GORUR, E. B.; KARAHAN, O.; BILIM, C.; ILKENTAPAR, S.; LUGA, E. *Very high strength (120 MPa) class F fly ash geopolymer mortar activated at different NaOH amount, heat curing temperature and heat curing duration*. **Construction and Building Materials**, v. 96, p. 673-678, 2015.

BASCAREVIC, Z. The resistance of alkali-activated cement-based binders to chemical attack. In: PACHECO-TORGAL, F.; LABRINCHA, A.; LEONELLI, C.; PALOMO, A.; CHINDAPRASIRT, P. *Handbook of Alkali-activated Cements, Mortars and Concretes*. United Kingdom: Elsevier, 1st ed., 2015.

BERNAL, S. A.; GUTIERREZ, R. B.; RODRIGUEZ, E. D. *Alkali-activated materials: cementing a sustainable future*. **Ingenieria y Competitividad**, v. 15, n. 2, p. 211-223, 2013.

BERNAL, S. A.; PROVIS, J. L. *Durability of Alkali-Activated Materials: Progress and Perspectives*. **Journal of American Ceramics Society**, v. 97, n. 4, p. 997-1008, 2014.

BERNAL, S. A.; PROVIS, J. L.; FERNÁNDEZ-JIMÉNEZ, A.; KRIVENKO, P. V.; KAVALEROVA, E.; PALACIOS, M.; SHI, C. *Binder Chemistry – High-Calcium Alkali-Activated Materials*. In: PROVIS, J.; van DEVENTER, J. S. J. *Alkali Activated Materials: State-of-the-Art Report*. New York, London: Springer, 2014.

BING-HUI, M.; ZHU, H.; XUE-MIN, C.; YAN, H.; SI-YU, G. *Effect of curing temperature on geopolymerization of metakaolin-based geopolymers*. **Applied Clay Science**, v. 99, p. 144-148, 2014.

BNDES (Banco Nacional de Desenvolvimento Econômico e Social) and CGEE (Centro de Gestão e Estudos Estratégicos). *Sugar cane-based bioethanol: energy for sustainable development*. 1st ed. Rio de Janeiro, Brazil, 2008;

BOUZÓN, N.; PAYÁ, J.; BORRACHERO, M.V.; SORIANO, L.; TASHIMA, M.M.; MONZÓ, J. *Refluxed rice husk ash/NaOH suspension for preparing alkali activated binders*. **Materials Letters**, p. 72-74, 2014.

BROUGH, A. R.; ATKINSON, A. *Sodium silicate-based, alkali-activated slag mortars Part I. Strength, hydration and microstructure*. **Cement and Concrete Research**, v. 32, p. 865-879, 2002.

CALLIGARIS, G. A.; FRANCO, M. K. K. D.; ALDRIGE, L. P.; RODRIGUES, M. S.; BERALDO, A. L.; YOKAICHIYA, F.; TURRILLAS, X.; CARDOSO, L. P. *Assessing the pozzolanic activity of cements with added sugar cane straw ash by synchrotron X-ray diffraction and Rietveld analysis*. **Construction and Building Materials**, v. 98, p. 44-50, 2015.

CASTALDELLI, V. N.; MORAES, J. C. B.; AKASAKI, J. L.; MELGES, J. L. P.; BORRACHERO, M. V.; SORIANO, L.; PAYÁ, J.; TASHIMA, M. M. *Study of the binary system fly ash/sugarcane bagasse ash (FA/SCBA) in SiO₂/K₂O alkali-activated binders*. **Fuel**, v. 174, p. 307-316, 2016.

CATAURO, M.; BOLLINO, F.; PAPALE, F.; LAMANNA, G. *Investigation of the sample preparation and curing treatment effects on mechanical properties and bioactivity of silica rich metakaolin geopolymer*. **Materials Science and Engineering C**, v. 36, p. 20-24, 2014.

CHENG, H.; LIN, K.L.; CUI, R.; HWANG, C. L.; CHANG, Y. M.; CHENG, T. W. *The effects of SiO₂/Na₂O molar ratio on the characteristics of alkali-activated waste catalyst-metakaolin based geopolymers*. **Construction and Building Materials**, v. 95, p. 710-720, 2015.

CHI, M. *Effects of modulus ratio and dosage of alkali-activated solution on the properties and micro-structural characteristics of alkali-activated fly ash mortars*. **Construction and Building Materials**, v. 99, p. 128-136, 2015.

CHINDAPRASIRT, P.; CHALEE, W. *Effect of sodium hydroxide concentration on chloride penetration and steel corrosion of fly ash-based geopolymer concrete under marine site*. **Construction and Building Materials**, v. 63, p. 303-310, 2014.

DAVIDOVITS, J. *Geopolymer Chemistry and Applications*. 3rd ed.; Institut Géopolymère: France, 2001

DAVIDOVITS, J. *Environmentally driven geopolymer cement applications*. **Geopolymer International Conference**, 2002.

DEB, P. S.; NATH, P.; SARKER, P. K. *The effects of ground granulated blast-furnace slag blending with fly ash and activator content on the workability and strength properties of geopolymer concrete cured at ambient temperature*. **Materials and Design**, v. 62, p. 32-39, 2014.

DUAN, P.; YAN, C.; ZHOU, W.; LUO, W.; SHEN, C. *An investigation of the microstructure and durability of a fluidized bed fly ash–metakaolin geopolymer after heat and acid exposure*. **Materials and Design**, v. 74, p. 125-137, 2015.

DUXSON, P.; PROVIS, J. L.; LUKEY, G. C.; MALLICOAT, S. W.; KRIVEN, W. M.; VAN DEVENTER, J. S. J. *Understanding the relationship between geopolymer composition, microstructure and mechanical properties*. **Colloids and Surfaces A**, v. 269, p. 47-58, 2005.

DUXSON, P.; FERNÁNDEZ-JIMENEZ, A.; PROVIS, J. L.; LUKEY, G. C.; PALOMO, A.; van DEVENTER, J. S. J. *Geopolymer technology: the current state of the art*. **Journal of Materials Science**, v. 42, p. 2917-2933, 2007.

FAOSTAT – Food and Agriculture Organization of the United Nations. Sugar cane production. Available in: <http://faostat3.fao.org/home/E>. Accessed in: 17 mar. 2016.

FERNÁNDEZ-JIMÉNEZ, A.; PUERTAS, F. *Structure of Calcium Silicate Hydrates Formed in Alkaline-Activated Slag: Influence of the Type of Alkaline Activator*. **Journal of American Ceramic Society**, v. 86, n. 8, p. 1389-1394, 2003.

FRÍAS, M.; VILLAR-COCIÑA, E.; SÁNCHEZ DE ROJAS, M. I.; VALENCIA-MORAES, E. *The effect that different pozzolanic activity methods has on the kinetic constants of the pozzolanic reaction in sugar cane straw-clay ash/lime systems: Application of a kinetic–diffusive model*. **Cement and Concrete Research**, Kidlington, v. 35, p. 2137-2142, 2005.

FRÍAS, M.; VILLAR-COCIÑA, E.; VALENCIA-MORAES, E. *Characterization of sugar cane straw waste as pozzolanic material for construction: Calcining temperature and kinetic parameters*. **Waste Management**, Kidlington, v. 27, p. 533-538, 2007.

GARCIA-LODEIRO, I.; PALOMO, A.; FERNÁNDEZ-JIMÉNEZ, A. *An overview of the chemistry of alkali-activated cement-based binders*. In: PACHECO-TORGAL, F.; LABRINCHA, A.; LEONELLI, C.; PALOMO, A.; CHINDAPRASIRT, P. *Handbook of Alkali-activated Cements, Mortars and Concretes*. United Kingdom: Elsevier, 1st ed., 2015.

GORHAN, G.; KURLU, G. *The influence of the NaOH solution on the properties of the fly ash-based geopolymer mortar cured at different temperatures*. **Composites: Part B**, v. 58, p. 371-377, 2014.

GUNASEKARA, C.; LAW, D. W.; SETUNGE, S.; SANJAYAN. *Zeta potential, gel formation and compressive strength of low calcium fly ash geopolymers*. **Construction and Building Materials**, v. 95, p. 592-599, 2015.

GUO, X.; SHI, H.; DICK, W. A. *Compressive strength and microstructural characteristics of class C fly ash geopolymer*. **Cement and Concrete Composites**, v. 32, p. 142–147, 2010.

- GUZMÁN, A.; GUTIÉRREZ, C.; AMIGÓ, V.; MEJIA, G. R.; DELVASTO, S. *Pozzolanitic evaluation of the sugar cane leaf*. **Materiales de Construcción**, Madrid, v. 61, n. 302, p.213-225, 2011.
- HAJJAJI, W.; ANDREJKOVICOVÁ, S.; ZANELLI, C.; ALSHAAER, M.; DONDI, M.; LABRINCHA, J. A.; ROCHA, F. *Composition and technological properties of geopolymers based on metakaolin and red mud*. **Materials and Design**, v. 52, p. 648-654, 2013.
- HE, J.; KIE, Y.; ZHANG, J.; YU, Y.; ZHANG, G. *Synthesis and characterization of red mud and rice husk ash-based geopolymer composites*. **Cement and Concrete Composites**, v. 37, p. 108-118, 2013.
- HEIKAL, M.; NASSAR, M. Y.; EL-SAYED, G.; IBRAHIM, S. M. *Characteristics and durability of alkali activated Egyptian blast-furnace slag-silica fume pastes*. **Journal of Basic and Environmental Sciences**, v. 1, p. 119-135, 2014.
- HOSSAIN, M. M.; KARIM, M. R.; HOSSAIN, M. K.; ISLAM, M. N.; ZAIN, M. F. M. *Durability of mortar and concrete containing alkali-activated binder with pozzolans: A review*. **Construction and Building Materials**, v. 94, p. 95-109, 2015.
- ISMAIL, I.; BERNAL, S. A.; PROVIS, J. L.; HAMDAN, S.; van DEVENTER, J. S. J. *Microstructural changes in alkali activated fly ash/slag geopolymers with sulfate exposure*. **Materials and Structures**, v. 46, p. 361-373, 2013.
- KAYA, K.; SOYER-UZU, S. *Evolution of structural characteristics and compressive strength in red mud–metakaolin based geopolymer systems*. **Ceramics International**, v. 42, p. 7406-7413, 2016.
- KAZEMIAN, A.; VAYGHAN, A. G.; RAJAPIOUR, F. *Quantitative assessment of parameters that affect strength development in alkali activated fly ash binders*. **Construction and Building Materials**, v. 93, p. 869-876, 2015.
- LEAL, M. R. L. V.; GALDOS, M. V.; SCARPARE, F. V.; SEABRA, J. E. A.; WALTER, A.; OLIVEIRA, C. O. F. *Sugar cane straw availability, quality, recovery and energy use: A literature review*. **Biomass and Bioenergy**, v. 53, p. 11-19, 2013a.
- LEAL, M. R. L. V.; WALTER, A. S.; SEABRA, J. E. A. *Sugarcane as an energy source*. **Biomass Conversion and Biorefinery**, v. 3, p. 17-26, 2013b.
- LEMOES, S. V.; DENADAI, M. S.; GUERRA, S. P. S.; ESPERANCINI, M. S. T.; BUENO, O. C.; TAKITANE, I. C. *Economic efficiency of two baling systems for sugar cane straw*. **Industrial Crops and Products**, v. 55, p. 97-101, 2014.
- LOMBARDI, G. M. R.; GIROTO, V. S.; LOMBARDI, N. M. R.; PERES, M. M.; SILVA, S. D. A.; ALVES, C. E. D.; ABÍLIO, R. S. *Uso Da Palha De Cana De Açúcar Como*

Fonte De Bioenergia Versus A Sua Contribuição Nutricional Quando Mantida No Solo. 7º Congresso Internacional de Bioenergia, São Paulo-SP, 2012.

MADURWAR, M. V.; RALEGAONKAR, R. V.; MANDAVGANE, S. A. *Application of agro-waste for sustainable construction materials: A review. Construction and Building Materials*, v. 38, p. 872-878, 2013.

MARJANOVI, N.; KOMLJENOVIC, M.; BASCAREVIC, Z.; NIKOLIC, V.; PETROVIC, R. *Physical-mechanical and microstructural properties of alkali-activated fly ash-blast furnace slag blends. Ceramics International*, v. 41, p. 1421-1435, 2015.

MARTIN, A.; PASTOR, J. Y.; PALOMO, A.; JIMÉNEZ, A. F. *Mechanical behaviour at high temperature of alkali-activated aluminosilicates (geopolymers). Construction Building Materials*, v. 93, p. 1188-1196, 2015.

MATIRENA, F.; MIDDENDORF, B.; DAY, R. L.; GEHRKE, M.; ROQUE, P.; MARTÍNEZ, L.; BETANCOURT, S. *Rudimentary, low tech incinerators as a means to produce reactive pozzolan out of sugar cane straw. Cement and Concrete Research*, Kidlington, v. 36, p. 1056-1061, 2006.

McLELLAN, B.; WILLIAMS, R.; LAY, J., van RIESSEN, A.; CORDER, G. *Costs and carbon emissions for geopolymer pastes in comparison to ordinary Portland cement. Journal of Cleaner Production*, v. 19, p. 1080-1090, 2011.

MELLADO, A.; CATALÁN, C.; BOUZÓN, N.; BORRACHERO, M. V.; MONZÓ, J. M.; PAYÁ, J. *Carbon footprint of geopolymeric mortar: study of the contribution of the alkaline activating solution and assessment of an alternative route. RSC Advances*, v. 4, 2014.

MELLADO, A.; PÉREZ-RAMOS, M. I.; MONZÓ, J.; BORRACHERO, M. V.; PAYÁ, J. *Resistance to acid attack of alkali-activated binders: Simple new techniques to measure susceptibility. Construction and Building Materials*, v. 150, p. 355-366, 2017.

MESA-PÉREZ, J. M.; ROCHA, J. D.; BARBOSA-CORTEZ, L. A.; PENEDO-MEDINA, M.; LUENGO, C. A.; CASCAROSA, E. *Fast oxidative pyrolysis of sugar cane straw in a fluidized bed reactor. Applied Thermal Engineering*, v. 56, p. 167-175, 2013.

MORAES, M. S. A.; GEORGES, F.; ALMEIDA, S. R.; DAMASCENO, F. C.; MACIEL, G. P. S.; ZINI, C. A.; JACQUES, R. A.; CARAMÃO, E. B. *Analysis of products from pyrolysis of Brazilian sugar cane straw. Fuel Processing Technology*, v. 101, p. 35-43, 2012.

NADZIRI, N.; ISMAIL, I.; HAMDAN, S. *Binding gel characterization of alkali-activated binders based on palm oil fuel ash (POFA) and fly ash. Journal of Sustainable Cement-Based Materials*, p. 1-4, 2017.

NIKOLIC, V.; KOMLJENOVIC, M.; BASCAREVIC, Z.; MARJANOVIC, N.; MILADINOVIC, Z.; PETROVIC, R. *The influence of fly ash characteristics and reaction*

conditions on strength and structure of geopolymers. Construction and Building Materials, v. 94, p. 361-370, 2015.

OLIVERA, D. C. G.; SALLES, J. D.; MORIY, B. A.; ROSSIGNOLO, J. A.; SAVASTANO JR., H. *Physical and Mechanical Performance of Mortars with Ashes from Straw and Bagasse Sugarcane. International Journal of Chemical, Molecular, Nuclear, Materials and Metallurgical Engineering*, v. 9, n. 1, 2015.

OZER, I.; SOYER-UZUM, S. *Relations between the structural characteristics and compressive strength in metakaolin based geopolymers with different molar Si/Al ratios. Ceramics International*, v. 41, p. 10192-10198, 2015.

PALOMO, A.; GRUTZECK, M. W.; BLANCO, M. T. *Alkali-activated fly ashes: A cement for the future. Cement and Concrete Research*, v. 29, p. 1323-1329, 1999.

PACHECO-TORGAL F.; ABDOLLAHNEJAD, Z.; CAMÕES, A. F.; JAMSHIDI, M.; DING, Y. *Durability of alkali-activated binders: A clear advantage over Portland cement or an unproven issue?. Construction and Building Materials*, v. 30, p. 400-405, 2012.

PACHECO-TORGAL, F.; CASTRO-GOMES, J.; JALALI, S. *Alkali-activated binders: A review. Part 1. Historical background, terminology, reaction mechanisms and hydration products. Construction and Building Materials*, v. 22, p. 1305-1314, 2008.

PACHECO-TORGAL, F.; CASTRO-GOMES, J.; JALALI, S. *Alkali-activated binders: A review. Part 2. About materials and binders manufacture. Construction and Building Materials*, v. 22, p. 1315-1322, 2008.

PACHECO-TORGAL, F.; LABRINCHA, A.; LEONELLI, C.; PALOMO, A.; CHINDAPRASIRT, P. *Handbook of Alkali-activated Cements, Mortars and Concretes*. United Kingdom: Elsevier, 1st ed., 2015.

PALOMO, A.; KRIVENKO, P.; GARCIA-LODEIRO, I.; KAVALEROVA, E.; MALTSEVA, O.; FERNÁNDEZ-JIMÉNES, A. *A review on alkaline activation: new analytical perspectives. Materiales de Construcción*, v. 64, n. 315, 2014.

PANIAS, D.; BALOMENOS, E.; SAKKAS, K. *The fire resistance of alkali-activated cement-based concrete binders. In: PACHECO-TORGAL, F.; LABRINCHA, A.; LEONELLI, C.; PALOMO, A.; CHINDAPRASIRT, P. Handbook of Alkali-activated Cements, Mortars and Concretes. United Kingdom: Elsevier, 1st ed., 2015.*

PAPA, E.; MEDRI, V.; LANDI, E.; BALLARIN, B.; MICCIO, F. *Production and characterization of geopolymers based on mixed compositions of metakaolin and coal ashes. Materials and Design*, 56, p. 409-415, 2014.

PELISSER, F.; GUERRINO, E. L.; MENDER, M.; MICHEL, M. D.; LABRINCHA, J. A. *Micromechanical characterization of metakaolin-based geopolymers. Construction and Building Materials*, v. 49, p. 547-553, 2013.

PEREIRA, A.; AKASAKI, J. L.; MELGES, J. L. P.; TASHIMA, M. M.; SORIANO, L. BORRACHERO, M. V.; MONZÓ, J.; PAYÁ, J. *Mechanical and durability properties of alkali-activated mortar based on sugarcane bagasse ash and blast furnace slag*. **Ceramics International**, v. 41, p. 13012-13024, 2015.

PEYS, A.; RAHIER, H.; PONTIKES, Y. *Potassium-rich biomass ashes as activators in metakaolin-based inorganic polymers*. **Applied Clay Science**, v. 119, p. 401-409, 2016.

PROVIS, J. Activating solution chemistry for geopolymers. In: PROVVIS, J.; van DEVENTER, J. S. J. *Geopolymers: Structure, processing, properties and industrial applications*. Oxford, Cambridge, New Delhi: Woodhead Publishing Limited, 2009.

PROVIS, J.; BERNAL, S. A. Binder Chemistry – Blended Systems and Intermediate Ca Content. In: PROVVIS, J.; van DEVENTER, J. S. J. *Alkali Activated Materials: State-of-the-Art Report*. New York, London: Springer, 2014.

PROVIS, J.; PALOMO, A.; SHI, C. *Advances in understanding alkali-activated materials*. **Cement and Concrete Research**, v. 78, p. 110-125, 2015.

PROVIS, J.; van DEVENTER, J. S. J. *Alkali Activated Materials: State-of-the-Art Report*. New York, London: Springer, 2014.

RAKHIMOVA, N. R.; RAKHIMOV, R. Z. *Alkali-activated cements and mortars based on blast furnace slag and red clay brick waste*. **Materials and Design**, v. 85, p. 324-331.

RANJBAR, N.; MEHRALI, M.; ALENGRAM U. J.; METSELAAR, H. S. C.; JUMAAT, M. Z. *Compressive strength and microstructural analysis of fly ash/palm oil fuel ash based geopolymer mortar under elevated temperatures*. **Construction and Building Materials**, v. 65, p. 114-121, 2014.

RASHAD, A. M. *A comprehensive overview about the influence of different admixtures and additives on the properties of alkali-activated fly ash*. **Materials and Design**, v. 54, p. 1005-1025, 2014.

RASHAD, A. M. *Alkali-activated metakaolin: A short guide for civil Engineer – An overview*. **Construction and Building Materials**, v. 41, p. 751-765, 2013a.

RASHAD, A. M. *Metakaolin as cementitious material: History, scours, production and composition – A comprehensive overview*. **Construction and Building Materials**, v. 41, p. 303-318, 2013b.

REIG, L.; SANZ, M. A.; BORRACHERO, M. V.; MONZÓ, J.; SORIANO, L.; PAYÁ, J. *Compressive strength and microstructure of alkali-activated mortars with high ceramic waste content*. **Ceramics International**, v. 43, n. 16, p. 13622-13634, 2017.

REIG, L.; TASHIMA, M. M.; BORRACHERO, M. V.; MONZÓ, J.; CHEESEMAN, C. R.; PAYÁ, J. *Properties and microstructure of alkali-activated red clay brick waste*. **Construction and Building Materials**, v. 43, p. 98-106, 2013a.

REIG, L.; TASHIMA, M. M.; SORIANO, L.; BORRACHERO, M. V.; MONZÓ, J.; PAYÁ, J. *Alkaline Activation of Ceramic Waste Materials*. **Waste Biomass Valorization**, v. 4, p. 729-736, 2013.

RIBEIRO, H.; FICARELLI, T. R. A. *Sugarcane Burning and Perspectives for Harvesters in Macatuba, São Paulo*. **Saúde Soc. São Paulo**, v. 19, n. 1, p. 58-63, 2010.

REJAMMA, R.; LABRINCHA, J. A.; FERREIRA, V. M. *Alkali activation of biomass fly ash–metakaolin blends*. **Fuel**, v. 98, p. 265-271, 2012.

RYU, G. S.; LEE, Y. B.; KOH, K. T.; CHUNG, Y. S. *The mechanical properties of fly ash-based geopolymer concrete with alkaline activators*. **Construction and Building Materials**, v. 47, p. 409-418, 2013.

SHI, C.; KRIVENKO, P. V.; ROY, D. *Alkali-Activated Cements and Concretes*. London and New York: Taylor and Francis, 2006.

TASHIMA, M. M.; AKASAKI, J. L.; CASTALDELLI, V. N.; SORIANO, L.; MONZÓ, J.; PAYÁ, J.; BORRACHERO, M. V. *New geopolymeric binder based on fluid catalytic cracking catalyst residue (FCC)*. **Materials Letters**, v. 80, p. 50-52, 2012a.

TASHIMA, M. M.; AKASAKI, J. L.; MELGES, J. L. P.; SORIANO, L.; MONZÓ, J.; PAYÁ, J.; BORRACHERO, M. V. *Alkali activated materials based on fluid catalytic cracking catalyst residue (FCC): Influence of SiO₂/Na₂O and H₂O/FCC ratio on mechanical strength and microstructure*. **Fuel**, v. 108, p. 833-839, 2013a.

TASHIMA, M. M.; SORIANO, L.; BORRACHERO, M. V. MONZÓ, J.; PAYÁ, J. *Effect of curing time on microstructure and mechanical strength development of alkali activated binders based on vitreous calcium aluminosilicate (VCAS)*. **Bulletin of Materials Science**, v. 36, n. 2, p. 245-249, 2013b.

TASHIMA, M. M.; SORIANO, L.; MONZÓ, J.; BORRACHERO, M. V.; PAYÁ, J. *Novel geopolymeric material cured at room temperature*. **Advances in Applied Ceramics: Structural, Functional and Bioceramics**, v. 112, n. 4, 2013b.

Tchakouté, H. K.; Rüschler, C. H.; Hinsch, M.; Djobo, J. N. Y.; Kamseu, E.; Leonelli, C. *Utilization of sodium waterglass from sugar cane bagasse ash as a new alternative hardener for producing metakaolin-based geopolymer cement*. **Chemie der Erde**, v. 77, p. 257-266, 2017.

TAWFIK, A.; EL-RAOOF, F. A.; KATSUKI, H.; MACKENZIE, K. J. D.; KOMARNENI, S. *K-Based Geopolymer from metakaolin: roles of K/Al ratio and water or steam Curing at different temperatures*. **Materialies de Construcción**, v. 66, n. 332, 2016.

TURNER, L. K.; COLLINS, F. G. *Carbon dioxide equivalent (CO₂-e) emissions: A comparison between geopolymer and OPC cement concrete*. **Construction and Building Materials**, v. 43, p. 125-130, 2013.

TIPPAYASAM, C.; BALYORE, P.; THAVORNITI, P.; KAMSEU, E.; LEONELLI, C.; CHINDAPRASIRT, P.; CHAYSUWAN, D. *Potassium alkali concentration and heat treatment affected metakaolin-based geopolymer*. **Construction and Building Materials**, v. 104, p. 293-297, 2016.

TURKER, H. H.; BALÇIKANLI, M.; DURMUS, I. H.; ÖZBAY, E.; ERDEMIR, M. *Microstructural alteration of alkali activated slag mortars depend on exposed high temperature level*. **Construction and Building Materials**, v. 104, p. 169-180, 2016.

UNICA (União da Indústria de Cana-de-açúcar). Produção de cana-de-açúcar, 2004/2005 - 2014/2015. 2014. Available in: <<http://www.unicadata.com.br>>. Accessed in: 16 mar. 2016.

WANG, H.; LI, H.; YAN, F. *Synthesis and mechanical properties of metakaolinite-based geopolymer*. **Colloids and Surfaces A**, v. 268, p. 1-6, 2005

YAO, Z. T.; JI, X. S.; SARKER, P. K.; TANG, J. H.; GE, L. Q.; XIA, M. S.; XI, Y. Q. *A comprehensive review on the applications of coal fly ash*. **Earth-Science Reviews**, v. 141, p. 105-121, 2015.

YUSUF, M. O.; JOHARI, M. A. M.; AHMAD, Z. A.; MASLEHUDDIN, M. *Strength and microstructure of alkali-activated binary blended binder containing palm oil fuel ash and ground blast-furnace slag*. **Construction and Building Materials**, v. 52, p. 504-510, 2014.

YUSUF, T. O.; ISMAIL, M.; USMAN, J.; NORUZMAN, A. H. *Impact of Blending on Strength Distribution of Ambient Cured Metakaolin and Palm Oil Fuel Ash Based Geopolymer Mortar*. **Advances in Civil Engineering**, 2014.

van DEVENTER, J. S. J.; PROVIS, J. L.; DUXSON, P. *Technical and commercial progress in the adoption of geopolymer cement*. **Minerals Engineering**, v. 29, p. 89-104, 2012.

VILLAR-COCIÑA, E.; VALENCIA-MORAES, E.; GONZÁLEZ-RODRIGUÉZ, R.; HERNÁNDEZ-RUÍZ, J. *Kinetics of the pozzolanic reaction between lime and sugar cane straw ash by electrical conductivity measurement: A kinetic-diffusive model*. **Cement and Concrete Research**, Kidlington, v. 33, p. 517-524, 2002.

VILLAQUIRÁN-CAICEDO, M. A.; GUITERRÉZ, R. M. *Synthesis of ternary geopolymers based on metakaolin, boiler slag and rice husk ash*. **DYNA**, v. 82, n. 194, p. 104-110, 2015.

ZHANG, H. Y.; KODUR, V.; QI, S. L.; CAO, L. WU, B. *Development of metakaolin-fly ash based geopolymers for fire resistance applications*. **Construction and Building Materials**, v. 55, p. 38-45, 2014.

ZHANG, Z.; PROVIS, J. L.; REID, A.; WANG, H. *Fly ash-based geopolymers: The relationship between composition, pore structure and efflorescence*. **Cement and Concrete Research**, v. 64, p. 30-41, 2014.

ZHANG, Z.; WANG, H.; PROVIS, J. L.; BULLEN, F.; REID, A.; ZHU, Y. *Quantitative kinetic and structural analysis of geopolymers. Part 1. The activation of metakaolin with sodium hydroxide*. **Thermochimica Acta**, v. 529, p. 22-33, 2012.

ZHANG, Z.; WANG, H.; ZHU, Y.; REID, A.; PROVIS, J. L.; BULLEN, F. *Using fly ash to partially substitute metakaolin in geopolymer synthesis*. **Applied Clay Science**, v. 88-89, p. 194-201, 2014.

ZHU, H.; ZHANG, Z. ZHU, Y.; TIAN, L. *Durability of alkali-activated fly ash concrete: Chloride penetration in pastes and mortars*. **Construction and Building Materials**, v. 65, p. 51-59, 2014.

3 POZZOLANIC REACTIVITY STUDIES ON SUGAR CANE STRAW ASH

The article entitled as "*Pozzolanic Reactivity Studies on a Biomass-Derived Waste from Sugar Cane Production: Sugar Cane Straw Ash (SCSA)*" by J. C. B. Moraes, J. L. P. Melges, J. L. Akasaki, M. M. Tashima, L. Soriano, J. Monzó, M. V. Borrachero, and J. Payá was published in the journal **ACS Sustainable Chemistry and Engineering**, v. 4 (8), p. 4273-4279, 2016.

Abstract: Biomass has gained in importance as an energy source in recent years. One of the crops that presents interesting opportunities with regard to biomass is sugar cane. In Brazil, sugar cane production is increasing for alcohol and sugar manufacture. Some byproducts, such as sugar cane straw, also are obtained during harvesting. Because of the calorific value of the sugar cane straw, its use as biomass is increasing. After the straw is burned to produce energy, an ash is obtained: sugar cane straw ash (SCSA). This waste needs an appropriate destination, and since the recent publication of successful studies using biomass derived-ashes as pozzolanic material, the present study aimed to assess the pozzolanic reactivity of sugar cane straw ash. The pozzolanic activity was assessed using a new and simple recently proposed method: evaluation of the electrical conductivity of calcium hydroxide (CH) and pozzolan suspensions, in which solid CH is initially present. These results were compared to those of two other well-established techniques: Fourier transformed infrared spectroscopy and thermogravimetric analysis. The evaluation by all three techniques is similar and shows that sugar cane straw ash is a good pozzolanic material: high lime fixation values for CH/SCSA mixes were determined by thermogravimetric analysis, and unsaturation with respect to CH in 3.5:6.5 CH/SCSA suspension.

Keywords: *Agroindustry residue, Pozzolan, Hydrated lime, Fourier-transformed infrared spectroscopy, Thermogravimetric analysis, Electrical conductivity measurement, Scanning electron microscopy.*

3.1 INTRODUCTION

Biomass has become an interesting source of energy in the last years. In the early 21st century, concern about the availability of nonrenewable resources and CO₂ emissions motivated an increase in research about biomass as an alternative energy source (GALLEZOT, 2008). The transformation of biomass into energy also allows the production of new inorganic materials for different applications (VASSILEV et al., 2013a; VASSILEV et al., 2013b; JAMES et al., 2012). In some cases, advanced materials based on porous silica nanoparticles have been obtained (ALYOSEFT et al., 2015; CHEN et al., 2013). One agricultural product that supplies biomass is sugar cane. In Brazil, the sugar cane crop has increased in recent years for the manufacture of alcohol and sugar, making Brazil the largest producer worldwide (FOOD AND AGRICULTURE ORGANIZATION OF THE UNITED NATIONS – FAOSTAT, 2016). In numbers, the harvest of sugar cane in Brazil was 632 million tons in 2014/2015, which represents an increase of 64% in the last 10 years (UNIÃO DA INDÚSTRIA DE CANA-DE-AÇÚCAR – UNICA, 2016). Formerly, the sugar cane harvest was performed using a burning process in the cultivation area; however, an Agro-Environmental Protocol (LEAL et al., 2013) was created in order to end this procedure. As a consequence, mechanized harvesting gained in importance. In the mechanized process, a byproduct composed of green and dry leaves is generated, sugar cane straw, of which about 140 kg is obtained per ton of sugar cane produced (LEAL et al., 2013; BNDES and CGEE, 2008). Initially, the straw was left on the field, but some authors recognized that the calorific value of the sugar cane straw could be used as biomass, in the same way as the sugar cane bagasse that is obtained from alcohol/sugar production (LEAL et al., 2013; MORAES et al., 2012). Recent studies have assessed the collection of this byproduct from the field (LEAL et al., 2013; LEMOS et al., 2014), and new practices for burning it to produce energy (MESA-PÉREZ et al., 2013). However, after obtaining energy from sugar cane straw by burning, waste is generated: sugar cane straw ash (SCSA). There is currently no mechanism for the valorization of this residue, and due to expected increases in sugar cane production and studies on the use the straw as an energy source, the production of SCSA will likely increase in the coming years. A good valorization method for this biomass-derived waste could be the partial replacement of Portland cement as a pozzolanic material. Some biomass-derived ashes have been successfully tested in cement and concrete as pozzolanic materials:

rice husk ash (CHAO-LUNG et al., 2011) and sugar cane bagasse ash (CORDEIRO et al., 2011). Pozzolan is an amorphous silica or alumina/silica material that reacts with calcium hydroxide (portlandite generated from Portland cement hydration) in an aqueous medium and generates cementing gels similar to those found for Portland cement (HEWLETT, 2008). The advantages of using biomass wastes such as pozzolans to partially replace Portland cement are technological (improving compressive strength and durability) and ecological (reducing both Portland cement consumption and the disposal of ashes in landfills) (MALHOTRA; MEHTA, 1996). The pozzolanic reactivity of a material can be assessed via studies of calcium hydroxide consumption using several techniques. Previously, reports on the reactivity of SCSA studied the behavior of Portland cement blends (GUZMÁN et al., 2011) and kinetic parameters (FRÍAS et al., 2007). In this article, the pozzolanic activity of SCSA obtained from an autocombustion process was assessed by means of electrical conductivity measurements as proposed by Tashima et al. (2014). This method consists of monitoring the electrical conductivity of suspensions composed of calcium hydroxide/pozzolan for 7 days. The SCSA reactivity results obtained by electrical conductivity measurements of suspensions were compared to those from other well-established techniques: Fourier transformed infrared spectroscopy (FTIR) and thermogravimetric analysis (TGA). The main advantage of electrical conductivity measurement is the easy preparation and relatively low cost of the test compared to the two other techniques for evaluating the pozzolanic potential of a material. In addition, SEM images were obtained in order to show the pozzolanic reaction products between SCSA and calcium hydroxide. This study aimed to assess the pozzolanic activity of SCSA and valorize this biomass waste, as well as to compare the results of a recently proposed and simple technique to those from other well-established methods.

3.2 MATERIALS AND METHODS

3.2.1 Materials

Sugar cane straw was obtained from a sugar cane plantation near Ilha Solteira (Sao Paulo, Brazil). The straw was burned in an autocombustion process with a maximum temperature of 700 °C. In this process, the sugar cane straw is initially ignited, and the

combustion heat maintains the process without any fuel added. The temperature was measured in different points and at several times. After burning, the SCSA was collected from the bottom of the furnace and passed through sieves in order to remove unburned particles. Finally, it was milled for 30 min in a planetary ball mill to reduce the particle diameter. Calcium hydroxide of high purity (>95% purity), supplied by Panreac S.A, was used for all pozzolanic reactivity tests.

3.2.2 Equipment

Electrical conductivity measurements were carried out using a Crison micro CM2201 instrument. pH measurements were obtained using a Crison micro PH2001 pH meter. In order to maintain the test temperature, a Julabo SW22 shaking water bath was used. Thermogravimetric analysis was performed using a Mettler Toledo TGA850 instrument, in a temperature range of 35–600 °C at a heating rate of 10 °C·min⁻¹ in an N₂ atmosphere (75 mL·min⁻¹ gas flow), where the samples were tested in sealed 100 µL pin-holed aluminum crucibles. Fourier transformed infrared spectroscopy was performed using a Bruker TENSOR 27 in the wavenumber range between 400 and 4000 cm⁻¹. SEM images of the calcium hydroxide/SCSA pastes were obtained using a JEOL JSM-6300 microscope. The chemical composition of SCSA was obtained through X-ray fluorescence (XRF) by means of a Philips Magix Pro XRF instrument. Methods. Electrical conductivity measurements were performed as proposed by Tashima et al. (2014). This followed method differs from others previously reported (LUXÁN et al., 1989; McCARTER; TRAN, 1996; WALKER; PAVÍA, 2011; PAYÁ et al., 2001): the main difference is related to the presence or not of solid calcium hydroxide in the tested suspensions. Some techniques (LUXÁN et al., 1989; McCARTER; TRAN, 1996; WALKER; PAVÍA, 2011) are based on the preparation of a saturated solution in Ca(OH)₂, and the decrease in electrical conductivity is measured when pozzolan is added. Another technique (PAYÁ et al., 2001) is based on the same type of measurement; however, the initial Ca(OH)₂ solution is unsaturated. In the test used in the actual study, there is an amount of undissolved Ca(OH)₂ in the initial suspension. In this way, two simultaneous processes take place: the consumption of dissolved Ca(OH)₂ and the dissolution of solid Ca(OH)₂. In tests according to Tashima's method, 1g of solid (the mixture of calcium hydroxide (CH) and pozzolan) and 50 mL of deionized water were

combined in an Erlenmeyer flask. The CH/SCSA suspensions (also named "systems" in the manuscript) were assessed at 40, 50, and 60 °C for 7 days in six different proportions: 2:8, 2.5:7.5, 3:7, 3.5:6.5, 4:6, and 4.5:5.5 (by mass). In addition, suspensions at 30 °C were also studied, where the relative amount of calcium hydroxide was decreased compared to the tests at higher temperature. At this temperature, the following proportions were evaluated: 0.5:9.5, 1:9, 1.5:8.5, 2:8, 2.5:7.5, and 3:7. The results of the loss of electrical conductivity (Lc) tests are presented as the percentage decrease in electrical conductivity, as reported by Tashima et al (2014). This parameter clarifies the electrical conductivity results and also takes into account the influence of the ions released by pozzolan. The pH of the suspensions was measured before the addition of the SCSCA and at the end of the test (7 days). At the end of the test, the suspensions evaluated at 40 °C were filtered, and the solid part retained on the filter was analyzed by TG. TG and FTIR studies were carried out for two CH/SCSCA pastes with proportions by mass of 3:7 and 5:5 at a constant water/binder rate of 0.80. The CH/SCSCA pastes were assessed after 1, 3, 7, and 28 days of curing at a temperature of 40 °C with relative humidity higher than 95%. At each curing time point, the pastes were milled in an agate mortar and mixed with acetone in order to stop the hydration process. They were then filtered and dried in a laboratory incubator for 30 min at 60 °C. SEM images of the fractured surface of the 3:7 paste were obtained after 28 days of curing at 40 °C. After each curing age, the SEM pastes were prepared by breaking samples and taking regular fracture images. They were then placed in acetone for 1h and, finally, dried for 30 min in a laboratory incubator at 60 °C.

3.3 RESULTS AND DISCUSSION

3.3.1 Sugar Cane Straw Ash Characterization

The chemical composition of SCSCA obtained from XRF analysis is shown in Table 3.1. SCSCA presents a SiO₂ content of 36.5%, which is lower than published values for sugar cane bagasse ash (CORDEIRO et al., 2011). Al₂O₃ and Fe₂O₃, other oxides that are important in the pozzolanic reaction (ASTM INTERNATIONAL, 2015), are found in minor amounts: 2.8% and 3.4%, respectively. The CaO content is 16.4%, a percentage much lower than that found for blast furnace slag or class C fly ash (HEWLETT, 2008). SCSCA does not

harden when mixed with water, suggesting that its hydraulic behavior could be negligible. The total alkali content (K_2O plus Na_2O) was 8.1%, which is considered high. However, such high values are very common in ashes produced by burning biomass (DEMIS et al., 2014). The C–S–H gel formed in the Portland cement hydration or in the pozzolanic reaction has the ability to incorporate alkali ions (Na^+ or K^+) (HONG; GLASSER, 1999). However, in the presence of reactive aggregates, alkali-silica expansion could take place when alkali-rich pozzolanic additions are used (THOMAS, 2011). Finally, the amount of LOI is relatively high (15.5%), due to the presence of organic matter; the combustion was incomplete and some cellulosic compounds remained. Regarding the phases present in SCSA, the XRD pattern showed the presence of an amorphous phase and crystalline phases mainly composed of quartz (SiO_2) and calcite ($CaCO_3$), which probably originate from the soil where the sugar cane straw was collected. It is therefore likely that the SiO_2 and CaO are present as crystals in the SCSA and do not take part in the pozzolanic reaction. Studies to determine the percentage of insoluble SCSA residue by acid and base treatment presented a value of 16.5%, which means that the SiO_2 -crystalline phase in the pozzolan represents about 45% of the total SiO_2 . The mean particle diameter (D_{med}), median particle diameter (D_{50}), and 90% passing particle diameter (D_{90}) of the SCSA were 14.7, 7.0, and 38.8 μm , respectively. Specific surface area was 0.595 m^2/g , and specific gravity was 2.25.

Table 3.1 – Chemical composition of SCSA by percentage

SiO_2	Al_2O_3	Fe_2O_3	CaO	K_2O	Na_2O	Cl	MgO	SO_3	P_2O_5	Others	LOI
36.5	2.8	3.4	16.4	7.9	0.2	0.4	7.3	4.4	4.0	1.2	15.5

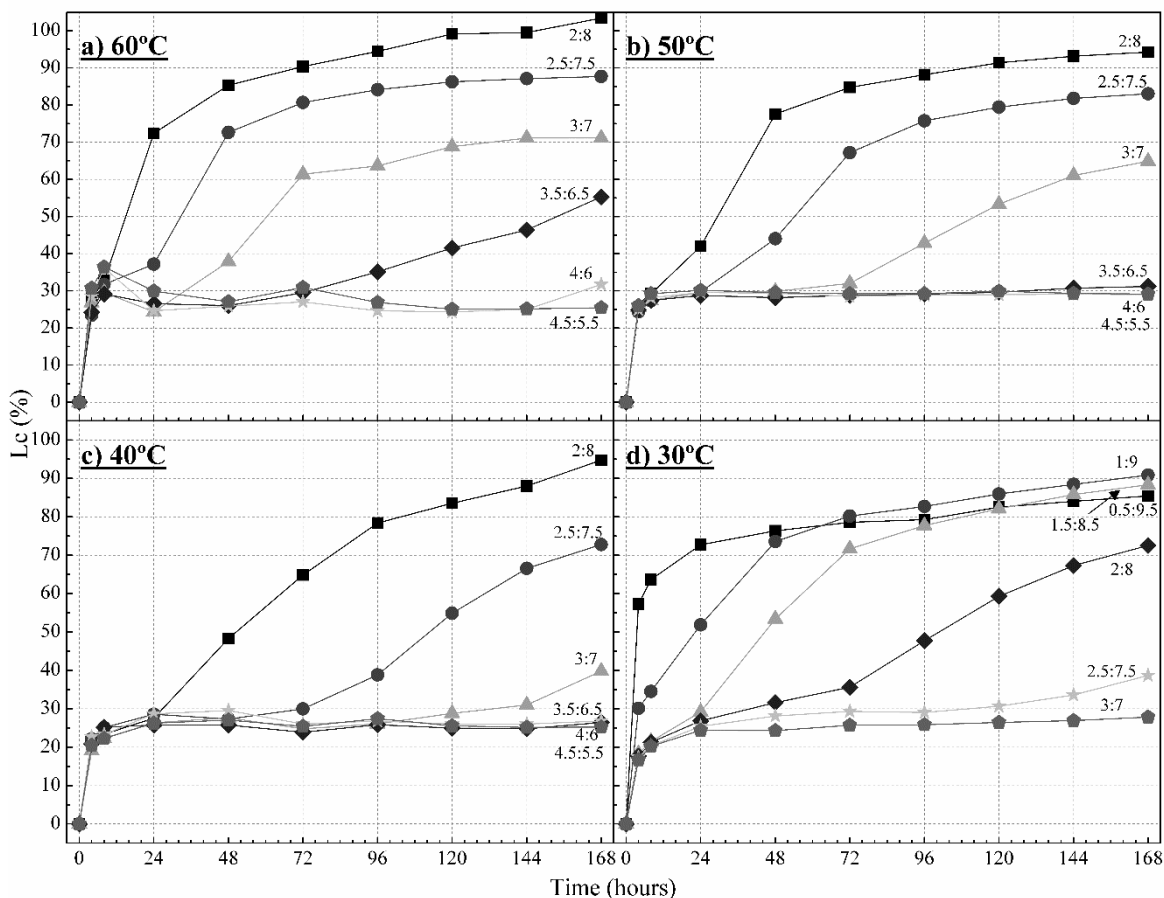
3.3.2 Electrical Conductivity Measurements

The principle of this test is based on the limited solubility of calcium hydroxide (CH) in water. Calcium hydroxide yields a saturated water solution if the quantity of dissolved hydroxide is lower than the amount of added hydroxide. Under these conditions, the concentration of Ca^{2+} and OH^- remains constant at a given temperature. Thus, the electrical conductivity of the suspension has a high value. If a pozzolan is added to the suspension, a reaction between Ca^{2+}/OH^- ions and the reactive fraction of the pozzolan takes place. This reaction decreases the concentration of ions, and consequently, the electrical

conductivity tends to diminish. However, the dissolution of solid calcium hydroxide present in the suspension maintains a constant concentration of Ca^{2+} and OH^- . While the solution remains saturated due to the dissolution of calcium hydroxide, the electrical conductivity remains constant. When the solid calcium hydroxide is exhausted, the solution becomes unsaturated, and the electrical conductivity starts to decrease. The time taken to achieve an unsaturated state depends on the CH/pozzolan proportion and the pozzolan reactivity. Highly reactive pozzolans reach the unsaturated state more quickly. The results of the loss of electrical conductivity (Lc) tests for suspensions studied at 30, 40, 50, and 60 °C over 7 days are shown in Figure 3.1. Two types of curves can be seen in the graphics. In one case, CH remains in the saturated state, and the Lc value is static during the 4–168 h testing period. In the other, an increase in the Lc value during the testing period is seen. This occurs when unsaturation is achieved because the pozzolanic reaction fixed the entire solid CH phase. The Lc value increases, for all systems, in the first 4 h due to the addition of SCSA addition to the suspension when adsorption of dissolved ions onto SCSA particles takes place. For the suspensions studied at 60 °C (Figure 3.1a), the 2:8 system presented a Lc value of over 70% after only 24 h, which represents a rapid consumption of the solid CH. For the 2.5:7.5 system, the Lc value is lower than the 2:8 system after 24 h (almost 40%); however, the suspension is also shown to be unsaturated. The 3:7 suspension presented an increase in the Lc value after 48 h, whereas the 3.5:6.5 and 4:6 systems only showed a rise in the Lc value after 96 and 168 h, respectively. The 4.5:5.5 system did not show any increase in Lc at this temperature, which means that the pozzolan could not consume all of the solid calcium hydroxide and that the unsaturated state was not achieved. It is well-known that chemical reactions (e.g., pozzolanic reaction) usually are slower when the temperature decreases. Thus, as expected, the loss in the conductivity of suspensions studied at 50 °C (Figure 3.1b) showed a slower unsaturation process than the suspensions tested at 60 °C. The 2:8 system presented an Lc value of 40% in the first 24 h. The 2.5:7.5 and 3:7 systems presented an increase in the Lc value after 48 and 72 h, respectively, whereas the final three suspensions (3.5:6.5, 4:6, 4.5:5.5) did not show any loss of conductivity. For the suspensions tested at 40 °C (Figure 3.1c), only the 2:8 system presented an increase in the Lc value after 48 h, taking a much longer time to reach the unsaturated state than at the higher temperatures. The 2.5:7.5 and 3:7 systems also showed an increase in the Lc value, after 72 and 120 h, respectively. As in the test at 50 °C, 3.5:6.5, 4:6, and 4.5:5.5, suspensions remained saturated until the end

of the test. According to the criteria proposed by Tashima et al. (2014), SCSA can be classified as a pozzolan with medium reactivity. This behavior is similar to that found for low densified silica fume (DSF-H). For testing at 30 °C (Figure 3.1d), considering that CH/SCSA suspensions of 3.5:6.5 did not reach unsaturation at 40 or 50 °C, lower CH/SCSA systems were tested (0.5:9.5, 1:9 and 1.5:8.5). For these suspensions tested at 30 °C, an increase in the Lc value was found for 0.5:9.5 (4 h), 1:9 (4 h), 1.5:8.5 (48 h), 2:8 (72 h), and 2.5:7.5 (144 h). However, the 3:7 suspension did not show any increase in the Lc value, meaning that SCSA could not consume enough calcium hydroxide to turn the suspension unsaturated at this temperature.

Figure 3.1 – Loss of electrical conductivity (Lc) of suspensions studied at (a) 60 °C; (b) 50 °C; (c) 40 °C; and (d) 30 °C



Additionally, pH measurements were carried out in order to assess the change in the concentration of OH^- . Thus, the pH of calcium hydroxide suspensions before the addition of SCSA and the pH of the suspension at the end of the test were measured. In general terms,

a significant decrease in pH was observed from the testing time at which unsaturation was reached, indicating that the OH^- concentration diminished. For samples in the saturated state, only minor changes in pH were observed, suggesting that the OH^- concentration remained constant. Figure 3.2 shows these variations in pH (ΔpH). It can be observed that for a given CH/SCSA proportion, a higher testing temperature results in a higher ΔpH . A straight line is shown for $\Delta\text{pH} = 0.2$ meaning that below this value the suspension remained saturated. As an exception, the ΔpH of the 4:6 CH/SCSA sample at 60 °C was below this value: in this case, the L_c value was at the limit of unsaturation (see Figure 3.1a), and consequently, the change in pH value was also at the limit.

Figure 3.2 – pH variation (ΔpH) of the CH/SCSA suspensions at each temperature studied

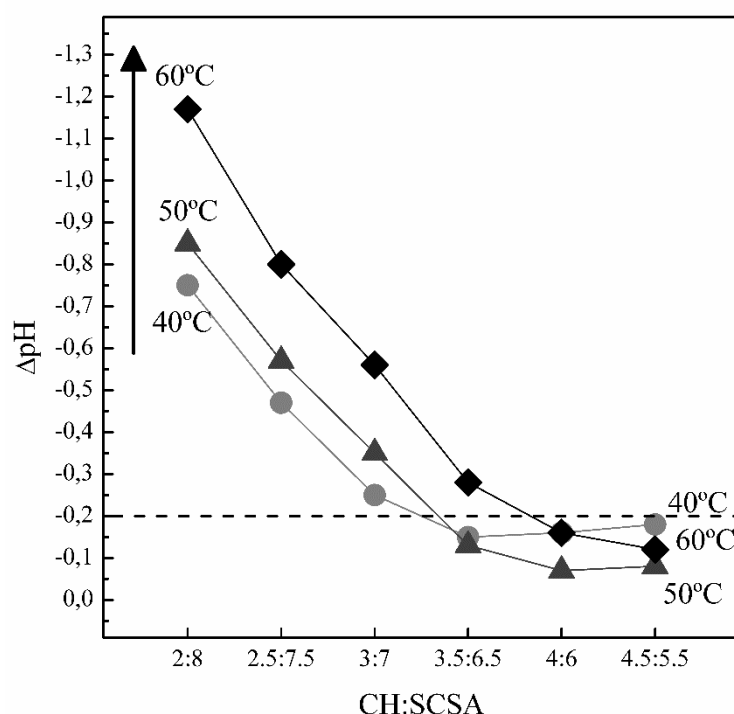
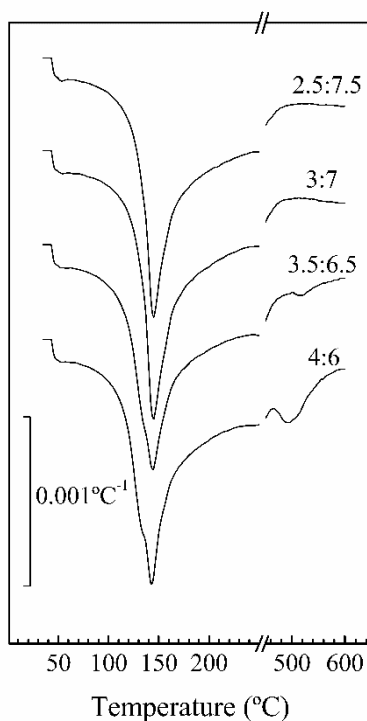


Figure 3.3 shows the DTG curves of the solid residue obtained by filtration of the suspensions after the end of electrical conductivity measurements at 40 °C. The main peak in the range 125–150 °C is from the dehydration of pozzolanic reaction products (mainly calcium silicate hydrates, C–S–H). The aim of this test is to assess the peak in the range 500–600 °C, which results from the dehydroxylation of the calcium hydroxide, according to the following equation: $\text{Ca}(\text{OH})_2 \rightarrow \text{CaO} + \text{H}_2\text{O}$. If this peak appears in the DTG curve, it

means that there is calcium hydroxide remaining in the solid residue after filtration, meaning that SCSA could not achieve an unsaturated suspension. From these results, it can be seen that only the 3.5:6.5 and 4:6 suspensions presented a peak at 500–600 °C, where the SCSA could not react with enough calcium hydroxide to result in an unsaturated suspension, confirming the results of the electrical conductivity measurements (Figure 3.1c). The suspensions 2.5:7.5 and 3:7 did not show calcium hydroxide in their DTG curves, also in good agreement with the electrical conductivity measurements.

Figure 3.3 – DTG curves of the solid part of the suspensions after electrical conductivity measurements at 40 °C.

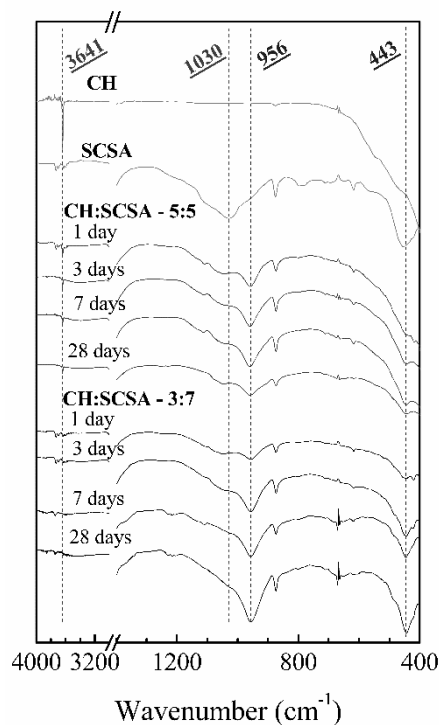


3.3.3 Fourier Transformed Infrared Spectroscopy

FTIR spectra of the 3:7 and 5:5 ratio CH/SCSA pastes after 1, 3, 7, and 28 days curing at a temperature of 40 °C are shown in Figure 3.4. The main vibration bands detected in this test were at 3641 (O–H vibration), 1030, 956, and 443 cm^{-1} (Si–O vibration). For the raw materials, the vibration band at 3641 cm^{-1} is related to calcium hydroxide (CH), and the peak at 1030 cm^{-1} is from the amorphous phase of the pozzolan (SCSA). For the pastes,

the four selected vibration bands have important roles in the pozzolanic reaction. With increasing curing age, the vibration band at 956 cm^{-1} and 443 cm^{-1} increases, whereas the other two peaks, at 3641 cm^{-1} and 1030 cm^{-1} , decrease. This results from the consumption of calcium hydroxide (vibration band at 3641 cm^{-1}) by the amorphous phase of SCSA (vibration band at 1030 cm^{-1}) with curing. Consequently, a new vibration band resulting from the pozzolanic reaction appears at 956 cm^{-1} . In both pastes, from the first day of curing the vibration band at 1030 cm^{-1} is reduced in intensity, showing dissolution of the amorphous network of the SCSA (dissolution of SiO_4 units), occurred mainly during the early part of the reaction. For the 5:5 CH/SCSA paste, the vibration band at 3641 cm^{-1} reduced from the first to the third day of curing and remained practically constant afterward. This means that the SCSA could not consume all of the calcium hydroxide after 28 days of curing, and the pozzolanic reaction occurred mainly in the first 7 days. The vibration band at 956 cm^{-1} was practically unchanged from days 1 to 28. For the 3:7 CH/SCSA paste, the peak at 3641 cm^{-1} almost disappeared after 1 day of curing. This suggests that the SCSA consumed almost all of the calcium hydroxide after this time. The peak at 875 cm^{-1} is related to C–O bond vibration from the carbonate anion. This peak appeared on the pure SCSA spectrum due to the presence of calcite (see Figure 3.4). In the CH/SCSA pastes, this peak is related to carbonate from the ash and from calcium hydroxide, and its intensity was maintained practically constant for all curing times, showing that the sample did not carbonated. The FTIR studies show that SCSA presents good reactivity since the pozzolanic reaction at both CH/SCSA proportions took place at early curing ages.

Figure 3.4 – FTIR spectra of 3:7 and 5:5 CH/SCSA pastes after 1, 3, 7, and 28 days of curing at 40 °C



3.3.4 Thermogravimetric Analysis

The DTG curves of the 5:5 and 3:7 CH/SCSA pastes from 1 to 28 days of curing at 40 °C are shown in Figure 3.5. The main peaks of these analyses are in the range 125–175 °C, which represents the dehydration of products from pozzolanic reaction and at 500–575 °C resulting from the dehydroxylation of calcium hydroxide. In the 5:5 paste, the 500–575 °C peak reduced from days 1 to 3 of curing and remained practically constant until 28 days, meaning that the pozzolanic reaction occurred in the first 3 days. The peak near 150 °C increased from days 1 to 3 of curing and did not show any changes after this time. This behavior is due to the pozzolanic reaction, which consumes the calcium hydroxide and forms cementing gels (mainly C–S–H). For the 3:7 paste, on the first day of curing there was no peak at 550 °C, as a result of complete calcium hydroxide consumption by the SCSA. Since the pozzolanic reaction took place within the first day, the peak related to the gel from this reaction (near to 150 °C) remained practically constant from 1 to 28 days of curing time. These results of thermogravimetric analysis are in accordance with those from the FTIR

studies. Table 3.2 shows the mass loss of pozzolanic reaction products (PP) and calcium hydroxide (PCH), as well the lime fixation of all pastes in the curing time studied. For the paste with a CH/SCSA proportion of 5:5, the lime fixation²⁹ had a high value after 1 day of curing (81.46%), suggesting the good pozzolanic reactivity from the SCSA. After 3 and 7 days, the lime fixation had similar values (92.76% and 92.29%, respectively), and after 28 days of curing, the lime fixation did not significantly change. Therefore, for the 5:5 CH/SCSA paste, the major pozzolanic reaction took place in the first day of curing. In the 3:7 CH/SCSA paste, the lime fixation was 100% within the first day of curing. At this proportion, the SCSA was able to consume all of the calcium hydroxide in only 1 day of curing. These DTG curves and lime fixation values show that the reactivity of the SCSA is of interest for potential applications. Concerning the mass loss from dehydration of the pozzolanic reaction products (PP), in both pastes studied, the values did not vary significantly with the curing time. Since the SCSA presents good reactivity, the major part of the pozzolanic reaction occurred in the first day of curing, resulting in only minor changes in the mass loss related to the dehydration of pozzolanic reaction products. These minor changes can be related to changes in water bonds of the C-S-H gels during the curing time. In previous studies (MORAES et al., 2015), more important changes in the mass loss related to formed hydrates at 20 °C were observed after the calcium hydroxide was completely combined, different from that found at 40 °C.

Figure 3.5 – DTG curves of 5:5 and 3:7 CH/SCSA pastes from 1 to 28 days of curing at 40 °C

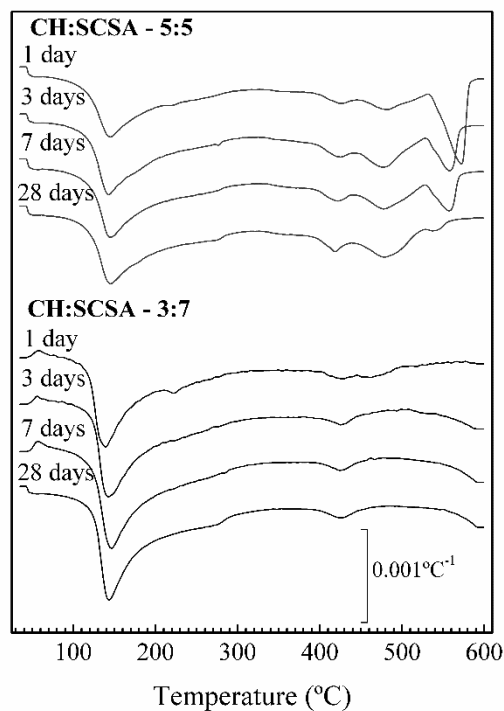


Table 3.2 – Mass loss related to the dehydration of pozzolanic reaction products (P_P) and calcium hydroxide (P_{CH}), and lime fixation of CH:SCSA pastes

CH:SCSA	Curing time (days)	P_P (%)	P_{CH} (%)	Lime fixation (%)
5:5	1	12.58	2.14	81.46
	3	14.03	0.90	92.76
	7	13.47	0.89	92.29
	28	13.94	0.17	98.50
3:7	1	13.50	0	100
	3	14.44	0	100
	7	15.05	0	100
	28	15.39	0	100

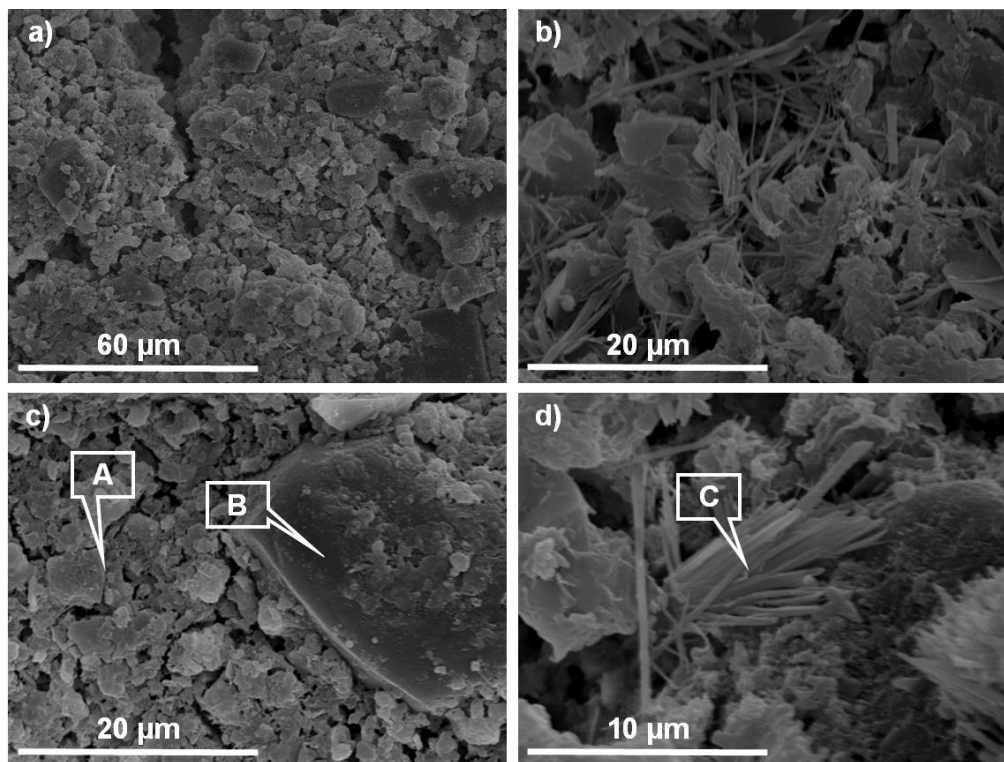
3.3.5 Comparison of Results from Different Techniques

The results of the three techniques for samples cured at 40 °C were compared. The three studies showed a high consumption of calcium hydroxide by the 3:7 CH/SCSA paste in the first days of testing. In electrical conductivity studies, the Lc started to increase after 120 h, whereas FTIR and TG studies showed no presence of calcium hydroxide after 3 days of curing. For studies with higher amounts of calcium hydroxide (4.5:5.5 for electrical conductivity studies and 5:5 for FTIR/TG studies), the SCSA did not consume all of the calcium hydroxide in the first 7 days of curing. For the 4.5:5.5 system, the Lc did not increase during the test, which means that the solution remained saturated. The DTG curve of the filtered material presented small amounts calcium hydroxide. FTIR/TG studies showed that the calcium hydroxide was not totally consumed after 7 days of curing. In general, the results from the electrical conductivity studies are similar to those found by the FTIR and TG techniques. The new method proposed by Tashima et al. (2014) has the advantage of being simpler and cheaper and also gave interesting results on pozzolanic reactivity behavior.

3.3.6 Scanning Electron Microscopy

SEM images of 3:7 pastes after 28 days of curing at 40 °C are shown in Figure 3.6. These images show a substantial presence of gel formed by the pozzolanic reaction. In addition, calcium hydroxide particles were not identified, indicating that all of it had been consumed by the SCSA (Figure 3.6a and Figure 3.6b). In Figure 3.6c, cementing gel is the main product. This gel is rich in calcium and silicon (spot A, mass percentage $\text{SiO}_2 = 35.7\%$; $\text{CaO} = 35.2\%$) and showed a Ca/Si atomic ratio of 1.06. In addition, a quartz particle can be seen surrounded by cementing gel (spot B). In Figure 3.6d, fibrillary C–S–H is highlighted. This phase is rich in calcium and silicon and also contained aluminum and iron (spot C, $\text{SiO}_2 = 38.3\%$; $\text{CaO} = 38.2\%$), with a Ca/Si atomic ratio of 1.07. This fibrous phase is also shown in Figure 3.6b.

Figure 3.6 – SEM images of 3:7 CH/SCSA paste after 28 days of curing cured at 40 °C



3.4 CONCLUSIONS

There is good potential for the valorization of sugar cane straw ash as a pozzolanic material. An increase in the use of biomass is inevitable because of the need for sustainable energy sources. The wastes generated from biomass burning show interesting properties as construction materials, and SCSCA seems likely to be used in the same way due to the promising results concerning its reactivity. In addition, the valorization of the ash in building construction has a sustainable profile since nonrenewable materials, such as Portland cement, can be replaced. The three techniques used in this study presented similar results for SCSCA reactivity. The electrical conductivity technique has the advantage of being simpler and cheaper than TGA and FTIR studies. The evaluation by thermogravimetric analysis shows high pozzolanic reactivity of SCSCA in CH/SCSCA mixes, finding values of lime fixation, for 5:5 proportion, higher than 80% after 1 day of curing at 40 °C and higher than 98% after 28 days. FTIR studies on CH/SCSCA pastes yielded important qualitative data: diminution of vibration bands related to raw materials (3641 cm^{-1} for CH and 1030 cm^{-1} for

SCSA) and increase of vibration bands related to pozzolanic reaction products (956 cm⁻¹). Electrical conductivity measurements let us classify the ash as medium reactivity type, accordingly to Tashima's method, similar to densified silica fume. Measurements of pH on these suspensions showed that a decrease in 0.2 units or higher confirms reaching an unsaturated state of the aqueous suspension. This study showed the potential for valorization of a biomass waste and assessed its pozzolanic reactivity using an interesting recently proposed technique.

REFERENCES

- ALYOSEFT, H. A.; SCHNEIDER, D.; WASSERSLEBEN, S.; ROGGENDORF, H.; WEIB, M.; EILERT, A.; DENECKE, R.; HARTMANN, I.; ENKE, D. *Meso/macroporous silica from miscanthus, cereal remnant pellets, and wheat straw*. **ACS Sustainable Chemistry and Engineering**, v. 3, n. 9, p. 2012–2021, 2015.
- ASTM C618–15. Standard Specification for Coal Fly Ash and Raw or Calcined Natural Pozzolan for Use in Concrete. ASTM International: West Conshohocken, PA, 2015.
- BNDES (Banco Nacional de Desenvolvimento Econômico e Social) and CGEE (Centro de Gestão e Estudos Estratégicos). *Sugar cane-based bioethanol: energy for sustainable development*. 1st ed. Rio de Janeiro, Brazil, 2008;
- CHAO-LUNG, H.; ANH-TUAN, B. L.; CHUN-SUN, C. *Effect of rice husk ash on the strength and durability characteristics of concrete*. **Construction and Building Materials**, v. 25, p. 3768–3772, 2011.
- CHEN, H.; WANG, W.; MARTIN, J. C.; OLIPHANT, A. J.; DOERR, P. A.; XU, J. F.; DEBORN, K. M.; CHEN, C.; SUN, L. *Extraction of lignocellulose and synthesis of porous silica nanoparticles from rice husks: a comprehensive utilization of rice husk biomass*. **ACS Sustainable Chemistry and Engineering**, v. 1, n. 2, p. 254–259, 2013.
- CORDEIRO, G. C.; TOLEDO FILHO, R. D.; ALMEIDA, R. S. *Influence of ultrafine wet grinding on pozzolanic activity of submicrometre sugar cane bagasse ash*. **Advances in Applied Ceramics**, v. 110, p. 453–456, 2011.
- DEMIS, S.; TAPALI, J. G.; PAPADAKIS, V. G. *An investigation of the effectiveness of the utilization of biomass ashes as pozzolanic materials*. **Construction and Building Materials**, v. 68, p. 291–300, 2014.
- FAOSTAT – Food and Agriculture Organization of the United Nations, Statistics Division. Sugar Cane Production. <http://faostat3.fao.org/home/E>.

FRÍAS, M.; VILLAR-COCIÑA, E.; VALENCIA-MORALES. *Characterisation of sugar cane straw waste as pozzolanic material for construction: calcining temperature and kinetic parameters*. **Waste Management**, v. 27, p. 533–538, 2007.

GALLEZOT, P. *Catalytic conversion of biomass: challenges and issues*. **ChemSusChem**, v. 1, p. 734–737, 2008.

GUZMÁN, A.; GUTIÉRREZ, C.; AMIGÓ, V.; GUTIÉRREZ, R. M.; DELVASTO, S. *Pozzolanic evaluation of the sugar cane leaf*. **Materiales de Construcción**, v. 61, p. 213–225, 2011.

HEWLETT, P. C. *Lea's Chemistry of Cement and Concrete*, 4th ed.; Elsevier: Oxford, 2008.

HONG, S. Y.; GLASSER, F. P. *Alkali bindings in cement pastes: Part I. The C-S-H phase*. **Cement and Concrete Research**, v. 29, p. 1893–1903, 1999.

JAMES, A. K.; THRING, R. W.; HELLE, S.; GHUMAN, H. S. *Ash management review applications of biomass bottom ash*. **Energies**, v. 5, n. 10, p. 3856–3873, 2012.

LEAL, M. R. L. V.; GALDOS, M. V.; SCARPARE, F. V.; SEABRA, J. E. A.; WALTER, A.; OLIVEIRA, C. O. F. *Sugar cane straw availability, quality, recovery and energy use: A literature review*. **Biomass Bioenergy**, v. 53, p. 11–19, 2013.

LEMOES, S. V.; DENADAI, M. S.; GUERRA, S. P. S.; ESPERANCINI, M. S. T.; BUENO, O. C.; TAKITANE, I. C. *Economic efficiency of two baling systems for sugar cane straw*. **Industrial Crops and Products**, v. 55, p. 97–101, 2014.

LUXÁN, M. P.; MADRUGA, F.; SAAVEDRA, J. *Rapid evaluation of pozzolanic activity of natural products by conductivity measurement*. **Cement and Concrete Research**, v. 19, n. 3, p. 63–68, 1989.

MALHOTRA, V. M.; MEHTA, P. K. *Pozzolanic and Cementitious Materials*; Gordon and Breach Publishers: Amsterdam, Vol. 1, 1996.

MCCARTER, W. J.; TRAN, D. *Monitoring pozzolanic activity by direct activation with calcium hydroxide*. **Construction and Building Materials**, v. 10, p. 179–184, 1996.

MESA-PÉREZ, J. M.; ROCHA, J. D.; BARBOSA-CORTEZ, L. A.; PENEDO-MEDINA, M.; LUENGO, C. A.; CASCAROSA, E. *Fast oxidative pyrolysis of sugar cane straw in a fluidized bed reactor*. **Applied Thermal Engineering**, v. 56, p. 167–175, 2013.

MORAES, J. C. B.; AKSAKI, J. L.; MELGES, J. L. P.; MONZÓ, J.; BORRACHERO, M. V.; SORIANO, L.; PAYÁ, J.; TASHIMA, M. M. *Assessment of sugar cane straw ash (SCSA) as pozzolanic material in blended Portland cement: Microstructural characterization of pastes and mechanical strength of mortars*. **Construction and Building Materials**, v. 94, p. 670–677, 2015.

MORAES, M. S. A.; GEORGES, F.; ALMEIDA, S. R.; DAMASCENO, F. C.; MACIEL, G. P. S.; ZINI, C. A.; JACQUES, R. A.; CARAMÃO, E. B. *Analysis of products from pyrolysis of Brazilian sugar cane straw*. **Fuel Processing Technology**, v. 101, p. 35–43, 2012.

PAYÁ, J.; BORRACHERO, M. V.; MONZÓ, J.; PERIS-MORA, E.; AMAHJOUR, F. *Enhanced conductivity measurement techniques for evaluation of fly ash pozzolanic activity*. **Cement and Concrete Research**, v. 31, n. 1, p. 41–49, 2001.

PAYÁ, J.; MONZÓ, J.; BORRACHERO, M. V.; VELÁZQUEZ, S.; BONILLA, M. *Determination of the pozzolanic activity of fluid catalytic cracking residue. Thermogravimetric analysis studies on FC3R–lime pastes*. **Cement and Concrete Research**, v. 33, p. 1085–1091, 2003.

TASHIMA, M. M.; SORIANO, L.; MONZÓ, J.; BORRACHERO, M. V.; AKASAKI, J. L.; PAYÁ, J. *New method to assess the pozzolanic reactivity of mineral admixtures by means of pH and electrical conductivity measurements in lime:pozzolan suspensions*. **Materiales de Construcción**, v. 64, n. 316, 12p., 2014.

THOMAS, M. *The effect of supplementary cementing materials on alkali-silica reaction: A review*. **Cement and Concrete Research**, v. 41, p. 1224–1231, 2011.

UNICA – União da Indústria de Cana-de-Açúcar Website. Sugar Cane Production. <http://www.unicadata.com.br/index.php?idioma=2>.

VASSILEV, S. V.; BAXTER, D.; ANDERSON, L. K.; VASSILEVA, C. G. *An overview of the composition and application of biomass ash. Part 1. Phase–mineral and chemical composition and classification*. **Fuel**, v. 105, p. 40–76, 2013.

VASSILEV, S. V.; BAXTER, D.; ANDERSON, L. K.; VASSILEVA, C. G. *An overview of the composition and application of biomass ash. Part 2. Potential utilisation, technological and ecological advantages and challenges*. **Fuel**, v. 105, p. 19–39, 2013.

WALKER, R.; PAVÍA, S. *Physical properties and reactivity of pozzolans, and their influence on the properties of lime–pozzolan pastes*. **Materials and Structures**, v. 44, p. 1139–1150, 2011.

4 PRELIMINARIES STUDIES ON SUGAR CANE STRAW ASH (SCSA) IN MORTARS OF PORTLAND CEMENT/SCSA AND BLAST-FURNACE SLAG/SCSA

The article entitled as "*Possibilities of reusing sugar cane straw ash in the production of alternative binders*" by J. C. B. Moraes, D. C. A. Queiroz, J. L. Akasaki, J. L. P. Melges, M. V. Borrachero, J. Payá and M. M. Tashima was published in the journal **Key Engineering Materials**, v. 668, p. 304-311, 2016.

Abstract: Sugar cane production is increasing in Brazil due the demand in manufacturing sugar and alcohol. During production process, several wastes are generated, such as sugar cane straw. After a burning process of this waste material, sugar cane straw ash (SCSA) is obtained, and may be used in the production of alternative binders. The aim of this paper is to assess the possibility of reuse SCSA as supplementary cementitious material in blended Portland cement mortars and as raw material in the production of alkali-activated binders. Blended Portland cement mortars were prepared using 0%, 20% and 30% of SCSA in replacement of Portland cement. For alkali-activated mortars, the activating solution is based on sodium hydroxide (NaOH) solution and different Slag/SCSA proportions in mass were assessed: 100/0, 75/25 and 50/50. Mechanical strength of mortars cured at room temperature was tested for 7 and 28 curing days. The results confirm that enhanced mechanical properties can be obtained for both alternative binders using SCSA on its composition.

Keywords: *Sugar cane straw ash, Portland cement, alkaline activation.*

4.1 INTRODUCTION

Portland cement is the one of the most used materials in the world, where the consumption in Brazil is about 59.4 million tons (SNIC, 2013) and the global consumption is about 3.7 billion tons (FICEM, 2013). Furthermore, to produce 1 ton of Portland cement requires about 2.8 ton of raw materials (GUO et al., 2010) and releases about 0.8 ton of CO₂, which represents 5%-8% of total CO₂ emission in the world (SHARP et al., 2010).

Many authors are researching new alternatives to minimize environmental problems related to the production of Portland cement. The use of supplementary cementitious materials are widely researched as alternative to reduce the Portland cement consumption. Mineral additions such as silica fume, blast furnace slag, fly ash (HEWLETT, 2008), rice husk ash and sugar cane bagasse ash (HEWLETT, 2008; PAYÁ et al., 2000; CORDEIRO et al., 2008; CORDEIRO et al., 2009) can be found in bibliography.

Another alternative is the use of alkali-activated binders, which has no Portland cement in its composition. Alkaline activation is a polymerization reaction, where an aluminosilicate material activated by an alkaline solution forms an amorphous pre-zeolitic structure (CASTALDELLI et al., 2013). The first application of alkaline activated binders was performed by Purdon in 1940, where the author used slag activated with sodium hydroxide (TORGAL et al., 2008). Nowadays, the use of aluminosilicate materials as fly ash and metakaolin (LIZCANO et al., 2012; RANJBAR et al., 2014) to produce alkali activated binders can also be found in bibliography. Binary system is used in order to improve the mechanical properties of alkali-activated binders, as slag/fly ash and slag/metakaolin (ONISEI et al., 2012; BERNAL et al., 2011).

This paper presents the use of sugar cane straw ash (SCSA). Sugar cane straw is a byproduct of the sugar cane production in the harvest process. Ripoli (1991) evaluated the calorific value of sugar cane straw as 1896 kcal/kg, which are higher than sugar cane bagasse. In addition, Ripoli, Gamero (2007) studied the best method to recover the sugar cane straw from field to generate energy. These researches show that the sugar cane straw is an important material to generate energy. However, in the process of burning to generate energy, a waste is obtained, the sugar cane straw ash. This paper intend to assess the SCSA as supplementary cementitious material in blended Portland cement mortars and as raw

material in the production of alkali-activated binders with slag. The Portland cement replacement for SCSA studied was 0%, 20% and 30%. The slag/SCSA proportions evaluated were 100/0, 75/25 and 50/50. The mechanical properties of specimens were assessed after 7 and 28 days of curing at 25°C.

4.2 EXPERIMENTAL

4.2.1 Materials and Equipment

Sugar cane straw ash (SCSA) is the main material in this work. Sugar cane straw was obtained from an agroindustry that produces alcohol through sugar cane. That material was burned in a furnace without temperature control to obtain the SCSA. The ash obtained was passed through sieves for removing large unburned particles and, after that, was milled for 50 minutes in a ball mill. The chemical characterization of the SCSA (Table 4.1) shows a reasonable content of SiO_2 and low content of Al_2O_3 and Fe_2O_3 . X-Ray Diffraction (DRX) of the SCSA (Figure 4.1) shows a deviation of the basis line between $\theta = 15^\circ$ and $\theta = 35^\circ$, characteristic of amorphous material. However, presence of quartz, calcite and diopside is noticed due the presence of soil among the ash. SEM images (Figure 4.2) reinforce results of DRX showing an amorphous structure of the SCSA.

Figure 4.1 – X-Ray Diffraction of SCSA

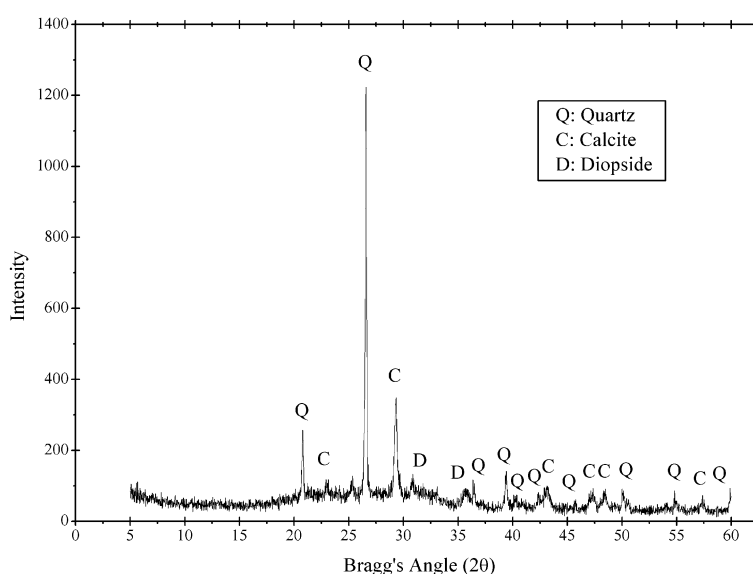
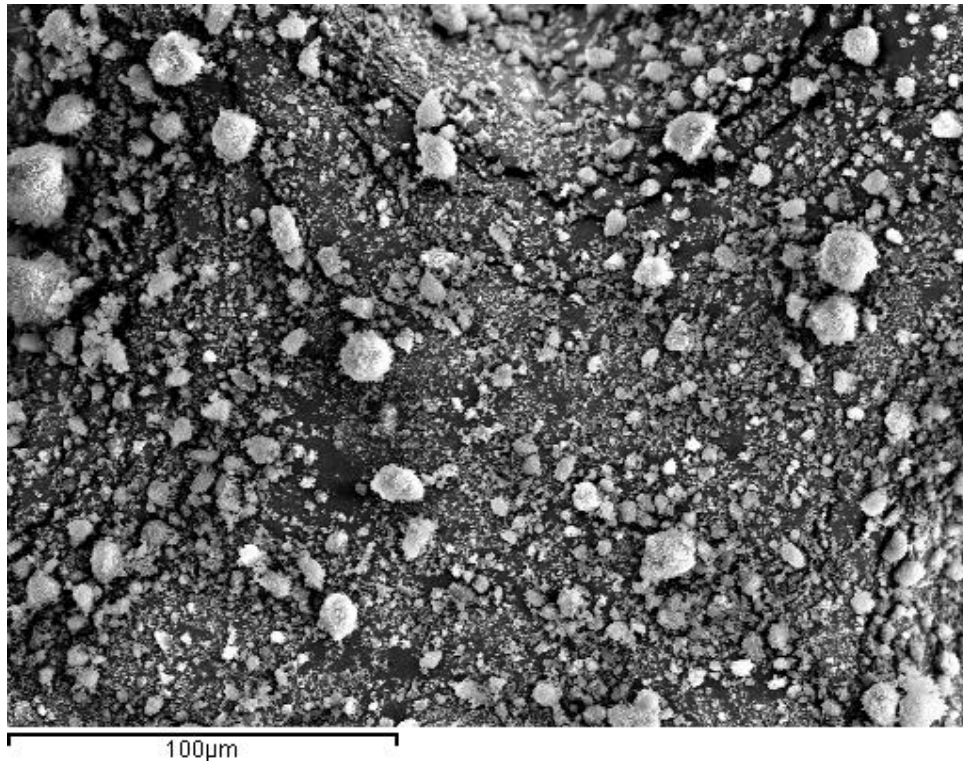


Figure 4.2 – SEM images of SCSA



In the preparation of Portland cement mortars, the Brazilian Portland cement used was the CPV – ARI Plus®, which has more than 95% of clinker in its composition. This Portland cement was used because has no pozzolan in its composition, which could interfere in the SCSA pozzolanic activity.

Blast furnace slag (BFS) was used in the preparation of alkali-activated mortars. The material was obtained from Ribas do Rio Pardo-MS, and its chemical composition is shown in Table 4.1.

In both mortars, the aggregate was standard natural sand (ABNT, 2014), obtained from Castilho-SP with fineness modulus of 2.05. Water was used from supply system of Ilha Solteira-SP.

Table 4.1 – Chemical composition of blast furnace slag (BFS) and sugar cane straw ash (SCSA)

Oxide	SiO ₂	Al ₂ O ₃	Fe ₂ O ₃	CaO	Na ₂ O	K ₂ O	SO ₃	Others	LOI
SCSA	36.5	2.8	3.4	16.4	0.2	7.9	4.4	12.9	15.5
BFS	33.0	11.5	0.6	43.5	0.3	0.4	1.89	8.1	0.1

The specimens were molded in cubes of 5x5x5 cm, cured at room temperature (25°C, RH~100%) and compressive strength of mortars were carried out in a universal test machine for 7 and 28 curing days.

4.2.2 Experimental Procedures

4.2.2.1 Portland cement mortars

Portland cement mortars were prepared with a water/binder ratio of 0.50 and a sand/binder ratio of 2.5, both in mass. These proportions ensure a good workability and mechanical properties of the mortars without superplasticizer, being possible to evaluate only the influence of SCSA in both characteristics.

The replacements of Portland cement by SCSA were 20% and 30% in mass, called CP20 and CP30 respectively. A mortar without SCSA called CP0 were prepared as a control. High proportion of SCSA is justified due to good results in literature with pozzolanic materials replacing considerable content of Portland cement (CORDEIRO et al., 2008; GUZMÁN et al., 2011; TASHIMA, 2012).

The specimens were cured at room temperature (RH~100% and 25°C) during 24 hours and then, they were demolded. After that, they were sealed in plastic containers, and cured in the same conditions mentioned above until the mechanical strength test. The compressive strength of mortars was assessed after 7 and 28 days of curing.

4.2.2.2 Alkali-activated mortars

Alkaline activated mortars were prepared with a water/cementitious materials ratio of 0.45 in mass, which is a lower value than compared to the Portland cement mortars. The

cementitious content was the sum of BFA and SCSA; sodium hydroxide was not considered. The sand/binder ratio was 2.5 in mass, as the Portland cement mortars. Sodium hydroxide solution was used as activating solution with Na^+ concentration of 8 mol.kg^{-1} .

The proportions of BFS/SCSA assessed were 100/0, 75/25 and 50/50, called AA0, AA25 and AA50, respectively. Differently of the Portland cement mortars, maximum slag replacement in alkali-activated mortars was 50% (CASTALDELLI, 2013).

Mortars specimens were demolded and cured using the same procedures as Portland cement mortars. The compressive strength was also performed after 7 and 28 days of curing.

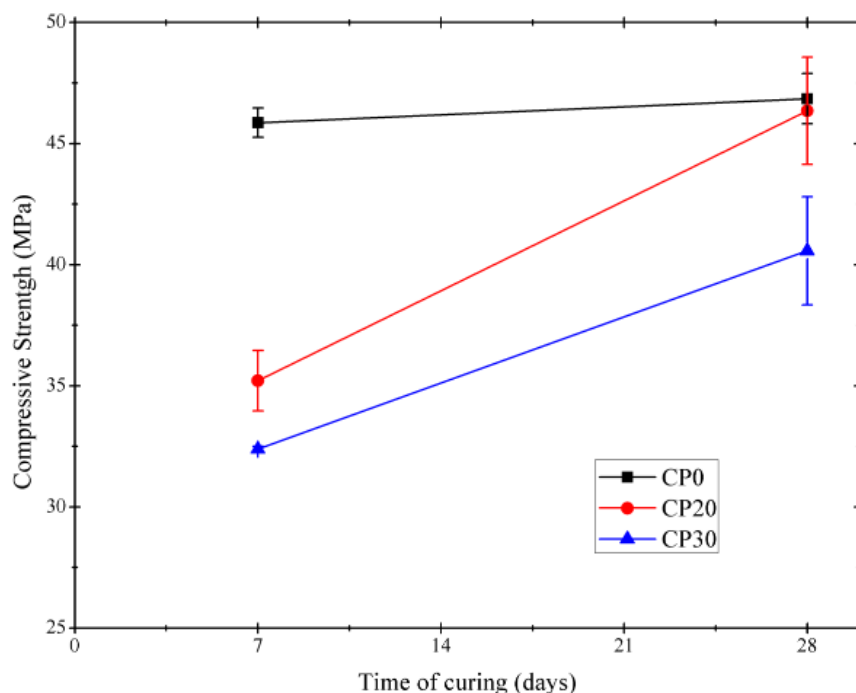
4.3 RESULTS AND DISCUSSIONS

4.3.1 Compressive Strength of Portland Cement Mortars

The results of compressive strength of Portland cement mortars are shown in Figure 4.3. After 7 days of curing, both CP20 and CP30 mortars presented lower compressive strength than CP0 (control mortar). The reduction of compressive strength from CP0 to CP20 is about 20% and from CP0 to CP30 is about 30%. These percentage values of reduction are similar to the percentage replacement of Portland cement by SCSA in both cases. Probably, it is due to SCSA did not start to react with the calcium hydroxide from cement hydration reaction.

After 28 days of curing, the compressive strength for both CP20 and CP30 increased to 46.36 MPa and 40.57 MPa, respectively. CP20 had about the same compressive strength than the CP0 (46.85 MPa), but the CP30 still is below of the control. For this curing age, the increase from the compressive strength of both blended mortars is related to the pozzolanic reaction. There is no significantly reduction from CP0 to CP20 and a reduction of 13.4% from CP0 to CP30. Both percentage values are significantly below than the replacement of Portland cement for SCSA (20% and 30%, respectively). The presence of amorphous SiO_2 in SCSA (36.5%) is the key for explaining the pozzolanic behavior (HEWLETT, 2008).

Figure 4.3 – Compressive strength of Portland cement mortars



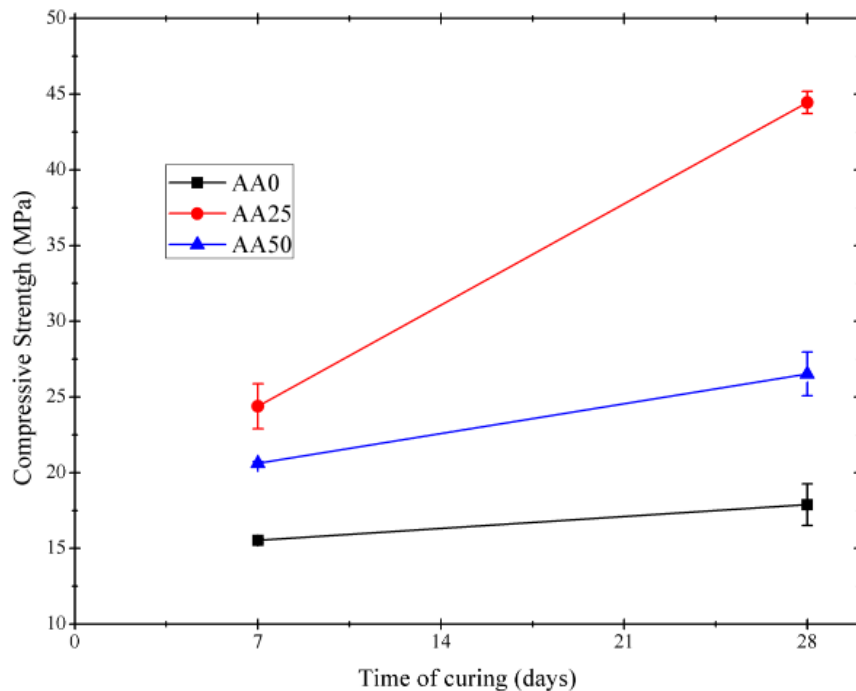
4.3.2 Compressive Strength of Alkaline Activated mortars

The results of compressive strength for alkaline activated mortars are shown in Figure 4.4. After 7 days of curing, AA25 and AA50 presented compressive strength (24.40 MPa and 20.62 MPa, respectively) higher than the corresponding to AA0 (15.52 MPa). It is noticed that the binary system with SCSA has higher compressive strength since earlier curing ages. The increase of compressive strength after 7 days of curing from AA0 to AA25 is 57.3%, and from AA0 to AA50 is 32.8%. This behaviour is attributed to the presence of reactive silica in SCSA: soluble silica in high alkaline medium plays a very important role in the formation of the C(N)-A-S-H gel and consequently in the yielded strength.

After 28 days of curing, AA25 and AA50 increased their compressive strength (44.45 MPa and 26.52 MPa, respectively). However, AA0 not increased significantly compressive strength (17.89 MPa). The increase of compressive strength after 28 days of curing from AA0 to AA25 is 148.5%, and from AA0 to AA50 is 49.1%. Apparently, the

curing period between 7 and 28 days favored the formation of more C(N)-A-S-H gel and consequently an increasing in the strength is produced.

Figure 4.4 – Compressive strength of alkaline activated mortars



4.4 CONCLUSIONS

The use of SCSA in the production of alternative binders showed to be a good possibility for reusing this waste material.

First, in Portland cement mortars, the SCSA replacement of 20% did not change the mechanical behavior from the control mortar after 28 days of curing. However, the SCSA replacement of 30% decreased 13.4% the compressive strength after 28 days of curing.

Finally, in alkali-activated mortars, the results of SCSA were better than compared to the Portland cement mortars. After 7 and 28 days of curing, both AA25 and AA50 presented higher compressive strength compared to AA0, indicating that blending BFS with SCSA is very interesting practice for enhancing mechanical properties.

REFERENCES

ASSOCIAÇÃO BRASILEIRA DE NORMAS TÉCNICAS – ABNT. NBR 7214 – Areia para ensaio de cimento. Rio de Janeiro, 2012.

BERNAL, S. A.; RODRÍGUEZ, E.; MEJÍA DE GUTIÉRREZ, R.; GORDILLO, M.; PROVIS, J.L. *Mechanical and thermal characterisation of geopolymers based on silicate-activated metakaolin/slag blends*. **Journal of Materials Science**, v. 46, p. 5477–5486, 2011.

CASTALDELLI, V. N.; AKASAKI, J. L.; MELGES, J. L. P.; TASHIMA, M. M.; SORIANO, L.; BORRACHERO, M. V.; MONZÓ, J.; PAYÁ, J. *Use of Slag/Sugar Cane Bagasse Ash (SCBA) Blends in the Production of Alkali-Activated Materials*. **Materials**, v. 6, 3108-3127, 2013.

CORDEIRO, G. C.; TOLEDO FILHO, R. D.; FAIRBAIRN, E. M. R. *Effect of calcination temperature on the pozzolanic activity of sugar cane bagasse ash*. **Construction and Building Materials**, v. 23, p. 3301-3303, 2009.

CORDEIRO, G. C.; TOLEDO FILHO, R. D.; TAVARES, L. M.; Fairbairn, E. M. R. *Ultrafine grinding of sugar cane bagasse ash for application as pozzolanic admixture in concrete*. **Cement and Concrete Research**, v. 39, p. 110-115, 2008.

FICEM - Inter-American Cement Federation. Statistical Report 2013.
http://www.ficem.org/estadisticas/statiscal_report_2013.pdf.

GUO, X.; SHI, H.; DICK, W.A. *Compressive strength and microstructural characteristics of class C fly ash geopolymer*. **Cement and Concrete Composites**, v. 32, p. 142–147, 2010.

GUZMÁN, A.; GUTIÉRREZ, C.; AMIGÓ, V.; MEJIA DE GUTIÉRREZ, R.; DELVASTO, S. *Pozzolanic evaluation of the sugar cane leaf*. **Materiales de Construcción**, v. 61, 213-225, 2011.

HEWLETT, P. C. *Lea's Chemistry of Cement and Concrete*, 4th ed.; Elsevier: Oxford, 2008.

LIZCANO, M.; KIM, H. S.; BASU, S.; RADOVI, M. *Mechanical properties of sodium and potassium activated metakaolin-based geopolymers*. **Journal of Materials Science**, v. 47, p. 2607-2616, 2012.

ONISEI, S.; PONTIKES, Y.; VAN GERVEN, T.; ANGELOPOULOS, V. N.; VELEA, T.; PREDICA, V.; Moldovan, P. *Synthesis of inorganic polymers using fly ash and primary lead slag*. **Journal of Hazardous Materials**, v. 205–206, p. 101–110, 2012.

PAYÁ, J.; MONZÓ, J.; BORRACHERO, M. V.; PERIS-MORA, E.; ORDÓÑEZ, L. M. *Studies on crystalline rice husk ashes and the activation of their pozzolanic properties*. **Waste Management**, v. 1, p. 493-503, 2000.

RANJBAR, N.; MEHRALI, M.; ALENGARAM, U. J.; METSELAAR, H. S. C.; JUMAAT, M. Z. *Compressive strength and microstructural analysis of fly ash/palm oil fuel ash based geopolymer mortar under elevated temperatures*. **Construction and Building Materials**, v. 65, p. 114-121, 2014.

RIPOLI, M. L. C.; GAMERO, C. A. *Palhiço de cana-de-açúcar: ensaio padronizado de recolhimento por enfardamento cilíndrico*. **Energia na Agricultura**, v. 22, n. 1, p. 75-93, 2007.

RIPOLI, M. L. C. Utilização do material remanescente de colheita de cana-de-açúcar [*Saccharum spp*] – Equacionamento dos balanços energético e econômico (In portuguese). 150 p. Habilitation Thesis – Escola Superior de Agricultura “Luiz de Queiroz”, Universidade de São Paulo, Piracicaba, 1991.

SINDICATO NACIONAL DA INDÚSTRIA DO CIMENTO – SNIC. Consumo Mensal de 2013. http://www.snic.org.br/numeros_dinamico.asp.

SHARP, J.H.; GARTNER, E.M.; MACPHEE, D.E. *Novel cement system (sustainability). Session 2 of the Fred Glasser cement science symposium*. **Advances in Cement Research**, v. 22, n. 4, p. 195–202, 2010.

TASHIMA, M. M. Producción y caracterización de materiales cementantes a partir del Silicoaluminato Cálcico Vítreo (VCAS). 454 p. PhD Thesis - Universitat Politècnica de València, Valencia, 2012.

TORGAL, F. P.; GOMES, J. C.; JALALI, S. *Alkali-activated binders: A review Part 1. Historical background, terminology, reaction mechanisms and hydration products*. **Construction and Building Materials**, v. 22, p. 1305-1314, 2008.

5 SUGAR CANE STRAW ASH AS SOLID PRECURSOR IN ALKALI-ACTIVATED BINDERS BASED ON BLAST FURNACE SLAG: SOLUTIONS WITH $[N^+]$ OF 8 MOL.KG⁻¹ AND SiO₂/Na₂O RATIOS OF 0-0.75

The article entitled as "*Increasing the sustainability of alkali-activated binders: The use of sugar cane straw ash (SCSA)*" by J. C. B. Moraes, M. M. Tashima, J. L. Akasaki, J. L. P. Melges, J. Monzó, M. V. Borrachero, L. Soriano and J. Payá and was published in the journal **Construction and Building Materials**, v. 124, p. 148-154, 2016.

Abstract: Alkali-activated binders are the new trend in building construction studies due their good mechanical properties and environmental advantages. These type of binders are obtained by a mixing of a solid precursor with an activating solution. In this study, the influence of sugar cane straw ash (SCSA) obtained from an auto-combustion process on blast-furnace slag (BFS) based alkali-activated binders was assessed as solid precursor. The studied proportions of BFS/SCSA were 100/0 (control), 85/15, 75/25, 67/33 and 50/50 (by mass). Regarding to the activating solutions, three different mixtures were used: only NaOH (8 mol.kg⁻¹ Na⁺) and two different combinations of NaOH with sodium silicate (8 mol.kg⁻¹ Na⁺ and SiO₂/Na₂O molar ratios of 0.50 and 0.75). The water/binder was maintained constant. To assess the influence of SCSA on BFS-alkali activated binders, mortars were evaluated in terms of compressive strength (3-90 days curing time at room temperature and 3 days at 65°C); and pastes were studied to justify these results by means of thermogravimetric analysis (TGA), Fourier transform infrared spectroscopy (FTIR) and field emission scanning electron microscopy (FESEM). The presence of SCSA in the binder greatly improved the compressive strength when compared to the control BFS mortars, reaching values higher than 50 MPa after 90 days. SCSA/BFS samples activated with sodium hydroxide yielded similar compressive strength values to those obtained for BFS mortars activated with sodium silicate. In the new binders, the partial replacement of BFS,

the total replacement of sodium silicate solution and a new way of valorizing sugar cane straw enhanced sustainability.

Keywords: *silicates, mechanical properties, biomass, renewable resources, microstructural characterization.*

5.1 INTRODUCTION

The development of sustainable construction materials is currently a new trend under investigation (PHAIR, 2006). Alkali-activated (AA) binders are being researched as an alternative construction material to replace the use of Portland cement (ROSTAMANI; BRENDLEY, 2003). This type of binder is obtained when a highly alkali concentrated solution activates, due to the high pH, a raw material, which can be metakaolin, fly ash, or blast furnace slag, among others (KUENZEL et al., 2013; NIKOLIC et al., 2015; RAKHIMOVA; RAKHIMOV, 2015). The advantages of using AA binders instead of Portland cement based-mixtures are both technological and environmental. In some cases, the compressive strength and durability of these binders are higher, and they are more sustainable since they consume less energy, release less CO₂ and the reuse of wastes (DAVIDOVITS, 2002; McLELLAN et al., 2011; DAVIDOVITS, 2001; MEJÍA et al., 2016, NIMWINYA et al., 2016). Although AA binders present advantages in terms of sustainability compared to the ordinary Portland cement (OPC), it is possible to increase even more the benefits from this type of material.

Blast furnace slag (BFS), one of the most commonly used raw materials in the production of AA binders, as it presents many advantages in terms of its technological properties (WANG et al., 1995). In recent years, blast furnace slag has been used in new AA systems with the addition of supplementary cementitious materials (RAKHIMOVA; RAKHIMOV, 2014; MARTINEZ-LOPEZ; ESCARLATE-GARCIA, 2016). This has become an interesting method in the cement industry, taking into account that the cost of blast furnace slag is on the same order as that of Portland cement (MEYER, 2009). Thus, the design of new binary blast furnace slag-based systems is an interesting topic. In the preparation of AA binders, the alkaline solution is the most pollutant, expensive reagent and consumes the most energy. In general, this solution is composed of alkaline hydroxides and silicates; the latter emit high amounts of CO₂ and have a high economic cost (MELLADO

et al., 2014). An alternative route is to reduce the use of alkaline silicates, replacing them with another more sustainable silicon source. As example, studies carried out on rice husk ash (RHA) in the preparation of alkaline solutions showed similar mechanical properties for AA systems when compared to a control solution prepared with silicate-based chemical reagents (BOUZÓN et al., 2014).

This paper introduces a new raw material to produce an AA binder: sugar cane straw ash (SCSA). Brazil is the major sugar cane producer in the world with a production of 632 million tons in 2014-2015, which represents an increase of 64% in the last ten years (UNIÃO DA INDÚSTRIA DE CANA-DE-AÇÚCAR – UNICA, 2016). The straw represents 15-20% of the total mass of sugar cane produced; during harvesting, this straw is abandoned on the field, producing some environmental and technical problems (LEAL et al., 2013). This residue could be transformed into ash by burning because it is a valuable biomass, yielding sugar cane straw ash (SCSA). An interesting destination for SCSA is in the construction materials sector (MORAES et al., 2015). In this particular study, it will be assessed as a component in an AA binder system with blast furnace slag. The huge amount of this waste generated and previous studies on agroindustry residues in AA binders support this study (PEREIRA et al., 2015; CASTALDELLI et al., 2013). SCSA from this study was obtained from an auto-combustion process of the straw. The ash was chemically and physically characterized, then assessed in BFS/SCSA systems (solid precursors) at these proportions: 100/0 (control), 85/15, 75/25, 67/33 and 50/50. Three alkaline solutions were designed to activate the precursor: an NaOH solution and two NaOH/sodium silicate solutions. The Na^+ concentration in these solutions was held constant, whereas the $\text{SiO}_2/\text{Na}_2\text{O}$ molar ratio (designated as ϵ) of the solution was varied to assess the influence of sodium silicate in the mixture. The compressive strength of the mortars, thermogravimetric analysis (TGA), Fourier transform infrared spectroscopy (FTIR), X-ray diffraction (XRD) and field emission scanning electron microscopy (FESEM) of the pastes were performed in order to assess the influence of SCSA on the BFS-based systems. The objective of this study was to valorize a waste from the agro-industry and reduce the use of a less sustainable material in the alkaline solution, i.e. sodium silicate. Additionally, savings in the consumption of BFS was an indirect goal.

5.2 MATERIALS AND METHODS

5.2.1 Materials and Equipment

The sugar cane straw was received from a sugar cane plantation near of Ilha Solteira (São Paulo, Brazil). This material was burned by an autocombustion process, in which the maximum temperature reached was 700°C. The residue from combustion was passed through sieves to remove the unburned matter, and the resulting ash was milled in a ball mill for 50 minutes in order to increase its reactivity. Blast furnace slag was obtained from Ribas do Rio Pardo (Mato Grosso do Sul, Brazil). Regarding the chemical composition, SCSA presented SiO₂, Al₂O₃, CaO as main components. Table 5.1 summarizes the chemical composition of the solid precursors (BFS and SCSA). . In their composition, the most interesting oxides for AA binders are the SiO₂, Al₂O₃ and CaO. AA binders based on BFS usually yields a (C,N)-A-S-H gel, whose mechanical properties can be improved by the use of siliceous source. The SCSA is this source in the present case, and replacing partially the BFS, can also improve the mechanical properties of the final AA binder (RAKHIMOVA; RAKHIMOV, 2014). In particle size studies, SCSA presented a mean particle diameter (D_{med}) and median particle diameter (D_{50}) of 18.1 and 10.6 μm respectively; for the BFS, these values were 27.5 and 21.4 μm , respectively.

Table 5.1 – Chemical composition of SCSA and BFS by weight percentage

Solid Precursors	SiO₂	Al₂O₃	Fe₂O₃	CaO	MgO	K₂O	SO₃	Cl	Others	LOI
SCSA	58.6	9.0	8.4	4.6	1.6	5.4	1.9	0.7	3.3	6.5
BFS	33.0	11.5	0.6	43.5	7.3	0.4	1.9	0.1	1.6	0.1

Both sodium hydroxide pellets (solid, 98% purity) and sodium silicate (solid, 18 wt% Na₂O, 63 wt% SiO₂) were supplied by Dinâmica Química. In the preparation of solution, NaOH pellets were dissolved in water, producing an increase in the temperature of the solution. When sodium silicate was used, it was added to the hot NaOH solution in order to facilitate the dissolution rate. Prepared solutions were used when they reached room temperature.

Mortars were assessed by compressive strength in an EMIC Universal Machine with a 2000 kN load limit at a loading rate of 0.5 MPa/s. The compressive strength was an average of testing values on three cubic mortars of 50 x 50 x 50 mm³. Regarding to the pastes studies, the TGA equipment used was a Mettler-Toledo TGA 850, where the specimen was heated in a 100 μ L sealed pin-holed aluminum crucible in the temperature range of 35-600°C, with a heating rate of 10°C.min⁻¹ and N₂ atmosphere (75 mL.min⁻¹ gas flow). FTIR was performed by a Bruker Tensor 27 in the range of 400 and 4000 cm⁻¹. XRD patterns were obtained by a Bruker AXS D8 Advance with a voltage of 40 kV, current intensity of 20 mA and a Bragg's angle (2θ) in the range of 5-70°. Finally, FESEM images were taken by a ZEISS Supra 55.

5.2.2 Alkali activated binder dosage

Five different BFS/SCSA proportions were assessed in this study: 100/0 (control), 85/15, 75/25, 67/33 and 50/50 (by mass). For the alkaline activating solution, the Na⁺ concentration was held constant at 8 mol.kg⁻¹, whereas three SiO₂/Na₂O molar ratio of the solution (ϵ) were assessed: 0 (only sodium hydroxide in the solution), 0.50 and 0.75. The water/binder proportion (being binder the sum of BFS and SCSA) was 0.45 and, for mortars, the selected sand/binder ratio was 2.5. Some mortars (ϵ = 0.75 with 67/33 and 50/50 ratios) presented rheological problems and they were not cast. Mortar specimens were assessed after 3 (25°C and 65°C, RH > 95%), 7, 28 and 90 curing days (only 25°C, RH > 95%). Paste samples were tested after 7, 28 and 90 curing days (25°C, RH > 95%) for TGA and FTIR studies; for XRD and FESEM analysis, only samples with 28 days of curing time (25°C, RH > 95%) were analyzed.

The nomenclature for AA binders studied in this paper is x-y/z, where the "x" is related to the alkaline activating solution design and "y/z" is the BFS/SCSA proportion in the mixture. The "x" can be N, SS50 and SS75, which are related the ϵ value equals to 0 (only sodium hydroxide in the solution), 0.50 and 0.75, respectively. Finally, the "y/z" values were 100/0, 85/15, 75/25, 67/33 and 50/50, as the already presented BFS/SCSA proportions. The specimen' names are provided in Table 5.2.

5.3 RESULTS AND DISCUSSION

The compressive strength (R_c) values of the mortars are summarized in Table 5.2. The mean data were obtained from three $50 \times 50 \times 50\text{mm}^3$ cubic specimens. In order to highlight the importance of SCSA in the mixture, a factor named γ is proposed (Figure 5.1), which represents the compressive strength ratio of a specimen with SCSA and its respective control ($R_{c\text{SCSA}} / R_{c\text{control}}$) under the same curing conditions. On one hand, it was observed that, for specimens with $\varepsilon = 0$, SCSA had an important role in the development of compressive strength. These mixtures presented higher strengths than the control sample after 3 days of curing, with γ factor values above 1.0 (Fig. 5.1a). On the other hand, for the samples activated with both sodium hydroxide and sodium silicate ($\varepsilon = 0.50$ and $\varepsilon = 0.75$), the compressive strengths of the SCSA mortars were similar or lower than their respective controls, with γ factor values lower than 1.0 after 3 days of curing (Fig. 5.1a). This behavior suggests that the presence of SCSA, when silicate anions are available in the prepared solution, does not provide any advantage, and produces a small delay in the cementing effect. This was especially marked for $\varepsilon = 0.75$. Curiously, at this early age, the strength of SS75-100/0 (12.8 MPa) was surpassed by some SCSA containing mortars with $\varepsilon = 0$ (e.g. 17.2 MPa for N-67/33), suggesting that dissolved silica from SCSA plays a similar role in the cementing reaction than silicate anions from sodium silicate. Similar trends were observed after 7 days of curing time (Fig. 5.1b). Interestingly, all SCSA specimens showed better strength results than the control sample after 28 days of curing, mainly for the specimens activated with only sodium hydroxide ($\varepsilon = 0$), which yielded significantly higher compressive strengths than the control sample. For this curing time, the γ factor reached for N-75/25 was above 2.5 (Fig. 5.1c). In contrast to the behavior observed after 3 and 7 days of curing, SCSA mortars with $\varepsilon = 0.50$ and $\varepsilon = 0.75$ gained important strength: after 28 days of curing, there was a positive effect when silicate anions were incorporated by means of both the alkaline solution and the ash. Thus, the γ factor was in the range of 1.67-1.89 for 15-25% SCSA mortars with $\varepsilon = 0.50$, and in the range of 1.13-1.19 for 15-25% SCSA samples with $\varepsilon = 0.75$ (Fig. 5.1c). Control mortars (only BFS) significantly increased in strength from 28 to 90 days of curing for all three activating solutions. Despite this, all SCSA containing mortars, after 90 days of curing, yielded similar or higher strength values than the control samples ($\gamma \geq 1$, Fig. 5.1d). Thus, for mortars with $\varepsilon = 0$, the γ factor values were in the range of 1.39-1.78, confirming the effectivity of the ash in the NaOH-alkali activated

BFS mortars. The contribution of silicate anions dissolved from the ash led to 90-day strength values similar to those obtained for BFS mortars with $\varepsilon = 0.50$ - 0.75 (e.g. 48.5 MPa for N-75/25 versus 51.2 MPa for SS50-100/0).

In order to assess strength development at higher curing temperatures, a set of mortars was cured at 65°C. For the studied BFS, the increase in curing temperature did not significantly increase the strength after 3 days of curing; only for the SS75-100/0 specimen was strength development much higher than for the mortar cured at 25°C (27.0 MPa versus 12.8 MPa). This behavior means that the presence of an important quantity of silicate anions in the mixture plays a decisive role in enhancing the mechanical properties with a high curing temperature. In an interesting way, for all SCSA containing mortars, the increase in curing temperature led to good strength development and, after 3 days, all samples yielded more than 20 MPa. Particularly, SS50-75/25 and SS50-67/33 reached 40 MPa. This behavior indicates that, at a high curing temperature, the role of SCSA, in terms of strength development, is much more effective than sodium silicate added in the activating solution. Thus, sodium silicate as a chemical reagent could be successfully replaced by SCSA, which also reduced the amount of BFS consumed.

These presented results confirm that is possible to obtain a more sustainable AA binder accordingly the following two factors: the reuse of a biomass waste and the replacement of the sodium silicate solution by an alternative siliceous source. As the biomass became a trend in energy generation in the last years (CHEN et al., 2015), the reuse of these wastes is a form of sustainability. Another issue is the CO₂ emission of the sodium silicate production, which is the highest one among the materials used in the AA binders design (MELLADO et al., 2014). Using a less pollutant siliceous source in the place of this activator increases the sustainable characteristic of the AA binder. The similarity on compressive strength of mortars with SCSA (ε equal to 0) and with only BFS (ε equal to 0.50 or 0.75) is the confirmation of the improvement in the new designed AA binder in terms of sustainability.

Table 5.2 – Specimens' names, compressive strength of mortars (MPa) and their standard deviations

Specimens' name	ϵ (SiO ₂ /Na ₂ O)	BFS/SCSA	Curing time				
			25°C				65°C
			3 days	7 days	28 days	90 days	3 days
N-100/0	0	100/0	10.7 ± 0.8	15.5 ± 0.2	16.9 ± 2.0	27.3 ± 0.8	11.9 ± 0.2
N-85/15		85/15	15.1 ± 0.3	25.1 ± 0.5	34.4 ± 0.3	37.9 ± 3.2	20.7 ± 0.3
N-75/25		75/25	15.9 ± 0.3	24.4 ± 1.9	44.4 ± 1.0	44.5 ± 2.0	25.7 ± 1.7
N-67/33		67/33	17.2 ± 0.2	23.9 ± 2.3	37.4 ± 3.7	43.6 ± 2.2	30.0 ± 1.4
N-50/50		50/50	10.6 ± 0.3	20.6 ± 0.1	26.5 ± 1.9	47.9 ± 1.2	34.3 ± 2.5
SS50-100/0	0.50	100/0	14.3 ± 0.4	25.6 ± 0.5	28.3 ± 2.1	51.2 ± 1.4	18.6 ± 0.8
SS50-85/15		85/15	15.8 ± 0.4	31.2 ± 0.7	47.2 ± 2.2	49.8 ± 3.1	31.8 ± 1.1
SS50-75/25		75/25	15.2 ± 0.1	25.6 ± 1.1	53.3 ± 2.9	49.2 ± 0.7	40.7 ± 2.0
SS50-67/33		67/33	13.2 ± 0.2	26.6 ± 0.1	38.1 ± 3.3	49.5 ± 1.2	40.4 ± 1.6
SS50-50/50		50/50	9.4 ± 0.6	18.4 ± 1.7	29.8 ± 2.9	50.8 ± 2.8	35.2 ± 1.6
SS75-100/0	0.75	100/0	12.8 ± 0.3	26.7 ± 0.6	39.3 ± 1.1	51.5 ± 4.1	27.0 ± 0.5
SS75-85/15		85/15	6.1 ± 0.2	19.1 ± 0.5	44.4 ± 2.9	56.0 ± 1.3	27.3 ± 0.6
SS75-75/25		75/25	4.8 ± 0.4	14.0 ± 0.5	46.8 ± 3.8	51.4 ± 3.1	32.6 ± 3.1

Figure 5.1 – Calculated γ factor for specimens with BFS/SCSA ratios of 85/15, 75/25, 67/33 and 50/50, in the ϵ value range of 0-0.75, after: a) 3 days of curing, b) 7 days of curing, c) 28 days of curing and d) 90 days of curing (at 25°C)

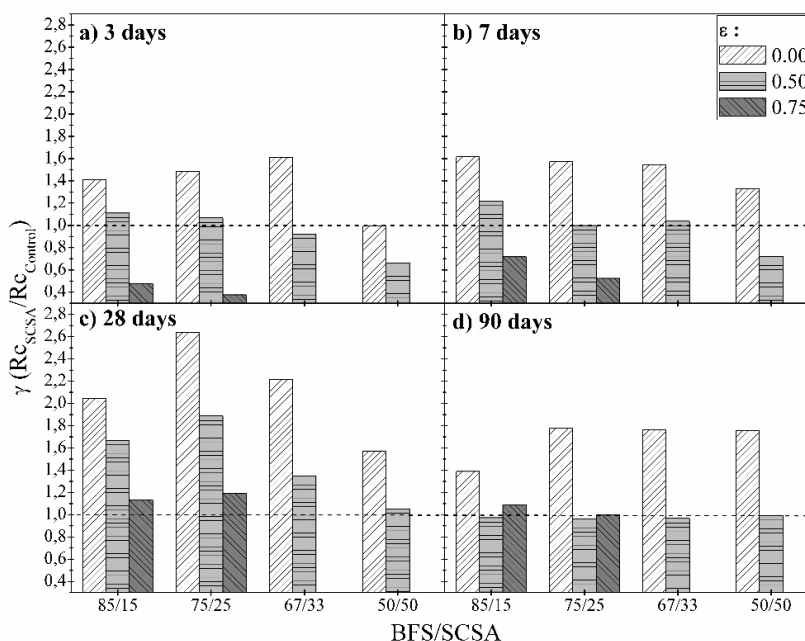


Figure 5.2 shows the DTG curves for N-100/0, N-75/25, N-50/50, SS50-100/0, SS50-75/25 and SS50-50/50 pastes cured for 7, 28 and 90 days at 25°C. Table 5.3 shows the mass losses of these pastes in the temperatures intervals of 35-180°C, 180-250°C and 250-600°C. In the DTG curves (Fig. 5.2a, Fig. 5.2b and Fig. 5.2c), the peaks in the range 140-155°C are related to the dehydration of (N,C)-A-S-H gel, whereas the peak at 180-200°C can be related to C-A-S-H compounds (e.g. stratlingite, C_2ASH_8) (PALOU et al., 2005; CHEN; BROUWERS, 2007). In general terms, the mass loss related to the (N,C)-A-S-H gel increased with the curing age for all mixtures, indicating that the formation of AA products was taking place. The presence of peaks at 180-200°C was found after 7 days (small peak or weak shoulder) and 28 days of curing (well-defined peak), and increased with the amount of SCSA in the mixture. After 90 days of curing, the peak related to C-A-S-H compounds disappeared, and the mass loss in the range of 180-250°C decreased (Table 5.3), indicating that Na^+ ions cross-linked with this compound and formed a (N,C)-A-S-H gel (PROVIS et al., 2015).

Figure 5.2 – DTG curves for the N-100/0 (a), SS50-100/0 (b), N-75/25 (c), SS50-75/25 (d), N-50/50 (e) and SS50-50/50 (f) pastes cured for 7, 28 and 90 days at 25°C

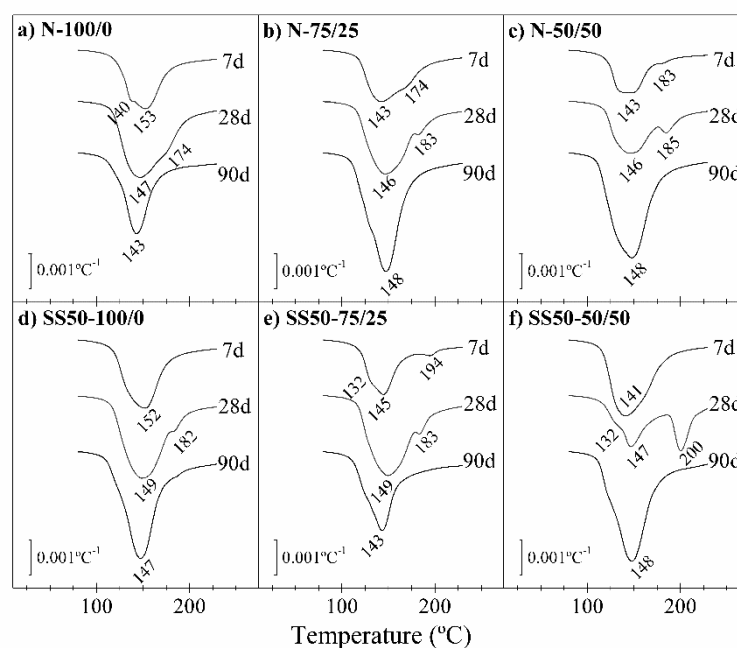
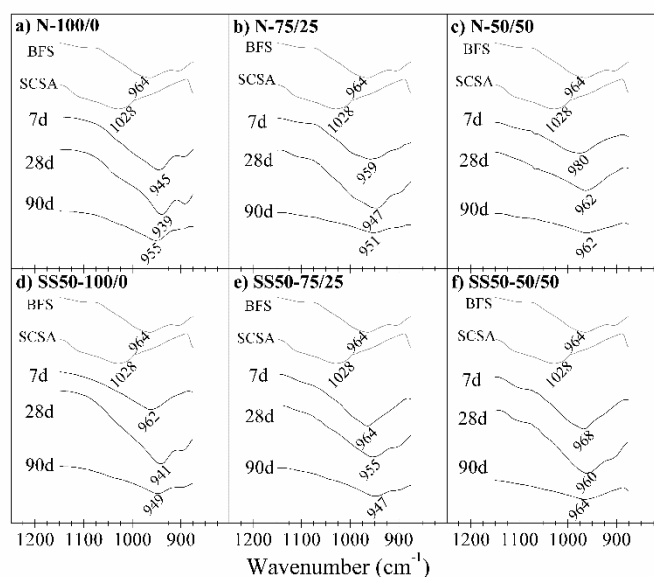


Table 5.3 – Mass losses for the N-100/0, N-75/25, N-50/50, SS50-100/0, SS50-75/25 and SS50-50/50) pastes cured for 7, 28 and 90 days at 25°C in defined temperatures ranges of TGA (35-180°C, 180-250°C and 250-600°C)

Curing time	Specimens' name	Mass loss in a temperature range (%)			
		35-180°C	180-250°C	250-600°C	TOTAL
7 days	N-100/0	7.61	2.47	3.52	13.60
	N-75/25	7.56	2.44	2.92	12.92
	N-50/50	5.67	1.58	3.35	10.60
	SS50-100/0	8.27	2.33	3.29	13.89
	SS50-75/25	5.95	2.10	3.89	11.94
	SS50-50/50	9.78	2.24	2.72	14.74
28 days	N-100/0	11.15	3.41	3.75	18.31
	N-75/25	10.41	3.34	3.83	17.58
	N-50/50	7.39	3.35	4.54	15.28
	SS50-100/0	10.75	3.28	3.77	17.80
	SS50-75/25	10.22	3.36	3.91	17.49
	SS50-50/50	5.75	4.66	6.67	17.08
90 days	N-100/0	8.89	2.85	4.51	16.25
	N-75/25	14.22	3.07	4.37	21.66
	N-50/50	14.25	2.92	4.15	21.32
	SS50-100/0	11.63	3.19	4.65	19.47
	SS50-75/25	8.46	3.18	6.62	18.26
	SS50-50/50	12.43	3.24	4.87	20.54

In the FTIR spectra (Figure 5.3), the main vibration bands of the raw materials and AA pastes are highlighted. First, regarding the raw materials, the main vibration bands of BFS and SCSA were 964 and 1028 cm^{-1} (Si(Al)-O-Si vibration), respectively. The pastes showed peaks in the range of 940-980 cm^{-1} (Si-O-T vibration, T = Si or Al) (PEREIRA et al., 2015). With an increase in the amount of SCSA in the mixture, the main vibration band shifted to higher wavenumber values. Since the main peak for SCSA has higher wavenumber vibration than the value for BFS, this justifies the higher wavenumber peaks in the pastes with the presence of ash. However, with curing age, the main vibration peak shifted to lower wavenumbers. This behavior is related to the formation of AA products, as shown in the DTG studies.

Figure 5.3 – FTIR spectra for the N-100/0 (a), SS50-100/0 (b), N-75/25 (c), SS50-75/25 (d), N-50/50 (e) and SS50-S50 (f) pastes cured for 7, 28 and 90 days at 25°C



The XRD patterns of the raw materials (BFS and SCSA) and the N-100/0 and N-50/50 pastes cured for 28 days at 25°C are shown in Figure 5.4. Mineralogical analysis showed that SCSA presented quartz (PDF Card #331161) and calcite (PDF Card #050586) as the main crystalline phases. The amorphous phase of the ash can be seen in the baseline deviation between the Bragg's angles of 17° and 33°. BFS showed the typical pattern of an amorphous material by presenting a baseline deviation in the range $2\theta = 20-35^\circ$. Regarding the pastes, a shift in the baseline deviation range was observed when compared to the raw materials in the 2θ range between 23° and 37°. This behavior is typical for the formation of cementing gels (PEREIRA et al., 2015; PROVIS et al., 2005). Another gel formation can be seen by the large peaks of C-S-H and C-A-S-H. Additionally, some crystalline phases were formed: N-100/0 showed peaks of katoite (PDF Card #380368), stratlingite (PDF Card #290285) and hydrotalcite (PDF Card #140191), produced during the activation process (PROVIS; BERNAL, 2014; PUERTAS et al., 2004). Termonatrite (PDF Card #080448) was also observed in the sample, probably due to the carbonation of the sample or transformation of the calcite into a sodium carbonate phase. A slightly different pattern was found for N-50/50. In this case, in addition to the previously mentioned phases containing aluminum or silicon, sodium zeolite phases were identified, i.e. hydrosodalite (PDF Card #311271) and hydrated nepheline (PDF Card #100460). The replacement of BFS by SCSA reduced the

Ca/Na atomic ratio and increases the (Si+Al)/Na ratio. Consequently, the formation of hydrosodalite and hydrated nepheline was favored.

Figure 5.4 – XRD patterns for the raw materials, BFS and SCSA, and for the N-100/0 and N-50/50 pastes, cured for 28 days at 25°C. (Keys: Q: Quartz; C: Calcite; W: Wollastonite; N: Termonatrite; T: Hydrotalcite; K: Katoite; S: Stratlingite; H: Hydrosodalite; P: Hydrated Nepheline)

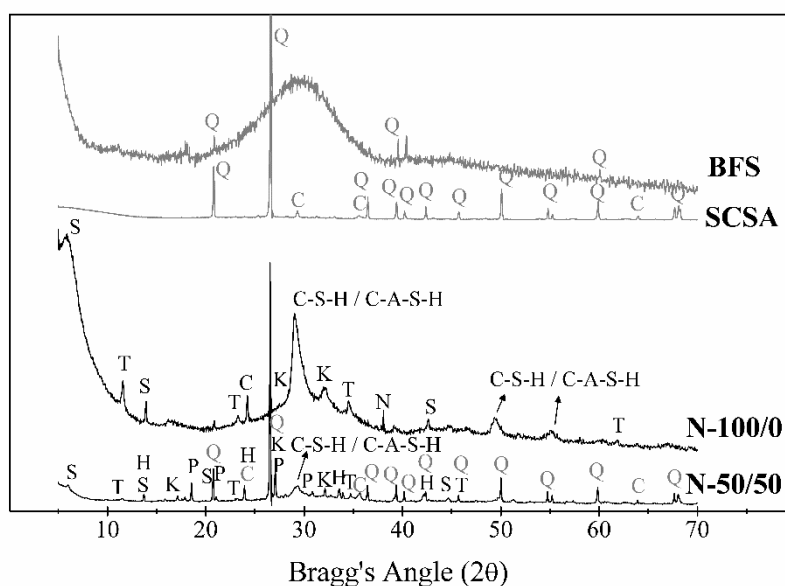
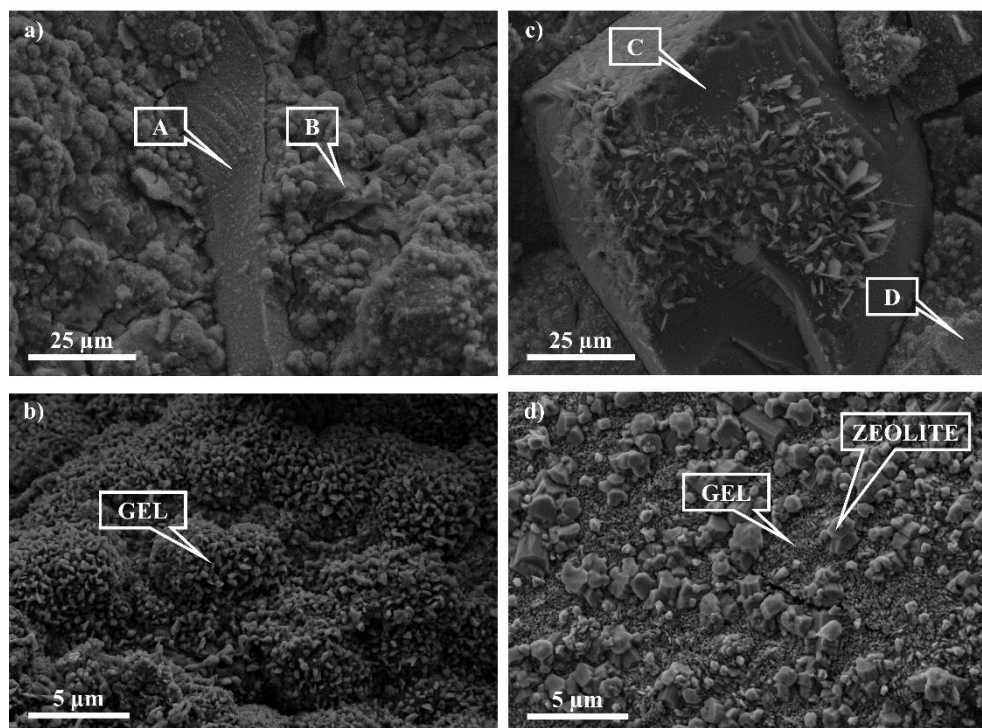


Figure 5.5 shows the FESEM images of the N-100/0 (Fig. 5.5a and 5.5b) and N-50/50 (Fig. 5.5c and 5.5d) pastes after 28 days of curing. In Figure 5.5a, a reacting BFS particle (Point A) and an (N,C)-A-S-H gel (Point B) can be seen; the gel had the following molar ratios: $\text{Al/Si} = 0.28 \pm 0.01$, $\text{Na/Si} = 1.07 \pm 0.05$ and $\text{Ca/Si} = 0.70 \pm 0.05$. In Figure 5.5c, a quartz particle from SCSA is indicated (Point C), surrounded by an (N,C)-A-S-H gel (Point D): this gel presented a higher amount of Si than that found in the control (molar ratios: $\text{Al/Si} = 0.27 \pm 0.01$, $\text{Na/Si} = 0.64 \pm 0.01$ and $\text{Ca/Si} = 0.55 \pm 0.09$). The presence of SCSA in the mixture favored the formation of gels richer in Si, since the added ash contains silicon as the main metallic element. In a higher magnification (Fig 5.5b for N-100/0 and Fig 5.5d for N-50/50), it can be seen that the gel of the AA binder with SCSA is more compact than that for the control one, which also can justify the best performance in the compressive strength test. In addition, zeolite crystals formation in the N-50/50 sample can be observed (Fig. 5.5d).

Figure 5.5 – FESEM images of N-100/0 (a and b) and N-50/50 (c and d) after 28 days of curing at 25°C.



5.4 CONCLUSIONS

The reactivity of SCSA in BFS-based alkali activated binders offers huge advantages. A sustainable material was obtained in this study. First, the replacement of BFS (15-50% by mass) by SCSA in NaOH activated systems provided excellent mechanical properties in the mortar, and similar or higher strengths than BFS systems (without SCSA) activated by NaOH/sodium silicate mixtures were achieved. Secondly, the use of SCSA reduced the use of the most expensive chemical reagent in these activated systems, i.e. sodium silicate. Finally, a high degree of valorization for these ashes was achieved by using them in this type of binder, and offers an interesting solution for managing sugar cane straw wastes. In summary, more sustainability was achieved by replacing BFS and sodium silicate in the design of new binders, and by the proposal of a new valorization method for sugar cane straw waste.

ACKNOWLEDGMENT

The authors would like to thanks to CNPq processo nº 401724/2013-1 and the "Ministerio de Educación, Cultura y Deporte" of Spain ("Cooperación Interuniversitaria" program with Brazil PHB-2011-0016-PC). Thanks are also given to the Electron Microscopy Service of the Universitat Politècnica de València.

REFERENCES

- BOUZÓN, N.; PAYÁ, J.; BORRACHERO, M. V.; SORIANO, L.; TASHIMA, M. M.; MONZÓ, J. *Refluxed rice husk ash/NaOH suspension for preparing alkali activated binders*. **Materials Letters**, p. 72-74, 2014.
- CASTALDELLI, V. N.; AKASAKI, J. L.; MELGES, J. L. P; TASHIMA, M. M.; SORIANO, L.; BORRACHERO, M. V.; MONZÓ, J.; PAYÁ, J. *Use of Slag/Sugar Cane Bagasse Ash (SCBA) Blends in the Production of Alkali-Activated Materials*. **Materials**, v. 6, p. 3108-3127, 2013.
- CHEN, W.; BROUWERS, H. J. H. *The hydration of slag, part 1: reaction models for alkali-activated slag*. **Journal of Materials Science**, v. 42, p. 428-443, 2007.
- CHEN, W. H.; PENG, J.; BI, X. T. *A state-of-the-art review of biomass torrefaction, densification and applications*. **Renewable and Sustainable Energy Reviews**, v. 44, p. 847-866, 2015.
- DAVIDOVITS, J. *Environmentally driven geopolymer cement applications*. **Geopolymer International Conference**, 2002.
- DAVIDOVITS, J. *Geopolymer Chemistry and Applications*. 3rd ed., Institut Géopolymère, France, 2001.
- KUENZEL, C.; NEVILLE, T. P.; DONATELLO, S.; VANDEPERRE, L.; BOCCACCINI, A. R.; CHEESEMAN, C. R. *Influence of metakaolin characteristics on the mechanical properties of geopolymers*. **Applied Clay Science**, v. 83-84, p. 308-314, 2013.
- LEAL, M. R. L. V.; GALDOS, M. V.; SCARPARE, F. V.; SEABRA, J. E. A; WALTER, A.; OLIVEIRA, C. O. F. *Sugarcane straw availability, quality, recovery and energy use: A literature review*. **Biomass Bioenergy**, v. 53, p. 11-19, 2013.
- MARTINEZ-LOPEZ, R.; ESCARLATE-GARCIA, J. I. *Alkali activated composite binders of waste silica soda lime glass and blast furnace slag: Strength as a function of the composition*. **Construction and Building Materials**, v. 119, p. 119-129, 2016.

McLELLAN, B.; WILLIAMS, R.; LAY, J.; VAN RIESSEN, A.; CORDER, G. *Costs and carbon emissions for geopolymer pastes in comparison to ordinary Portland cement*. **Journal of Cleaner Production**, v. 19, p. 1080-1090, 2011.

MEJÍA, J. M.; GUTIÉRREZ, R. M.; MONTES, C. *Rice husk ash and spent diatomaceous earth as a source of silica to fabricate a geopolymeric binary binder*. **Journal of Cleaner Production**, v. 118, p. 113-139, 2016.

MELLADO, A.; CATALÁN, C.; BOUZÓN, N.; BORRACHERO, M. V.; MONZÓ, J. M.; PAYÁ, J. *Carbon footprint of geopolymeric mortar: study of the contribution of the alkaline activating solution and assessment of an alternative route*. **RSC Advances**, v. 4, p. 23846, 2014.

MEYER, C. *The greening of the concrete industry*. **Cement and Concrete Composites**, v. 31, p. 601-605, 2009.

MORAES, J. C. B.; AKASAKI, J. L.; MELGES, J. L. P.; MONZÓ, J.; BORRACHERO, M. V.; SORIANO, L.; PAYÁ, J.; TASHIMA, M. M. *Assessment of sugar cane straw ash (SCSA) as pozzolanic material in blended Portland cement: Microstructural characterization of pastes and mechanical strength of mortars*. **Construction and Building Materials**, v. 94, p. 670-677, 2015.

NIKOLIC, V.; KOMLJENOVIC, M.; BAŠCAREVIC, Z.; MARJANOVIC, N.; MILADINOVIC, Z.; PETROVIC, R. *The influence of fly ash characteristics and reaction conditions on strength and structure of geopolymers*. **Construction and Building Materials**, v. 94, p. 361-370, 2015.

NIMWINYA, E.; ARJHARN, W.; HORPIBULSUK, S.; PHOO-NGERNKHAM, T.; POOWANCUM, A. *A sustainable calcined water treatment sludge and rice husk ash geopolymer*. **Journal of Cleaner Production**, v. 119, 128-134, 2016.

PALOU, M.; MAJLING, J.; DOVÁI, M.; KOZANKIVÁ, J.; MOJMDAR, S. B. *Formation and stability of crystallohydrates in the non-equilibrium system during hydration of sab cements*. **Ceramics-Silikáty**, v. 49, p. 230-236, 2005.

PEREIRA, A.; AKASAKI, J. L.; MELGES, J. L. P.; TASHIMA, M. M.; SORIANO, L.; BORRACHERO, M. V.; MONZÓ, J.; PAYÁ, J. *Mechanical and durability properties of alkali-activated mortar based on sugarcane bagasse ash and blast furnace slag*. **Ceramics International**, v. 41, p. 13012-13024, 2015.

PHAIR, J. W. *Green chemistry for sustainable cement production and use*. **Green Chemistry**, v. 8, p. 763-780, 2006.

PROVIS, J. L.; BERNAL, S. A. *Geopolymers and Related Alkali-Activated Materials*. *Annual Review of Materials Research*, v. 44, p. 299-327, 2014.

PROVIS, J.L.; LUKEY, G. C.; van DEVENTER, J. S. J. *Do geopolymers actually contain nanocrystalline zeolites? A reexamination of existing results.* **Chemistry of Materials**, v. 17, p. 3075-3085, 2005.

PROVIS, J. L.; PALOMO, A.; SHI, C. *Advances in understanding alkali-activated materials.* **Cement and Concrete Research**, v. 78, p. 110-125, 2015.

PUERTAS, F.; FERNÁNDEZ-JIMÉNEZ, A.; BLANCO-VARELA, M. T. *Pore solution in alkali-activated slag cement pastes. Relation to the composition and structure of calcium silicate hydrate.* **Cement and Concrete Research**, v. 34, p. 139-148, 2004.

RAKHIMOVA, N. R.; RAKHIMOV, R. Z. *Alkali-activated cements and mortars based on blast furnace slag and red clay brick waste.* **Materials and Design**, v. 85, p. 321-331, 2015.

RAKHIMOVA, N. R; RAKHIMOV, R. Z. *A review on alkali-activated slag cements incorporated with supplementary materials.* **Journal of Sustainable Cement-Based Materials**, v. 1, p. 61-74, 2014.

ROSTAMI, H.; BRENDLEY, W. *Alkali Ash Material: A Novel Fly Ash-Based Cement.* **Environmental Science and Technology**, v. 37, p. 3454-3457, 2003.

Sugarcane production. **UNICA – União da Indústria de Cana-de-Açúcar Website**; <http://www.unicadata.com.br/index.php?idioma=2>

WANG, S. D.; PU X. C.; SCRIVENER K. L.; PRATT P. L. *Alkali-activated slag cement and concrete: a review of properties and problems.* **Advances in Cement Research**, v. 7, p. 93-102, 1995.

6 SUGAR CANE STRAW ASH AS SOLID PRECURSOR IN ALKALI-ACTIVATED BINDERS BASED ON BLAST FURNACE SLAG: SOLUTIONS WITH $[N+]$ OF 4 MOL.KG^{-1} AND $\text{SiO}_2/\text{Na}_2\text{O}$ RATIOS OF 0-0.75

The article entitled as "*Effect of sugar cane straw ash (SCSA) as solid precursor and the alkaline activator composition on alkali-activated binders based on blast furnace slag (BFS)*" by J. C. B. Moraes, M. M. Tashima, J. L. Akasaki, J. L. P. Melges, J. Monzó, M. V. Borrachero, L. Soriano and J. Payá and was published in the journal **Construction and Building Materials**, v. 144, p. 214-224, 2017.

Abstract: Alkali-activated materials (AAM) comprise one of the solutions to diminish the use of Portland cement in building construction and, consequently, a reduction in the environmental problems related to CO_2 emissions and energy consumption may be achieved. These kinds of binders are obtained when a mineral precursor (calcium silicate or aluminosilicate material) is mixed with an alkaline solution. In this study, the blast furnace slag (BFS) combined with a new waste from the sugar cane industry, sugar cane straw ash (SCSA), is utilised. This new residue was studied replacing partially the blast furnace slag in BFS/SCSA proportions of 100/0, 85/15, 75/25, 67/33 and 50/50. The alkaline solution concentration plays an important role in obtaining AAM with good mechanical properties. Therefore, this paper intends to assess the influence of the activating solution (composed of sodium hydroxide and sodium silicate) through different $\text{H}_2\text{O}/\text{Na}_2\text{O}$ (called η) and $\text{SiO}_2/\text{Na}_2\text{O}$ (called ϵ) molar ratios. For BFS/SCSA proportions of 100/0 and 75/25, the η values assessed were 22, 28 and 37, whereas the ϵ values selected were 0 and 0.75. In order to study the effects of SCSA in the mixture, other BFS/SCSA proportions (0-50% replacement) were assessed by only η and ϵ ratios of 28 and 0-0.75, respectively. To reach these objectives, mortars and pastes were manufactured in order to study their behaviour in the following tests: compressive strength (3, 7, 28 and 90 days of curing at 25°C), Fourier transform infrared spectroscopy (FTIR), thermogravimetric analysis (TGA), X-ray

diffraction (XRD), mercury intrusion porosimetry (MIP) and field emission scanning electron microscopy (FESEM). The results showed that the alkaline solution influenced the compressive strength development, and specimens reached more than 60 MPa after 90 days of curing. In addition, the mortars with SCSA and without sodium silicate presented similar values of compressive strength to those samples with only BFS and sodium silicate, showing that the ash can replace the sodium silicate, which is the pollutant and an expensive chemical reagent, yielding a sustainable binder. Therefore, SCSA presented good results and is a promising material in alkali-activated binders.

Keywords: *environmentally friendly material, biomass waste, compressive strength, microstructural studies, sustainability*

6.1 INTRODUCTION

Alkali-activated materials (AAM) development is one of the newest trends in binder for building construction. In a previous study can be found more details about AMM definition, their advantages and the most common raw materials (MORAES et al., 2016a). Now it will be focus on important support studies for this present research.

In recent decades, assessment of the reuse of biomass ashes in inorganic binders (mainly Portland cement) has been an important focus of attention (PARIS et al., 2016). In addition, in the last few years, the use of biomass ashes as supplementary mineral admixtures in alkali-activated BFS-based binders has notably increased (PAYÁ et al., 2015). The combination of BFS and palm oil fuel ashes (POFA) is noticeable (YUSUF et al., 2014; ISLAM et al., 2014). In these studies, the authors obtained a higher compressive strength with the 20% replacement of BFS by POFA compared to the control after 28 days of curing (YUSUF et al., 2014); this percentage was increased to 30% without any important loss of mixture properties (ISLAM et al., 2014). In the case of residues derived from the sugarcane industry, some examples have recently been reported regarding sugarcane bagasse ash (SCBA) (PEREIRA et al., 2015; CASTALDELLI et al., 2013). The presence of SCBA from an autocombustion process in BFS/SCBA ratio of 75/25 resulted in slightly higher compressive strength than the control after 90 days of curing. In durability studies, the alkali-activated binders were compared to Portland cement mixtures in ammonium chloride, acetic

acid and sodium sulphate attacks, where the new type of binders exhibited better behaviour than conventional ones (PEREIRA et al., 2015). In another study with the SCBA produced in an industrial combustion, the ash can be utilised until a 40% replacement of BFS is reached, and yields an important contribution in the mechanical strength of BFS/SCBA mixtures.

Another interesting biomass derived from the sugarcane crop is sugarcane straw, which is produced in large amounts and is usually abandoned in land. This biomass could be transformed into reactive ash (sugarcane straw ash, SCSA) for reuse in inorganic binders (MORAES et al., 2016b): interesting sustainability issues have been described in terms of saving energy and raw materials for cement and concrete. The SCSA is obtained from the combustion of sugar cane straw, a waste that increased in the last few years for two reasons: the expansion of sugar cane production in many countries and the trend to use a mechanized harvesting. Related the first reason, an example can be given: sugar cane production in Brazil expanded from 385,000 tons in 2005/2006 to 670,000 tons in 2015/2016, which represents an increase of 74% in only one decade (União da Indústria de Cana-de-Açúcar – UNICA). The main reason for this increase is high demand in the production of ethanol (MORAES et al., 2015). Following the second reason, several protocols prohibited the open field burning in crop fields before collecting the sugar cane, due to safety and environmental issues. After the mechanised harvesting process, sugar cane straw is obtained, which is mostly left on the field to cover the bare soil; however, some of it can be reused without affecting this protection (LEAL et al., 2013). This straw presents an interesting calorific value, and there are some studies about selected ways to collect it in order to produce energy by a burning procedure; sugar cane bagasse is already being utilised in this way (MORAES et al., 2013; LEAL et al., 2013, MESA-PÉREZ et al., 2013; LEMOS et al., 2014). After the combustion of the straw, an ash rich in silica is generated: sugar cane straw ash (SCSA).

In an early published paper (MORAES et al., 2016a), SCSA was used to replace BFS in AAM. The results demonstrated the high reactivity of SCSA, especially for those mixtures activated with NaOH solution. In this case, the concentration of the solution was 8 mol.kg⁻¹. In addition, other alkali activators tested contained a mixture of NaOH and waterglass (studied solutions presented 0.5 and 0.75 SiO₂/Na₂O molar ratios), maintaining the concentration of Na⁺ at a constant level. In this case, the goal was to produce the solubilisation of the silica present in the SCSA by means a high alkaline solution, and

consequently the required quantities of NaOH and waterglass were high. In these conditions, compressive strength of 90-days mortars of BFS/SCSA activated mixtures were similar or higher than those found for only BFS activated system.

Regarding the alkaline activating solution, the reported papers showed that the most utilised alkali sources are sodium hydroxide and sodium silicate (waterglass) (SHI; KRIVENKO, 2006). The concentration of these solutions and the $\text{SiO}_2/\text{Na}_2\text{O}$ molar ratio are crucial parameters to reach interesting mechanical properties, since variations on the solution concentration and relative dosage with respect to the solid precursor can provide different compressive strengths after a given curing age, as reported in some studies (TASHIMA et al., 2013; OZER; SOYER-UZUN, 2015; AYDIN; BARADAN, 2014). In this way, the influence of the solution concentration to a given solid precursor should be studied in order to achieve the optimum dosage.

Seriously, the use of silicates in the preparation of alkaline solutions is responsible for the most greenhouse gas emissions related to AAM; however, this chemical compound becomes very important in the mechanical strength development of the AAM. One possibility is to prepare sodium carbonate-silicate mixes, for partially reducing the silicate source (BERNAL et al., 2016). Another possibility is replacing the waterglass with another siliceous source. Some authors used residues in the preparation of the alkaline solution, such as rice husk ash and glass waste, and obtained compressive strengths of mortars similar to the control ones prepared with sodium silicate (BOUZÓN et al., 2014; PUERTAS et al., 2014; TCHAKOUTÉ et al., 2016). Another alternative possibility is to reduce the quantity of alkali compounds (especially sodium silicate) by blending solid silica-rich wastes with the precursor. In this paper, binary BFS/SCSA systems have been tested, where one of the solid precursors (SCSA) is rich in reactive silica.

The research had two objectives: the first was to add value for an ash derived from a residue in the sugar cane industry, SCSA, as a way to reduce the use of sodium silicate in AAM; the second one was to study the influence of the alkaline solution concentration on the mechanical properties of these proposed AAM based on a BFS/SCSA binary system. SCSA was already studied as a solid precursor in a previous study (MORAES et al., 2016a). In this former study, only one $\text{H}_2\text{O}/\text{Na}_2\text{O}$ molar ratio was assessed, with different $\text{SiO}_2/\text{Na}_2\text{O}$ molar ratios. Authors observed that the mechanical behaviour from mortars composed by BFS/SCSA activated with only sodium hydroxide is similar to ones with only BFS mixed

with NaOH and sodium silicate. This result means that the SCSA is a silica source similar than the sodium silicate in AAM. Regarding to the present study, the activating solution varied for both molar ratios: $\text{H}_2\text{O}/\text{Na}_2\text{O}$ (called η) and $\text{SiO}_2/\text{Na}_2\text{O}$ (called ε). The η values in the studied mixtures were 22, 28 and 37 (they were approximately to the corresponding solutions 5, 4 and 3 mol.kg^{-1} of Na^+ respectively), whereas the ε values were 0 (only sodium hydroxide) and 0.75. With respect to the solid precursors, the following BFS/SCSA proportions (by weight) were assessed: 100/0, 85/15, 75/25, 67/33 and 50/50. Compressive strengths of mortars were assessed until 90 days of curing at 25°C. Microstructural analyses of pastes were performed by powder X-ray diffraction (XRD), Fourier transform infrared spectroscopy (FTIR), thermogravimetric analysis (derivative DTG curves), mercury intrusion porosimetry (MIP) and field emission scanning electron microscopy (FESEM).

6.2 MATERIALS AND METHODS

6.2.1 Materials

The main material of this study is the sugar cane straw ash (SCSA). The straw was collected in a sugar cane plantation close to Ilha Solteira city (São Paulo, Brazil). Afterwards, it was transformed by means of an autocombustion process with a maximum combustion temperature of 700°C, yielding a residual ash. Since this residue presents a certain amount of unburned particles, the ash was passed through sieves to remove them. Finally, the passed powder was milled in a ball mill for 50 minutes to reduce and homogenise the ash particles, and then the SCSA was ready to be tested. The blast furnace slag (BFS) was acquired from the Ribas do Rio Pardo (Mato Grosso do Sul, Brazil). The chemical composition of both SCSA and BFS are shown in Table 6.1. BFS showed the typical chemical composition: CaO , SiO_2 and Al_2O_3 were the main oxides. SCSA had SiO_2 as the main component (58.6%), and Al_2O_3 and Fe_2O_3 were also significant components. Regarding the particle size of the solid precursors, SCSA presents a mean particle diameter (D_{med}) and median particle diameter (D_{50}) of 18.1 μm and 10.6 μm , respectively; for the BFS, these values are 27.5 and 21.4 μm , respectively. In the alkaline solution preparation, sodium hydroxide (solid, 98% purity) and sodium silicate (solid, 18 wt% Na_2O , 63 wt% SiO_2) supplied by Dinâmica Química were

used. For mortar preparation, natural sand with a fineness modulus of 2.05 and specific gravity of 2667 kg/m³ was obtained from Castilho City (São Paulo, Brazil).

Table 6.1 – Chemical characterisation of the solid precursors utilised in this paper (BFS and SCSA)

Solid Precursor	SiO₂	Al₂O₃	Fe₂O₃	CaO	MgO	K₂O	SO₃	Cl	Others	LOI
SCSA	58.6	9.0	8.4	4.6	1.6	5.4	1.9	0.7	3.3	6.5
BFS	33.0	11.5	0.6	43.5	7.3	0.4	1.9	0.1	1.6	0.1

6.2.2 Alkali activated binders’ dosage and preparation

In this study, six different alkaline solutions were prepared, in order to assess their influence on the mechanical properties of the designed AAM. The H₂O/Na₂O molar ratios assessed (called η) were 22, 28 and 37. For each η value, there were two SiO₂/Na₂O (called by ϵ) molar ratios evaluated in this study: 0 (only sodium hydroxide in the solution) and 0.75. Regarding the solid precursors, for the intermediary η ratio of 28, the BFS/SCSA proportions studied (y/z) to evaluate the influence of the ash in AAM systems were 100/0, 85/15, 75/25, 67/33 and 50/50. For the other η values (22 and 37), the BFS/SCSA proportions assessed were 100/0 and 75/25. Therefore, the total studied mixes in this paper was eighteen, as summarised in Table 6.2. In all mixes (pastes and mortars), the water/precursor ratio was maintained at a constant level of 0.45. For mortars, natural sand was added in the proportion solid precursor/sand of 1/2.5. The dosages nomenclature proposed in this study is η - ϵ -y/z and specimen names are also shown in Table 6.2.

Regarding the preparation of AAMs, first, the alkaline solution was prepared. Since the dissolution of sodium hydroxide in water releases heat, the resulting solution was left to reach room temperature. Afterwards, the solid precursor was mixed with the alkaline solution, until proper homogenisation was attained. For mortars, sand was finally added and mechanically stirred for 3 minutes. Pastes and mortars were cured at 25°C and relative humidity higher than 95% until the tests age.

Table 6.2 – Mixture dosage and specimen's names and tests carried out: compressive strength (Rc), X-ray diffraction (XRD), Fourier transform infrared spectroscopy (FTIR), Thermogravimetric analyses (TGA), Mercury intrusion porosimetry (MIP) and Field emission scanning electron microscopy (FESEM)

Specimen's name	H ₂ O/Na ₂ O molar ratio (η)	SiO ₂ /Na ₂ O molar ratio (ε)	BFS / SCSA (y/z)	Testing ages (days)					
				Rc	XRD	FTIR	TGA	MIP	FESEM
22-0-100/0	22	0	100/0	3-7-28-90	-	-	-	-	-
22-0-75/25			75/25		-	-	-	-	-
22-0.75-100/0		0.75	100/0	3-7-28-90	-	-	-	-	-
22-0.75-75/25			75/25		-	-	-	-	-
28-0-100/0	28	0	100/0	3-7-28-90	90	7-28-90	7-28-90	90	90
28-0-85/15			85/15		-	-	-	-	-
28-0-75/25			75/25		90	7-28-90	7-28-90	90	90
28-0-67/33			67/33		-	-	-	-	-
28-0-50/50		0.75	50/50	3-7-28-90	-	-	-	-	-
28-0.75-100/0			100/0		90	7-28-90	7-28-90	90	90
28-0.75-85/15			85/15		-	-	-	-	-
28-0.75-75/25			75/25		90	7-28-90	7-28-90	90	90
28-0.75-67/33	37	0	67/33	3-7-28-90	-	-	-	-	-
28-0.75-50/50			50/50		-	-	-	-	-
37-0-100/0		0	100/0		-	-	-	-	-
37-0-75/25			75/25		-	-	-	-	-
37-0.75-100/0	37	0.75	100/0	3-7-28-90	-	-	-	-	-
37-0.75-75/25			75/25		-	-	-	-	-

6.2.3 Test procedures for pastes and mortars

XRD patterns were accomplished by a Bruker AXS D8 Advance with a voltage of 40 kV, current intensity of 20 mA and a Bragg's angle (2θ) in the range of 5-70°. FTIR spectra were obtained by a Bruker Tensor 27 in the range of 400 and 4000 cm⁻¹. The DTG curves were carried out by a TGA Mettler-Toledo TGA 850, where the specimen was heated in a 70 µL alumina crucible in the temperature range of 35-1000°C, with a heating rate of 20°C.min⁻¹ and air atmosphere (75 mL.min⁻¹ gas flow). Mercury intrusion porosimetry (MIP) was carried out by a Micrometrics Instrument Corporation AutoPore IV 9500, using intrusion pressure from 6.6 kPa to 402.2 MPa, representing measurement diameter pores in

the range of 222.2 μm and 3.6 nm. Finally, field emission scanning electron microscopy (FESEM) images were taken by a ZEISS Supra 55 in fractured surface sample covered with carbon in order to evaluate the gel structure and chemical composition. Some micrographs were taken by using an in-lens system, which virtually eliminates aberrations, resulting in optimal spatial resolution; clearer and less electrostatically distorted images were recorded. XRD, FTIR, TGA, MIP and FESEM tests were carried out at different ages, according to Table 6.2.

Mortars were cast in a cubic mould of 50 x 50 x 50 mm³ and tested in an EMIC Universal Machine with a load limit of 2000 kN. Compressive strengths of mortars were assessed after 3, 7, 28 and 90 days of curing at 25°C and relative humidity (RH) was higher than 95% for all dosages studied.

6.3 RESULTS AND DISCUSSION

6.3.1 Compressive strength of mortars

Compressive strength results of mortars are summarised in Table 6.3. BFS mortars activated with $\varepsilon = 0$ (22-0-100/0, 28-0-100/0 and 37-0-100/0) showed the lowest strengths. At early ages (3 and 7 days), the mortar with the highest concentrated activating solution (22-0-100/0) yielded lower strengths than the other mortars activated with other NaOH solutions: this behaviour suggested that high sodium concentration did not have advantages in terms of early strength development. For longer curing times (28 and 90 days), all BFS mixes activated with NaOH yielded similar strength (25-33 MPa at 28 days and 34-36 MPa at 90 days). BFS samples activated with $\varepsilon = 0.75$ solution (22-0.75-100/0, 28-0.75-100/0 and 37-0.75-100/0) showed higher strengths when compared to mortars activated with $\varepsilon = 0$ solution. Thus, strengths reached after 7 days for $\varepsilon = 0.75$ systems were similar to those obtained for $\varepsilon = 0$ after 90 days of curing. This behaviour revealed the important role of sodium silicate in the activation of BFS. BFS mortars with $\varepsilon = 0.75$ yielded very high strengths after 28 and 90 days: 53-61 and 64-67 MPa, respectively.

Related to the influence of the partial replacement of BFS by the sugar cane straw ash (SCSA) in the AAM, specimens for all η values without the sodium silicate ($\varepsilon = 0$) showed a significant improvement compared to the corresponding ones with BFS and $\varepsilon = 0$.

Thus, noticeably, strengths reached for samples with BFS/SCSA=75/25 (25% replacement of BFS) were in the range 50-57 MPa at 28 days and in the 56-59 MPa at 90 days. These values, compared to those obtained for BFS activated mortars with $\varepsilon = 0$, represent increasing mean values of 86% and 66% at 28 and 90 days, respectively. These values were slightly lower than those found for BFS activated with $\varepsilon = 0.75$ solutions, which means that the role played by SCSA in the BFS/SCSA mixtures with $\varepsilon = 0$ was comparable to that for sodium silicate. Curiously, for the earliest curing age (3 days) the effect of the SCSA was negligible with $\varepsilon = 0.75$: for BFS/SCSA samples activated with $\eta = 22$ and $\eta = 28$ solutions; similar strengths to that found for BFS systems with $\varepsilon = 0$ were reached. In contrast, BFS/SCSA samples activated with $\eta = 37$ yielded only 1.9 MPa (BFS with $\varepsilon = 0$ sample yielded 13.4MPa), which means that the lowest sodium concentration solution was not very effective in the dissolution of reactive silica from SCSA at this age (SONG; JENNIGS, 1999).

Specifically, for the BFS/SCSA with $\eta = 28$ samples, different replacement SCSA percentages were studied (15, 25, 33 and 50% replacements). The replacement interval of 25-50% mortars did not show a difference in the compressive strength values after 90 days of curing, being slightly superior to the 15% replacement. Additionally, the compressive strength development from the BFS/SCSA ratio of 75/25 presented better results than the 67/33 and 50/50 mixtures, since the results of the early curing times of that blend are significantly higher than these ones.

Regarding the specimens with sodium silicate ($\varepsilon = 0.75$), the BFS/SCSA 75/25 mixture presented slightly lower 90-day compressive strengths than the control ones for the three η values tested, which is different to that which occurred for the blends with $\varepsilon = 0$. However, for early curing ages, the strengths for SCSA-containing systems were significantly lower. This behaviour suggests that, at early ages, the dissolution of silica from SCSA and the presence of silicate anions in the solution have a negative effect on the strength development.

Again for the $\eta = 28$ mixtures, SCSA percentages in the range 15-33% presented better compressive strength development until the 90th day of the study, whereas 50% showed worse results than those. The presence of SCSA in mixtures with $\varepsilon = 0.75$ did not show any difference compared to the control one. From these compressive strength results, the optimal BFS/SCSA proportions are 75/25 and 67/33. Noticeably, the BFS/SCSA 50/50

sample did not set before 7 days of curing, which strengthens the proposed idea regarding the bad compatibility between SCSA and sodium silicate for a good early strength development (MORAES et al., 2016a). In these cases, a large amount of silicate in solution is produced because the sodium silicate in the activator and the solubilisation of silica from SCSA by NaOH. In these conditions, the silicate/BFS ratio was notably increased (especially for 50% replacement of BFS by SCSA) and the effective NaOH concentration for achieving BFS was drastically diminished (ESCALANTE-GARCIA et al., 2003).

The use of sodium silicate ($\varepsilon = 0.75$) only showed beneficial results to the BFS/SCSA proportion of 100/0: for the all η values, the final compressive strength of this solid precursor proportion showed higher results when compared to those without sodium silicate. When BFS was partially replaced by SCSA, the use of sodium silicate did not favour the mortar strength development. The final compressive strength (90 days) of the mortars with sodium silicate is similar to those that do not have this reagent, and also negatively affected the mechanical strength development: the compressive strength of SCSA-mortars with $\varepsilon = 0$ showed higher compressive strength at early ages when compared to the specimens with the $\varepsilon = 0.75$ ones. Making an overview of all of the results, the comparison between the specimens with SCSA activated with only sodium hydroxide (SCSA percentages in the interval 15-50% and $\varepsilon = 0$) and those without SCSA activated with sodium hydroxide and silicate (SCSA percentage of 0% and $\varepsilon = 0.75$) may be highlighted.

Table 6.3 – Compressive strength of mortars (MPa) and their standard deviations

Specimen name	Compressive strength (MPa)			
	25°C, RH > 95%			
	3 days	7 days	28 days	90 days
22-0-100/0	11.8 ± 0.2	16.5 ± 0.5	25.0 ± 1.1	35.7 ± 0.5
22-0-75/25	10.2 ± 0.2	29.0 ± 1.8	57.4 ± 0.4	58.8 ± 2.3
22-0.75-100/0	15.2 ± 0.1	33.1 ± 1.5	55.8 ± 4.3	67.2 ± 0.4
22-0.75-75/25	6.5 ± 0.1	23.3 ± 1.3	56.7 ± 0.7	62.1 ± 2.3
28-0-100/0	16.1 ± 0.7	21.4 ± 0.8	32.8 ± 1.2	34.7 ± 4.1
28-0-85/15	7.1 ± 0.1	18.1 ± 0.9	41.2 ± 2.2	50.0 ± 1.9
28-0-75/25	11.3 ± 2.4	26.9 ± 0.7	54.0 ± 1.0	57.0 ± 2.5
28-0-67/33	3.1 ± 0.1	9.5 ± 0.6	46.0 ± 4.2	57.2 ± 4.9
28-0-50/50	2.8 ± 0.1	3.2 ± 0.7	35.0 ± 0.1	57.3 ± 2.0
28-0.75-100/0	20.3 ± 1.1	36.2 ± 2.0	60.4 ± 4.8	64.5 ± 1.5
28-0.75-85/15	3.5 ± 0.1	17.1 ± 0.4	42.4 ± 1.9	65.6 ± 3.2
28-0.75-75/25	3.2 ± 0.2	13.6 ± 0.6	48.7 ± 4.0	63.6 ± 4.3
28-0.75-67/33	5.4 ± 0.1	18.5 ± 0.5	52.7 ± 0.7	63.1 ± 1.7
28-0.75-50/50	-	-	21.1 ± 0.5	50.4 ± 1.2
37-0-100/0	13.4 ± 0.1	19.0 ± 0.5	29.6 ± 0.7	36.0 ± 1.4
37-0-75/25	1.9 ± 0.0	12.3 ± 0.5	50.8 ± 1.1	56.6 ± 1.6
37-0.75-100/0	15.3 ± 0.9	33.0 ± 1.5	53.4 ± 2.1	64.2 ± 3.0
37-0.75-75/25	1.7 ± 0.1	10.7 ± 0.1	53.3 ± 1.3	58.6 ± 4.5

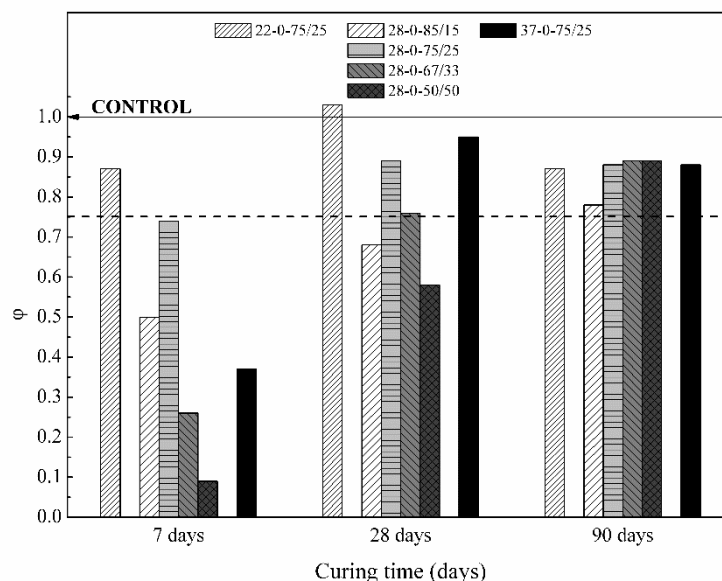
In order to assess the importance of the SCSA contribution, and the possibility to compare their mortars with the control ones (BFS/SCSA=100/0) with sodium silicate, an ϕ ratio is proposed in this study. This ϕ parameter is the ratio between the compressive strength of a mortar with a certain BFS/SCSA proportion different than 100/0 (y/z , being 85/15, 75/25, 67/33 or 50/50), a determined η value and $\varepsilon = 0$ ($R_{c\eta-0-y/z}$) over the control one (only BFS), with the same H_2O/Na_2O ratio and activated with sodium silicate solution ($\varepsilon = 0.75$) for the same curing time ($R_{c\eta-0.75-100/0}$), as in Equation 6.1:

$$\phi = \frac{R_{c\eta-0-y/z}}{R_{c\eta-0.75-100/0}} \quad (6.1)$$

The ϕ values for 7, 28 and 90 days of curing are presented in Figure 6.1. After 7 days of curing, the specimen with $\eta = 22$ presented a compressive strength that was slightly

lower than the control (22-0.75-100/0), and reached an ϕ value of 0.87. The sample 28-0-75/25 showed a lower rate of 0.74, whereas the other specimens presented ϕ ratios lower than 0.50. This behaviour can be explained by taking into account that the commercial sodium silicate was already dissolved in the aqueous medium, which means that the reaction process occurs faster than in the mortars with SCSA, leading to a higher compressive strength at early curing ages. On the other hand, after 28 days, the effect of SCSA in the development of the strength gained in importance: 22-0-75/25, 28-0-75/25 and 37-0-75/25 specimens showed ϕ values over than 0.80, indicating that the SCSA contribution as a silica source mainly occurred in the 7-28 days of curing period. For this curing time, it is highlighted that the 22-0-75/25 reached compressive strength slightly above the control, since the ϕ value of this mortar was 1.04. The higher amount of Na^+ was shown to be beneficial in the first 28 days of curing, because this mortar presented a compressive strength similar to the control and ϕ values always over 0.80. Regarding the SCSA content, the mortars with $\eta = 28$ showed that the optimum replacement was 25%, due to the highest ϕ value for 28-0-75/25 system ($\phi=0.89$) at this curing age. After 90 days of curing, all mortars showed ϕ values in the range from 0.80-0.90, confirming that the SCSA can be used as a silica source in alkali-activated binders based on BFS. Interestingly, for BFS/SCSA = 75/25 systems, the values of ϕ over 0.75 at 90 days confirm that the use of SCSA is interesting from two points of view: the partial replacement of BFS and the total replacement of sodium silicate. At this curing time, neither the quantity of Na^+ nor the percentage of SCSA utilised in the mortar had a significant affect.

Figure 6.1 – Values of the ϕ ratio for mortars containing SCSA at 7, 28 and 90 days of curing

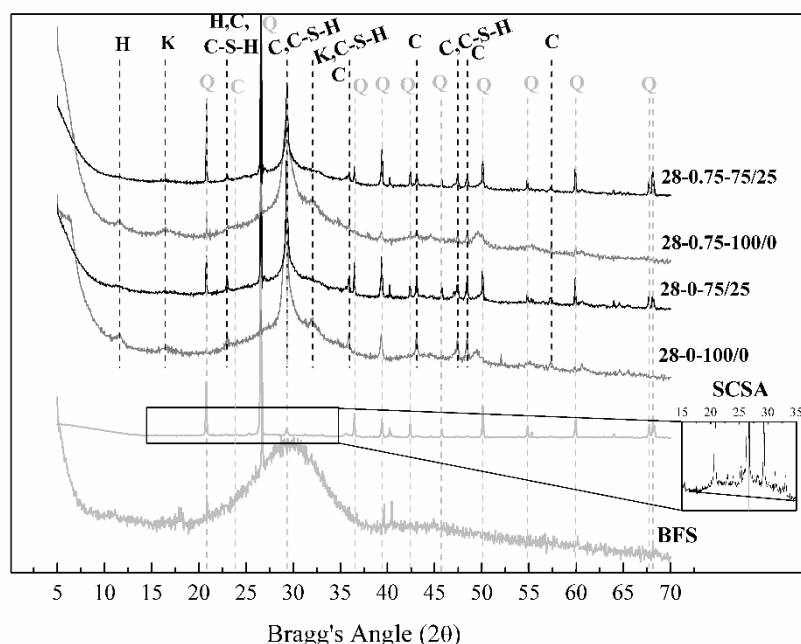


6.3.2 Microstructural studies

XRD patterns of the raw materials (BFS and SCSA) and the pastes 28-0-100/0, 28-0-75/25, 28-0.75-100/0 and 28-0.75-75/25 after 90 days of curing are shown in Figure 6.2. Firstly, regarding the raw materials BFS and SCSA, XRD patterns show a baseline deviation in the Bragg's Angle range of 17-33° and 20-35°, respectively, which is characteristic of the presence of amorphous phases. The presence of an important amount of quartz (PDF Card #331161) in SCSA meant that this baseline deviation was only easily identified by enlargement of the diffractogram in the 20-35° range. In addition, calcite (PDF Card #050586) was present in the ash. Regarding XRD patterns of pastes, a baseline deviation in the 2θ range of 22-38° was observed in all cases. This behaviour was observed in other studies of the alkaline activation of BFS (MORAES et al., 2016a; PEREIRA et al., 2015). The XRD pattern for 28-0-100/0 showed the strongest broad peak centred at 29.32° and a broad weaker peak at 32.08°, which can be associated with the presence of C-S-H gel (probably this gel has sodium and aluminium, (C,N)-A-S-H phase); additionally, the peak from calcite in the very close 2θ value of 29.32° overlapped. The presence of calcite in this sample was confirmed by the identification of other related peaks: 22.97, 35.93, 43.09,

47.39, 48.44 and 57.35°. This calcite was due to the slight carbonation of the sample, according to the results from thermogravimetric analysis. A small quantity of quartz was also identified, which comes from the BFS, suggesting that this crystalline phase did not react in the process after 90 days of curing. Finally, minor phases were also identified: hydrotalcite ($\text{Mg}_6\text{Al}_2\text{CO}_3(\text{OH})_{16}\cdot\text{H}_2\text{O}$, PDFcard 140191) and katoite ($\text{Ca}_3\text{Al}_2(\text{SiO}_4)(\text{OH})_8$, PDFcard 380368). The XRD pattern for 28-0.75-100/0 was similar to the above-described sample without sodium silicate, suggesting that the nature of the crystalline phases was not influenced by the nature of the chemical activator. For samples containing SCSA (28-0-75/25 and 28-0.75-75/25), the main peak belonged to quartz phase, suggesting that this crystalline phase did not react towards the alkaline medium. Similar peaks to BFS-containing pastes were identified: calcite and (C,N)-A-S-H. This means that the nature of the crystalline products did not strongly influence the hydration of BFS by the presence of SCSA.

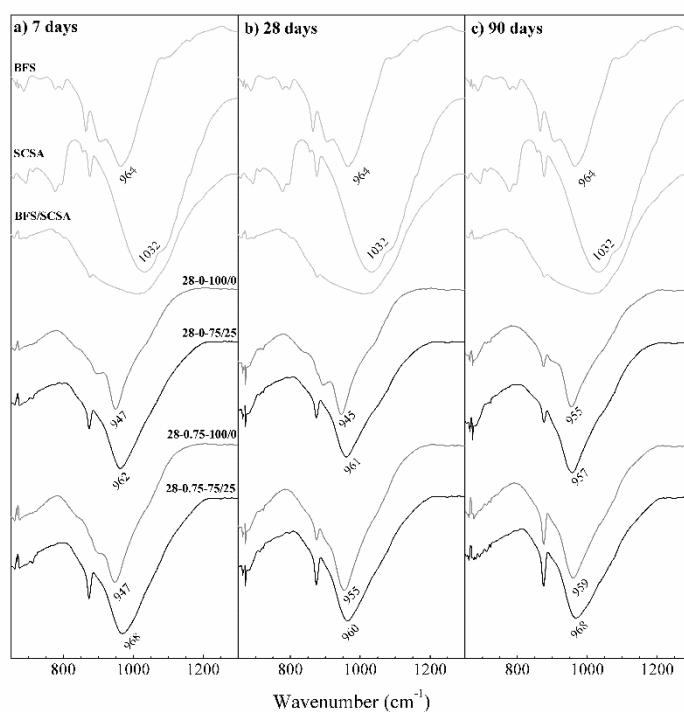
Figure 6.2 – XRD patterns of the raw materials (BFS and SCSA) and the pastes 28-0-100/0, 28-0-75/25, 28-0.75-100/0 and 28-0.75-75/25 after 90 days of curing (Key: Q: quartz; C: calcite, H: hydrotalcite; K, katoite; C-S-H: calcium silicate hydrate)



FTIR spectra of the raw materials (BFS, SCSA and a BFS/SCSA mixture by proportion of 75/25 before combining with the alkaline solution) and the pastes 28-0-100/0, 28-0-75/25, 28-0.75-100/0 and 28-0.75-75/25 after 7, 28 and 90 days of curing are shown in

Figure 6.3. The broadband in the range from 800-1270 cm^{-1} may be highlighted, as this is related to the amorphous Si-O-T vibrations of the raw materials and pastes (being T Si or Al) (MORAES et al., 2016a; ISMAIL et al., 2014). Firstly, regarding the raw materials, the BFS spectrum presented a broadband centred at 964 cm^{-1} ; the SCSA spectrum also showed a broadband, in this case centred at 1032 cm^{-1} . A blend of BFS/SCSA was also assessed in order to visualise the modification on the spectrum when raw materials are combined with the alkaline solution before the reaction. In this case, the broadness of the band was much larger than those for raw materials (from 810 to 1270 cm^{-1}) as a consequence of the sum of absorptions from both materials. This more flattened broadband must be taken as the starting point for monitoring the hydration evolution by FTIR.

Figure 6.3 – FTIR spectra of the raw materials (BFS and SCSA) and the pastes 28-0-100/0, 28-0-75/25, 28-0.75-100/0 and 28-0.75-75/25 after 7, 28 and 90 days of curing



Regarding the AAM pastes after 7 days of curing (Fig. 6.3a), it can be seen that the strongest peaks are in the interval of 940-970 cm^{-1} , which is the wavenumber region for the (C,N)-A-S-H gels from the BFS activation (MORAES et al., 2016a; ISMAIL et al., 2014). The changes observed in the band position for both BFS and BFS/SCSA systems can be

related to the effect of Al/Si and Ca/Si ratios: the decrease of these values induces an increase in the wavenumber band (SALIH et al., 2015; RAVIKUMAR; NEITHALATH, 2012). As the aluminium content for both raw materials is very low, the changes in the wavenumbers is more related to changes in the Ca/Si ratio. In addition, the dissolution of silica-glassy part from SCSA (whose band absorption was higher in energy than the one found for gel) that reacts with BFS particles and forms part of the gel can also shift the broadband position to a lower wavenumber. In general, for BFS samples, the broadband peak energy increased with curing time, with this increase being higher for sodium silicate activated paste (28-0.75-100/0). This suggests that silicate tetrahedral anions are more strongly linked in the (C,N)-A-S-H gel. On the contrary, BFS/SCSA samples did not show a significant shift to higher energy in the broadband FTIR peak with curing time. This behaviour can be explained as follows: despite the formation of a more linked structure with the presence of SCSA (as suggested by compressive strength behaviour), part of glassy silica from SCSA was reacted to form cementing gel. In this way, the intensity of the absorption related to SCSA was diminished, and the resulting peak of the overlapped absorptions from the unreacted SCSA and the formed gel did not shift to higher energies. In the case of BFS specimens (without SCSA), the difference between the main peak of raw material (964 cm^{-1}) and the peak associated with the formed gel ($945\text{-}959\text{ cm}^{-1}$) in the activated pastes was very low; the influence of the raw BFS consumed through the reaction was negligible in the FTIR absorption overlap. The absorption band related to the presence of carbonates (875 cm^{-1}) was easily identified in SCSA and in all pastes which contain this ash. This FTIR peak increased with curing time, suggesting the carbonation of the pastes during the curing process. This carbonation process also affected the BFS pastes. Thus, after 7 days of curing, the peak centred at 875 cm^{-1} was not shown for 28-0-100/0 and 28-0.75-100/0 pastes; however, after 28 curing days, paste activated by sodium silicate showed this peak, and both pastes showed this absorption peak after 90 curing days.

TGA results (derivative thermogravimetric curve, DTG) on the pastes 28-0-100/0, 28-0-75/25, 28-0.75-100/0 and 28-0.75-75/25 after 7, 28 and 90 days of curing are presented in Figure 6.4. In this study, the main peaks and most important mass losses were at the temperatures of 110-165, 200-250 and $580\text{-}620^{\circ}\text{C}$. Therefore, Table 6.4 is presented with the mass losses in the following important temperature ranges of $35\text{-}250^{\circ}\text{C}$ (P_g , mass loss related to the formed gel), $450\text{-}650^{\circ}\text{C}$ and the total mass loss (P_t) obtained in the test (35-

1000°C). DTG peaks in the range 110-160°C are related to the dehydration of (C,N)-A-S-H or C-S-H gels from the activation of the BFS (PEREIRA et al., 2015; ABDALQADER et al., 2016). The peak placed at 200-250°C is associated with the decomposition C-A-S-H gels (e.g. stratlingite or C_2ASH_8) (PEREIRA et al., 2015; EL-DIDAMONY, 2012). Finally, the peaks observed in the range of 580-600°C are related to the decomposition of calcium carbonate. This decomposition temperature range is noticeably lower than that observed for calcite from natural source (700-850°C): this is probably due to the particle size of the $CaCO_3$ crystals produced in the carbonation process, which is a poorly crystallised phase (ABDALQADER et al., 2015) and to the presence of sodium ions, both influencing the decrease in temperature decomposition.

In general terms, it can be noticed that the mass losses increased with curing time, and for a given curing age, they increased with the presence of SCSA and/or sodium silicate: 28-0-100/0 presented the lowest total mass loss, and also presented the lowest mass losses for the ranges 35-250 and 450-650°C. For early age SCSA-containing samples (7 days), the peak centred in the range from 450-650°C was very intense, as can be seen in DTG curves (Figure 6.4). This was probably due, on the one hand, to the initial calcium carbonate present in the ash, as confirmed by XRD, and on the other hand by the higher carbonation rate of the sample with the presence of SCSA. For medium curing times (28 days), sample 28-0.75-100/0 also showed this peak, and the same long curing time (90 days) was seen in the 28-0-100/0 sample. These results suggest that the formation of the compound that decomposes at this temperature range is formed in all of the studied systems; however, the rate of formation changed depending on the mixture.

Linear relationships have been found between the mass loss calculated from the thermogravimetric analysis and the developed compressive strength of mortar (Figure 6.5). As a consequence of the alkaline activation reaction progress, more hydrates are formed and more strength is developed. Thus, mass loss in the range 35-250°C (P_g , related to low temperature water releasing from cementing gel) increased with compressive strength. A similar trend was found for total mass loss (P_t , in the range 35-1000°C).

Figure 6.4 – DTG curves of the pastes 28-0-100/0, 28-0-75/25, 28-0.75-100/0 and 28-0.75-75/25 after 7, 28 and 90 days of curing

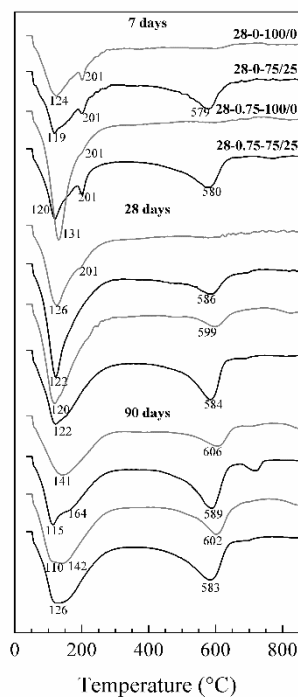
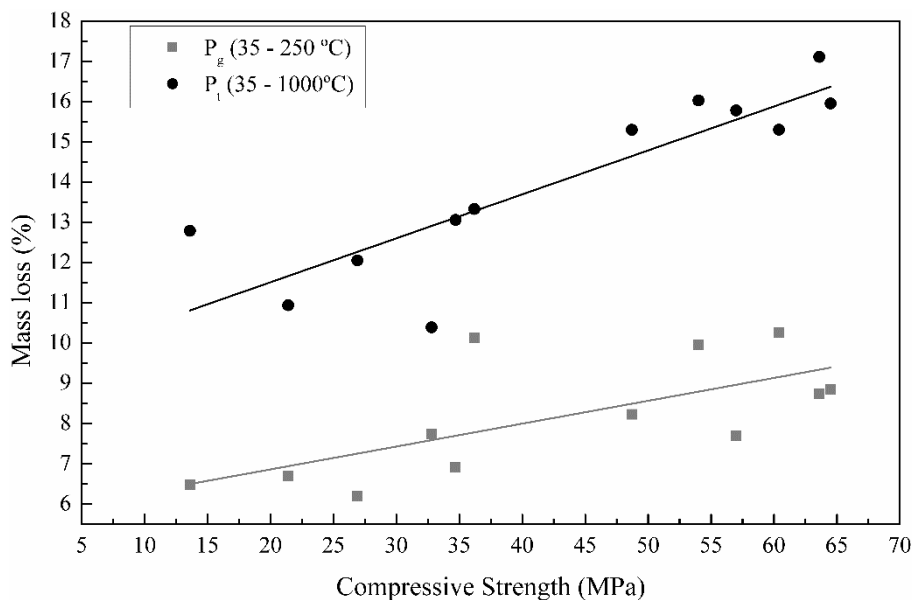


Table 6.4 – Mass losses (%) for the pastes 28-0-100/0, 28-0-75/25, 28-0.75-100/0 and 28-0.75-75/25 after 7, 28 and 90 days of curing at different temperature ranges (35-250°C, 450-650°C, and total mass loss 35-1000°C)

Specimen	Mass losses (%)								
	7 days			28 days			90 days		
	35-250	450-	Total	35-250	450-	Total	35-250	450-	Total
	°C (P _g)	650 °C	(P _t)	°C (P _g)	650 °C	(P _t)	°C (P _g)	650 °C	(P _t)
28-0-100/0	6.70	1.50	10.94	7.74	0.93	10.39	6.92	3.16	13.06
28-0 -75/25	6.20	3.57	12.05	9.96	3.36	16.03	7.69	5.37	15.78
28-0.75-100/0	10.14	1.03	13.33	10.25	2.44	15.30	8.85	4.18	15.95
28-0.75-75/25	6.47	3.99	12.79	8.23	4.72	15.30	8.73	5.45	17.11

Figure 6.5 – Relationships between thermogravimetric mass losses for pastes (P_g , 35-250°C; and P_t , 35-1000°C) and the compressive strength of mortars.



MIP results for the pastes 28-0-100/0, 28-0-75/25, 28-0.75-100/0 and 28-0.75-75/25 after 90 days of curing are summarised in Table 6.5. The influence of SCSA in total porosity was insignificant for pastes activated with only sodium hydroxide (28.42 and 28.44% for 28-0-100/0 and 28-0-75/25, respectively); however, for the specimens with $\varepsilon = 0.75$, the paste with the ash presented greater porosity than its respective control (24.28 and 27.66% for 28-0.75-100/0 and 28-0.75-75/25, respectively). Taking into account the Hg retained in the intrusion-extrusion cycle, the presence of SCSA reduced the tortuosity in the paste from their respective controls (35.15 and 43.52%, respectively for $\varepsilon = 0$, and 27.85 and 38.75% for $\varepsilon = 0.75$, in that order). Probably, the presence of a fine powder (finer than BFS) and the production of cementing gel from its solution-precipitation process, yielded a more homogeneous capillary and gel pore networks, with the lower formation of ink-bottle pores.

Regarding the volume pore distribution of the pastes, differential and accumulated distribution MIP curves are depicted in Figure 6.6. Differential distribution curves (Figure 6.6a) showed two main types of pores for all tested pastes: capillary pores in the 100 to 5000 nm range (similar to large capillary pore network defined by Mindness et al. (2002) for OPC pastes, and small capillary and gel pores in the range 3 to 30 nm. Interestingly, SCSA containing pastes showed a low volume of Hg intruding into the highest size pores, being lower than 0.02 mL/g of paste (see Table 6.5). Contrarily, for samples without SCSA, this

value was higher than 0.04 mL/g of paste. This means that SCSA reacted in the alkaline medium and produced a refined pore size in this range. This pore refinement produced smaller pores, and the intruded Hg volume was significantly higher for these smaller pores: in this way, the median pore diameter for SCSA containing AAMs was very low (9.14 and 7.04 nm for $\varepsilon = 0$ and $\varepsilon = 0.75$ respectively). Interestingly, the presence of the sodium silicate in the activated BFS sample (28-0.75-100/0) produced a beneficial effect on the reduction of porosity, and gel pore volume was very low compared to the other pastes. Probably, the presence of dissolved silicate in the activating solution favoured the formation of a denser gel with a gel pore size lower than 3 nm. This is the reason for the high mean diameter in volume (diameter of the pore size for which 50% of Hg volume was intruded): the value of 272 nm was due to the low gel pore volume. Thus, for silicate-activated BFS mortar, good mechanical properties were achieved.

Figure 6.6 – MIP curves of the pastes 28-0-100/0, 28-0-75/25, 28-0.75-100/0 and 28-0.75-75/25 after 90 days of curing: a) differential, and b) accumulated distribution

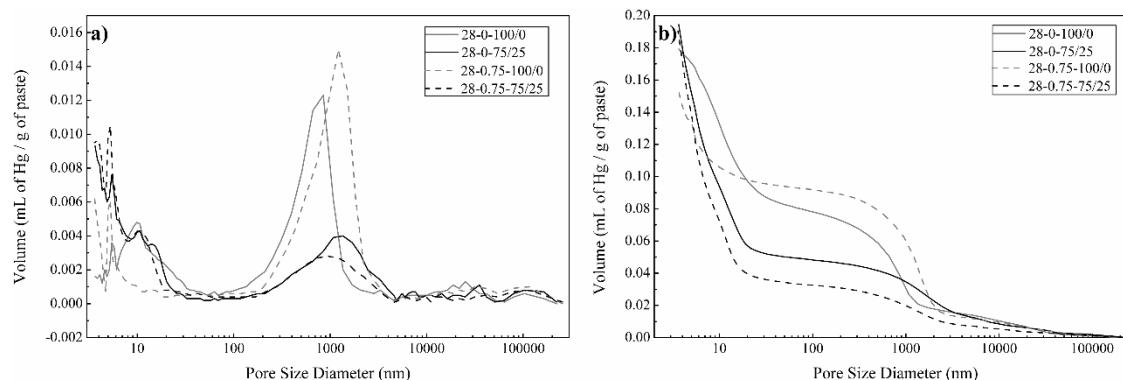
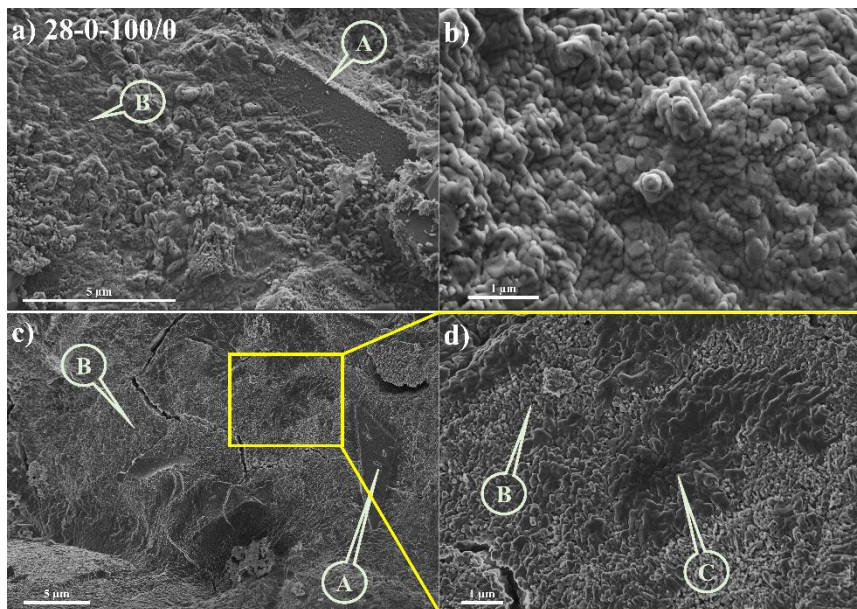


Table 6.5 – MIP results of the pastes 28-0-100/0, 28-0-75/25, 28-0.75-100/0 and 28-0.75-75/25 after 90 days of curing

Specimen	Total porosity (%)	Total pore area (m ² /g)	Median pore diameter		Volume (mL of Hg/g of paste) and percentage			Hg retained (%)
			Volume (nm)	Area (nm)	> 5000 nm	5000 - 100 nm	< 100 nm	
28-0-100/0	28.42	43.06	27.04	7.62	0.0139 (7.74%)	0.064 (35.67%)	0.1013 (56.54%)	43.52
28-0-75/25	28.44	91.44	9.14	5.12	0.0126 (6.39%)	0.0355 (17.98%)	0.1463 (74.06%)	35.16
28-0.75-100/0	24.28	42.99	545.80	5.02	0.0118 (7.63%)	0.0801 (51.55%)	0.0633 (40.82%)	27.85
28-0.75-75/25	27.66	102.15	7.04	5.06	0.0072 (3.77%)	0.0254 (13.33%)	0.1578 (82.9%)	38.75

FESEM images of the pastes 28-0-100/0, 28-0-75/25, 28-0.75-100/0 and 28-0.75-75/25 after 90 days of curing are presented in the Figures 6.7-10. Regarding the paste with NaOH-activated BFS (28-0-100/0, Fig. 6.7), a particle of the solid precursor can be observed (BFS, spot A in Fig 6.7a) with some binding gel products (spot B, Fig 6.7a) around it. EDS analysis on the unreacted BFS particle gave the following atomic ratios: Ca/Si=0.76, Al/Si=0.33 and Na/Si=0.02. Most of the sample was occupied by the porous gel shown in the Fig 6.7b: it was formed by an imbricated set of irregular gel particles with sizes in the 200-50nm range. This gel was analysed by EDS, resulting in the following atomic ratios: Ca/Si = 0.83 ± 0.05 , Al/Si = 0.34 ± 0.02 , and Na/Si = 0.39 ± 0.06 . The Si:Al:Ca proportion was 0.46:0.14:0.38, which corresponds to a C-A-S-H gel according to Abdalqader et al. (2016). FESEM micrographs taken by using an in-lens system (Fig 6.7c) showed a very homogeneous binding gel, and some small areas are covered by a denser gel (spot C, Fig 6.7d).

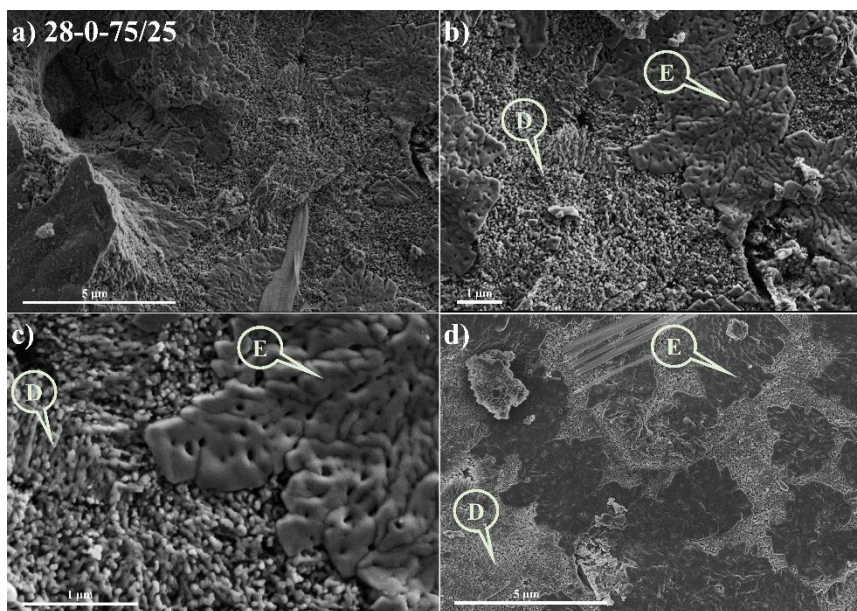
Figure 6.7 – FESEM micrographs of BFS activated paste with NaOH (28-0-100/0): a) general view of the paste with an unreacted BFS particle (spot A) and gel (spot B); b) detailed view of the gel; c) in-lens micrograph showing BFS unreacted particle (spot A) and main gel (spot B); d) enlarged zone from c), in which a denser gel is shown (spot C).



In Figure 6.8, some FESEM micrographs for 28-0-75/25 paste are depicted. In Figure 6.8a, a general view of the gel is presented. In figures 6.8b and 6.8c, the presence of two different types of formed gels is noteworthy (see spots D and E). In spot D, the gel appears to be made of small particles (size under 50 nm), which are smaller than those obtained in the 28-0-100/0 specimen. In addition, its composition shows similar values to that obtained for porous gel in the 28-0-100/0 paste: $\text{Ca/Si} = 0.84 \pm 0.03$, $\text{Al/Si} = 0.28 \pm 0.02$, and $\text{Na/Si} = 0.37 \pm 0.04$. In this case, the Si:Al:Ca proportion was 0.47:0.13:0.40, which also corresponds to a C-A-S-H gel. The Na/Si atomic ratio was similar to 28-0-100/0 paste (0.37 vs 0.39) despite the higher quantity of Si in the 28-0-75/25 paste due to the presence of SCSA. In contrast, the other gel (see spot E) showed a different morphology: more compacted, denser particles larger than 200 nm and irregularly hollowed (holes smaller than 50 nm size). This gel resulted in the following atomic ratios: $\text{Ca/Si} = 0.65 \pm 0.08$, $\text{Al/Si} = 0.28 \pm 0.02$, and $\text{Na/Si} = 0.30 \pm 0.05$. The Si:Al:Ca proportion was 0.52:0.14:0.34, which corresponds to a C(N)-A-S-H gel according to Abdalqader et al. (2016). The presence of SCSA in the mix favoured the formation of gels with a lower percentage of Ca and higher percentage of Na. Additionally, if the Na/Ca and (Na+K)/Ca ratios are compared, the influence on the composition of the gel can be noticed due to the K contained in the ash. Thus, the Na/Ca and (Na+K)/Ca ratios for 28-0-100/0 were very similar: 0.47 ± 0.06 and 0.52 ± 0.06 respectively. In contrast, gels in 28-0-75/25 paste showed much higher values for (Na+K)/Ca than for Na/Ca (for porous gel, 0.59 ± 0.01 vs. 0.44 ± 0.03 ; for compacted gel, 0.69 ± 0.12 vs. 0.47 ± 0.13). Figure 6.8d shows the distribution of both gels, porous and compacted, taken by using an in-lens system: darker zones belong to compacted gels and lighter ones to porous gels.

Figure 6.8 – FESEM micrographs of BFS/SCSA activated paste with NaOH (28-0-75/25):

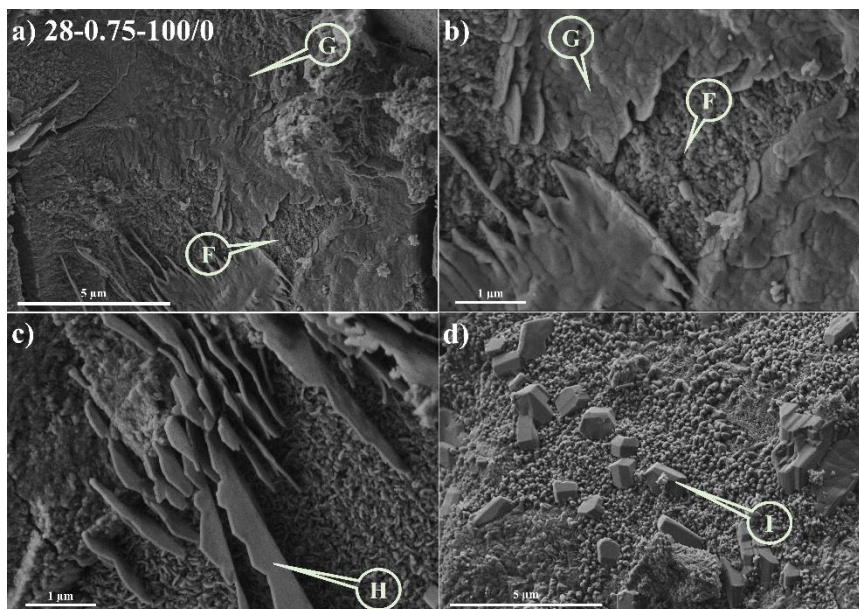
a) general view of the paste; b) general view of formed gels (spot D shows a porous gel, and spot E, a compacted gel); c) detailed view of both gels; d) in-lens view (lighter area for porous gel, and darker are for compacted gel).



Regarding the specimen of BFS activated with both sodium hydroxide and silicate, Fig. 6.9a shows a general view of the microstructure, in which a large zone is covered by a compacted gel (spot G) with a smaller area covered by a more porous gel (spot F). Both types of formed gel can also be seen in the enlarged zone (Fig 6.9b). The porous gel (see spot F, Fig 6.9b) is similar to porous gel found in the microstructure of the 28-0-75/25 paste; the denser gel (see spot G, Fig 6.9b) is a continuous gel similar in composition to the one found in 28-0-75/25 paste (spot D). Also, some crystalline formations have been found: in Fig 6.9c, sheet-like crystals which were surrounded by a porous gel with the following composition (atomic ratios): $\text{Ca/Si} = 0.85 \pm 0.03$, $\text{Al/Si} = 0.29 \pm 0.01$, and $\text{Na/Si} = 0.09 \pm 0.03$. This chemical composition suggested that this phase is a C-A-S-H gel, and probably the crystals are stratlingite, $\text{Ca}_2\text{Al}_2(\text{SiO}_2)(\text{OH})_{10} \cdot 2.5\text{H}_2\text{O}$. In Fig 6.9d, some well-formed crystals, with a size of around 500 nm, were found. It was very difficult to perform chemical analysis because of the influence of the surrounding matrix, but interestingly the Na/Ca atomic ratio was very high (1.20 ± 0.02). This atomic ratio and the carbonation (ZAHARAKI; KOMNITSAS, 2009) of the sample (accordingly to TGA studies) allowed us

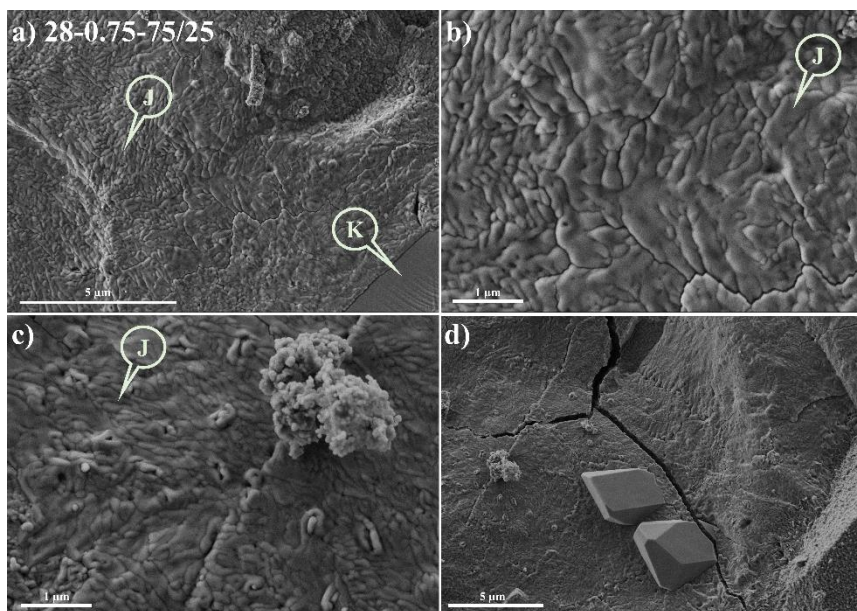
to conclude that they are pirssonite, $\text{Na}_2\text{Ca}(\text{CO}_3)_2 \cdot 2\text{H}_2\text{O}$. They can be formed due to carbonation of the sample.

Figure 6.9 – FESEM micrographs of BFS activated paste with NaOH and sodium silicate (28-0.75-100/0): a) general view of the paste with some gel formation (spot F shows a porous gel, and spot G, a compacted gel); b) detailed view of formed gels; c) detailed view of sheet-like crystals (spot H, stratlingite); d) pirssonite crystals surrounded by gels.



In Fig. 6.10, some micrographs of the 28-0.75-75/25 paste are depicted. Fig 6.10a show a general view of the microstructure, in which much of the shown area is covered by a compacted gel (spot J). In the bottom-right corner of this micrograph, a particle of quartz was identified (probably from the SCSA, spot K). Figures 6.10b and 6.10c showed a detailed arrangement of the compacted gel (spot J): this gel was very similar to the compacted gel found for 28-0 -75/25 paste (see Fig 6.8c, spot D), in this case with a less hollowed pattern. Finally, in Fig 6.10d, pirssonite crystals (2-3 μm size) are shown, produced by the carbonation process.

Figure 6.10 – FESEM micrographs of BFS/SCSA activated paste with NaOH and sodium silicate (28-0.75-75/25): a) general view of the paste with some gel formation (spot J) and a quartz particle (spot K); b) detailed view of compacted gel; c) detailed view of gel; d) pirssonite crystals surrounded by gels.



6.4 CONCLUSIONS

BFS alkali activated materials (AAM) activated by alkaline solutions in the $\text{H}_2\text{O}/\text{Na}_2\text{O}$ (η) range of 22 to 37 (equivalent to a Na^+ molality of 5 to 3 mol.kg^{-1}) and the corresponding systems with the replacement of BFS by sugarcane straw ash (SCSA) were studied. NaOH and a mixture of NaOH+sodium silicate solutions, $\text{SiO}_2/\text{Na}_2\text{O}$ ratios (ϵ) of 0 and 0.75 respectively, were assessed as activating solutions. In terms of mortar compressive strength behaviour, the replacement of BFS by SCSA did not negatively affect the mechanical performance produced. Interestingly, this replacement enabled the strength behaviour respect to the NaOH activated BFS-AAM: increases in the strength were 86% and 66% at 28 and 90 days, respectively. Moreover, these strength values were slightly lower than those obtained for sodium silicate BFS-AAMs (at 90 days of curing, reached 80-90% of the strength for BFS-mortar). Also, the strength behaviour due to the influence of SCSA content (assessed on the interval of 15-50% replacement of BFS) did not show differences at 90 days of curing, which represents an interesting advantage in terms of the design and dosage of the AAMs. The optimum BFS/SCSA proportion was 75/25 due to its better

compressive strength developed in the early curing time with respect to other tested replacements. Regarding the effect of the alkaline solution, the η ratio also did not influence the compressive strength at 90 days of curing; however, the strength evolution was significantly affected by the replacement: very early aged (3 days) mortars containing SCSA yielded low strength values. From microstructural studies, the significant role of SCSA in the development of the gel formed due to the alkali activation process was investigated. From XRD, TG and FTIR analyses, no differences in the nature of the cementing gel were found between the tested pastes. However, mercury intrusion porosimetry (MIP) measurements highlighted the critical reduction in the capillary pore volume for SCSA-containing pastes compared to the NaOH-BFS activated system. The high gel pore volume from MIP and the presence of compacted gel identified by FESEM in the SCSA systems agreed with the good mechanical behaviour of SCAS-activated mortars. A high proportion of a C(N)-A-S-H compacted gel was observed in these SCSA-systems, in a similar way to the observations for BFS activated with sodium silicate. From a general point of view, despite the low alkali concentration in the activation solutions, the SCSA plays an important role in the development of the binding ability of the alkali-activated paste. For these systems, a replacement of sodium silicate in the activating solution by the dosage of SCSA in the precursor can be proposed as a way to yield highly sustainable binders. Thus, interesting mixtures containing SCSA can be designed, which yield a similar performance to BFS systems, meaning that good valorisation of this biomass waste can be carried out for low alkalinity-activated materials.

ACKNOWLEDGMENTS

The authors would like to thanks to CNPq processo nº 401724/2013-1 and the "Ministerio de Educación, Cultura y Deporte" of Spain ("Cooperación Interuniversitaria" program with Brazil PHB-2011-0016-PC). Thanks are also given to the Electron Microscopy Service of the Universitat Politècnica de València.

REFERENCES

- ABDALQADER, A. F.; JIN, F.; AL-TABBAA, A. A. *Development of greener alkali-activated cement: utilisation of sodium carbonate for activating slag and fly ash mixtures. Journal of Cleaner Production*, v. 113, p. 66-75, 2016.
- AYDIN, S.; BARADAN, B. *Effect of activator type and content on properties of alkali-activated slag mortars. Composites Part B: Engineering*, v. 57, p. 166-172, 2014.
- BERNAL, S. A.; NICOLAS, R. S.; van DEVENTER, J. S. J.; PROVIS, J. L. *Alkali-activated slag cements produced with a blended sodium carbonate/sodium silicate activator. Advances in Cement Research*, v.28, p. 262-273, 2016.
- BOUZÓN, N.; PAYÁ, J.; BORRACHERO, M. V.; SORIANO, L.; TASHIMA, M. M.; MONZÓ, J. *Refluxed rice husk ash/NaOH suspension for preparing alkali activated binders. Materials Letters*, p. 72-74, 2014.
- CASTALDELLI, V. N.; AKASAKI, J. L.; MELGES, J. L. P; TASHIMA, M. M.; SORIANO, L.; BORRACHERO, M. V.; MONZÓ, J.; PAYÁ, J. *Use of Slag/Sugar Cane Bagasse Ash (SCBA) Blends in the Production of Alkali-Activated Materials. Materials*, v. 6, p. 3108-3127, 2013.
- EL-DIDAMONY, H.; AMER, A. A.; ELA-ZIZ, H. A. *Properties and durability of alkali-activated slag pastes immersed in sea water. Ceramics International*, v. 38, p. 3773-3780, 2012.
- ESCALANTE-GARCIA, J. I.; FUENTES, A. F.; GOROKHOVSKY, A.; FRAIRE-LUNA, P.E.; MENDONZA-SUAREZ, G. *Hydration products and reactivity of blast-furnace slag activated by various alkalis. Journal of the American Ceramic Society*, v. 86, p. 2148-53, 2003.
- ISLAM, A.; ALENGARAM, U. J.; JUMAAT, M. Z.; BASHAR, I. I. *The development of compressive strength of ground granulated blast furnace slag-palm oil fuel ash-fly ash based geopolymer mortar. Materials and Design*, v. 56, p. 833-841, 2014.
- ISMAIL, I.; BERNAL, S. A.; PROVIS, J. L.; NICOLAS, R. S.; HAMDAN, S. van DEVENTER, J. S. J. *Modification of phase evolution in alkali-activated blast furnace slag by the incorporation of fly ash. Cement and Concrete Composites*, v. 45, p. 125-135, 2014.
- LEAL, M. R. L. V.; GALDOS, M. V.; SCARPARE, F. V.; SEABRA, J. E. A; WALTER, A.; OLIVEIRA, C. O. F. *Sugarcane straw availability, quality, recovery and energy use: A literature review. Biomass Bioenergy*, v. 53, p. 11-19, 2013.
- LEMO, S. V.; DENADAI, M. S.; GUERRA, S. P. S.; ESPERANCINI, M. S. T.; BUENO, O. C.; TAKITANE, I. C. *Economic efficiency of two baling systems for sugarcane straw. Industrial Crops and Products*, v. 55, p. 97-101, 2014.

MESA-PÉREZ, J. M.; ROCHA, J. D.; BARBOSA-CORTEZ, A.; PENEDO-MEDINA, M.; LUENGO, C. A.; CASCAROSA, E. *Fast oxidative pyrolysis of sugar cane straw in a fluidised bed reactor*. **Applied Thermal Engineering**, v. 56, p. 167-175, 2013.

MINDNESS, S.; YOUNG, J. F.; DARWIN, D. *Concrete*, second ed., Pearson, London, 2002.

MORAES, B. S.; ZAIAT, M.; BONOMI, A. *Anaerobic digestion of vinasse from sugarcane ethanol production in Brazil: Challenges and perspectives*. **Renewable and Sustainable Energy Reviews**, v. 44, p. 888-903, 2015.

MORAES, J. C. B.; MELGES, J. L. P.; AKASAKI, J. L.; TASHIMA, M. M.; SORIANO, L.; MONZÓ, J.; BORRACHERO, M. V.; PAYÁ, J. *Pozzolanic Reactivity studies on a biomass-derived waste from sugar cane production: Sugar Cane Straw Ash (SCSA)*. **ACS Sustainable Chemistry and Engineering**, v. 4, p. 4273-4279, 2016b.

MORAES, J. C. B.; TASHIMA, M. M.; AKASAKI, J. L.; MELGES, J. L. P.; MONZÓ, J.; BORRACHERO, M. V.; SORIANO, L.; PAYÁ, J. *Increasing the sustainability of alkali-activated binders: the use of sugar cane straw ash (SCSA)*. **Construction and Building Materials**, v. 124, p. 148-154, 2016a.

OZER, I.; SOYER-UZUN, S. *Relations between the structural characteristics and compressive strength in metakaolin based geopolymers with different molar Si/Al ratios*. **Ceramics International**, v. 41, p. 10192-10198, 2015.

PARIS, J. M.; ROESSLER, J. G.; FERRARO, C. C.; DEFORD, H. D.; TOWNSEND, T. G. *A review of waste products utilized as supplements to Portland cement in concrete*. **Journal of Cleaner Production**, v. 121, p. 1-18, 2016.

PAYÁ, J.; MONZÓ, J.; BORRACHERO, M. V.; TASHIMA, M. M. *Reuse of aluminosilicate industrial waste materials in the production of alkali-activated concrete binders*. In: PACHECO-TORGAL, F.; LABRINCHA, J.A.; LEONELLI, C.; PALOMO, A.; CHINDAPRASIRT, P. *Handbook of Alkali-activated Cements, Mortars and Concretes*, first ed. Cambridge, Woodhead Publishing and Elsevier, Waltham, Kidlington, 2015.

PEREIRA, A.; AKASAKI, J. L.; MELGES, J. L. P.; TASHIMA, M. M.; SORIANO, L.; BORRACHERO, M. V.; MONZÓ, J.; PAYÁ, J. *Mechanical and durability properties of alkali-activated mortar based on sugarcane bagasse ash and blast furnace slag*. **Ceramics International**, v. 41, p. 13012-13024, 2015.

PUERTAS, F.; TORRES-CARRASCO, M. *Use of glass waste as an activator in the preparation of alkali-activated slag. Mechanical strength and paste characterisation*. **Cement and Concrete Research**, v. 57, p. 95-104, 2014.

RAVIKUMAR, D.; NEITHALATH, N. *Effects of activator characteristics on the reaction product formation in slag binders activated using alkali silicate powder and NaOH*. **Cement and Concrete Composites**, v. 34, p. 809-818, 2012.

SALIH, M. A.; FARZADNIA, N.; ALI, A. A. A.; DEMIRBOGA, R. *Development of high strength alkali activated binder using palm oil fuel ash and GGBS at ambient temperature*. **Construction and Building Materials**, v. 93, p. 289-300, 2015.

SHI, C.; KRIVENKO, P. V.; Roy, D. *Alkali-Activated Cements and Concretes*, Taylor and Francis, London and New York, 2006.

SONG, S.; JENNIGS, H. M. *Pore solution chemistry of alkali-activated ground granulated blast-furnace slag*. **Cement and Concrete Research**, v. 29, p. 159-170, 1999.

Sugarcane production. **UNICA – União da Indústria de Cana-de-Açúcar Website**; <http://www.unicadata.com.br/index.php?idioma=2>

TASHIMA, M. M.; AKASAKI, J. L.; MELGES, J. L. P.; SORIANO, L.; MONZÓ, J.; PAYÁ, J.; BORRACHERO, M. V. *Alkali activated materials based on fluid catalytic cracking catalyst residue (FCC): Influence of $\text{SiO}_2/\text{Na}_2\text{O}$ and $\text{H}_2\text{O}/\text{FCC}$ ratio on mechanical strength and microstructure*. **Fuel**, v. 108, p. 833-839, 2013.

TCHAKOUTÉ, H. K.; RÜSCHER, C. H.; KONG, S.; KAMSEU, E.; LEONELLI, C. *Comparison of metakaolin-based geopolymer cements from commercial sodium waterglass and sodium waterglass from rice husk ash*. **Journal of Sol-Gel Science and Technology**, v. 78, p. 492-506, 2016.

YUSUF, M. O.; JOHARI, M. A. M.; AHMAD, Z. A.; MASLEHUDDIN, M. *Evolution of alkaline activated ground blast furnace slag-ultrafine palmoil fuel ash based concrete*. **Materials and Design**, v. 55, p. 387-393, 2014.

ZAHARAKI, D.; KOMNITSAS, K. *Effect of additives on the compressive strength of slag-based inorganic polymers*. **Global NEST Journal**, v. 11, p. 137-146, 2009.

7 SUGAR CANE STRAW ASH AS SOLID PRECURSOR IN ALKALI-ACTIVATED BINDERS BASED ON BLAST FURNACE SLAG: SOLUTIONS WITH [N+] OF 6-10 MOL.KG⁻¹

The article entitled as "*Optimum use of sugar cane straw ash (SCSA) in alkali-activated binders based on blast furnace slag (BFS)*" by J. C. B. Moraes, M. M. Tashima, J. L. P. Melges, J. L. Akasaki, J. Monzó, M. V. Borrachero, L. Soriano and J. Payá was accepted in the **Journal of Materials in Civil Engineering**.

Abstract: Alkali-activated binders (AAB) are a material obtained from the combination of a solid precursor and an alkaline activating solution. In this study, one solid precursor utilised was blast furnace slag (BFS) and the other was an agro waste: sugar cane straw ash (SCSA). Sodium hydroxide was used for preparing activating solutions. In order to reach the potential reactivity of the SCSA, a study varying the BFS/SCSA mass ratio and H₂O/Na₂O molar ratio was carried out. The BFS/SCSA ratio varied from 100/0 to 70/30, and H₂O/Na₂O was studied in the range of 11.1–18.5. To fulfil this objective, specimens were assessed by their compressive strength of mortars and microstructural studies of pastes (XRD, TGA, FTIR, FESEM) in the curing time range of 3–90 days at 25 °C. Results from these tests showed that the best BFS/SCSA and H₂O/Na₂O ratios were 70/30 and 18.5, respectively. This study revealed an interesting valorisation of the SCSA as a complementary precursor in BFS-based alkali-activated binders due to the improvement of mechanical properties and the reduction in the consumption of BFS in AAB.

KEYWORDS: *Agro Waste, Optimum Replacement, Microstructural Studies, Compressive Strength.*

7.1 INTRODUCTION

The recent concerns in the last decades about the reduction of three worldwide problems, which are high CO₂ (greenhouse gas) emissions, the use of non-renewable raw materials and energy consumption, have increased the investigation of new sustainable and environmentally friendly materials (SHI et al., 2011; MADLOOL et al., 2013; TURNER et al., 2013; USÓN et al., 2013; ZHANG et al., 2014). In building construction, these concerns are related to the current widespread use of Portland cement, which is one of the most used materials in the world (SHEN et al., 2014). In this binder production process, a total energy of 3000 MJ is spent per ton of clinker, and the raw materials (mainly limestone and clay) involved in this manufacturing procedure are from non-renewable sources (USÓN et al., 2013). As concerns the greenhouse gas emissions from cement production, it is responsible for emitting 5–7% of the total world emissions (TURNER et al., 2014). Therefore, in order to reduce the consumption of Portland cement, a new type of environmentally friendly material that are being widely studied is presented as an interesting option: alkali-activated binders (AAB) (PROVIS et al., 2015). These binders are obtained when a highly concentrated alkaline solution is mixed with a solid precursor (usually an amorphous aluminosilicate), and this combination generates binding gels with mechanical properties and durability similar to or even better than Portland cement mixtures (PROVIS et al., 2014; PACHECO-TORGAL et al., 2015). The environmentally friendly characteristics of AAB come from the reduced CO₂ emissions and energy consumption (DUXSON et al., 2007; van DEVENTER et al., 2010; TURNER et al., 2013), as well as the use of by-products from important industries as solid precursors in their mixtures, such as blast-furnace slag (BFS) and fly ash (FA) (PROVIS 2014; PACHECO-TORGAL 2015). One of the most studied precursors in AAB is blast-furnace slag (SHI et al., 2006). This precursor can be easily activated by the addition of an alkali hydroxide solution. Regarding the activating solution, it has an important role in the development of the mechanical properties of the AAB (WANG et al., 1995; TASHIMA et al., 2013; AYDIN et al., 2014; OZER et al., 2015). The most utilised reagent is sodium hydroxide (NaOH) (PROVIS et al., 2014; PACHECO-TORGAL et al., 2015). In the activation of BFS with NaOH, the main reaction compound is C(N)-A-S-H gel. The Na⁺ sourced from the hydroxide is important to balance the extra negative

charge from the AlO_4^{5-} when it replaces the SiO_4^{4-} in the tetrahedrally coordinated form, and it helps to form a more polymerised gel (PROVIS et al., 2014; PACHECO-TORGAL et al., 2015). Therefore, the Na^+ concentration has an important role in the final gel structure. Another important issue is the OH^- concentration sourced from the hydroxide: previous studies showed that the use of sodium hydroxide is beneficial to accelerate the reaction process of BFS (SONG et al., 1999; SONG et al., 2000). However, at very high values of pH (> 13.0), which are obtained by using more than 1M of NaOH, the anions (silica and alumina) take an important role in the gel structure development (FERNÁNDEZ-JIMÉNEZ et al., 2003).

BFS presents an important environmental impact advantage when compared to Portland cement: the CO_2 emissions are up to 85% less than the conventional one (ÖZBAY et al., 2016). However, the increased use of BFS in the cement industries has resulted in the monetary cost of this binder increasing in the same way (MEYER, 2009). Thus, an option that investigators are researching to reduce the use of BFS is through the employment of binary systems. These systems consist in partially replacing the BFS with another mineral admixture in order to maintain or even increase the properties of the newly designed alkali-activated binder. In the recent bibliography, some examples can be found of binders utilised in binary systems with BFS, such as fly ash (CHI et al., 2013), red clay brick waste (RAKHIMOVA et al., 2015) and metakaolin (BORGES et al., 2016). An alternative to reduce the cost of the final alkali-activated binders and also to increase even more their environmentally friendly and sustainable characteristics is the use of ashes from biomass wastes as solid precursors. One example of agro waste is sugar cane bagasse ash (SCBA). Previous studies on binary BFS/SCBA systems have shown that is possible to utilise them together with some improvement in the mechanical properties of alkali-activated binders (CASTALDELLI et al., 2013; PEREIRA et al., 2015).

In this scenario of using biomass wastes, another residue has been increasing in Brazil in recent years: sugar cane straw. Two main factors explain this increase: the expansion of sugarcane production and the trend to use mechanized harvesting. As concerns the first reason, sugar cane production grew by 166% since the beginning of this century until 2016, mainly due to the production of ethanol to be used as a car fuel (MORAES et al., 2015a; UNIÃO DA INDÚSTRIA DE CANA-DE-AÇÚCAR, 2016). Regarding the mechanized harvesting factor, it has increased because a protocol signed in Brazil prohibited

pre-burning the sugar cane plant in the field – a process that makes it easier to harvest the sugar cane – due to environmental and safety issues (LEAL et al., 2013). Therefore, mechanized harvesting has been shown to be a suitable method to pick sugar cane. However, after this procedure, a waste is generated that contains mainly the leaves from the crop: the sugar cane straw. Like sugar cane bagasse, this waste has an interesting calorific value as shown by some authors (LEAL et al., 2013; UZUN et al., 2017), and can be used as a biomass to produce energy. Hence, researchers are studying methods to optimise the collection process, and the best burning method for this material to obtain the maximum energy recovery (LEMOS et al., 2014; ALVES et al., 2015). There is a high probability that this waste will become a trend to obtain energy from the burning process. However, after obtaining energy from the biomass through this procedure, a residue is generated that needs to be valorised: sugar cane straw ash (SCSA). This ash is basically formed by amorphous silica with good pozzolanic reactivity, as shown in a previous study (MORAES et al., 2016a). When the SCSA was assessed as a partial replacement for Portland cement, it could be used up to a 30% replacement percentage without significant changes in the mechanical properties (MORAES et al., 2015b). The new goal of employing SCSA is to utilise it in combined systems with blast-furnace slag in alkali-activated binders. SCSA is an important source of amorphous SiO_2 to the mixture, which means that its presence causes changes in the gel composition of BFS-based AAB. Hence, there are optimum amounts of both sodium hydroxide and SCSA that can be incorporated into the mixture to achieve the best mechanical properties. A previous study of a BFS/SCSA system activated by 8 molar NaOH solution showed that the ash improved the compressive strength from early ages when compared to the BFS mortars (MORAES et al., 2016b). In this study, the best replacements of BFS by SCSA found for 7 and 28 days curing times were 15 and 25%.

This present paper assesses the effect of the NaOH concentration of the alkaline solution on the activation of a binary BFS/SCSA system in order to achieve the best compressive strength development and calculate the cementing efficiency of SCSA in BFS-based AAB. For this purpose, a set of dosages were prepared in this investigation: the BFS/SCSA proportions assessed were 100/0, 90/10, 80/20 and 70/30, while the $\text{H}_2\text{O}/\text{Na}_2\text{O}$ molar ratios studied were 11.1, 12.3, 13.9, 15.9 and 18.5. This study was carried out on mortars and pastes: the former were assessed by their compressive strength, and the latter were analysed by X-ray diffraction (XRD), Fourier transform infrared spectroscopy (FTIR),

thermogravimetric analysis (TGA), and field emission scanning electron microscopy (FESEM).

7.2 MATERIALS AND METHODS

7.2.1 Materials

The solid precursors utilised in this study were blast-furnace slag (BFS) and sugar cane straw ash (SCSA). BFS was obtained from Ribas do Rio Pardo (Mato Grosso do Sul, Brazil). SCSA was prepared in three steps: straw calcination, following by sieving and, finally, milling the passing ash. Firstly, the burning process of the sugar cane straw was carried out by an autocombustion process (MORAES et al., 2016b). The remaining ash was sieved (0.297 mm, MESH #50) to remove some unburned particles and impurities. The final step was milling the passing material for 50 minutes. The chemical composition obtained from X-ray fluorescence (XRF) of both materials is given in Table 7.1. It can be seen that the SCSA presents SiO_2 as the main compound. Regarding the BFS, the main oxides are SiO_2 , Al_2O_3 and CaO . The particle sizes of BFS and SCSA are shown through mean (D_{med}) and median (D_{50}) diameters: the former material presents values of 21.0 and 13.4 μm , respectively; whereas these values for the ash are 18.1 and 10.6 μm . Regarding the activating solution, only sodium hydroxide pellets were utilised (NaOH, solid, purity higher than 99%), provided by Dinâmica Química. For mortars manufacturing, natural sand was utilised with a specific gravity of 2667 kg/m^3 and fineness modulus of 2.05 and was supplied from Castilho city (Sao Paulo, Brazil).

Table 7.1 – Chemical composition of the raw materials sugar cane straw ash (SCSA) and blast furnace slag (BFS) in weight percentages

Solid Precursors	SiO_2	Al_2O_3	Fe_2O_3	CaO	MgO	K_2O	SO_3	Cl	Others	LOI
SCSA	58.6	9.0	8.4	4.6	1.6	5.4	1.9	0.7	3.3	6.5
BFS	42.1	11.0	1.7	33.6	8.2	1.6	0.1	0.1	1.6	0.1

7.2.2 Design of alkali-activated binders

The optimum use of SCSA on BFS-based AAB was determined by varying the Na^+ concentration in the alkaline solution (represented by the $\text{H}_2\text{O}/\text{Na}_2\text{O}$ molar ratio) and the proportion of solid precursors (BFS/SCSA mass ratio). The designed AAB presented $\text{H}_2\text{O}/\text{Na}_2\text{O}$ molar ratio values of 11.1, 12.3, 13.9, 15.9 and 18.5, corresponding to Na^+ concentrations of 10, 9, 8, 7 and 6 mol.kg^{-1} , respectively (five ratios). For each of these ratio values, the BFS/SCSA proportions assessed were 100/0 (control), 90/10, 80/20 and 70/30 (four proportions). Therefore, the total number of dosages studied was twenty. The nomenclature proposed for these dosages is x-y/z, where the "x" is related to the $\text{H}_2\text{O}/\text{Na}_2\text{O}$ molar ratios presented previously (for simplicity, "x" values were 11, 12, 14, 16 and 19), while "y/z" is associated with the BFS/SCSA proportions assessed in this study. With respect to the water/binder (w/b, the binder being the sum of BFS and SCSA) and aggregate/binder (a/b) ratios, they were maintained as constants: the former ratio was 0.45 for both pastes and mortars, while the latter proportion was 2.5 for mortars (both ratios by mass).

7.2.3 Tests carried out for pastes and mortars

For the macrostructural studies, the compressive strength of mortars was measured by an EMIC Universal Machine with a 2000 kN load limit at a loading rate of 0.5 MPa/s. In this test, three cubic mortars of 50 x 50 x 50 mm^3 were tested to obtain an average of the compressive strength and the standard deviation. In the following microstructural studies, the pastes were evaluated by X-ray diffraction (XRD), Fourier transform infrared spectroscopy (FTIR), thermogravimetric analysis (TGA), field emission scanning electron microscopy (FESEM) and energy-dispersive X-ray spectroscopy (EDS). XRD was performed by a Bruker AXS D8 Advance, with a voltage of 40 kV and current intensity of 20 mA, where the Bragg's angle (2θ) assessed was in the range of 5–70° with a step of 0.02° and step time of 2 s/step. The FTIR equipment utilised was a Bruker Tensor 27 in the wavenumber range of 400 and 4000 cm^{-1} , the scan frequency was 0.25 s^{-1} and the resolution was 4 cm^{-1} . TGA studies were carried out by a Mettler-Toledo TGA 850 thermobalance, where the specimen was heated in a 70 μL alumina crucible in the temperature range of 35–1000 °C, with a heating rate of 20 $^{\circ}\text{C.min}^{-1}$ in an air atmosphere (75 mL.min^{-1} gas flow).

Finally, FESEM images and EDS results were taken by a ZEISS Supra 55 in fractured specimens covered with carbon. Micrographs were taken with an extra high tension (EHT) of 2 kV, whereas for EDS analysis was 20 kV. The working distance (WD) for both cases was 5-8 mm. EDS analysis was obtained by an average of at least five points in different regions of the sample.

Regarding the testing ages and curing conditions, all the designed mortars were evaluated by their compressive strength after 3, 7, 28 and 90 days of curing at 25 °C and relative humidity (RH) higher than 95%. Related to the pastes samples, selected mixes were assessed after 7, 28 and 90 days of curing in the same conditions of the mortars (curing temperature and RH) as for the FTIR and TGA tests. For XRD, FESEM and EDS tests, samples were analysed only after 90 days of curing in the same conditions. The information on these tests and the dosages utilised for each experiment are summarized in Table 7.2.

Table 7.2 – Specimen names, mixture designs (H₂O/Na₂O and BFS/SCSA ratios) and tests performed: compressive strength (R_c), X-ray diffraction (XRD), Fourier transform infrared spectroscopy (FTIR), thermogravimetric analysis (TGA) and field emission scanning electron microscopy (FESEM)

Specimen name	H ₂ O/Na ₂ O	BFS/SCSA	Tests ages (days)				
			R _c	XRD	FTIR	TG	FESEM
19-100/0	18.5	100/0	3-7-28-90	90	7-28-90	7-28-90	90
19-90/10		90/10		-	7-28-90	7-28-90	-
19-80/20		80/20		90	7-28-90	7-28-90	90
19-70/30		70/30		-	7-28-90	7-28-90	-
16-100/0	15.9	100/0	3-7-28-90	-	-	-	-
16-90/10		90/10		-	-	-	-
16-80/20		80/20		-	-	-	-
16-70/30		70/30		-	-	-	-
14-100/0	13.9	100/0	3-7-28-90	-	-	-	-
14-90/10		90/10		-	-	-	-
14-80/20		80/20		90	7-28-90	7-28-90	90
14-70/30		70/30		-	-	-	-
12-100/0	12.3	100/0	3-7-28-90	-	-	-	-
12-90/10		90/10		-	-	-	-
12-80/20		80/20		-	-	-	-
12-70/30		70/30		-	-	-	-
11-100/0	11.1	100/0	3-7-28-90	-	-	-	-
11-90/10		90/10		-	-	-	-
11-80/20		80/20		90	7-28-90	7-28-90	90
11-70/30		70/30		-	-	-	-

7.3 RESULTS AND DISCUSSION

7.3.1 Compressive strength of mortars

a) Influence of the $\text{H}_2\text{O}/\text{Na}_2\text{O}$ molar ratio

The influence of the $\text{H}_2\text{O}/\text{Na}_2\text{O}$ molar ratio on the compressive strength of mortars is illustrated in Figure 7.1. The assessed BFS/SCSA proportions were 100/0 (Fig. 7.1a), 90/10 (Fig. 7.1b), 80/20 (Fig. 7.1c) and 70/30 (Fig. 7.1d) after 3, 7, 28 and 90 days of curing. It is first observed that the highest $\text{H}_2\text{O}/\text{Na}_2\text{O}$ molar ratio yielded the greatest compressive strength in the analysed curing ages for all proportions of solid precursors. Additionally, for a given BFS/SCSA proportion and curing time, it is noticed that there is a linear relationship between the values of compressive strength and the $\text{H}_2\text{O}/\text{Na}_2\text{O}$ ratio. Therefore, a fitting straight line is proposed for each curing time of a given BFS/SCSA relation. The slope values of the proposed straight line were also obtained. Therefore, the straight lines generated will be discussed by their slope values (Table 7.3). The slope value indicates the impact on the compressive strength development of the $\text{H}_2\text{O}/\text{Na}_2\text{O}$ molar ratios: a high slope value means that the compressive strength is more affected by variation of $\text{H}_2\text{O}/\text{Na}_2\text{O}$ relations.

On one hand, the presence of SCSA up to 20% in the mixture did not cause significant changes: the slope values of BFS/SCSA proportions of 90/10 and 80/20 are similar to the control. In other words, the effect of the sodium content on the compressive strength of mixtures with SCSA percentages of 0–20% was similar. On the other hand, the proportion of 70/30 showed the highest slope values, which means that there is more influence of the activator concentration for this proportion of SCSA in the mixture. It was observed in previous studies with sodium silicate that the Na^+ concentration influenced more significantly the compressive strength development than for a system without sodium silicate (WANG et al., 1995; AYDIN et al., 2012; AYDIN et al., 2014). This behaviour was also observed when the SCSA was utilised, which was suggested by a higher slope values for BFS/SCSA proportion of 70/30. From these results, it can be concluded that the best $\text{H}_2\text{O}/\text{Na}_2\text{O}$ molar ratio was 18.5, independently of the BFS/SCSA proportion assessed.

Figure 7.1 – Influence of the H_2O/Na_2O ratio by line adjustment on BFS/SCSA proportions of 100/0 (a), 90/10 (b), 80/20 (c) and 70/30 (d) after 3, 7, 28 and 90 days of curing at 25 °C

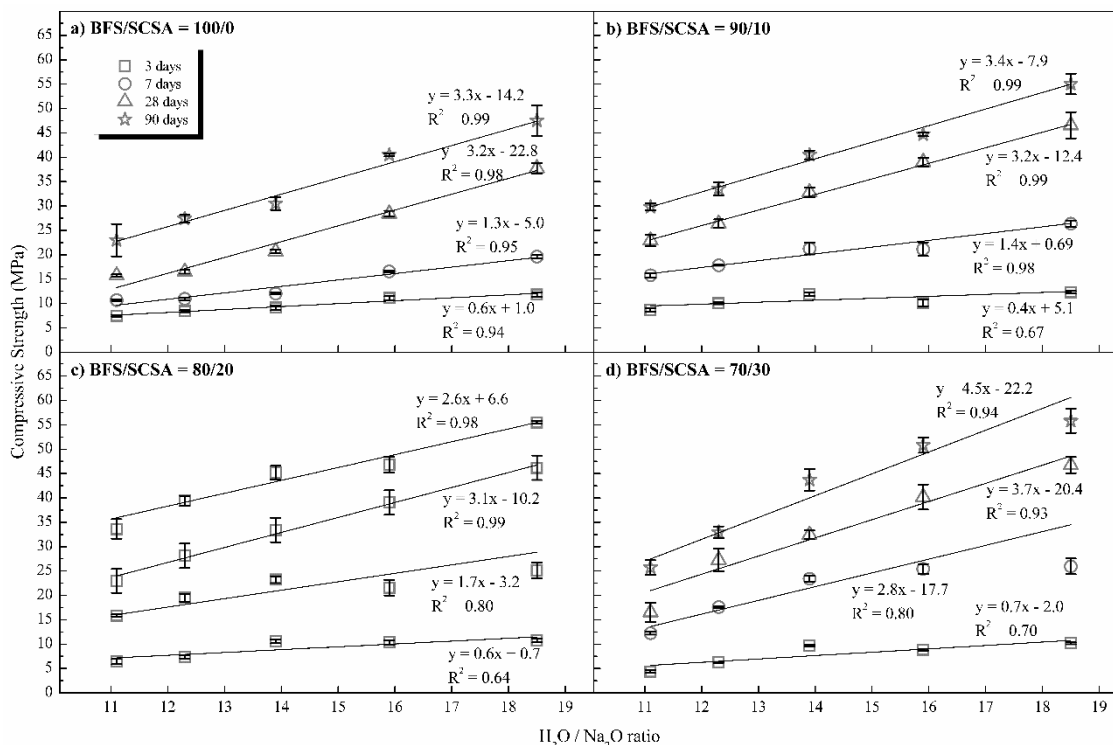


Table 7.3 – Slope values from the graphic compressive strength versus H_2O/Na_2O ratio for the four BFS/SCSA proportions

BFS/SCSA	Slope value			
proportion	3 days	7 days	28 days	90 days
100/0	0.6	1.3	3.2	3.3
90/10	0.4	1.4	3.2	3.2
80/20	0.6	1.7	3.1	2.6
70/30	0.7	2.8	3.7	4.5

b) Influence of the SCSA replacement percentage

The relative influence of the SCSA replacement in the mixtures was described by a σ_{SCSA} factor. This factor represents the relative contribution of the SCSA to the compressive strength of AAB mortars. The calculated factor is obtained by the compressive strength of a SCSA-mortar with a given H_2O/Na_2O molar ratio ($R_{x-y/z}$) from which the compressive strength of its respective control ($R_{x-100/0}$) is subtracted, corrected by the relative percentage

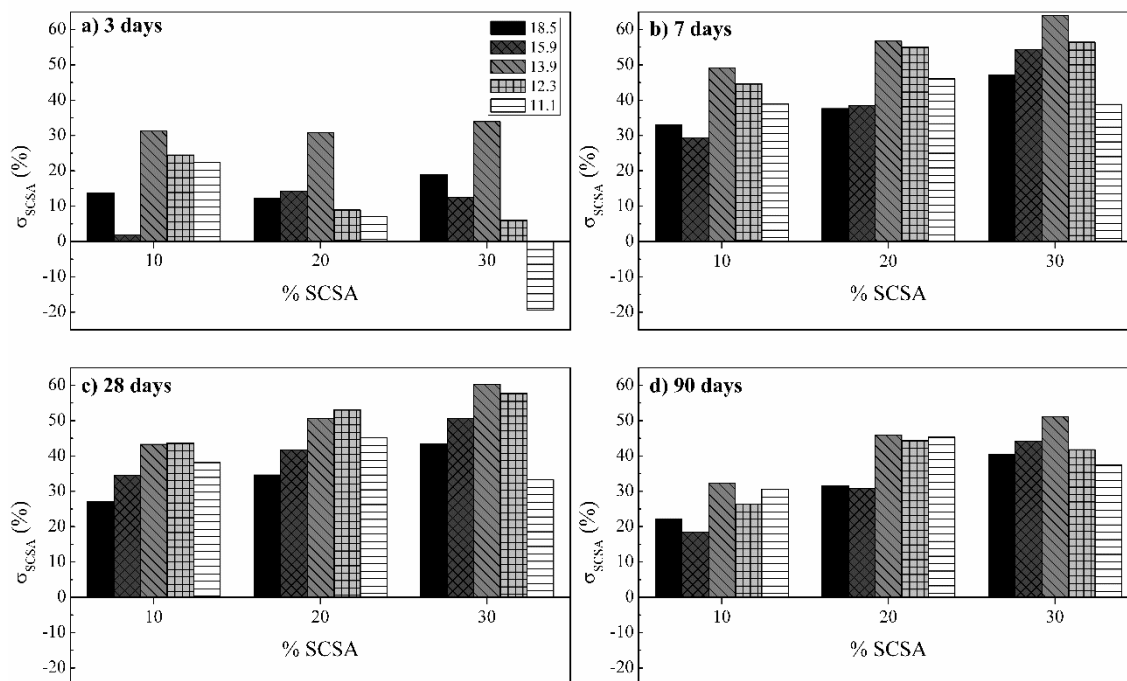
of BFS in the mixture, which is the ratio of BFS mass (m_{BFS}) over the total binder mass ($m_{BFS} + m_{SCSA}$). The σ_{SCSA} factor is calculated from Equation 7.1 as follows:

$$\sigma_{SCSA}(\%) = \frac{R_{x-y/z} - R_{x-100/0} \left(\frac{m_{BFS}}{m_{BFS} + m_{SCSA}} \right)}{R_{x-y/z}} * 100 \quad (7.1)$$

The results of the σ_{SCSA} factor are shown in Figure 7.2 for the following curing times: 3 (Fig. 7.2a), 7 (Fig. 7.2b), 28 (Fig. 7.2c) and 90 (Fig. 7.2d) days. The σ_{SCSA} values of all mixtures presented positive values (except for 11-70/30 after 3 days of curing), showing that the SCSA contributed positively in all mixture proportions and all curing ages.

It is also observed that with the increase of SCSA in the mixture, the contribution of the ash in the compressive strength increases also: the SCSA percentage of 30% reached the highest values. In addition, a high contribution at the curing times of 7–90 days was noticed, where SCSA is responsible for 30–65% of the developed compressive strength. The highest SCSA contribution was observed for the H_2O/Na_2O molar ratio of 13.9: this Na^+ concentration probably activates the SiO_4^{4-} anions from the ash better (the best SiO_2/Na_2O ratio). This H_2O/Na_2O molar ratio does not mean that this is the best compressive strength in terms of absolute values, but the ratio of 13.9 is the one that most favours the use of SCSA in this case. In general terms, these values show that SCSA makes an important contribution to the development of the compressive strength of the mortars for all H_2O/Na_2O molar ratios.

Figure 7.2 – σ_{SCSA} factor for SCSA percentage replacements of 10, 20 and 30% after: a) 3; b) 7; c) 28; and d) 90 days of curing at 25 °C.



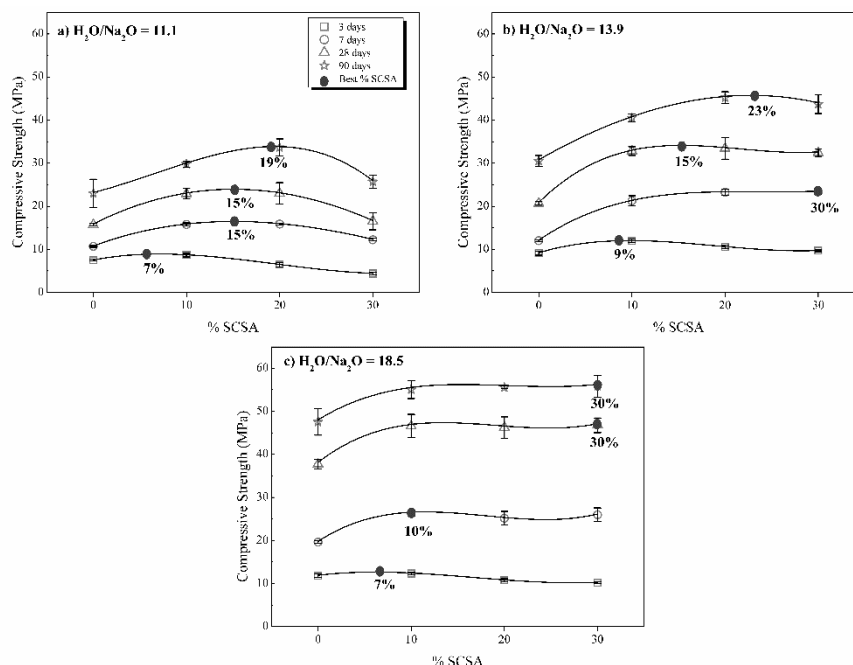
c) Optimum BFS/SCSA proportion

Studies to determine the optimum BFS/SCSA proportion through compressive strength results are illustrated in Figure 7.3. This figure shows plots of compressive strength versus the SCSA percentage in the mixture (% SCSA) for H_2O/Na_2O molar ratios of 11.1 (Fig. 7.3a), 13.9 (Fig. 7.3b) and 18.5 (Fig. 7.3c) after 3, 7, 28 and 90 days of curing. A fitting cubic function is proposed in order to obtain mathematically the optimum percentage of SCSA (highest compressive strength value) for each curing time. The best BFS/SCSA proportion was represented by points in the fitting curve with the respective optimum percentage of SCSA written below.

The proposed fitting cubic function showed that, after 3 days of curing, it is already interesting to use SCSA in alkali-activated binders, since the best SCSA percentage was in the range of 7–9%. The SiO_4^{4-} groups from SCSA work as a silica source from sodium silicate (MORAES et al., 2016), explaining the higher strength of SCSA mortars with respect to the control. Additionally, the filler effect of SCSA particles in the matrix may be also taken into account in the first curing days. Over the curing time, the optimum BFS/SCSA

proportion moved to a higher SCSA percentage. This can be seen through 7, 28 and 90 days of curing, where the optimum percentage of SCSA was in the intervals of 10–30%, 15–30% and 19–30%, respectively. Another fact noted was that, with the increase of Na^+ molarity (decrease in the $\text{H}_2\text{O}/\text{Na}_2\text{O}$ molar ratio), the optimum percentage of SCSA moves to lower values: $\text{H}_2\text{O}/\text{Na}_2\text{O}$ ratios of 18.5, 13.9 and 11.1 had the optimum percentage at 30, 23 and 19%, respectively, after 90 days of curing. For low $\text{H}_2\text{O}/\text{Na}_2\text{O}$ ratios, increasing the amount of SCSA over the optimum value reduces the compressive strength due to problems in products formation. Previous studies concluded that a high presence of sodium combined with a great amount of amorphous silica (in this case, sourced from the high percentages of SCSA) favours crystalline structures or soft gels that reduce the compressive strength (SCHILLING et al., 1994; JAMBUNATHAN et al., 2013; YUSUF et al., 2014; RASHAD et al., 2016). This problem is not observed for lower amounts of sodium, since the $\text{H}_2\text{O}/\text{Na}_2\text{O}$ molar ratio of 18.5 with 30% of SCSA presented the highest compressive strength. However, percentages of SCSA over 30% with low Na^+ molarity present hardening problems (MORAES et al., 2017). It can be concluded that it is more interesting to use percentages of SCSA in the range of 20–30% until the curing time assessed (90 days).

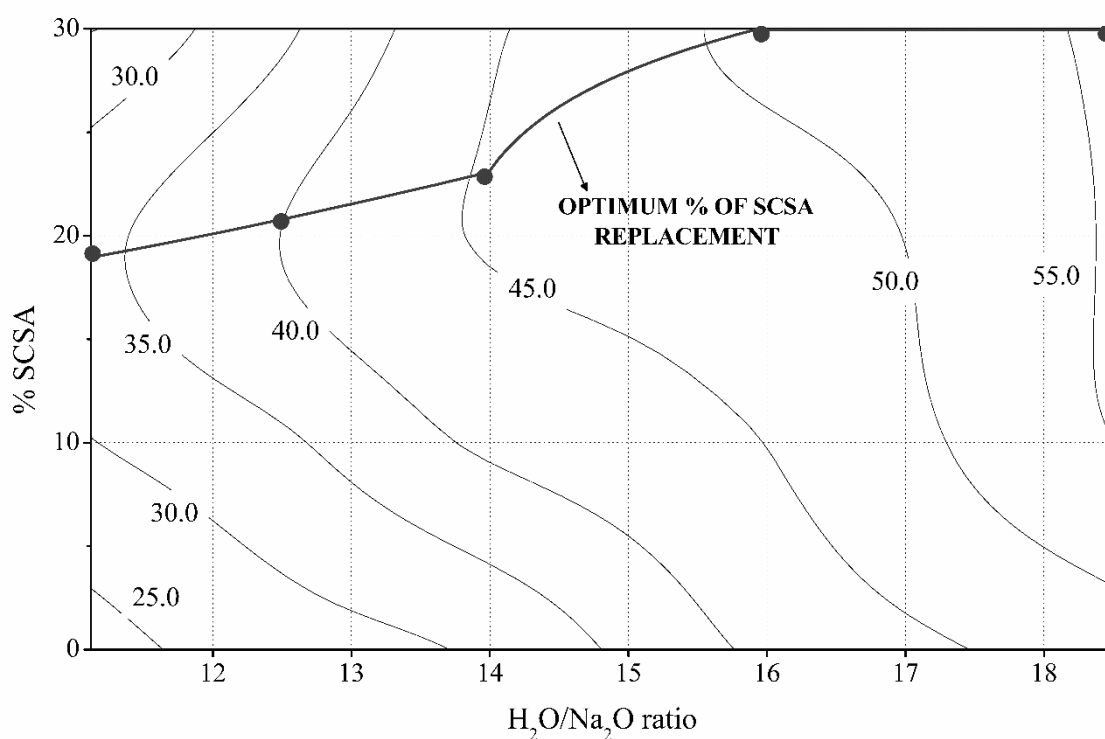
Figure 7.3 – Best BFS/SCSA proportion for the $\text{H}_2\text{O}/\text{Na}_2\text{O}$ ratios of: a) 11.1; b) 13.9; and c) 18.5 after 3, 7, 28 and 90 days of curing at 25 °C.



d) Optimum use of SCSA in BFS-based alkali-activated binders

Figure 7.4 shows a non-linear fitting surface of compressive strength in a graph of the SCSA percentage in the mixture (% SCSA) versus the H_2O/Na_2O molar ratio considering the results after 90 days of curing. The optimum percentage of SCSA for each H_2O/Na_2O molar ratio was calculated by the fitting cubic function in the last item, and it is represented in this figure by points connected by a solid curve. It is observed that the highest compressive strength is obtained with increase of the SCSA and H_2O/Na_2O molar ratio. Therefore, the optimum use of SCSA in BFS-based alkali-activated binders is obtained with a BFS/SCSA proportion of 70/30 and H_2O/Na_2O molar ratio of 18.5.

Figure 7.4 – Non-linear fitting surface of compressive strength values considering all the results after 90 days of curing. Points linked by a solid curve represent the optimum percentage of SCSA in the mixture.



7.3.2 Microstructural studies

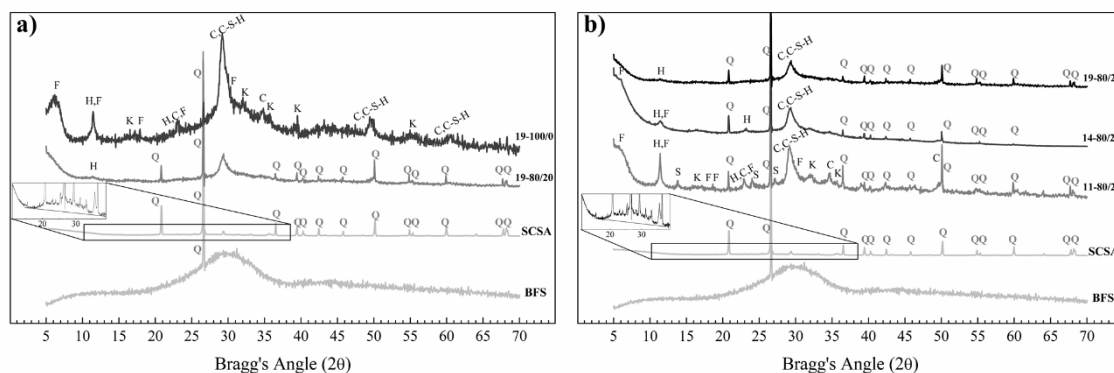
7.3.2.1 X-ray diffraction (XRD)

X-ray diffractions of both raw materials (BFS and SCSA) and the alkali-activated pastes are shown in Figure 7.5 for pastes with 90 days of curing. Fig. 7.5a presents the patterns of the pastes 19-100/0 (control) and 19-80/20 in order to investigate the influence of the SCSA on the BFS-based alkali-activated binders. Firstly, as concerns the raw materials, the BFS pattern showed a baseline deviation in the Bragg's angle range of $19\text{--}37^\circ$ related to the amorphous phase of this precursor. On the other hand, the only crystalline phase determined was quartz (PDF Card #331161). Turning to the SCSA pattern, it presented a baseline deviation from the amorphous phase in the Bragg's angle range of $20\text{--}35^\circ$ shown in the amplification of the diffractogram. Crystalline phases detected in the SCSA were quartz and calcite (PDF Card #050586). Regarding the diffractogram of the pastes, the addition of SCSA to the mixture did not alter the formation of crystalline phases in this case. The crystalline phases determined in both pastes were hydrotalcite (PDF Card #140191), which is common in the alkaline activation of BFS (Pereira 2015; Moraes 2016b; Abdalqader 2016), katoite (PDF Card #380368) and faujasite (PDF Card #391380). The only difference observed was the presence of quartz, but this comes from the SCSA composition and it was not formed during the reaction process of the alkali-activated binders. The amorphous phase behaviour of the pastes also did not show any difference: their diffractograms presented the same baseline deviation in the interval of $2\theta = 20\text{--}40^\circ$. This shift in the baseline deviation interval from the raw materials (2θ in the range of $19\text{--}37^\circ$ and $20\text{--}35^\circ$ for BFS and SCSA, respectively) in the paste (2θ in the range of $20\text{--}40^\circ$) was also observed in previous studies (PEREIRA et al., 2015; MORAES et al., 2016b; SHEARER et al., 2016). The authors attributed this behaviour to the formation of cementing gels. Another indication on the formation of reaction products is the broad peak centred at 29.17° from the semi-crystalline C-S-H, which was present in both pastes.

Fig. 7.5b illustrates the patterns of the 20% SCSA-containing pastes 19-80/20, 14-80/20 and 11-80/20 in order to assess the influence of the activator concentration on the pastes. The results showed that the alkaline solution concentration influenced the formation of some crystalline phases in the specimens. As can be observed, the higher the presence of

Na^+ , the stronger the crystalline peaks are in the diffractogram. The stronger peak from the semi-crystalline C-S-H (placed at 2θ equal to 29.17°) can be related to the generation of a more crystalline gel structure, i.e., it possibly means the formation of a less polymerised structure that can explain the lower compressive strength with increase of the Na^+ concentration (SCHILLING et al., 1994; JAMBUNATHAN et al., 2013; YUSUF et al., 2014; RASHAD et al., 2016). In addition, the paste with the lowest $\text{H}_2\text{O}/\text{Na}_2\text{O}$ molar ratio presented the formation of a zeolite type: hydrosodalite (PDF Card #100401). Previous studies also concluded that a higher concentration of the activator induces the formation of this zeolite (HANJITSUWAN et al., 2014).

Figure 7.5 – X-ray diffraction patterns of the raw material and pastes after 90 days of curing: a) BFS and SCSA (raw materials), 19-100/00 and 19-80/20 (pastes); b) BFS and SCSA (raw materials), 19-80/20, 14-80/20 and 11-80/20 (pastes). Key: Q: quartz; C-S-H: semi-crystalline C-S-H; H: hydrotalcite; K: katoite; F: faujasite; C: calcite; S: hydrosodalite



7.3.2.2 Fourier transform infrared spectroscopy (FTIR)

Figure 7.6 shows the FTIR spectra of the raw materials (BFS, SCSA and BFS/SCSA before mixing with the alkaline solution) and pastes cured after 7, 28 and 90 days. In these spectra, the main band was detected within the wavenumber interval of 850 to 1200 cm^{-1} among the range of $400\text{--}4000\text{ cm}^{-1}$ that was obtained in the test. That wavenumber range is related to bond vibrations of amorphous Si-O-T (T being Si or Al). The position of the band within that interval is associated with the chemical composition of the raw material and, in the case of pastes, it is related to the structure and composition of the formed products

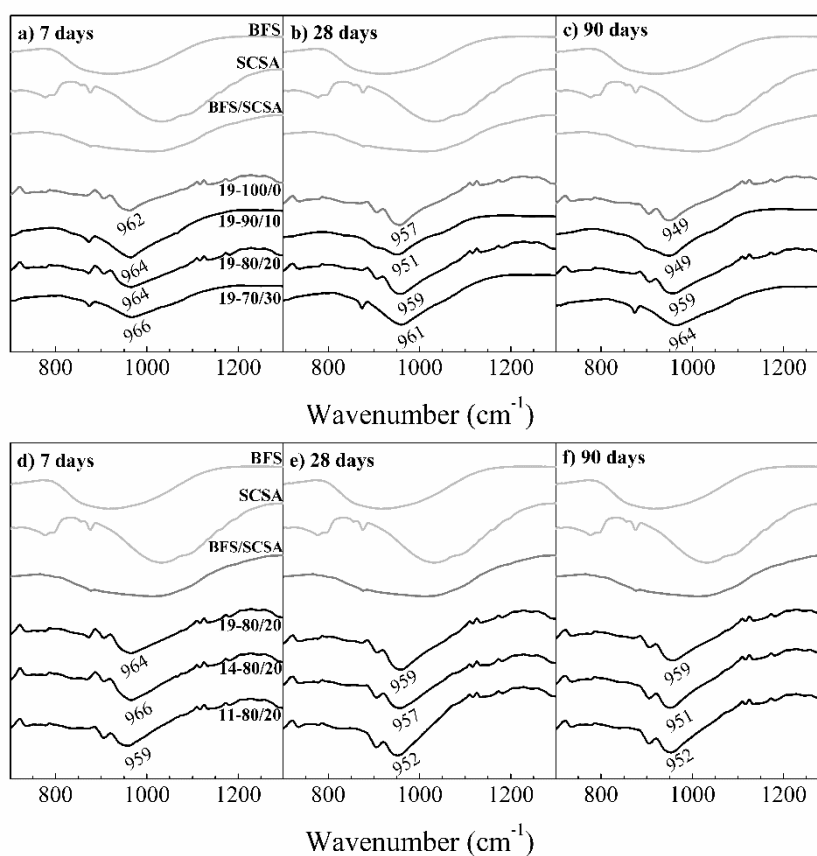
(ISMAIL et al., 2014). Therefore, the FTIR discussion will be focused on variations or differences observed in band positions among the studied spectra. On one hand, the first difference in band positions was observed between both raw materials. The SCSA spectrum presented more absorption at higher wavenumber values than the BFS one (around 1050 and 900 cm^{-1} , respectively). This behaviour is caused by the content of calcium as one of the most abundant elements in the chemical composition of BFS. In the case of the BFS/SCSA blend spectrum, it was observed that the broadness of the main band is the sum of the infrared absorptions of both BFS and SCSA. On the other hand, variation between the raw materials and pastes was also observed: the band position of the pastes shifted when compared to those from the raw materials. The strong absorption of SCSA and BFS was in the wavenumbers of 1050 and 900 cm^{-1} , respectively, whereas for the pastes it was around 950 cm^{-1} . In addition, it was noticed that the BFS/SCSA blend presented a broader band than the pastes. This is explained by the dissolution of the Si-O-T links from the raw materials, followed by the formation of alkali-activated gels (SHEARER et al., 2016; ISMAIL et al., 2014; SALIH et al., 2015; RAVIKUMAR et al., 2012).

Fig. 7.6a, Fig. 7.6b and Fig. 7.6c illustrate the FTIR spectra of the 19-100/0, 19-90/10, 19-80/20 and 19-70/30 pastes (same $\text{H}_2\text{O}/\text{Na}_2\text{O}$ ratio and four different BFS/SCSA proportions). The aim is to study the SCSA's influence on the alkali-activated binders based on BFS. In these spectra of pastes, the absence of the strongest energy absorption from SCSA (around 1050 cm^{-1}) shows that the ash reacted with the BFS and formed binding gels. In general terms, the presence of SCSA up to 30% of percentage replacement did not significantly alter the spectra with respect to the control. It is observed that the SCSA-pastes presented a slightly higher wavenumber value of the strongest peak than the control. This can be attributed to the formation of a gel with higher Si content and a more polymerised structure (SHEARER et al., 2016; RAVIKUMAR et al., 2015; ZHANG et al., 2012; LI et al., 2017). This can be explained by the fact that gels with more Si can incorporate more alkalis in their structure, forming a more linked network (RAVIKUMAR et al., 2015). This gel development is related to the better mechanical response from the SCSA-mortars in compressive strength tests.

Regarding the study of the influence of the alkaline activator, Fig. 7.6d, Fig. 7.6e and Fig. 7.6f represent the FTIR spectra of 19-80/20, 14-80/20 and 11-80/20 pastes (three different $\text{H}_2\text{O}/\text{Na}_2\text{O}$ ratios and the same BFS/SCSA proportion). Once again, minor changes

are observed among the three spectra, showing that this technique does not offer, in this case, enough information in terms of changes in the nature of the gel. It is only observed that the increase in the $\text{H}_2\text{O}/\text{Na}_2\text{O}$ molar ratio of pastes resulted in shifting the wavenumber of the centred peak to higher values. This means that the lowering Na^+ concentration in the mixture formed a denser structure, explaining the highest compressive strength obtained from the mortars with a low concentration of sodium: in a previous study, it was observed that the increase in the Na/Ca ratio in the mixture caused a poor densification of the gel (BAKHAREV et al., 1999).

Figure 7.6 – FTIR spectra of the raw materials (BFS and SCSA) and pastes cured for: a and d) 7 days; b and e) 28 days; and c and f) 90 days at 25 °C. Study on the effect of SCSA content (see a, b and c graphs). Study on the effect of the sodium hydroxide concentration (see d, e and f graphs)



7.3.2.3 Thermogravimetric analysis (TGA)

The TGA results are described by both mass losses in Table 7.4 and DTG curves in Figure 7.7 of the pastes after 7, 28 and 90 days of curing. Table 7.4 is divided into two sections: the SCSA influence and activator concentration effect. The peaks determined in these curves were in the range of 130–160, 200–210, 380–420 and 750–800 °C. The first peak (130–160 °C) is related to the dehydration of the C-S-H or C(N)-A-S-H gels from the alkaline activation of BFS, while the second peak (200–220 °C) is related to C-A-S-H products (PEREIRA et al., 2015; MORAES et al., 2016b; MYERS et al., 2013). The third peak, placed at 380–420 °C, is due to the dehydration of the hydrotalcite that was detected in the XRD analysis (JIN et al., 2015). Finally, the last peak detected is attributed to the decomposition of CaCO_3 (BERNAL et al., 2013). The most important information about mass loss in these results comes from the analysis in the decomposition range of 100–250 °C and the total mass loss.

Fig. 7.7a, Fig. 7.7b and Fig. 7.7c show the DTG curves of the study of the influence of the SCSA for the following pastes 19-100/0, 19-90/10, 19-80/20 and 19-70/30 after 7 (Fig. 7.7a), 28 (Fig. 7.7b) and 90 (Fig. 7.7c) days of curing. After 7 days of curing, the mass losses from the SCSA pastes were slightly higher than the control one, as observed in Table 7.4. This means that, at an early age, the role of SCSA is important in the formation of gel. Another fact observed was that the centred peak of the decomposition of C-S-H/C(N)-A-S-H gels (in the range of 130–160 °C) of the SCSA-pastes 19-80/20 and 19-70/30 are positioned at higher values than the 19-100/0 and 19-90/10 ones. This possibly reveals the formation of products with strongly bonded water for those pastes, explaining the improved compressive strength at this age (ISMAIL et al., 2014). In the 28-day curing time, the SCSA-pastes had their mass loss increased compared to the control one, suggesting a continuity in the hydration process. Related to the DTG curves, it can be noticed that the peak from the C-A-S-H hydration (in the range of 200–220 °C) disappeared in the SCSA-containing pastes. This can be explained by the formation of C(N)-A-S-H gels by the cross-linking among the tobermorite chains of the gel structure (more polymerised gel) (MYERS et al., 2013). Probably, the dissolved silica from SCSA contributed to 3D polymerisation and a higher compressive strength was achieved. Another fact observed is that the centred peak from the C-S-H/C(N)-A-S-H dehydration shifted to higher temperatures for all analysed pastes.

Finally, after 90 days of curing, the control paste showed an increase in the mass loss, while the loss values of the SCSA-pastes were reduced. This result is in contrast with the increase in the compressive strength values in the curing interval of 28–90 days. It can be explained by the improvement in the densification and polymerisation of the gel, where the condensation of OH groups releases H₂O molecules (HAHA et al., 2011). This process means that the dehydration mass loss from the gels is lowered, explaining the increase in the compressive strength of the mortars.

Fig. 7.7d, Fig. 7.7e and Fig. 7.7f illustrate the DTG curves to assess the activator concentration effect after 7 (Fig. 7.7d), 28 (Fig. 7.7e) and 90 (Fig. 7.7f) days of curing for the following pastes: 19-80/10, 14-80/20 and 11-80/20. In the first curing time analysed (7 days), the increase in the Na⁺ concentration caused an increase in the mass loss of the pastes. However, this fact did not follow the compressive strength behaviour (Table 7.3), since the mortars with higher H₂O/Na₂O molar ratio presented the best strength values. This behaviour can be attributed to zeolite formation in the mixtures with the highest sodium content from early ages, because the dehydration of this crystalline structure occurs in the same temperature range as the gels (PUERTAS et al., 2003; BERNAL et al., 2011; GENCEL et al., 2013). After 28 days of curing, the three pastes presented similar mass loss values. However, the pastes with lower concentrations of Na⁺ showed a greater increase in the mass loss in the interval of 7–28 days of curing: 19-80/20 had a mass loss of 9.83% at 7 days that rose to 15.83% (6% of absolute increase) at 28 days, while the 11-80/20 presented 14.60% and 15.24% (0.64% of increase), respectively. This behaviour is similar to those found in compressive strength results, where the 19-80/20 showed more strength development than the 11-80/20 one in the 7–28 days curing time interval. This means that this increase in the mass loss can be related to new gel formation. In the last curing time studied (90 days), both 14-80/20 and 11-80/20 pastes showed no difference from 28 days of curing. On the contrary, the 19-80/20 paste presented a reduction in the total mass loss: this behaviour may be related to the gel polymerisation (HAHA et al., 2011).

Figure 7.7 – DTG curves of the pastes: 19-100/0, 19-90/10, 19-80/20 and 19-70/30 cured after a) 7 days, b) 28 days and c) 90 days; and 19-80/20, 14-80/20 and 11-80/20 cured after d) 7 days, e) 28 days and f) 90 days.

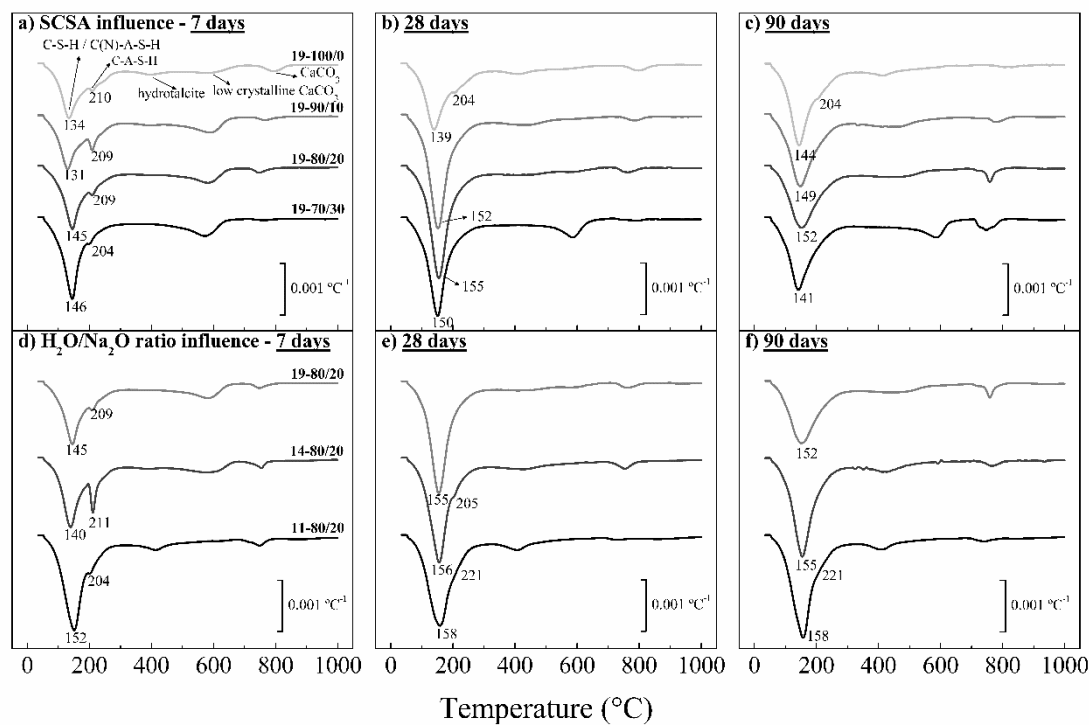


Table 7.4 – Mass losses from TGA curves in the 35–250 °C range ($P_{35-200^{\circ}\text{C}}$) and the total mass loss in 35–1000 °C range (P_T) in pastes cured for 7, 28 and 90 days at 25 °C

Data analysis	Specimen	$P_{35-250^{\circ}\text{C}}$			P_T		
		7 days	28 days	90 days	7 days	28 days	90 days
SCSA influence	19-100/0	9.26	10.94	13.31	18.21	18.59	20.84
	19-90/10	9.46	16.01	12.42	20.25	23.70	21.30
	19-80/20	9.83	15.83	11.75	19.58	23.45	20.94
	19-70/30	10.94	13.84	12.11	19.89	23.29	23.82
Activator concentration effect (H ₂ O/Na ₂ O molar ratio variation)	19-80/20	9.83	15.83	11.75	19.58	23.45	20.94
	14-80/20	11.52	15.05	15.00	22.22	23.89	23.66
	11-80/20	14.60	15.24	15.94	25.04	23.76	24.57

7.3.2.4 *Field emission scanning electron microscopy (FESEM) and Energy-dispersive X-ray spectroscopy (EDS)*

FESEM micrographs of the pastes are shown in Figure 7.8 for the samples 19-100/0 (Fig. 7.8a) and 19-80/20 (Fig. 7.8b) cured after 90 days to study the influence of SCSA. In Fig. 7.8a, the formation can be observed of a homogeneous gel (gel 1) by activating only the BFS (spot A). At a higher magnification, this observed gel presented a dense surface with some roughness. The composition of gel 1 can be represented by means of the following molar ratios: $\text{Ca/Si} = 0.8 \pm 0.1$, $\text{Na/Si} = 0.3 \pm 0.1$, $\text{Mg/Si} = 0.3 \pm 0.1$ and $\text{Al/Si} = 0.3 \pm 0.1$. At spot B, a reacting BFS particle with some superficial gels formation can be seen. In this case, the molar ratios are $\text{Ca/Si} = 1.3$, $\text{Na/Si} = 0.1$, $\text{Mg/Si} = 0.2$ and $\text{Al/Si} = 0.2$: it can be seen that the relative content of sodium was significantly lower than that observed for gel 1, suggesting that most of the BFS particles are unreacted. In the case of the paste with SCSA (Fig. 7.9b), the formation can be seen of two different products at spot C (gel 2) and D (gel 3). Related to the first spot, gel 2 presents a compact and smooth surface with molar ratios of $\text{Ca/Si} = 0.9 \pm 0.1$, $\text{Na/Si} = 0.3 \pm 0.1$, $\text{Mg/Si} = 0.1 \pm 0.1$ and $\text{Al/Si} = 0.2 \pm 0.1$. Gel 3 from the second spot shows the formation of some stacked products with molar ratios of $\text{Ca/Si} = 0.9 \pm 0.1$, $\text{Na/Si} = 1.0 \pm 0.2$, $\text{Mg/Si} < 0.1$ and $\text{Al/Si} = 0.2 \pm 0.1$. Besides the difference in the form of both gels, gel 3 presents a higher content of Na in its composition than gel 2 and the absence of magnesium. Probably, the magnesium was not detected because this gel 3 was developed mainly from the reaction of SCSA (the BFS had 8.2% of MgO, a significantly higher value than that for SCSA, 1.6% according to Table 7.1). Comparing both pastes, 19-100/0 and 19-80/20, gel 2 from the sample with SCSA presented a denser structure than gel 1 from the control sample. Probably, this gel formation explains the higher compressive strength of the SCSA mortars. In addition, gel 3 (with composition of C,N-S(A)-H) presumably also contributes to enhancing the mechanical development.

Figure 7.8 – FESEM micrographs of the pastes: a) 19-100/0; and b) 19-80/20 cured after 90 days.

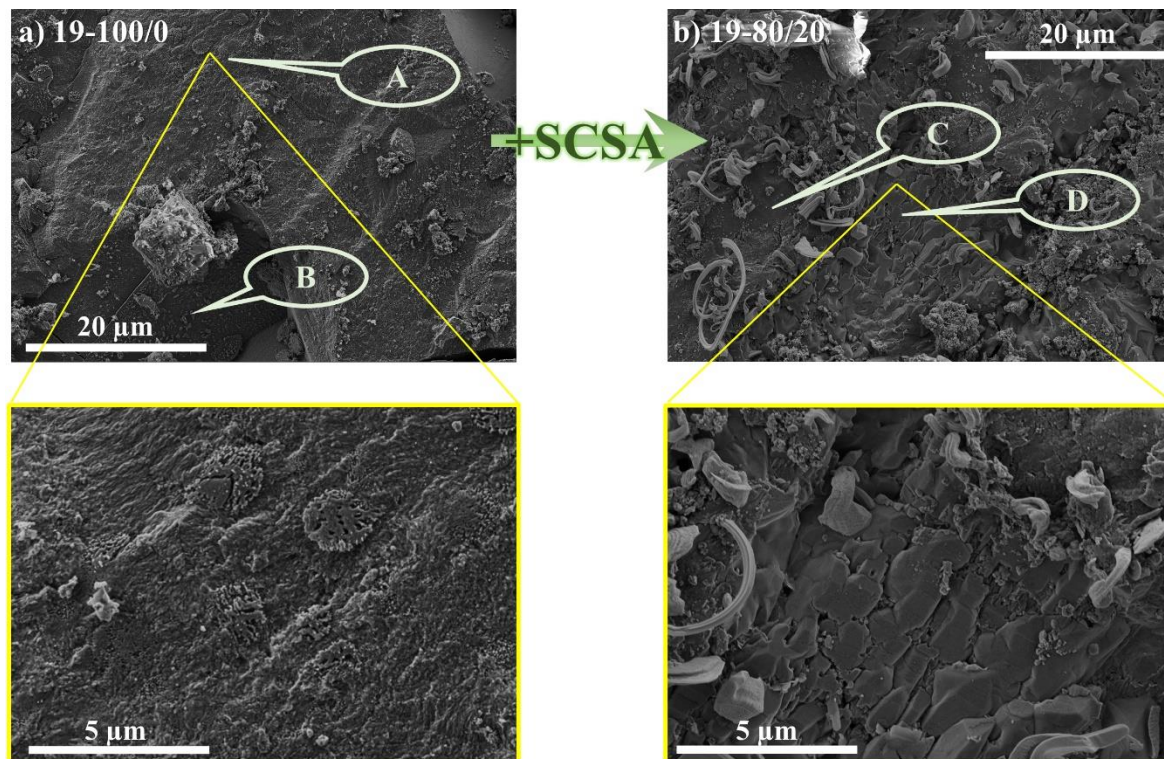
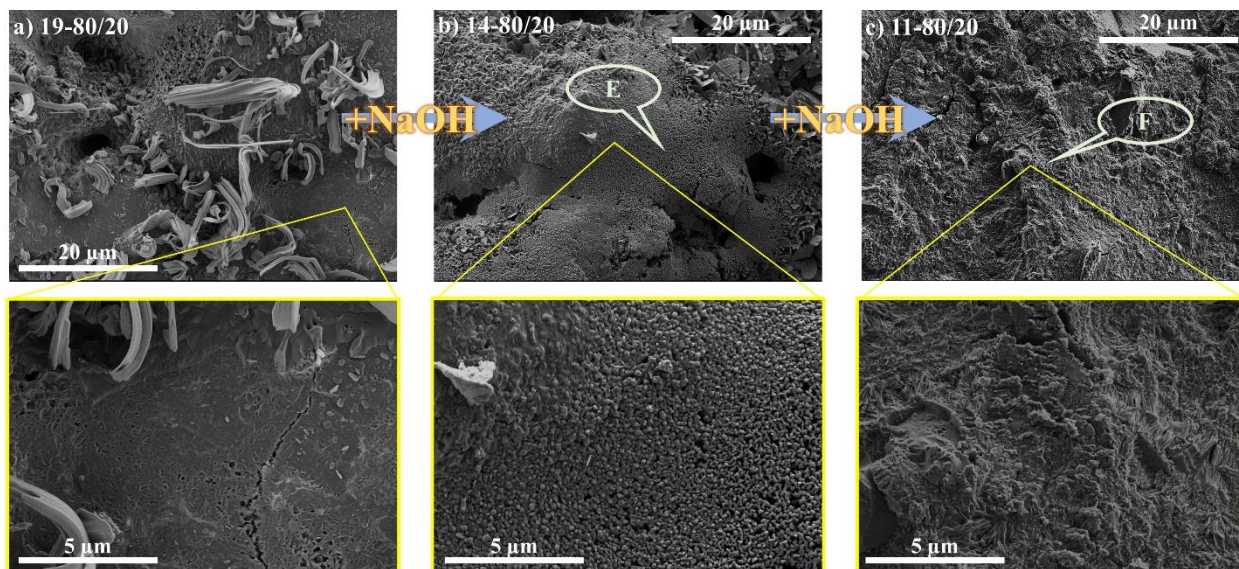


Fig. 7.9 illustrates the micrographs of the pastes 19-80/20 (Fig. 7.9a), 14-80/20 (Fig. 7.9b) and 11-80/20 (Fig. 7.9c) after 90 days of curing in order to study the influence of the activator on the microstructure of the samples. The 19-80/20 sample was described in the previous paragraph. In the case of the 4-80/20 paste (Fig. 7.9b), the formation can be seen of several products, gel 4 (spot E) being the most common product observed in the paste. At higher magnification, this product formation is seen to be a group of small particles with low porosity, although it is less compacted than gel 2 in the 19-80/20 paste. Finally, the overview of the paste 11-80/20 is shown in Fig. 7.9c. In general terms, it is noticed that there is the presence of only one gel formation (gel 5). At higher magnification (spot F), this gel shows a very porous and rough surface compared to gels 2 and 4. The chemical composition of gel 5 is represented by molar ratios of $\text{Ca/Si} = 0.9 \pm 0.1$, $\text{Na/Si} = 0.3 \pm 0.1$, $\text{Mg/Si} = 0.3 \pm 0.1$ and $\text{Al/Si} = 0.2 \pm 0.1$. Comparing the gel formation from the pastes, when the Na^+ concentration increases, a more porous structure is observed. This behaviour may explain why the mortars with the lowest Na^+ concentration presented the highest compressive strength.

Figure 7.9 – FESEM micrographs of the pastes: a) 19-80/20; b) 14-80/20; and c) 11-80/20 cured after 90 days.



7.4 CONCLUSIONS

The SCSA was assessed in alkali-activated binders when partially replacing the BFS in the range percentages of 0–30%, where the increase of ash content in the mixture was in intervals of 10%. The alkaline solutions were designed with only NaOH, varying the H_2O/Na_2O molar ratio in the interval of 11.1–18.5. In 3–90 curing days, the activating solution was found to have an important role in the mechanical development of the AAB. The compressive strength data showed better results for the highest H_2O/Na_2O molar ratio (18.5) of activating solution in all BFS/SCSA proportions. The relative influence of SCSA replacement was calculated by means of the σ_{SCSA} factor: BFS/SCSA equal to 70/30 reached the highest mechanical development for activating solutions with a H_2O/Na_2O molar ratio higher than 13.9. In general, the compressive strength development of the BFS-based system was enhanced by the presence of SCSA. XRD studies on BFS/SCSA pastes showed that most of the reaction products are amorphous. With the increase of the sodium concentration in the activator, more crystalline phases (faujasite and hydrosodalite) were produced. FTIR spectroscopy studies showed the consumption of amorphous phase from SCSA and confirmed the best development for systems with the highest H_2O/Na_2O molar ratio.

Thermogravimetric studies showed the effect of SCSA on the hydration process: in the first 28 days of reaction, the combined water in the gels was higher than that found in the BFS control pastes, although at the longer curing time of 90 days, a polymerisation process was observed, which has been related to the strength gain at this curing age. FESEM studies revealed the changes in the nature of the gels formed in the reactions: the gels in SCSA/BFS mixtures contained less magnesium and aluminium and more sodium and calcium than was found for BFS control paste. Additionally, the increase of sodium in activating solution yielded more porous gel, which agrees with the mechanical behaviour. This study revealed an interesting valorisation of the SCSA as an additional precursor in BFS-based alkali-activated binders, in view of the improvement of mechanical properties and the reduction in the consumption of BFS in AAB.

ACKNOWLEDGEMENTS

The authors would like to thank CNPq processo n° 401724/2013-1, CNPq processo n° 140779/2015-0 and the "Ministerio de Educación, Cultura y Deporte" of Spain ("Cooperación Interuniversitaria" program with Brazil PHB-2011-0016-PC). Thanks are also given to the Electron Microscopy Service of the Universitat Politècnica de València.

REFERENCES

- ABDALQADER, A. F.; JIN, F.; AL-TABBAA, A. A. *Development of greener alkali-activated cement: utilisation of sodium carbonate for activating slag and fly ash mixtures. Journal of Cleaner Production*, v. 113, p. 66-75, 2016.
- ALVES, M.; PONCE, G. H. S. F.; SILVA, M. A.; ENSINAS, A. V. *Surplus electricity production in sugarcane mills using residual bagasse and straw as fuel. Energy*, v. 91, p. 751-757, 2015.
- AYDIN, S.; BARADAN, B. *Mechanical and microstructural properties of heat cured alkali-activated slag mortars. Materials and Design*, v. 35, p. 374-383, 2012.
- AYDIN, S.; BARADAN, B. *Effect of activator type and content on properties of alkali-activated slag mortars. Composites Part B: Engineering*, v. 57, p. 166-172, 2014.
- BAKHAREV, T.; SANJAYAN, J. G.; CHENG, Y. B. *Alkali activation of Australian slag cements. Cement and Concrete Research*, v. 29, p. 113-120, 1999.

BERNAL, S. A.; PROVVIS, J. L.; WALKEY, B.; NICOLAS, R. A.; GEHMAN, J. D.; BRICE, D. G.; KILCULLEN, A. R.; DUXSON, P.; van DEVENTER, J. S. J. *Gel nanostructure in alkali-activated binders based on slag and fly ash, and effects of accelerated carbonation*. **Cement and Concrete Research**, v. 53, p. 127-144, 2013.

BERNAL, S. A.; RODRÍGUEZ, E. D.; GUTIÉRREZ, R. B.; GORDILLO, M.; PROVVIS, J. L. *Mechanical and thermal characterisation of geopolymers based on silicate-activated metakaolin/slag blends*. **Journal of Materials Science**, v. 46, p. 5477-5486, 2011.

BORGES, P. H. R.; BANTHIA, N.; ALCAMAND, H. A.; VASCOLCELOS, W. L.; NUNES, E. H. M. *Performance of blended metakaolin/blastfurnace slag alkali-activated mortars*. **Cement and Concrete Composites**, v. 71, p. 42-52, 2016.

BROUGH, A. R.; ATKINSON, A. *Sodium silicate-based, alkali-activated slag mortars. Part I. Strength, hydration and microstructure*. **Cement and Concrete Research**, v. 32, p. 865-879, 2002.

CASTALDELLI, V. N.; AKASAKI, J. L.; MELGES, J. L. P.; TASHIMA, M. M.; SORIANO, L.; BORRACHERO, M. V.; MONZÓ, J.; PAYÁ, J. *Use of slag/sugar cane bagasse ash (SCBA) blends in the production of alkali-activated materials*. **Materials**, v. 6, p. 3108-3127, 2013.

CHI, M.; HUANG, R. *Binding mechanism and properties of alkali-activated fly ash/slag mortars*. **Construction and Building Materials**, v. 40, p. 291-298, 2013.

DUXSON, P.; PROVVIS, J. L.; LUKEY, G. C.; van DEVENTER, J. S. J. *The role of inorganic polymer technology in the development of 'green concrete'*. **Cement and Concrete Research**, v. 37, p. 1590-1597, 2007.

FERNÁNDEZ-JIMÉNEZ, A.; PUERTAS, F. *Effect of activator mix on the hydration and strength behaviour of alkali-activated slag cements*. **Advances in Cement Research**, v. 15, n. 3, p. 129-136, 2003.

GENCEL, O.; SUTCU, M.; ERDOGMUS, E.; KOC, V.; CAY, V. V.; GOK, M. S. *Properties of bricks with waste ferrochromium slag and zeolite*. **Journal of Cleaner Production**, v. 59, p. 111-119, 2013.

HAHA, M. B.; SAOUT, G. L.; WINNEFELD, F.; LOTHENBACH, B. *Influence of activator type on hydration kinetics, hydrate assemblage and microstructural development of alkali activated blast-furnace slags*. **Cement and Concrete Research**, 41, 301-310, 2011.

HANJITSUWAN, S.; HUNPRATUB, S.; THONGBAI, P.; MAENSIRI, S.; SATA, V.; CHINDAPRASIRT, P. *Effects of NaOH concentrations on physical and electrical properties of high calcium fly ash geopolymer paste*. **Cement and Concrete Composites**, v. 45, p. 9-14, 2014.

ISMAIL, I.; BERNAL, S. A.; PROVIS, J. L.; NICOLAS, R. S.; HAMDAN, S.; van DEVENTER, J. S. J. *Modification of phase evolution in alkali-activated blast furnace slag by the incorporation of fly ash*. **Cement and Concrete Composites**, v. 45, p. 125-135, 2014.

JAMBUNATHAN, N.; SANJAYAN, J. G.; PAN, Z.; LI, G.; LIU, Y.; KORAYEM, A. H.; DUAN, W. H.; COLLINS, F. *The role of alumina on performance of alkali-activated slag paste exposed to 50 °C*. **Cement and Concrete Research**, v. 54, p. 143-150, 2013.

JIN, F.; GU, K.; AL-TABBAA, A. *Strength and hydration properties of reactive MgO-activated ground granulated blastfurnace slag paste*. **Cement and Concrete Research**, v. 57, p. 8-16, 2015.

JUENGER, M. C. G.; WINNEFELD, F.; PROVIS, J. L.; IDEKER, J. H. *Advances in alternative cementitious binders*. **Cement and Concrete Research**, v. 41, p. 1232-1243, 2011.

LEAL, M. R. L. V.; GALDOS, M. V.; SCARPARE, F. V.; SEABRA, J. E. A; WALTER, A.; OLIVEIRA, C. O. F. *Sugarcane straw availability, quality, recovery and energy use: A literature review*. **Biomass Bioenergy**, v. 53, p. 11-19, 2013.

LEMO, S. V.; DENADAI, M. S.; GUERRA, S. P. S.; ESPERANCINI, M. S. T.; BUENO, O. C.; TAKITANE, I. C. *Economic efficiency of two baling systems for sugarcane straw*. **Industrial Crops and Products**, v. 55, p. 97-101, 2014.

LI, C.; SUN, H.; LI, L. *A review: The comparison between alkali-activated slag (Si+Ca) and metakaolin (Si+Al) cements*. **Cement and Concrete Research**, v. 40, p. 1341-1349, 2010.

LI, N.; FARZADNIA, N.; SHI, C. *Microstructural changes in alkali-activated slag mortars induced by accelerated carbonation*. **Cement and Concrete Research**, v. 100, p. 214-226, 2017.

MADLOOL, N. A.; SAIDUR, R.; RAHIM, N. A.; KAMALISARVESTANI, M. *An overview of energy savings measures for cement industries*. **Renewable and Sustainable Energy Reviews**, v. 19, p. 18-29, 2013.

MAJCHRZAK-KUCEBA, I. *A simple thermogravimetric method for the evaluation of the degree of fly ash conversion into zeolite material*. **Journal of Porous Materials**, v. 20, p. 407-415, 2013.

MEYER, C. *The greening of the concrete industry*. **Cement and Concrete Composites**, v. 31, p. 601-605, 2009.

MORAES, B. S.; ZAIAT, M.; BONOMI, A. *Anaerobic digestion of vinasse from sugarcane ethanol production in Brazil: Challenges and perspectives*. **Renewable and Sustainable Energy Reviews**, v. 44, p. 888-903, 2015a.

MORAES, J. C. B.; AKASAKI, J. L.; MELGES, J. L. P.; MONZÓ, J.; BORRACHERO, M. V.; SORIANO, L.; PAYÁ, J.; TASHIMA, M. M. *Assessment of sugar cane straw ash (SCSA) as pozzolanic material in blended Portland cement: Microstructural characterization of pastes and mechanical strength of mortars*. **Construction and Building Materials**, v. 94, p. 670-677, 2015b.

MORAES, J. C. B.; MELGES, J. L. P.; AKASAKI, J. L.; TASHIMA, M. M.; SORIANO, L.; MONZÓ, J.; BORRACHERO, M. V.; PAYÁ, J. *Pozzolanic Reactivity studies on a biomass-derived waste from sugar cane production: Sugar Cane Straw Ash (SCSA)*. **ACS Sustainable Chemistry and Engineering**, v. 4, p. 4273-4279, 2016a.

MORAES, J. C. B.; TASHIMA, M. M.; AKASAKI, J. L.; MELGES, J. L. P.; MONZÓ, J.; BORRACHERO, M. V.; SORIANO, L.; PAYÁ, J. *Increasing the sustainability of alkali-activated binders: the use of sugar cane straw ash (SCSA)*. **Construction and Building Materials**, v. 124, p. 148-154, 2016b.

MORAES, J. C. B.; TASHIMA, M. M.; AKASAKI, J. L.; MELGES, J. L. P.; MONZÓ, J.; BORRACHERO, M. V.; SORIANO, L.; PAYÁ, J. *Effect of sugar cane straw ash (SCSA) as solid precursor and the alkaline activator composition on alkali-activated binders based of blast furnace slag (BFS)*. **Construction and Building Materials**, v. 144, p. 214-224, 2017.

MYERS, R. P.; BERNAL, S. A.; NICOLAS, R. A.; PROVIS, J. L. *Generalized structural description of calcium–sodium aluminosilicate hydrate gels: The cross-linked substituted tobermorite model*. **Langmuir**, v. 29, p. 5294-5306, 2013.

ÖZBAY, E.; ERDEMİR, M.; DURMUS, H. I. *Utilization and efficiency of ground granulated blast furnace slag on concrete properties – A review*. **Construction and Building Materials**, v. 105, p. 423-434, 2016.

OZER, I.; SOYER-UZUN, S. *Relations between the structural characteristics and compressive strength in metakaolin based geopolymers with different molar Si/Al ratios*. **Ceramics International**, v. 41, p. 10192-10198, 2015.

PACHECO-TORGAL, F.; LABRINCHA, J. A.; LEONELLI, C.; PALOMO, A.; CHINDAPRASIRT, P. *Handbook of Alkali-activated Cements, Mortars and Concretes*. 1st ed. Woodhead Publishing and Elsevier, Cambridge, Waltham, Kidlington, 2015.

PEREIRA, A.; AKASAKI, J. L.; MELGES, J. L. P.; TASHIMA, M. M.; SORIANO, L.; BORRACHERO, M. V.; MONZÓ, J.; PAYÁ, J. *Mechanical and durability properties of alkali-activated mortar based on sugarcane bagasse ash and blast furnace slag*. **Ceramics International**, v. 41, p. 13012-13024, 2015.

PROVIS, J. L.; van DEVENTER, J. S. J. *Alkali Activated Materials: State-of-the-Art Report*. 1st ed. Springer, Dordrecht, Heidelberg, New York, London, 2014.

PROVIS, J. K.; PALOMO, A.; SHI, C. *Advances in understanding alkali-activated materials*. **Cement and Concrete Research**, v. 78, n. 10, p. 110-125, 2015.

- PUERTAS, F.; FERNÁNDEZ-JIMÉNEZ, A. *Mineralogical and microstructural characterisation of alkali-activated fly ash/slag pastes*. **Cement and Concrete Composites**, v. 25, p. 287-292, 2003.
- PUERTAS, F.; FERNÁNDEZ-JIMÉNEZ, A.; BLANCO-VARELA, M. T. *Pore solution in alkali-activated slag cement pastes. Relation to the composition and structure of calcium silicate hydrate*. **Cement and Concrete Research**, v. 34, p. 139-148, 2004.
- RAKHIMOVA, N. R.; RAKHIMOV, R. Z. *Alkali-activated cements and mortars based on blast furnace slag and red clay brick waste*. **Materials and Design**, v. 85, p. 324-331, 2015.
- RASHAD, A. A.; ZEEDAN, S. R.; HASSAN, A. A. *Influence of the activator concentration of sodium silicate on the thermal properties of alkali-activated slag pastes*. **Construction and Building Materials**, v. 102, p. 811-820, 2016.
- RAVIKUMAR, D.; NEITHALATH, N. *Effects of activator characteristics on the reaction product formation in slag binders activated using alkali silicate powder and NaOH*. **Cement and Concrete Composites**, v. 34, p. 809-818, 2012.
- SALIH, M. A.; FARZADNIA, N.; ALI, A. A. A.; DEMIRBOGA, R. *Development of high strength alkali activated binder using palm oil fuel ash and GGBS at ambient temperature*. **Construction and Building Materials**, v. 93, p. 289-300, 2015.
- SCHILLING, P. J.; ROY, A.; EATON, H. C.; MALONE, P. G.; BRABSTON, W. N. *Microstructure, strength, and reaction products of ground granulated blast-furnace slag activated by highly concentrated NaOH solution*. **Journal of Materials Research**, v. 9, n. 1, p. 188-97, 1994.
- SHI, C.; FERNÁNDEZ JIMÉNEZ, A.; PALOMO, A. *New cements for the 21st century: The pursuit of an alternative to Portland cement*. **Cement and Concrete Research**, v. 41, n. 7, p. 750-763, 2011.
- SHI, C.; KRIVENKO, P. V.; Roy, D. *Alkali-Activated Cements and Concretes*, Taylor and Francis, London and New York, 2006.
- SHEARER, C. R.; PROVIS, J. L.; BERNAL, S. A.; KURTIS, K. E. *Alkali-activation potential of biomass-coal co-fired fly ash*. **Cement and Concrete Research**, v. 73, p. 62-74, 2016.
- SHEN, L.; GAO, T.; ZHAO, J.; WANG, L.; WANG, L.; LIU, L.; CHEN, F.; XUE, J. *Factory-level measurements on CO₂ emission factors of cement production in China*. **Renewable and Sustainable Energy Reviews**, v. 34, p. 337-349, 2014.
- SONG, S.; JENNIGS, H. M. *Pore solution chemistry of alkali-activated ground granulated blast-furnace slag*. **Cement and Concrete Research**, v. 29, p. 159-170, 1999.

SONG, S.; SOHN, D.; JENNINGS, H. M.; MASON, T. O. *Hydration of alkali-activated ground granulated blast furnace slag*. **Journal of Materials Science**, v. 35, p. 249-257, 2000.

Sugarcane production. **UNICA – União da Indústria de Cana-de-Açúcar Website**; <http://www.unicadata.com.br/index.php?idioma=2>

TASHIMA, M. M.; AKASAKI, J. L.; MELGES, J. L. P.; SORIANO, L.; MONZÓ, J.; PAYÁ, J.; BORRACHERO, M. V. *Alkali activated materials based on fluid catalytic cracking catalyst residue (FCC): Influence of SiO₂/Na₂O and H₂O/FCC ratio on mechanical strength and microstructure*. **Fuel**, v. 108, p. 833-839, 2013.

TASHIMA, M. M.; REIG, L.; SANTINI JR, M. A.; MORAES, J. C. B.; AKASAKI, J. L.; PAYÁ, J.; BORRACHERO, M. V.; SORIANO, L. *Compressive strength and microstructure of alkali-activated blast furnace slag/sewage sludge ash (GGBS/SSA) blends cured at room temperature*. **Waste and Biomass Valorization**, v. 8, n. 5, p. 1441-1451, 2016.

TURNER, L. K.; COLLINS, F.K. *Carbon dioxide equivalent (CO₂-e) emissions: A comparison between geopolymer and OPC cement concrete*. **Construction and Building Materials**, v. 43, p. 125-130, 2013.

USÓN, A. A.; LÓPEZ-SABIRÓN, A. M.; FERREIRA, G.; SASTRESA E. L. *Uses of alternative fuels and raw materials in the cement industry as sustainable waste management options*. **Renewable and Sustainable Energy Reviews**, v. 23, p. 242-260, 2013.

UZUN, H.; YILDIZ, Z.; GOLDFARB, J. L.; CEYLAN, S. *Improved prediction of higher heating value of biomass using an artificial neural network model based on proximate analysis*. **Bioresource Technology**, v. 234, p. 122-130, 2017.

van DEVENTER, J. S. J.; PROVIS, J. L.; DUXSON, P.; BRICE, D. G. *Chemical research and climate change as drivers in the commercial adoption of alkali activated materials*. **Waste and Biomass Valorization**, v. 1, p. 145-155, 2010.

WANG, S. D.; SCRIVENER, J. K.; PRAT, P. L. *Factors affecting the strength of alkali-activated slag*. **Cement and Concrete Research**, v. 24, n. 6, p. 1033-1043, 1994.

YUSUF, M. O.; JOHARI, M. A. M.; AHMAD, Z. A.; MASLEHUDDIN, M. *Influence of curing methods and concentration of NaOH on strength of the synthesized alkaline activated ground slag-ultrafine palm oil fuel ash mortar/concrete*. **Construction and Building Materials**, v. 66, p. 541-548, 2014.

ZHANG, Z.; PROVIS, J. L.; REID, A.; WANG, H. *Geopolymer foam concrete: An emerging material for sustainable construction*. **Construction and Building Materials**, v. 56, p. 113-127, 2014.

ZHANG, Z.; WANG, H.; PROVIS, J. L. *Quantitative study of the reactivity of fly ash in geopolymerization by FTIR*. **Journal of Sustainable Cement-Based Materials**, v. 1, n. 4, p. 154-166, 2012.

8 SUGAR CANE STRAW ASH AS SILICA SOURCE TO PRODUCE THE ACTIVATING SOLUTION IN ALKALI-ACTIVATED BINDERS BASED ON BLAST FURNACE SLAG

The article entitled as “*New use of sugar cane straw ash (SCSA) in alkali-activated materials: a silica source in the preparation of the alkaline activator*” by J. C. B. Moraes, A. Font, L. Soriano, J. L. Akasaki, M. M. Tashima, J. Monzó, M. V. Borrachero and J. Payá is going to be sent to journal **Cement and Concrete Research**.

Abstract: In order to obtain alkali-activated materials (AAM) with good performance, it is necessary to utilise silicates to produce the activating solution, which is an expensive and highly pollutant chemical reagent. In this way, this paper presented a new silica source to produce the activating reagent: the sugar cane straw ash (SCSA). This new reagent (an aqueous suspension) was prepared with SCSA and NaOH by means of a thermal bottle. The ash reacting time inside the thermal bottle (τ) was assessed from 0-48 hours, and SCSA amount in the suspension (represented by $\text{SiO}_2/\text{Na}_2\text{O}$ ratio, ϵ) was analysed from 0-1.82. Compressive strengths obtained after 3 curing days at 65 °C from mortars based on blast-furnace slag (BFS) showed the best τ was equal to 24 hours and the ϵ was 1.46. Comparing these systems with another two silica sources, sodium silicate and rice husk ash, the SCSA showed lower results than the former and similar results than the latter.

KEYWORDS: *Thermal Treatment, Microstructure, Compressive Strength, Alkali Activated Cement, Granulated Blast-Furnace Slag.*

8.1 INTRODUCTION

Alkali-activated materials (AAM) are alternative binders to the use of Portland cement. Their advantages over the most common binder are lower energy consumption and lesser CO₂ emission (PACHECO-TORGAL et al., 2015; PROVIS; van DEVENTER, 2015). AAM are obtained by mixing an amorphous aluminosilicate (solid precursor) with an alkaline solution (or activating solution), where the product from this chemical reaction hardens and forms a material with interesting mechanical properties (PACHECO-TORGAL et al., 2015; PROVIS; van DEVENTER, 2015). Examples of usual solid precursors are blast furnace slag, metakaolin and fly ash. Regarding to the alkaline solution, the most common reagents are alkali hydroxides and silicates (PACHECO-TORGAL et al., 2015; PROVIS; van DEVENTER, 2015).

The use of wastes in AAM have become a trend in the last years (KOURTI et al., 2010; BERNAL et al., 2016; TORNIOLO; BOCCACCINI, 2017). In this way, this paper described the utilisation of a waste from the agroindustry: the sugar cane straw ash (SCSA), an ash rich in amorphous silica (SiO₂). The management of this waste is an interesting issue due the increase of sugar cane production in Brazil in the last years: in 2014, 736.11 million tonnes of sugarcane were collected in this country, that is approximately 40% of the worldwide production (FOOD AND AGRICULTURE ORGANIZATION OF THE UNITED NATIONS – FAOSTAT, 2017). In previous works, this ash was successfully assessed as construction material in cementitious systems (FRÍAS et al., 2007; MARTIRENA; MONZÓ, 2017). Specifically in alkali-activated materials, SCSA was evaluated as solid precursor in combined systems with blast furnace slag (BFS) (MORAES et al., 2016). Now, this paper presents another use of SCSA in AAM: become a source of silica in the production of alkaline solution. The SiO₄⁴⁻ anion is a key to produce AAM with good performance because it favours the formation of a denser and stronger structure (PACHECO-TORGAL et al., 2015; PROVIS; van DEVENTER, 2015). Currently, an important reactive part of the silicon is provided by sodium silicate, which is widely used in combination with sodium hydroxide to produce the activating solution (PACHECO-TORGAL et al., 2015; PROVIS; van DEVENTER, 2015). However, the main disadvantage of sodium silicate is regarding in its production, since it is the most expensive and the highest emitter of greenhouse gases among the AAM raw materials (NAZARI; SANJAYAN, 2016).

In this way, one of the main trends in the next years would be to study new sources of silica to produce the alkaline solution (PROVIS et al., 2015a, 2016; PROVIS et al., 2017). Examples of these sources that were recently investigated are rice husk ash (RHA) (BOUZÓN et al., 2014; MEJÍA et al., 2013), spent diatomaceous earth (MEJÍA et al., 2016), glass waste (PUERTAS;TORRES-CARRASCO, 2014; TORRES-CARRASCO; PUERTAS, 2015) and sugar cane bagasse ash (TCHAKOUTÉ et al., 2017).

The main objective of this paper is to assess the potential of SCSA as silica source to prepare the alkaline solution. SCSA was utilised in combination with sodium hydroxide to produce an aqueous NaOH/SCSA suspension. The study was divided in three parts: 1) optimum time for dissolving the ash to prepare the activating reagent, 2) influence of SCSA amount in the activating reagent, and 3) comparison of SCSA to commercial and alternative silica sources. NaOH/SCSA activating suspension was prepared by means of a thermal bottle, so the first part of the study was to assess the optimum time on leaving the ash dissolving in the bottle. Following to the second part, different $\text{SiO}_2/\text{Na}_2\text{O}$ molar ratios were evaluated in order to obtain the most effective amount of SCSA in the activating reagent. Finally, in the third part, NH/SCSA activating reagent was compared to other two systems: NaOH/SS and NaOH/RHA. The solid precursor selected for this study was the blast furnace slag (BFS). In order to assess the effectiveness of SCSA to produce alkaline activator reagents, mortars were evaluated by their compressive strength. In addition, microstructural properties of the corresponding pastes were tested by X-ray diffraction (XRD), Fourier transform infrared spectroscopy (FTIR), thermogravimetric analysis (TGA) and field emission scanning electron microscopy (FESEM).

8.2 EXPERIMENTAL

8.2.1 Materials and equipment

Blast-furnace slag was supplied by Cementval S.A (Puerto de Sagunto, Spain) in form of large grains and it was milled in a ball mill for 30 minutes in order to obtain a fine material that can be used as solid precursor in AAM. Chemical composition of BFS is shown in Table 8.1. BFS is mostly composed by CaO (40.2%), SiO_2 (29.9%), Al_2O_3 (10.6%) and MgO (7.4%). Its mean particle diameter (D_{mean}) was 25.6 μm . Sodium

hydroxide (NaOH, which was called by NH when is regarding to solution composition and specimens' nomenclature) is the chemical reagent utilised to prepare the alkaline solutions. This material was used in form of pellets, and it was supplied by Panreac S.A. (purity of 98%). In mortars' preparation, natural sand from Caolines Lapiedra (Lliria, Valencia, Spain) with fineness modulus of 4.30 was utilised.

Sugar cane straw ash (SCSA) was utilised as silica source to produce the activating solution. In order to prepare the ash, firstly, straw was collected from sugar cane plantations near to Ilha Solteira city (São Paulo, Brazil). Then, the collected straw was transformed in the ash by means of an autocombustion process. This procedure had a duration time of 6 hours, and the maximum temperature reached in this combustion was 700 °C. This ash contained some unburned particles, it was sieved (MESH #50, opening of 300 µm) to remove them. Finally, the passing ash was milled in a ball mill for 50 minutes in order to reduce liquid absorption ability and to enhance rheological properties of the fresh AAM. Table 8.1 shows the chemical composition of SCSA, where the major compound was SiO₂ (58.6 wt%), and also significant percentage of Al₂O₃ (9.0 wt%) and Fe₂O₃ (8.4 wt%) as main compounds. D_{mean} of SCSA after the milling process was 18.1 µm. Insoluble residue determination was also carried out for SCSA (34 wt%).

Rice husk ash (RHA) was another silica source utilised to produce the activating solution. This ash served as a comparison material to SCSA. RHA was supplied by DACSA S.A (Tabernes Blagues, Spain) and it was utilised as received. Its chemical composition is summarized in the Table 8.1: the main oxide was SiO₂ (85.6 wt%). The ash had a D_{mean} of 62.3 µm. RHA was utilised without milling because a previous study concluded that the particle diameter of this ash did not influence on mechanical properties of AAM (BOUZÓN et al., 2014). Unlike RHA, the use of unground SCSA presented rheological problems during the AAM preparation (important water adsorption), this was the reason because SCSA was milled for reaching appropriate workability of the samples.

Commercial sodium silicate (SS) was also utilised in this study as a silica source. This chemical reagent was acquired from Merck, and its chemical composition was 8 wt% Na₂O, 28% wt% SiO₂ and 64% wt% H₂O.

Table 8.1 – Chemical composition of BFS, SCSA and RHA in wt%

Raw materials	SiO ₂	Al ₂ O ₃	Fe ₂ O ₃	CaO	MgO	K ₂ O	SO ₃	Cl	Others	LOI
BFS	29.9	10.6	1.3	40.2	7.4	0.6	1.9	-	2.6	5.5
SCSA	58.6	9.0	8.4	4.6	1.6	5.4	1.9	0.7	3.3	6.5
RHA	85.6	0.3	0.2	1.8	0.5	3.4	0.3	0.3	0.6	7.0

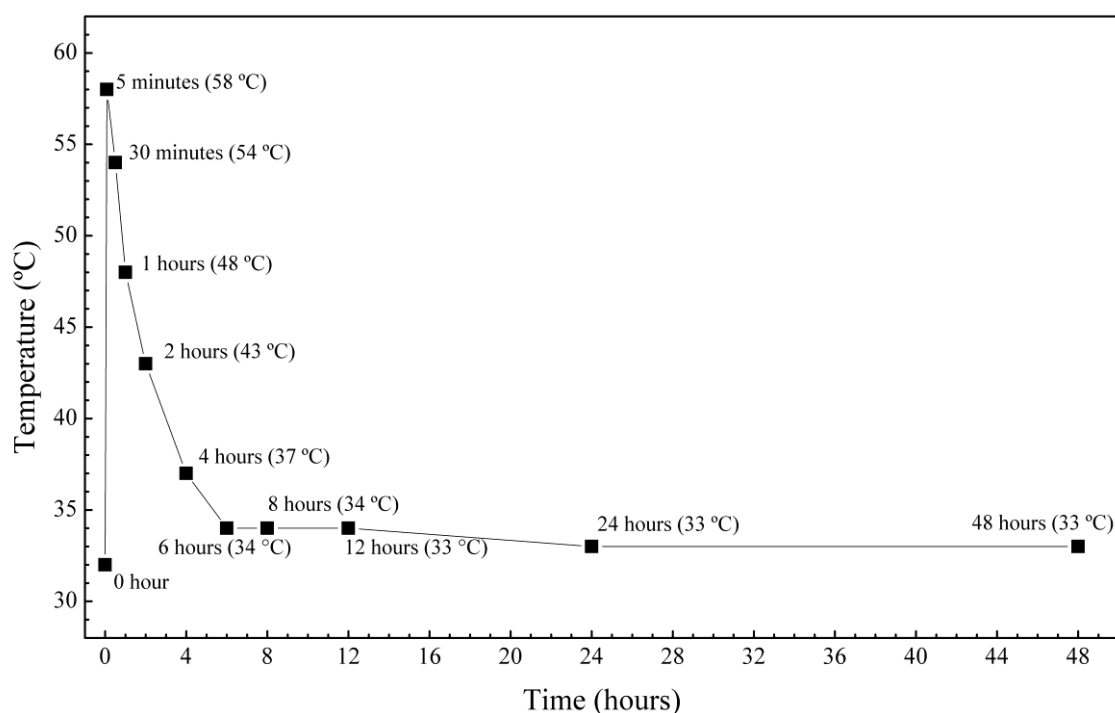
8.2.2 Alkali-activated materials preparation

Alkali-activated materials designed for this study had three parameters that were maintained as constants along the study: the water/BFS ratio, the sand/BFS ratio (for mortars) and the Na⁺ molality were held as 0.45, 3.0 and 4 mol.kg⁻¹, respectively. The preparation of alkaline solution has an important role in this study. Four different systems were performed: NH/SCSA, NH/RHA, only NH (NH/-) and NH/SS. The amount of SCSA, RHA and SS used to produce the alkaline solution is represented in terms of the SiO₂/Na₂O molar ratio in the solution (called by ϵ). In the case of this study, the ϵ value can only be varied by the amount of the silica source that is added to the activating solution, since the Na⁺ molarity was maintained constant. The ϵ values analysed for SCSA containing suspensions were 0.73, 1.09, 1.46 and 1.82. For sodium silicate and RHA, only SiO₂/Na₂O molar ratio of 1.46 was assessed. In the case of the solution with only NaOH, obviously the SiO₂/Na₂O molar ratio was equal to 0.

Regarding to the preparation of activating solutions composed by NH/SCSA and NH/RHA, they were produced by means of a thermal bottle. As the NaOH dissolution in water releases heat, using a thermal bottle would beneficiate from this heat for extended time in order to improve the dissolution rate of ash particles. Regarding to preparation steps of these both systems, firstly the ash (SCSA or RHA) was dry mixed with NaOH in the thermal bottle. Then, water was added over the solids, and the solution was stirred for 1 minute. Finally, the thermal bottle was sealed by a cap, and the suspension was maintained covered until a determined time (called by τ) to dissolve the ash. Part of the ash was not dissolved, then activating suspensions were obtained rather activating solutions ("activating solution" will be used as general term along the paper). In this study, the τ times assessed for SCSA were 0 (in this case, the ash was added as solid precursor together with BFS), 6, 24 and 48

hours, whereas, for RHA, the only thermal bottle-treating time was 24 hours. A monitoring of the temperature of the sodium hydroxide solution (4 mol.kg^{-1}) inside the thermal bottle was carried out. The Figure 8.1 shows the temperature in function of the time from 0 until 48 hours. The water before to mix with sodium hydroxide (0 hours) was in the temperature of 32°C . The system reached 58°C after 5 minutes and started to decrease until 6 hours, time that the temperature of the solution reached a constant temperature (around of 35°C). After the thermal bottle treatment, the solution (suspension) was left until reach room temperature. Prepared suspensions were not filtered, and they were used as obtained. In the case of preparing solutions composed by NaOH or NaOH/sodium silicate, chemical reagents were mixed with water in a common beaker. The beaker was sealed with plastic film, and solution was left to reach room temperature.

Figure 8.1 – Temperature evolution with time in the dissolution of sodium hydroxide (32.4 g) in water (202.5 g) inside the thermal bottle



For mortars manufacturing, BFS was mixed with the prepared solution until attain proper homogenisation (60 seconds). The prepared paste was stirred with natural sand (150 seconds). The resulting mortar was vibrated in a prismatic mould ($40 \times 40 \times 160 \text{ mm}^3$), and

then stored under controlled temperature (20 or 65 °C) and relative humidity (100%) conditions until compressive strength tests. The pastes produced for microstructural analyses were kept in the same conditions as the mortars.

8.2.3 Tests procedures

Compressive strength tests were carried out on mortars by means of a universal test machine according to the UNE-EN 196-1 standard. Pastes were assessed by X-ray diffraction (XRD), Fourier transform infrared spectroscopy (FTIR), thermogravimetric analysis (TGA) and field emission scanning electron microscopy (FESEM). XRD patterns were obtained by a Bruker AXS D8 Advance with a voltage of 40 kV, current intensity of 20 mA and a Bragg's angle (2θ) in the range of 5-70°, with a step of 0.02° and 2 s/step. FTIR spectra were accomplished by a Bruker Tensor 27 in the range of 400 and 4000 cm^{-1} . TGA were performed by a TGA Mettler-Toledo TGA 850, where the specimen was heated in a 70 μL alumina crucible in the temperature range of 35-1000 °C, with a heating rate of 20 $^{\circ}\text{C}.\text{min}^{-1}$ and dry air atmosphere (75 $\text{mL}.\text{min}^{-1}$ gas flow). In this test, mass losses and derivative curves (DTG curve) were extracted from the TG curve. Finally, FESEM images were taken by a ZEISS Supra 55 in fractured surface sample covered with carbon. In EDS studies, the extra high tension (EHT) was 20 kV and the working distance (WD) was 6-8 mm.

Mortars and pastes were assessed after 3 days of curing at 65 °C and relative humidity of 100%. Only for compressive strength test in the Section 3 of the study (comparison of SCSA to others silica source) that were carried out a curing time of 28 days at 20 °C and relative humidity of 100%. Table 8.2 summarizes the tests performed and the selected mixtures assessed for each test.

8.2.4 Alkali-activated materials studies

The aim of the paper was to assess the potential of SCSA as silica source in the preparation of activating solution. In this way, the study on mortars was divided in three sections: 1) To obtain the optimum treatment time on leaving the ash in the thermal bottle; 2) To determine the optimum SCSA amount in the activating solution; and 3) To compare

the NH/SCSA suspension to some different silica sources: NH/SS (solution) and NH/RHA (suspension) systems. The both optimum thermal bottle time and SCSCA amount in the solution were selected by compressive strength reached at 3 days curing time at 65 °C. In the first section of the study, four different periods of leaving the ash dissolving in the thermal bottle with the NaOH (also called as thermal bottle time, τ) were assessed in order to obtain the optimum time. The assessed τ values were 0, 6, 24 and 48 hours. In this part, the ϵ ratio was maintained as a constant of 1.46. Following to the second section of the study, the influence of SCSCA amount were assessed by varying the ϵ ratio. Then, the assessed ϵ ratios were 0 (this solution contains only NaOH), 0.73, 1.09, 1.46 and 1.82 (they are common values in the alkaline activation of blast furnace slag (SHI et al., 2006)). In this case, the τ was held as a constant time selected from the previous section (24 hours). Finally, in the third section of the study, NH/SCSCA solutions with ϵ of 1.46 and thermal bottle time of 24 hours was compared to the following systems with the same ϵ : NH/SS and NH/RHA with τ of 24 hours. Four selected mixtures to study their microstructure in pastes were manufactured: two produced by the activating solution with NH/SCSCA (ϵ equal to 1.46, τ times of 0 and 24 hours), one prepared by means of a NaOH solution ($\epsilon = 0$), and the last one produced by a solution of NH/SS ($\epsilon = 1.46$).

The nomenclature adopted for these dosages are X- ϵ - τ , where: X is the alkaline solution system (NH, SCSCA, RHA or SS); ϵ is the $\text{SiO}_2/\text{Na}_2\text{O}$ molar ratio; and τ is only defined for the solutions with SCSCA and RHA. Table 8.2 summarizes the three study sections, dosages assessed and their respective nomenclatures.

Table 8.2 – Mixtures and tests carried out

Study Section	Activating Solution	SiO ₂ /Na ₂ O molar ratio (ϵ)	Thermal bottle time (τ)	Nomenclature	Testing ages	
					Compressive strength tests	Microstructural tests (XRD, FTIR, TG and FESEM)
1	NH/SCSA	1.46	0	SCSA-1.46-0	3 days (65 °C)	3 days
			6	SCSA-1.46-6		-
			24	SCSA-1.46-24		3 days
			48	SCSA-1.46-48		-
			-	NH-0		3 days
2	NH/SCSA	0.73	24	SCSA-0.73-24	3 days (65 °C)	-
		1.09		SCSA-1.09-24		-
		1.46		SCSA-1.46-24		3 days
		1.82		SCSA-1.82-24		-
		-		-		-
3	NH/SS	1.46	-	SS-1.46	3 days (65 °C)	3 days
	NH/SCSA		24	SCSA-1.46-24	and 28 days	3 days
	NH/RHA		24	RHA-1.46-24	(20 °C)	-

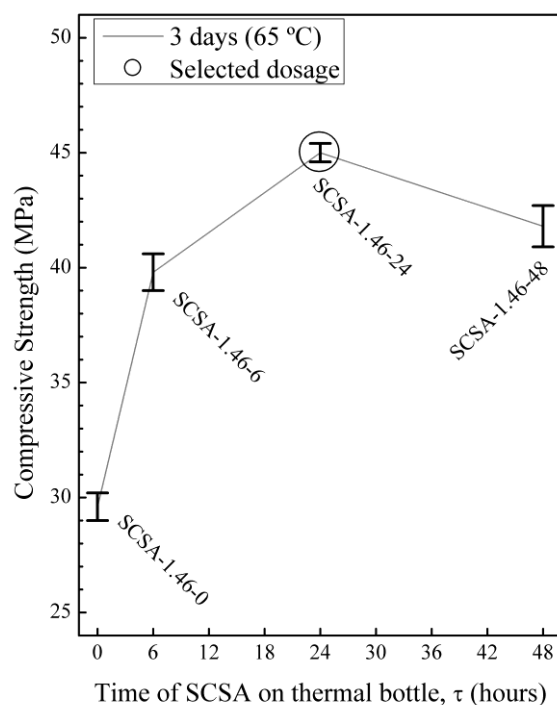
8.3 RESULTS AND DISCUSSION

8.3.1 Effect of the thermal bottle time (τ) for SCSA/NaOH suspensions (Section 1)

Different activating reagents based on SCSA were obtained by mixing, in a thermal bottle, with NaOH and water (variable τ at a constant ϵ). The dissolution heat of NaOH in water benefited the dissolution of SCSA. Prepared suspensions were not filtered, and they were used as obtained. Compressive strengths of SCSA-1.46-0, SCSA-1.46-6, SCSA-1.46-24 and SCSA-1.46-48 after 3 days of curing at 65 °C are shown in the Figure 8.2. It is observed that the thermal bottle time (τ) had crucial effect on the compressive strength development and showed to be beneficial until a τ of 24 hours: SCSA-1.46-24 mortar showed the highest compressive strength (45.0 MPa). On one hand, these results suggest that the use of thermal bottle accelerated the silica dissolution from SCSA in the activating solution. The

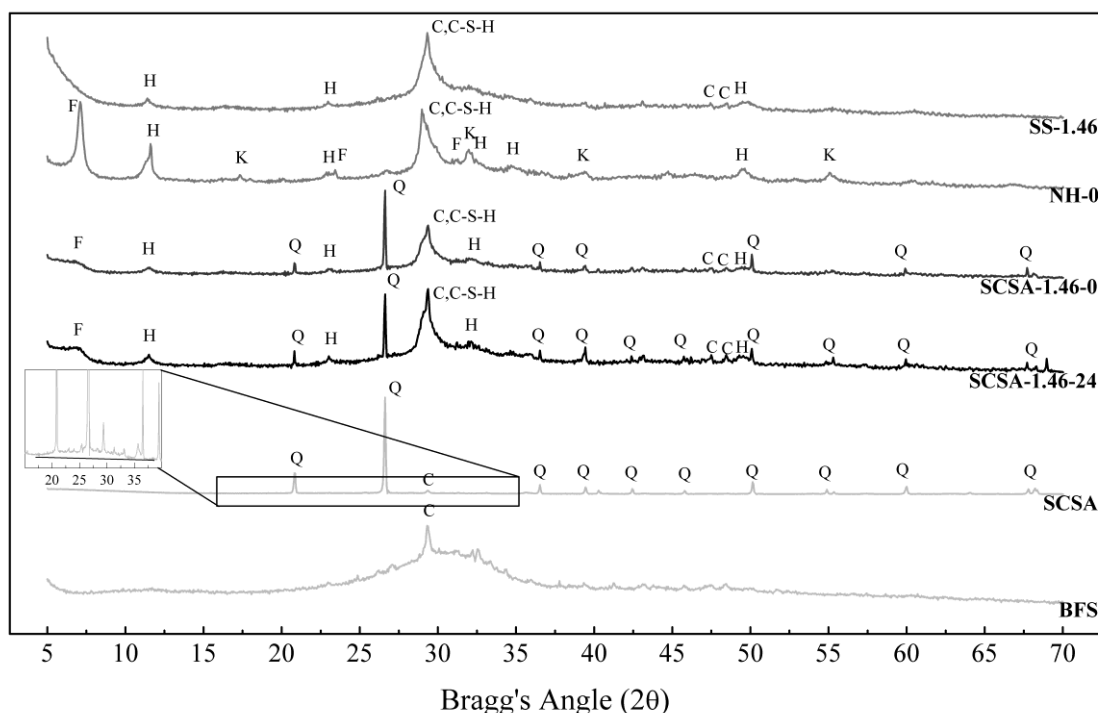
more presence of SiO_4^{4-} anions in the alkaline solution probably favoured the formation of more cementing gel when reacted to BFS. The suspension temperature at high temperature (maximum of 58°C) observed from 0 to 6 hours (Figure 8.1) favoured the SCSA dissolution, as can be noticed comparing the compressive strength development for SCSA-1.46-0 and SCSA-1.46-6. However, even the solution reached a constant temperature after 6 hours, some SCSA dissolution must be carried out due the high alkaline condition: the compressive strength for SCSA-1.46-24 was higher than the SCSA-1.46-6 one. On the other hand, it is not advantageous to utilise the thermal bottle beyond the τ of 24 hours: SCSA-1.46-48 (41.8 MPa) reached slightly lower compressive strength than the SCSA-1.46-24. It was observed that the sodium silicate produced from the silica in SCSA suffered a gelification (BOUZÓN et al., 2014). Probably, this formed gel did not take part in the formation of alkali-activated materials products, which contributes to the decrease in the compressive strength. Therefore, it can be concluded that the optimum thermal bottle time (τ) was 24 hours for SCSA.

Figure 8.2 – Compressive strength values of mortars (cured at 65°C for 3 days) with activator prepared by thermal bottle treatment in different reaction time (τ) of 0, 6, 24 and 48 hours



XRD patterns for raw materials (BFS and SCSA), and SCSA-1.46-24 and SCSA-1.46-0 pastes cured after 3 days at 65 ° are depicted in the Figure 8.3. The baseline deviation observed in the diffractograms of raw materials and pastes is due the presence of amorphous phase in their composition. In the BFS and SCSA diffractograms, the baseline deviation was observed in the Bragg's Angle range of 22-37° and 17-35°, respectively. In the case of the ash, this baseline deviation was only detected by the enlargement of the diffractogram, because the large quantity of quartz. There were no differences among the baseline deviations of the prepared pastes, suggesting that they formed similar gel of (N,C)-A-S-H (ISMAIL et al., 2014). In addition to some amorphous phase, crystalline compounds were also observed in the diffractograms. In XRD patterns of the raw materials, some crystalline phases detected were calcite (CaCO_3 , PDF Card #050586) for both BFS and SCSA, and quartz (SiO_2 , PDF Card #331161) for SCSA. In the case of pastes, it was identified a formation of faujasite ($\text{Na}_2\text{Al}_2\text{Si}_4\text{O}_{12} \cdot 8\text{H}_2\text{O}$, PDF Card #391380) and hydrotalcite ($\text{Mg}_6\text{Al}_2\text{CO}_3(\text{OH})_{16} \cdot \text{H}_2\text{O}$, PDF Card #140191). Also C-S-H phase was observed (probably a (C,N)-A-S-H phase by the presence of sodium and aluminum in the reaction). The broad XRD peak associated to this gel overlapped to the main calcite XRD peak. However, other peaks related to the presence of calcite were observed, which indicates that some slight carbonation of the samples took place during the curing process or in the sample handling. Regarding to thermal bottle time (τ) influence, SCSA-1.46-24 and SCSA-1.46-0 presented similar diffractogram patterns. Some differences may be highlighted: larger XRD peaks related to faujasite and hydrotalcite were observed when τ is increased. Additionally the main band for the C-S-H gel in the range of 28.3-30.3° was different in size: the paste prepared by means of a thermal bottle showed stronger intensity than the sample produced by the SCSA without the bottle treatment. Areas under main XRD peaks for quartz (A_Q) and C-S-H (A_{gel}) were measured utilising the Graphing Software Origin Pro 8 in the range of the analysed peak and not taking in account the baseline deviation. The area ratio $\phi = A_{gel}/A_Q$ were calculated for both pastes. The ϕ value for SCSA-1.46-24 was 5.58 while for SCSA-1.46-0 was 2.87. Assuming that quartz fraction in SCSA was not dissolved in the preparation of the suspension and did not react with BFS, these ϕ values suggest a formation of more reaction products when $\tau = 24\text{h}$.

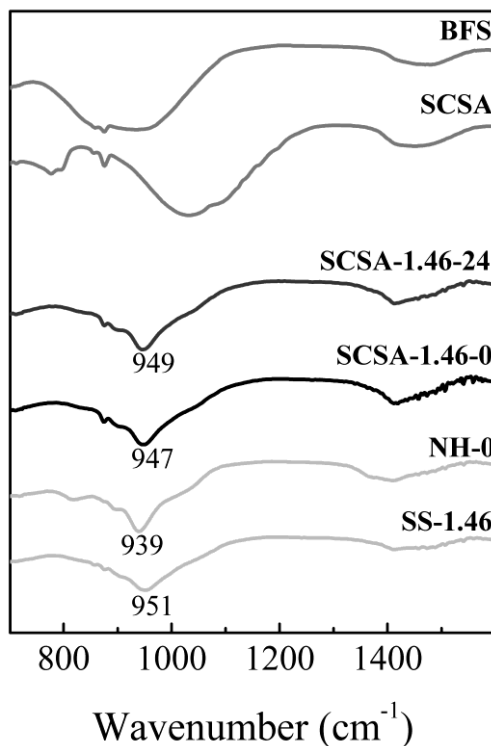
Figure 8.3 – XRD patterns of raw materials (SCSA and BFS) and pastes (SCSA-1.46-24, SCSA-1.46-0, NH-0 and SS-1.46) cured after 3 days at 65 °C. Keys: Q: quartz; C: calcite; H: hydrotalcite; F: faujasite; C-S-H: calcium silicate hydrate; K: katoite.



FTIR spectra of raw materials, BFS and SCSA, and pastes SCSA-1.46-24 and SCSA-1.46-0 cured after 3 days at 65 °C, are represented in the Figure 8.4. The main bands detected in the spectra for raw materials and pastes were in the wavenumber ranges of 800-1250 cm^{-1} (stretching mode of Si-O) and 1400-1550 cm^{-1} (stretching mode of O-C-O bonds). The band in the range of 1400-1550 cm^{-1} was due to the presence of calcite in raw materials and also to the carbonation of the samples, as observed in XRD analysis. In this case, the most important wavenumber interval is within of 800-1250 cm^{-1} because in this wavenumber range are observed the main differences among spectra. BFS and SCSA presented broad bands in the wavenumber ranges of 800-1050 and 900-1250 cm^{-1} , respectively, while the pastes showed narrower bands in the interval of 900-1050 cm^{-1} with a centred peak near to 950 cm^{-1} . This behaviour is justified by the dissolution of the raw materials particles, and following by the formation of alkali-activated materials products (FERNÁNDEZ-

JIMÉNEZ; PUERTAS, 2003). In the case of both pastes produced with SCSA, they did not present significant differences between them, indicating that their gel nature is similar.

Figure 8.4 – FTIR spectra of raw materials (SCSA and BFS) and pastes (SCSA-1.46-24, SCSA-1.46-0, NH-0 and SS-1.46) cured after 3 days at 65 °C



TGA results are represented in Figure 8.5 (DTG curves) and Table 8.3 (mass losses) for the pastes SCSA-1.46-24 and SCSA-1.46-0 after 3 days of curing at 65 °C. In the DTG curves for these pastes, four peaks were observed in the following temperatures: 140, 400, 550 and 800 °C. The first peak, centred at 140 °C, is related to the decomposition of (C,N)-A-S-H or N-A-S-H products. Peak at 400 °C was identified as the decomposition of hydrotalcite, and the peaks at 550 and 800 °C were related to the decomposition of carbonates (BERNAL et al., 2017). Normally, carbonates decompose in the temperature range of 700-850 °C. However, the formation of a poorly crystallised phase and the presence of sodium ions caused a decrease in the temperature decomposition of carbonates to 550 °C (BERNAL et al., 2017). Table 8.3 shows the mass losses in two different temperature intervals in order to emphasize the study on formation of the reaction products: 35-300 °C (P_{35-300}) and 300-1000 °C ($P_{300-1000}$). Similar mass losses in the range of 35-300 °C (12.67 and 11.68%,

respectively) were observed suggesting that the amount of hydration products formation was in the same order of magnitude. This fact means that differences in compressive strengths are not directly related to the percentage of combined water, and it may be analysed from the point of view in the distribution of products into the cementing matrix.

Figure 8.5 – DTG curves of pastes (SCSA-1.46-24, SCSA-1.46-0, NH-0 and SS-1.46) cured after 3 days at 65 °C (numbers close to main peaks are in °C)

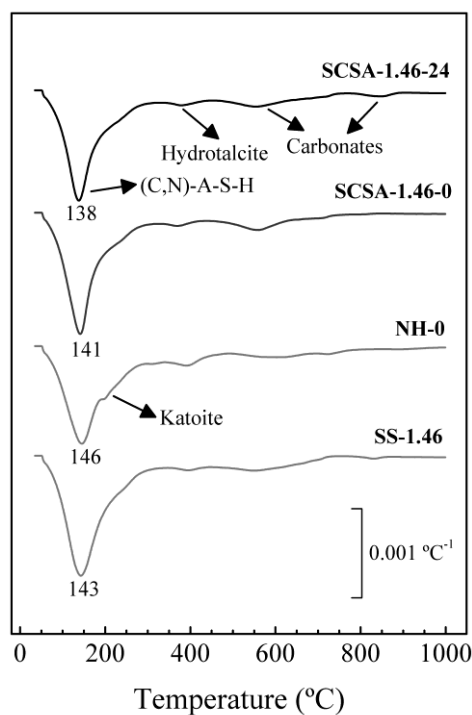
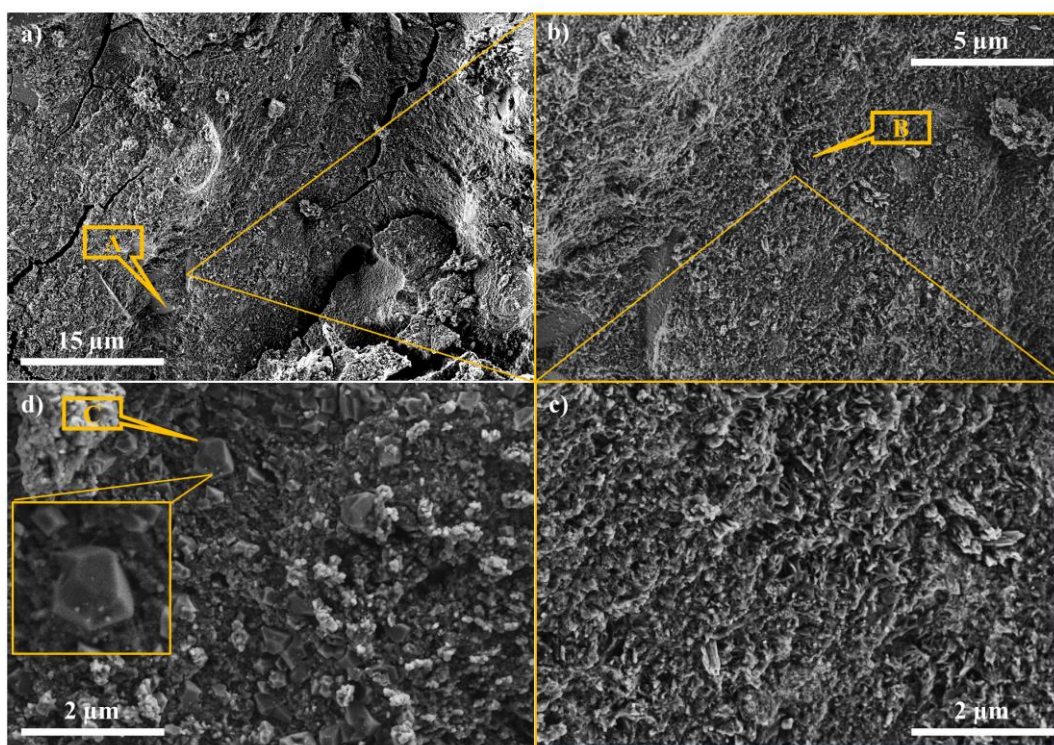


Table 8.3 – Mass losses (%) of the pastes SCSA-1.46-24, SCSA-1.46-0, NaOH and SS-1.46 cured after 3 days at 65 °C in the test temperature intervals of 35-300 °C (P₃₅₋₃₀₀) and 300-1000 °C (P₃₀₀₋₁₀₀₀)

Specimen	Mass Losses (%)		
	P ₃₅₋₃₀₀	P ₃₀₀₋₁₀₀₀	TOTAL
SCSA-1.46-24	11.68	5.57	17.25
SCSA-1.46-0	12.67	5.06	17.73
NaOH	12.40	5.76	18.16
SS-1.46	14.50	5.19	19.69

Figure 8.6 shows FESEM micrographs for the SCSA-1.46-24 paste after 3 days of curing at 65 °C. In a general view of the fractured surface paste (Fig. 6a), it is observed a dense and amorphous structure (as the previous tests suggested). A compacted gel was observed and scarce unreacted particles of blast furnace slag (Spot A) were also identified. There were not found unreacted SCSA particles. The formed gels (Spot B) can be seen at a higher magnification at Fig. 6b and Fig. 6c: they present a form of very small and irregular in shape particles (less than 0.2 µm in diameter) that are piled each other in a homogeneous pattern, yielding a low porosity matrix. EDS analysis from this gel (eight points) give the following molar ratios of $\text{Ca/Si} = 0.95 \pm 0.07$, $\text{Al/Si} = 0.32 \pm 0.03$, $\text{Na/Al} = 1.34 \pm 0.05$ and $\text{Mg/Si} = 0.13 \pm 0.05$. This gel is considered as the (C,N)-A-S-H product. In the Fig. 6d, some microcrystals (Spot C) are distributed into gel matrix (probably faujasite crystals).

Figure 8.6 – FESEM micrographs of the paste SCSA-1.46-24

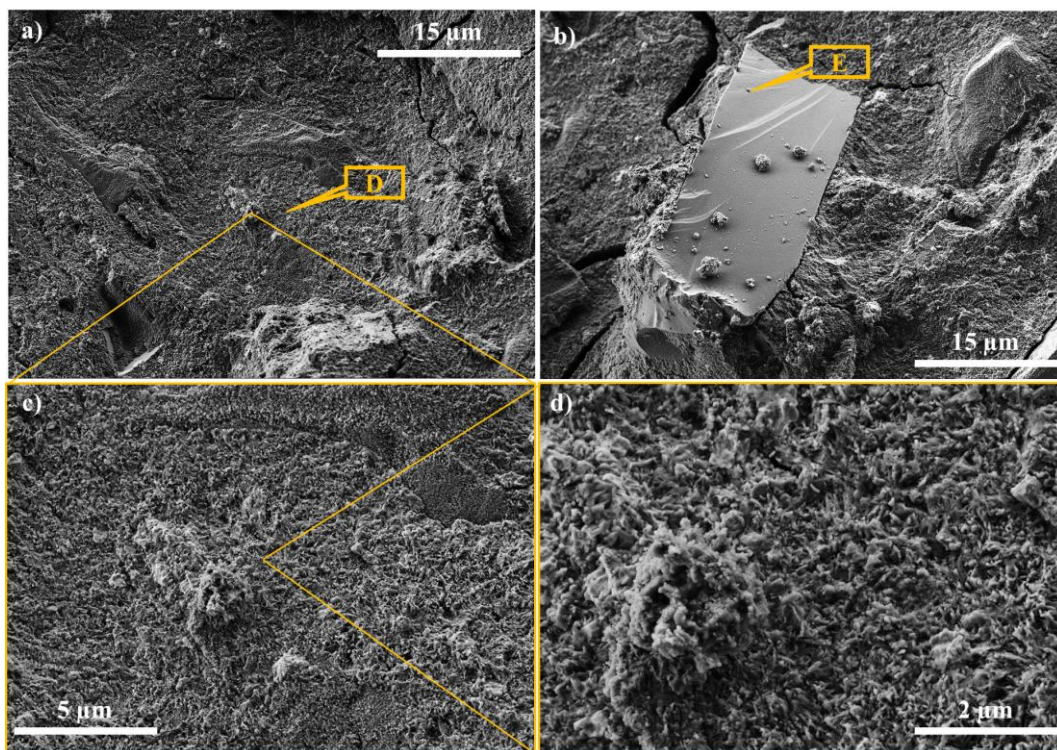


FESEM images of the paste SCSA-1.46-0 cured after 3 days at 65 °C are shown in the Figure 8.7. In the Figure 8.7a, it can be observed a dense structure similar to the SCSA-1.46-24 paste at Spot D. Fig. 7b shows a quartz particle from SCSA in the Spot E surrounded by gel. Magnifications of the Fig. 7a are shown in Fig. 7c and Fig. 7d. The formed gel is also

composed by small hydration products as those found for the SCSA-1.46-24 paste. Regarding to chemical composition of gel in SCSA-1.46-0, the molar ratios were: $\text{Ca/Si} = 0.92 \pm 0.06$, $\text{Al/Si} = 0.33 \pm 0.01$, $\text{Na/Al} = 1.86 \pm 0.12$ and $\text{Mg/Si} = 0.18 \pm 0.05$. The Ca/Si , Al/Si and Mg/Si ratios in SCSA-1.46-0 paste were similar to that found in the SCSA-1.46-24. The larger difference was found for Na/Al ratio in the formed gel, despite both pastes were produced with the same composition.

It has been reported (GAO et al., 2015) that the strength development of AAM depends on the ε value of the activating solution, and, for BFS systems, ε values lower than 1.0 yields low compressive strength. In both SCSA pastes, the theoretical ε value was 1.46, however for SCSA-1.46-0 there is less solubilized silica and, consequently, the real ε is lower than that for SCSA-1.46-24. In these conditions, more Na^+ is incorporated to the formed gel, and then the strength contribution is significantly lower (34.2% lower strength was obtained for mortars, see Figure 8.2). Thus, the chemical composition of the gel formed has a decisive contribution on the strength of the matrix.

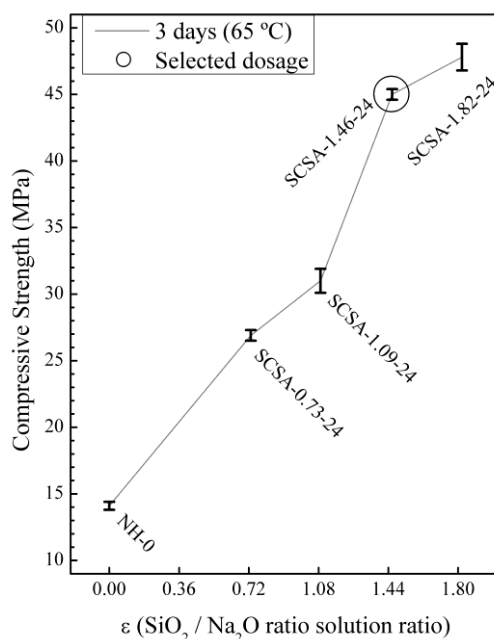
Figure 8.7 – FESEM micrographs of the paste SCSA-1.46-0



8.3.2 Effect of the $\text{SiO}_2/\text{Na}_2\text{O}$ molar ratio (ϵ) for SCSA/NaOH suspensions (Section 2)

Compressive strength of the mixtures NH-0, SCSA-0.73-24, SCSA-1.09-24, SCSA-1.46-24 and SCSA-1.82-24 were represented in the Figure 8.8 after 3 days of curing at 65 °C. It is observed that the SCSA amount (represented by ϵ , the $\text{SiO}_2/\text{Na}_2\text{O}$ molar ratio of the solution) influenced the compressive strength of the mortars for a constant τ value (24 h). The increase of the SCSA quantity in the solution also generates an increase in the compressive strength of mortars. A noticeable result was that all the samples with the ash (compressive strength results in the range of 26.9-47.8 MPa) presented significantly better results than the mortar with only NaOH (14.1 MPa). As expected, the dissolved SiO_4^{4-} from SCSA influenced positively the formation of a stronger structure. The dosage selected for the sequence of the study (Section 3) was the SCSA-1.46-24. Although the SCSA-1.82-24 (47.8 MPa) presented slightly higher compressive strength than SCSA-1.46-24 (45.0 MPa), this later mortar presented better rheological properties than the former one.

Figure 8.8 – Compressive strength values of mortars (cured at 65 °C for 3 days) with activator prepared by thermal bottle treatment in different $\text{SiO}_2/\text{Na}_2\text{O}$ molar ratio (ϵ) of 0 (only NaOH), 0.73, 1.09, 1.46 and 1.82



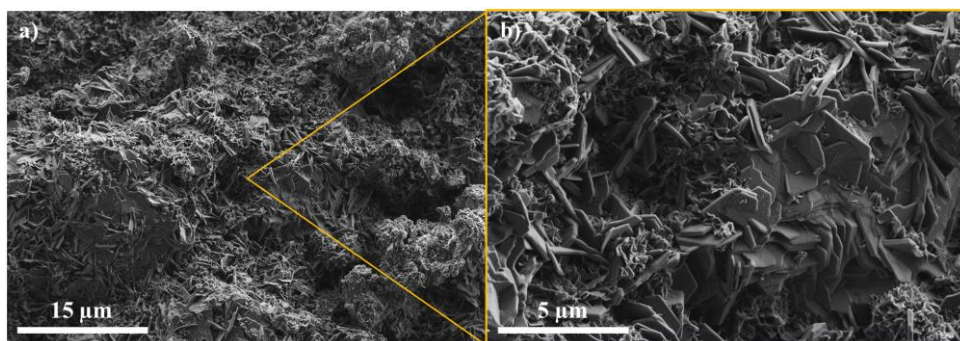
XRD results showed important differences between NaOH and SCSA-1.46-24 pastes (Figure 8.3). In the case of former paste, it was presented more intense peaks of crystalline phases (faujasite and hydrotalcite) than SCSA sample. In addition, katoite was also formed in this paste. The high formation of crystalline compounds were already noticed in a previous study, where the use of only NaOH solution causes a production of more ordered phases than a sample produced by solution with a combination of sodium hydroxide and a silica source (as sodium silicate) (ESCALANTE-GARCÍA et al., 2003; BUCHWALD et al., 2007). The more formation of ordered structures can justify the lowest compressive strength results for this mixture.

In the FTIR studies (Figure 8.4), the SCSA paste presented its main Si-O peak located in higher wavenumber than the paste produced with only NaOH. Probably the increase of silica content for SCSA system in the mixture caused a stronger gel, justifying the higher compressive strength of mortars produced with SCSA.

Regarding to TGA studies (Figure 8.5 and Table 8.3), NaOH sample presented similar mass loss to the other pastes besides the low compressive strength. As noticed in the XRD analysis, NaOH sample had strong formation of crystalline compounds, as faujasite and katoite ($\text{Ca}_3\text{Al}_2(\text{SiO}_4)(\text{OH})_8$, PDF Card #380368), that decompose at approximately temperatures of 140 °C and 200 °C, respectively. In these temperatures are also observed the decomposition of alkali-activated materials gels. Probably, great part of the mass loss of NH-0 sample in the range of 35-300 °C is related to those crystalline phases decomposition and not to cementing gels dehydration. This observation explains the mass loss of NH-0 specimen to be comparable to other pastes, even the compressive strength was very low.

Figure 8.9 presents the FESEM micrographs of NH-0 sample after 3 days of curing at 65 °C. Differently to observed in the previously described SCSA pastes, the structure of NH-0 paste is more crystalline and porous. This kind of structure was already expected due the results from the above described results. Regarding to the chemical composition of the paste, Ca/Si, Al/Si, Na/Al and Mg/Si molar ratios of the formed product are 1.18 ± 0.02 , 0.38 ± 0.02 , 1.89 ± 0.15 and 0.07 ± 0.01 . The Ca/Si ratio in this case is higher than for SCSA pastes (1.18 vs. 0.95-0.92). It is clearly noticed that the NH-0 paste presents less silicon than SCSA samples, which probably the lack of it caused a formation of a more crystalline, porous and softer structure with lower compressive strength.

Figure 8.9 – FESEM micrographs of the paste NH-0



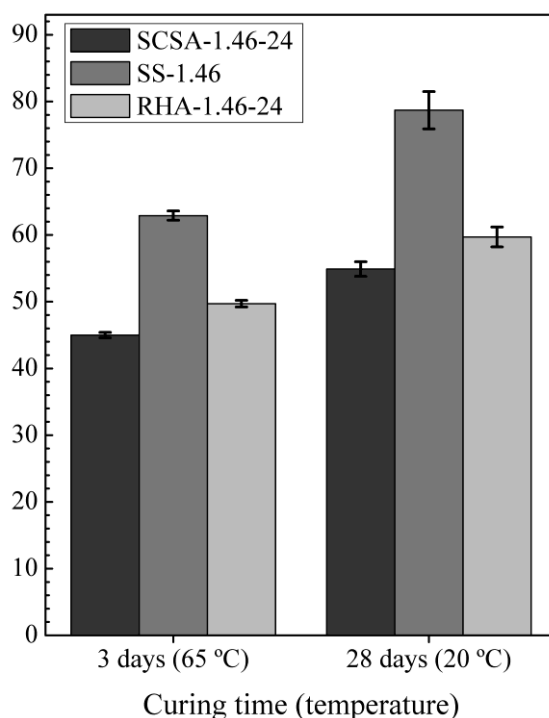
8.3.3 Comparison of SCSA to others silica sources (Section 3)

Compressive strength of SCSA-1.46-24 was compared to SS-1.46 and RHA-1.46-24 samples after 3 days at 65 °C and after 28 days at 20 °C (Figure 8.10). The highest compressive strength was reached by the SS-1.46 system with 62.9 MPa and 78.8 MPa for 3 (at 65 °C) and 28 (at 20 °C) curing time respectively. In the case of both systems with ashes, SCSA and RHA, they presented similar results on the compressive strength of mortars: SCSA mortar presented a compressive strength of 45 and 54.9 MPa for 3 and 28 days, respectively, whereas RHA blend reached 49.7 and 59.7 MPa for the same curing ages. In all cases, developed strength at 20°C was better. Although the calculated $\text{SiO}_2/\text{Na}_2\text{O}$ ratio was equal for the three mixtures, reliably the presence of non-dissolved silica from the ashes caused the lower compressive strength. It was difficult to determine the amount of solubilized silica after the treatment in the thermal bottle: the gelification of the suspension (which impeded the filtration of it). It is obvious that quartz present in SCSA was not dissolved, which generated less solubilized silica. This is the reason that strength for RHA samples was slightly higher.

Despite the SCSA did not present the same result as the commercial sodium silicate (reached a value between 75-80% of the compressive strength obtained for SS-1.46), the ash has the potential to be utilised as silica source to produce the activating solution. In a previous study, spent diatomaceous earth was assessed in the production of alternative solutions in a fly ash/metakaolin system (MEJÍA et al., 2016). However, in this case, the compressive strength of pastes obtained from this solution was approximately 50% of the results for control with sodium silicate. In the same study, the spent diatomaceous earth presented similar results than the rice husk ash. Waste glass was also utilised as silica source

to produce the activating solution (PUERTAS; TORRES-CARRASCO, 2014). In a system based on BFS, the pastes produced by the solution with the waste presented approximately 75-80% of the compressive strength of the control, which is similar than SCSA results in the present paper. More recently, sugar cane bagasse ash was evaluated as silica source in the production of activating solution (TCHAKOUTÉ et al., 2017). This new solution presented similar results in compressive strength tests than the waste glass and rice husk ash in metakaolin-based AAM.

Figure 8.10 – Comparison of compressive strength values of mortars (cured at 65 °C for 3 days and 20 °C for 28 days) obtained from SCSA, SS and RHA



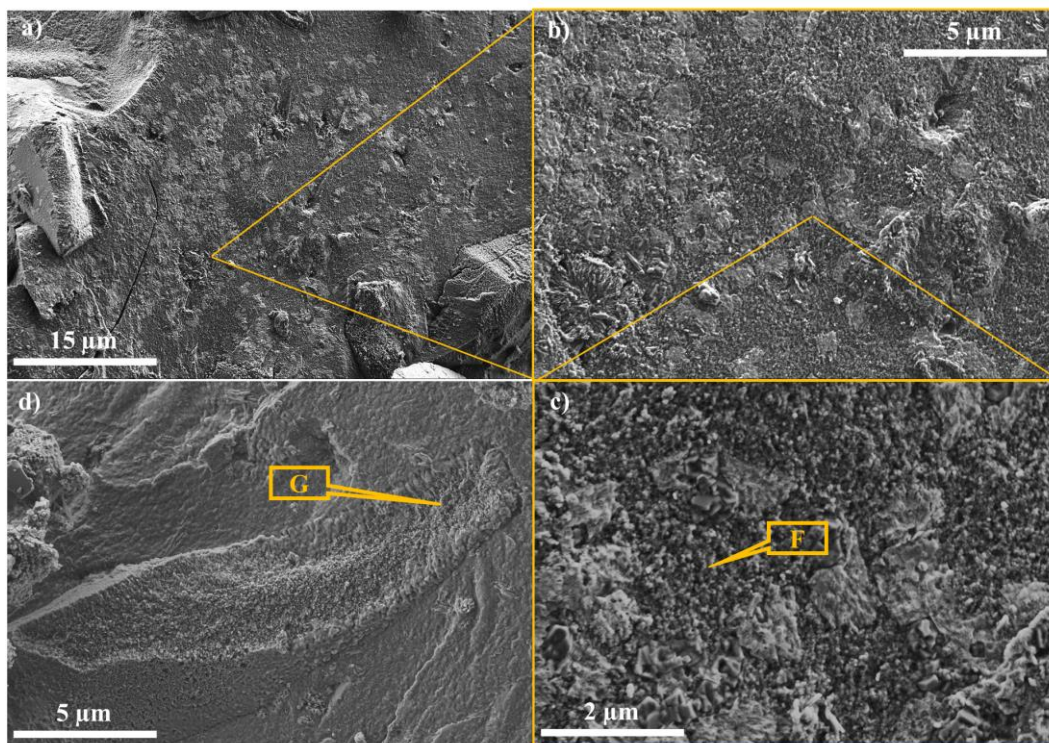
XRD patterns of SCSA-1.46-24 and SS-1.46 presented differences (Figure 8.3): the main one is the obvious absence of quartz in SS-1.46. SCSA-1.46-24 diffractogram presented, additionally, faujasite that was not observed in the SS-1.46 sample. Hydrotalcite and calcite were identified in SS-1.46, showing peaks of low intensity. Probably, this fact and the higher content of soluble silica let to explain the highest compressive strength obtained for this mixture.

FTIR studies (Figure 8.4) did not let to differentiate SCSA-1.46-24 and SS-1.46, only just a small difference in the energy of the main Si-O band. This result suggests that the chemical nature of the formed hydrates is similar.

In TGA results (Figure 8.5 and Table 8.3), mass loss of SS-1.46 was higher than the SCSA-1.46-24. It can be related to the more formation of cementing gels, which justifies the highest compressive strength. In addition, the shape of the DTG curve of both SCSA pastes are more similar to the specimen produced with sodium silicate than the NaOH: deep peak related to the mass loss of the dehydration of (C,N)-A-S-H products and no peaks related to decomposition of C-A-S-H compounds. This behaviour suggests that SCSA pastes presented similar products formation to the sodium silicate paste.

FESEM micrographs of SS-1.46 paste after 3 days of curing at 65 °C are depicted in the Figure 8.11. It can be noticed that this paste presented an amorphous and dense structure, principally in the magnification at Spot F (Fig. 11c). Comparing Fig. 11c to Fig. 6c (SCSA-1.46-24), it can be noted that the compactness of the former was slightly lower than that found for SCSA paste. In addition, the formed gel was similar to the ones observed in the SCSA pastes. Regarding to gel composition, Ca/Si, Al/Si, Na/Al and Mg/Si molar ratios are 0.90 ± 0.04 , 0.23 ± 0.02 , 2.40 ± 0.16 and 0.09 ± 0.03 . Ca/Si ratio was slightly lower than to the SCSA paste ones, probably due more silica is chemically combined from the sodium silicate solution. In the Fig. 11d, a BFS particle covered by reaction products was observed at Spot G. The chemical composition for this spot was Ca/Si = 1.09 ± 0.13 , Al/Si = 0.45 ± 0.11 , Na/Al = 1.19 ± 0.26 and Mg/Si = 0.64 ± 0.26 . Comparing the Spot G to Spot F, the former presented higher ratios of Ca/Si, Al/Si and Mg/Si than the latter. The more relative presence of Ca, Al and Mg respect to Si suggests that the BFS particle was partially reacted.

Figure 8.11 – FESEM micrographs of the paste SS-1.46



8.4 CONCLUSIONS

SCSA was successfully utilised as silica source to produce the alkaline activating reagent for producing BFS-based AAM materials, by means of its partial dissolution in a thermal bottle. The dissolution heat in water of NaOH facilitates the dissolution of silica from the SCSA and it was not necessary to filter the obtained suspensions for yielding good behaviour as activating reagent, which facilitates its implementation in AAMs. Compressive strength tests of mortars showed that the optimum time on leaving the ash dissolving in the thermal bottle in the NaOH solution was 24 hours. The optimum amount of SCSA, represented by the $\text{SiO}_2/\text{Na}_2\text{O}$ molar ratio of the solution (ϵ), was 1.46. Besides the SCSA samples presented lower mechanical properties compared to specimens produced with a the commonly used NH/SS solution, the ash-based systems showed significantly better results than the samples prepared with the solution with only NaOH: the alkaline treatment of SCSA in the thermal bottle with NaOH produced a very reactive alkaline activator for BFS-based AAMs. From the microstructural studies, it can be concluded that SCSA pastes presented

similar characteristics than matrices obtained with sodium silicate-based reagent: dense and amorphous gels with comparable Ca/Si, Al/Si and Na/Al molar ratios were identified.

ACKNOWLEDGMENTS

The authors would like to thank CNPq processo n° 401724/2013-1 and CNPq processo n° 140779/2015-0. Thanks are also given to the Electron Microscopy Service of the Universitat Politècnica de València.

REFERENCES

- BERNAL, S. A.; GUTIERREZ, R. M.; PROVIS, J. L.; ROSE, V. *Effect of silicate modulus and metakaolin incorporation on the carbonation of alkali silicate-activated slags*. **Cement and Concrete Research**, v. 40, p. 898-907, 2010.
- BERNAL, S. A.; RODRÍGUEZ, E. D.; KIRCHHEIM, A. P.; PROVIS, J. L. *Management and valorisation of wastes through use in producing alkali-activated cement materials*. **Journal of Chemical Technology and Biotechnology**, v. 91, p. 2635-2388, 2016.
- BUCHWALD, A.; HILBIG, H.; KAPS, C. *Alkali-activated metakaolin-slag blends—performance and structure in dependence of their composition*. **Journal of Materials Science**, v. 42, p. 3024-3032, 2007.
- BOUZÓN, N.; PAYÁ, J.; BORRACHERO, M. V.; SORIANO, L.; TASHIMA, M. M.; MONZÓ, J. *Refluxed rice husk ash/NaOH suspension for preparing alkali activated binders*. **Materials Letters**, v. 115, p. 72-74, 2014.
- ESCALANTE-GARCÍA, J.I.; FUENTES, A.F.; GOROKHOVSKY, A.; FRAIRE-LUNA, P.E.; MENDONZA-SUAREZ, G. *Hydration Products and Reactivity of Blast-Furnace Slag Activated by Various Alkalis*. **Journal of American Ceramic Society**, v. 86, p. 2148-53, 2003.
- FERNÁNDEZ-JIMÉNEZ, A.; PUERTAS, F. *Structure of Calcium Silicate Hydrates Formed in Alkaline-Activated Slag: Influence of the Type of Alkaline Activator*. **Journal of American Ceramic Society**, v. 86, n. 8, p. 1389-1394, 2003.
- Food and Agriculture Organization of the United Nations – FAOSTAT.
<http://www.fao.org/faostat/en/#home>.
- FRÍAS, M.; VILLAR-COCIÑA, E.; VALENCIA-MORALES, E. *Characterisation of sugar cane straw waste as pozzolanic material for construction: Calcining temperature and kinetic parameters*. **Waste Management**, v. 27, p. 533-538, 2007.

GAO, X.; YU, Q. L.; BROUWERS, H. J. H. *Reaction kinetics, gel character and strength of ambient temperature cured alkali activated slag-fly ash blends*, **Construction and Building Materials**, v. 80, p 105-115, 2015.

KOURTI, I.; RANI, D.A.; DEEGAN, D.; BOCCACCINI, A. R.; CHEESEMAN, C.R. *Production of geopolymers using glass produced from DC plasma treatment of air pollution control (APC) residues*. **Journal of Hazardous Materials**, v. 176, p. 704-709, 2010.

ISMAIL, I.; BERNAL, S. A.; PROVIS, J. L.; NICOLAS, R. S.; HAMDAN, S.; van DEVENTER, J. S. J. *Modification of phase evolution in alkali-activated blast furnace slag by the incorporation of fly ash*. **Cement and Concrete Composites**, v. 45, p. 125-135, 2014.

MARTIRENA, F.; MONZÓ, J. *Vegetable ashes as Supplementary Cementitious Materials*. **Cement and Concrete Research**, 2017.

MEJÍA, J. M.; GUTIÉRREZ, R. M.; MONTES, C. *Rice husk ash and spent diatomaceous earth as a source of silica to fabricate a geopolymeric binary binder*. **Journal of Cleaner Production**, v. 118, p. 133-139, 2016.

MEJÍA, J. M.; GUTIÉRREZ, R. M.; PUERTAS, F. *Rice husk ash as a source of silica in alkali-activated fly ash and granulated blast furnace slag systems*. **Materiales de Construcción**, v. 63, p. 361-375, 2013.

MORAES, J. C. B.; TASHIMA, M. M.; AKASAKI, J. L.; MELGES, J. L. P; MONZÓ, J.; BORRACHERO, M. V.; SORIANO, L.; PAYÁ, J. *Increasing the sustainability of alkali-activated binders: The use of sugar cane straw ash (SCSA)*. **Construction and Building Materials**, v. 124, p. 148-154, 2016.

NAZARI, A.; SANJAYAN, J. *Handbook of Low Carbon Concrete*, Butterworth-Heinemann, 2016.

PACHECO-TORGAL, F.; LABRINCHA, A.; LEONELLI, C.; PALOMO, A.; CHINDAPRASIRT, P. *Handbook of Alkali-activated Cements, Mortars and Concretes*. United Kingdom: Elsevier, 1st ed., 2015.

PROVIS, J. L. *Alkali-activated materials*. **Cement and Concrete Research**, 2017.

PROVIS, J. L.; PALOMO, A.; SHI, C. *Advances in understanding alkali-activated materials*. **Cement and Concrete Research**, v. 78, p. 110-115, 2015.

PROVIS, J; van DEVENTER, J. S. J. *Alkali Activated Materials: State-of-the-Art Report*. New York, London: Springer, 2014.

PUERTAS, F.; TORRES-CARRASCO, M. *Use of glass waste as an activator in the preparation of alkali-activated slag. Mechanical strength and paste characterisation*. **Cement and Concrete Research**, v. 57, p. 95-104, 2014.

SHI, C.; KRIVENKO, P. V.; ROY, D. *Alkali-Activated Cements and Concretes*. London and New York: Taylor and Francis, 2006.

TCHAKOUTÉ, H. K.; RÜSCHER, C. H.; HINSCH, M.; DJOBO, J. N. Y.; KAMSEU, E.; LEONELLI, C. *Utilization of sodium waterglass from sugar cane bagasse ash as a new alternative hardener for producing metakaolin-based geopolymer cement*. **Chemie der Erde**, v. 77, p. 257-266, 2017.

TONIOLO, N.; BOCCACCINI, A. R. *Fly ash-based geopolymers containing added silicate waste. A review*. **Ceramics International**, v. 43, p. 14545-14551, 2017.

TORRES-CARRASCO, M.; PUERTAS, F. *Waste glass in the geopolymer preparation. Mechanical and microstructural characterisation*. **Journal of Cleaner Production**, v. 90, p. 397-408, 2015.

UNE-EN 196-1 2005. *Methods of Testing Cement – Part 1, Determination of Strength*, 2005.

9 GENERAL CONCLUSIONS

Sugar cane straw ash (SCSA) was successfully assessed as both solid precursor and silica source for the activating solution in alkali-activated binders based on blast furnace slag (BFS) with NaOH solutions.

SCSA obtained from an autocombustion process showed high reactivity since early curing times (see Chapters 3 and 4). Studies of thermogravimetric analysis (TGA) and Fourier transform infrared spectroscopy (FTIR) on pastes of SCSA and calcium hydroxide (CH) showed that the ash consumed all the CH in the first 3 days of curing at 40 °C. In the electrical conductivity tests, the SCSA was classified as medium reactivity (Chapter 3). Regarding to the use of the SCSA in mortars of Portland cement (as pozzolan) and blast-furnace slag (alkali-activated binders), the ash high reactivity was observed after 3 days of curing, where the SCSA-mortars presented similar or higher compressive strength.

As solid precursor in alkali-activated binders, SCSA partially replacing the BFS improved the alkali-activated mortars activated with NaOH for Na^+ concentration of 4-10 mol.kg^{-1} (see Chapters 5, 6 and 7). Compressive strength of SCSA-mortars activated with only NaOH reached higher values than the control with only blast-furnace slag/NaOH. In addition, the role of SCSA in the mixture was similar to the sodium silicate: SCSA mortars activated with only NaOH reached comparable compressive strength to a mortar with only BFS activated by both, sodium silicate and sodium hydroxide (see Chapters 5 and 6). Microstructural studies showed that the SCSA-containing mixtures presented a denser gel than one with only BFS and favoured the formation of zeolites. Therefore, the optimum use of SCSA in alkali-activated binders was replacing the BFS until 30% and using a Na^+ concentration between 4-6 M

In the last part of the thesis, SCSA was successfully utilised as silica source in sodium solutions to produce a BFS-based alkali-activated binders (see Chapter 8). A certain amount of SCSA was mixed with NaOH in a thermal bottle during a determined time to produce the activating solution. The optimum dissolution time was 24 hours, and the optimum amount of SCSA, represented by the $\text{SiO}_2/\text{Na}_2\text{O}$ molar ratio of the solution, was 1.46. Comparing the solution produced with SCSA/NaOH to other solutions, it presented similar better results in compressive strength tests to a solution prepared with only NaOH.

Related to other silica sources, SCSA/NaOH samples presented similar results to RHA/NaOH ones, and lower values when it was compared to the commercial sodium silicate and NaOH specimens. Microstructural analysis showed that the specimens produced from the SCSA-activating solution presented more similar results to the samples obtained from the sodium silicate/NaOH than the specimens produced by the activating solution with only NaOH.

10 PROPOSALS FOR FUTURE STUDIES

A proposal for continuing this work is to test the produced alkali-activated binders in durability tests, as chemical and temperature attacks. These tests can indicate the appropriate application for these new binders.

Another proposal is to utilise the SCSA with others solid precursors (metakaolin, fly ash, etc.). These studies can increase the possibilities of using the ash in alkali-activated binders.

Finally, it is proposed the application of SCSA in alkali-activated binders in different ways: structure repairs, masonry, structural elements, etc.